SOME ASPECTS OF TWO-PHASE FLOW, HEAT TRANSFER AND DYNAMIC INSTABILITIES IN MEDIUM AND HIGH PRESSURE STEAM GENERATORS

H. Ç. ÜNAL

SOME ASPECTS OF TWO-PHASE FLOW, HEAT TRANSFER AND DYNAMIC INSTABILITIES IN MEDIUM AND HIGH PRESSURE STEAM GENERATORS

PROEFSCHRIFT

TER VERKRIJGING VAN DE GRAAD VAN DOCTOR IN DE TECHNISCHE WETENSCHAPPEN AAN DE TECHNISCHE HOGESCHOOL DELFT, OP GEZAG VAN DE RECTOR MAGNIFICUS PROF. IR. B. P. TH. VELTMAN VOOR EEN COMMISSIE AANGEWEZEN DOOR HET COLLEGE VAN DEKANEN, TE VERDEDIGEN OP WOENSDAG 18 MAART 1981 DES MIDDAGS OM 16.00 UUR

DOOR

Hüseyin Çetin ÜNA

werktuigbouwkundig ingenieur

geboren te Uşak - Turkije

Dit proefschrift is goedgekeurd door de promotoren
PROF.DR.IR. G. OOMS en PROF.IR. D.G.H. LATZKO

ABSTRACT

Experimental data for void fraction, incipient point of boiling, initial point of net vapour generation, bubble dynamics, dryout, two-phase flow pressure drop and density-wave oscillations were obtained in long, sodium heated steam generator tubes of different geometries for a wide range of operating conditions and at medium and high pressures.

The present 1036 data and the 1664 data from literature taken in sodium and electrically heated steam generator tubes were correlated accurately using theoretical models or phenomenological equations. The established correlating equations contribute to the thermal and hydrodynamic design and the safe operation of medium- and high-pressure steam generators.

The phenomena related to some aspects of two-phase flow, heat transfer and density-wave oscillations in these steam generators were disclosed. These also include the distribution factor in small- and medium-size diameter steam generator tubes, the characteristic of the transitions at the incipient point of boiling and initial point of net vapour generation, bubble growth during subcooled nucleate flow boiling, the importance of the equivalent length for dryout in non-uniformly heated steam generator tubes and the mechanism of density-wave oscillations in once-through steam generator tubes.

CONTENTS

Chapter Five

Chapter Six

NOMENCLATURE

A, cross-sectional area [m^2];

A_o, cross-sectional area at the outlet of riser [m^2];

B, volume of photographical test section [m^3];

Bo, boiling number on water/steam side, [$q/(G\lambda)$];

C, distribution parameter;

C_d, drag coefficient;

c, specific heat capacity at constant pressure or specific heat capacity of material of heating surface [J/kgK];

D, bubble or plug diameter [m];

D_c, a fraction of maximum bubble diameter [m];

D_d, diameter of dry area under the bubble [m];

D_m, maximum bubble diameter [m];

$D(t)$, instantaneous bubble diameter [m];

$D_p(t)$, diameter of the total contact area of a bubble with the heating surface [m];

d, inside diameter of a circular tube or hydraulic diameter [m];

d_c, mean coil diameter [m];

d_1, inner diameter of annulus [m];

d_2, outer diameter of annulus [m];

e, total number of plugs and bubbles in photographical test section;

Fr, Froude number on water/steam side, $[G/(g\ d\ \rho_l^2)]$;

Fr_c, Froude number (based on coil diameter) on water/steam side, $[G^2/(g\ d_c\ \rho_l^2)]$;

f, Fanning friction factor;

G, mass velocity on water/steam side [kg/m^2s];

g, acceleration of gravity [m^2/s];

H, enthalpy on water/steam side [J/kg];

ΔH, dimensionless inlet subcooling enthalpy, $[(H_l - H_i)/H_l]$;

h, single-phase forced convection heat transfer coefficient [W/m^2K];

h_c, heat transfer coefficient for the loss of heat from a bubble to the surrounding liquid [W/m^2K];

J, volumetric flux density [m/s];

$\bar{J}$, average volumetric flux density of a two-phase mixture [m/s];

j, number of bubbles in a sample;

K, inlet throttling coefficient; i.e., pressure loss coefficient of an orifice or a flow control valve installed at the inlet of a tube, defined by equation (7.3);

K_A, flow parameter;

k, thermal conductivity [W/mK];

L, tube length [m];

l, length of a heat transfer region [m];

m, number of axial positions;

N, sum of pressure loss coefficients of bends along a straight tube or a serpentine;

n, number of data;

Nu, Nusselt number on water/steam side, [h/(kd)];

P, outlet pressure on water/steam side [N/m^2];

P_r, reduced pressure (i.e., P divided by critical pressure);

Pr, Prandtl number on water/steam side, (c μ/k);

ΔP, total pressure drop on water/steam side [N/m^2];

ΔP_{lo}, frictional pressure drop if water with total mass flow flows in a steam generator tube [N/m^2];

ΔP_{tp}, total two-phase flow pressure drop on water/steam side [N/m^2];

ΔP_a, acceleration pressure drop on water/steam side [N/m^2];

ΔP_f, frictional pressure drop on water/steam side [N/m^2];

ΔP_g, gravitational pressure drop on water/steam side [N/m^2];

Q, power [W];

q, heat flux on water/steam side [W/m^2];

q_c, rate of heat transfer from a bubble per unit area [W/m^2];

q_d, peripheral average dryout heat flux [W/m^2];

q_h, heat flux to bubble from the thin liquid layer under it [W/m^2];

Re, Reynolds number on water/steam side, (Gd/μ);

r, radial coordinate; r = 0 at the centre of the tube [m];

S, slip ratio;

T, temperature on water/steam side [K];

T_{sat}, saturation temperature on water/steam side [K];

t, time [s];

t_c, bubble collapse time [s];

t_m, maximum bubble growth time [s];

t_t, bubble life time [s];

ΔT_{sat}, superheating of the liquid (i.e., difference between wall temperature and saturation temperature of the liquid) [K];

$\overline{\Delta T}_{sat}$, initial superheating of the thin liquid layer under the bubble [K];

ΔT_{sub}, subcooling of the liquid (i.e., difference between saturation temperature and bulk liquid temperature) [K];

U, overall coefficient of heat transfer [W/m^2K];

u, liquid bulk velocity [m/s];

Δu, difference between the time-averaged bubble or plug velocity and the local liquid velocity [m/s];

V, velocity of the vapour phase, or instantaneous bubble or plug velocity [m/s];

$\overline{V}_a$, time-averaged bubble or plug velocity [m/s];

V_d, weighted mean drift velocity [m/s];

V_v, weighted mean velocity of the vapour phase [m/s];

v_d, drift velocity [m/s];

v_1, mean velocity of the vapour phase [m/s];

v_2, mean velocity of the liquid phase [m/s];

W, mass flow [kg/s];

X, thermodynamic steam quality, $[(H_o - H_l)/\lambda]$;

$\overline{X}$, steam quality by weight (i.e., true steam quality);

x,y,z, Cartesian coordinates [m];

Y_{41}-Y_{727}, constants or functions defined in the text; first number denotes the chapter and the remainder the sequence;

Y_{A1}, Y_{A2}, constants defined in Appendix 1.

GREEK SYMBOLS

α, void fraction;

$\bar{\alpha}$, void fraction, average over the cross section;

β, vapour volumetric rate ratio;

δ, wall thickness [m];

ζ, axial length [m];

θ, temperature on sodium side [K];

λ, latent heat of evaporation [J/kg];

μ, dynamic viscosity [kg/ms];

ρ, density [kg/m^3];

$\bar{\rho}$, average density in a heat transfer region [kg/m^3];

σ, surface tension [N/m];

Δ, instability temperature difference [K];

τ, transit time of a fluid particle [s];

τ^+, dimensionless transit time;

ϕ, volumetric flow rate [m^3/s];

ψ, period [s].

SUBSCRIPTS

a, refers to average;

B, refers to boiling region;

b, refers to bulk condition;

bt, refers to termination of boiling;

d, refers to dryout location;

e, refers to equivalent length;

F, refers to condition for pool boiling or fully developed boiling;

h, refers to heated length or heated surface;

I, refers to inside position in a helical coil;

IC, refers to outlet condition at the start of instabilities;

IPB, refers to incipient point of boiling;

IPNVG, refers to initial point of net vapour generation;

i, refers to inlet condition;

L, refers to liquid phase;

l, refers to water at the state of saturation;

M, refers to measured value;

n, refers to sodium side;

P, refers to predicted value,

p, refers to preheat region;

pa, refers to average over the periphery of a helical coil;

R-22, refers to Refrigerant-22;

o, refers to outlet condition;

S, refers to the beginning of superheated steam region;

s, refers to superheated steam region;

t, refers to total;

v, refers to vapour phase at the state of saturation;

w, refers to water/steam side.

Chapter One

GENERAL INTRODUCTION

This thesis is based on the papers of the author [U1-U11]. Nine of them were published [U1, U9], and one will appear in due course [U11]. An other paper has been submitted for publication [U10]. Two of the papers were written in collaboration with others [U6, U11].

Instead of presenting the thesis in the form of collected reprints of the papers, they were rewritten, thus their contents could be arranged systematically. This permitted also the elimination of the common parts of the papers and the presentation of the extensive experimental data.

The aim of the thesis is to enlighten the phenomena related to some aspects of two-phase flow, heat transfer and dynamic instabilities, especially density wave oscillations in medium and high pressure steam generators and to derive accurate models and correlations for the thermal and hydrodynamic design and the safe operation of these steam generators. A small part of the thesis is devoted to the economical aspects of the nuclear power in Turkey.

Two-phase flow and dynamic instabilities have been extensively studied in the literature during the last two decades in connection with the development of nuclear reactors and space vehicles. In spite of huge amounts of accumulated data, some practically important two-phase flow and instability phenomena connected with the design and safe operation of the medium and high pressure steam generators are not yet well fully understood; consequently for the evaluation of these phenomena there exist no adequate methods, as demonstrated in Chapter 3 to 7 of this thesis. One of the reasons for this is the lack of systematic experimental data. In this connection, extensive studies were carried out in the "Division of Technology for Society" of "The Netherlands Organisation for Applied Scientific Research", (MT-TNO), as a part of the supporting research for the design and construction of a 300 MWe prototype fast breeder reactor, i.e., SNR-300, with sodium as a coolant. The SNR-300 project is supported by four governments, (i.e., Germany, Belgium, Luxembourg and The Netherlands). Within the framework of this project, TNO assisted NERATOOM, an engineering and contracting company, in the development of steam generators, heat exchangers and sodium pumps, and executed in parallel a base programme in the field of sodium technology

[H1]. The funds for this program of sodium technology were provided by the Dutch Ministry of Economic Affairs.

The present thesis reports the results of a small part of the research carried out in MT-TNO for the SNR-300 project. The thesis consists of eight chapters. Although in the Introduction Section of each chapter, the subject and the aim of the chapter including the state of art of the subject are given in detail, the contents of the thesis are briefly mentioned here for the convenience of the reader.

The second chapter describes the experimental apparatus. Tests were carried out using six long test tubes (one vertical test tube, two test tubes, each comprised of a vertical tube and a V-shaped horizontal tube and three helical coils) and one large scale model evaporator in two test rigs. The test tubes and the evaporator were heated with sodium.

The third chapter deals with void fraction. Due to lack of data for the interphase phenomena, the void fraction is at present the only means used to describe steady state or unsteady state two-phase flow and is consequently of vital importance to predict the two-phase flow instabilities [S8]. For the calculation of the two-phase flow pressure drop, the void fraction has to be known. In that chapter the theoretical model of Zuber and Findlay [Z2] for the evaluation of the void fraction was verified first by experiments carried out in small diameter vertical steam generator tube for P = 4.1 - 18 MN/m^2 and G = 51 - 2237 kg/m^2s. This verification simplified the model significantly and gave the accurate values of the parameters used in the model. These values differed substantially from those given in the literature. Thereafter the results obtained were shown to apply to predict the void fraction accurately for the adiabatic and diabatic flow of steam/water mixtures in small and medium size vertical circular and rectangular tubes and vertical annuli for P = 1 - 13.8 MN/m^2 and G = 127 - 3504 kg/m^2s. For this purpose 642 data were used. 62 of them were obtained during the present study. Experimental data and correlations were also presented for void fraction in coiled steam generator tubes for P = 4 - 18 MN/m^2 and G = 429 - 1518 kg/m^2s. For the above pressure range, no data for void fraction are reported for water. The total number of present data was 44. The behaviour of the void fraction in a helical coil appears to be different from that in a vertical or horizontal tube. The tests for void fraction were performed with an unconventional method, i.e., with a high speed photographic technique. This method was first used in TNO.

The fourth chapter deals with the incipient point of boiling and initial point of net vapour generation. These points are of importance not only for understanding boiling phenomena but also for the evaluation of the void fraction [K7], two-phase flow instabilities [S1, S2] and heat transfer surfaces in steam generators. In vertical and helically coiled circular steam generator tubes, the incipient point of boiling was measured for $P = 4 - 18$ MN/m^2 and $G = 757 - 2208$ kg/m^{2}s and the initial point of net vapour generation for $P = 4 - 18$ MN/m^2 and $G = 1435 - 2203$ kg/m^{2}s. For the measurements a direct method, i.e., a high speed photographic technique was used. The present 22 data and 57 data from the literature for the incipient point of boiling of water for $P = 0.15 - 19.6$ MN/m^2 and $G = 470 - 17355$ kg/m^{2}s and 86 data from the literature for water and Refrigerant-22 for the initial point of net vapour generation for $P = 0.1 - 13.7$ MN/m^2 and $G = 132 - 2818$ kg/m^{2}s were correlated with the aid of a dimensionless number derived from a phenomenological heat transfer equation (or model) established by the present author [U12] for the subcooled nucleate flow boiling of water. A scaling law to predict the initial point of net vapour generation for liquids different from water were also given. It was shown that the above mentioned points are closely connected with the heat transfer mechanism of the subcooled nucleate flow boiling.

The fifth chapter presents work on bubble dynamics. This is of importance for a basic understanding of the boiling phenomenon and is closely related to the rate of heat transfer [T3] and void fraction [G1]. A heat transfer controlled bubble model was established first for the subcooled nucleate flow boiling of water, considering also the statistical aspects of a bubble population. The model yielded three semi-empirical correlations to predict the bubble growth rate, maximum bubble diameter and maximum bubble growth time. The 12 data obtained with a high speed photographic technique for $P = 4.1 - 17.7$ MN/m^2 and 48 data given in the literature for $P = 0.1 - 10.3$ MN/m^2 were then found to fit the correlations well. The model revealed the fact that the dry area under a bubble growing in the subcooled nucleate flow boiling region of a steam generator tube disappears beyond about 1 MN/m^2. Experimental data and a correlation were also presented for the drag coefficients for the bubble and plug flows for $P = 4.3 - 18$ MN/m^2 and $G = 51 - 107$ kg/m^{2}s.

The sixth chapter reports experimental data for the dryout and two-phase flow pressure drop obtained in three long sodium heated circular helically coiled steam generator tubes for P = 14.7 - 20.2 MN/m^2 and G = 112 - 1829 kg/m^2s, and P = 14.9 - 20 MN/m^2 and G = 296 - 1829 kg/m^2s, respectively. The importance of the evaluation of the dryout and two-phase flow pressure drop for the design and the safe operation of the steam generators need not to be repeated here. As discussed in detail in that chapter, the RMS errors in the prediction of the dryout heat flux with the well excepted five correlations from the 215 data obtained in a non-uniformly heated steam generator tube vary between 39.8% and 111.5%. A similar conclusion was also drawn for the well-known two two-phase flow pressure drop correlations. Therefore the 203 data obtained for dryout heat flux in the present study and 674 data given in the literature for short and long uniformly heated circular tubes and for a long non-uniformly heated circular tube for P = 4.3 - 20.2 MN/m^2 and G = 399 - 5542 kg/m^2s were correlated to predict the dryout heat flux within 20% accuracy for 98% of the time with a RMS error of 9.01%. It appears that the so-called equivalent length hypothesis should have physical significance for the mechanism of dryout, and that the effect of centrifugal forces on the inception of dryout in a helical coil disappears beyond about $d_c/d = 38.9$. Using 369 data an accurate correlation for the determination of the two-phase flow pressure drop was also established for P = 14.3 - 20.1 MN/m^2 and G = 296 - 3498 kg/m^2s.

The seventh chapter deals with two-phase flow instabilities, especially with the density wave oscillations. First, data were obtained for the inception conditions of these oscillations in four long, once-through sodium heated steam generator tubes and in a large scale model evaporator for P = 5.3 - 19.1 MN/m^2 and G = 187 - 1365 kg/m^2s. All the test tubes and the evaporator operated in the forced convection mode. Thereafter it was shown that the density wave oscillations in a forced convection once-through steam generator tube are time delay oscillations and, that the length of the superheated steam region and the transit time in this region practically govern the mechanism of these oscillations. An empirical relation was also established for this mechanism. Using this mechanism the data for the density wave oscillations from forced convection once-through steam generator tubes can be correlated in different ways. Two correlations were presented for this application. The correlations are very accurate.

The first correlation predicts the power at the start of density wave oscillations within 8% accuracy for 87% of the time from the 351 data obtained in the present study and from the 62 data given in the literature for once-through steam generator tubes and a steam generator tube in which no superheated steam was produced for P = 4.1 - 17.3 MN/m^2 and G = 118 - 2088 kg/m^2s. The RMS error for all the 413 data is 5.97%. All the data considered were obtained in forced convection systems. In order to use this correlation it is sufficient to know two operating conditions (i.e., pressure and inlet subcooling) and the geometry. The second correlation applies only to forced convection once-through steam generator tubes and predicts the power at the start of the density wave oscillations from 380 data obtained in the present study and in the literature for P = 4.3 - 19.1 MN/m^2 and G = 118 - 1365 kg/m^2s within 7.5% accuracy for 98% of the time with a RMS error of 3.33%. A correlating equation to predict the period of these oscillations for P =4.1 - 19 MN/m^2 and G = 262 - 2088 kg/m^2s in once-through steam generator tubes and in a steam generator tube in which no superheated steam was produced was also established. With a few exceptions, stability models in literature were always used in the form of a computer program to predict the inception conditions and the period of the density wave oscillations. In general, a stability model can not predict the power at the start of these oscillations better than to about 10% accuracy. The accuracy of stability models given in the literature can be much less than 10%, as demonstrated in [B9, N3]. Most literature models are based on linearized equations of conservation, and thus they are per definition not suitable for the determination of the period of these oscillations. The present correlations practically eliminate the use of complicated stability models in the form of computer programs at least for the ranges of geometries and operating conditions considered in this study in so far the prediction of the inception conditions of the density wave oscillations in forced convection once-through steam generator tubes are concerned, since the correlations were derived from the physical mechanism of these oscillations and they are very accurate. The 110 data given in the literature for the inception conditions of the density wave oscillations in natural circulation steam generator tubes for different geometries and for P = 0.2 - 7.1 MN/m^2 and G = 519 - 1230 kg/m^2s were also correlated accurately in order to support the fact that the

simple correlations are sufficient to determine the inception conditions of these oscillations. In that chapter experimental data were also presented for the flow pattern instabilities detected in vertical and helically coiled steam generator tubes during the subcooled nucleate flow boiling of water. These instabilities appear to be due to the suppression of bubble growth.

The eighth chapter gives the conclusions of this study. In the thesis in total about 2700 data were analysed and correlated. 1036 of these data were obtained in the present work.

In two-phase flow it is customary to describe a phenomenon with different terms. The following is therefore considered useful to be clarified.

Subcooled nucleate flow boiling is a transition between the forced convection and the fully developed boiling regimes; it is also referred in the literature to as "partial nucleate boiling", "forced convection surface boiling", or simply "surface boiling". In this type of boiling, the liquid bulk temperature is below the saturation temperature.

The terms "dryout", "burnout" and "boiling crisis" apply to the same phenomenon. Dryout heat flux is practically identical to the heat flux at the departure from nucleate boiling.

A once-through steam generator tube is per definition the tube in which superheated steam is produced.

In two-phase flow the dimensionless numbers used for the correlation of the experimental data are not, in general, derived from the well known three classical methods of the dimensional analysis (i.e., the Buckingham method, the Rayleigh method and the use of differential equations) [K4]. As shown in [I2], the dimensionless numbers which characterize fully the dynamics of two-phase flow are numerous and it is practically impossible to take all of them into account when correlating the data. The same applies also to a steady-state two-phase flow.

In the present study almost all the dimensionless numbers used for the correlation of data were derived from theoretical models (or phenomenological equations). Thereafter the models and consequently the assumptions used to establish the models were verified with the results of present experiments and with the results of experiments of several investigators or vice versa. One essential requirement for these verifications is that

the ranges of geometries and operating conditions of these experiments have to be as wide as possible. This was also fulfilled. The above, i.e., the logical grouping of the variables into dimensionless numbers, can then be accepted without hesitation, as indicated in a classical text book [M3].

The paper on the economic aspects of nuclear power in Turkey is presented in Appendix 4. This paper outlines Turkey's energy resources, the past, present and future electric power situations and the large hydro and thermal power plant projects, planned and studied by the State Planning Department to be built possibly during the time covered by the second or the third five-year plan (1967 - 1972 or 1972 - 1977). The data are reviewed to obtain a future power balance. Then an economical comparison is made of the power plant projects with the 300-, 400-, 500- and 700-MW(e) BWR and PHWR nuclear power plants on the basis of the unit energy cost. The results obtained indicate that nuclear energy should be seriously considered for the production of electricity in Turkey.

Chapter Two

EXPERIMENTAL APPARATUS

The tests reported were carried out in two test rigs, the SWISH rig (i.e., Subcritical Water Investigation in Sodium Heated heat transfer rig) and 50 MW SCTF (i.e., 50 MW Sodium Component Test Facility). The rigs and the test tubes used in these rigs are briefly described below.

2.1 SWISH RIG

2.1.1 The Rig

The flow diagram of the rig is shown in Fig. 2.1 where the high pressure part of the rig is drawn in heavy lines and the low pressure part in fine lines. The rig was constructed from stainless steel,

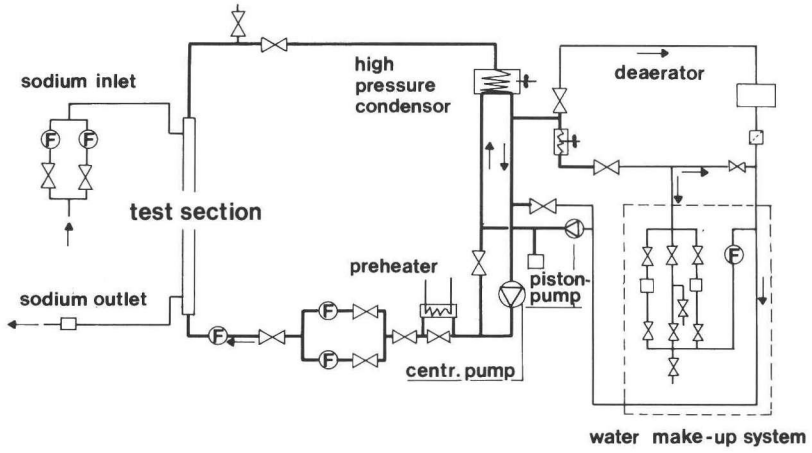

Fig. 2.1 Flow diagram of the SWISH rig

grade AISI-316, for supercritical operating conditions (i.e., 500°C at 30 MN/m^2). The maximum available temperature was 650°C. The ID and OD of the piping used for constructing the water/steam side were 20 and 30 mm, respectively. For the construction of the sodium side a piping of 40 mm ID and 44 mm OD was used. The capacity of the centrifugal pump on the water/steam side was 5 m^3/h at 2 MN/m^2 developed head and the capacity of the electromagnetic pump on the sodium side was 20 m^3/h at 0.5 MN/m^2

developed head.

The sodium in the rig was heated electrically. The maximum available power was about 830 kW including the power of the preheater. After an operating period of approximately 6 years this power decreased to about 500 kW due to failure of some electrical heaters that were not replaced. An air cooled condenser was used on the water/steam side.

For each test tube used for stability experiments headers were mounted at the inlet and outlet of the test tube. Between these two headers, a comparatively large diameter by-pass pipe was mounted; thus the total pressure drop in the test tube was constant. The by-pass pipe is not shown separately in Fig. 2.1, but it is included in the part indicated as test section. The total length of a test tube was the length between the inlet header and the outlet header. Flow control valves were mounted at a test tube just after the inlet header.

During high pressure operation the pressure was regulated by an automatic control valve and the piston pump. The deaerator then served as an expansion tank. The volume of the high pressure part of the loop was approximately 0.05 m^3, excluding the test tube and by-pass.

All the measurements were carried out with precalibrated instruments and collected with an on-line data acquisition system and processed by a Hewlett-Packard-2116-B computer. This computer had a 32 kilo-bytes core memory and 1000 kilo-bytes auxiliary disc memory for data storage. Almost all the evaluation and correlation work was carried out either with this computer or with a large Hewlett-Packard-21MX computer with 256 kilo-bytes core memory and 50 mega-bytes auxiliary disc memory. Throughout this study, properties of water, steam, sodium and Refrigerant-22 were evaluated from [A6, D6, D7, H3].

Demineralised water with an oxygen content of less than 15 ppb, a conductivity of less than 0.5 μS/cm and a pH between 8.5 and 9 was used during the tests.

In total six test tubes were used in the above described rig.

2.1.2 TEST TUBES

2.1.2.1 Test Tube 1 (TT1)

This test tube of 7.86 mm ID and 12 mm OD was manufactured from

stainless steel, grade AISI-316. The sodium side surrounding the test tube was constructed in the form of seven annuli, as shown in Fig. 2.2. From the base the first three annuli were 1.977 m long and the last four annuli were 0.989 m long. The distance between the successive annuli was 16 mm. The inner wall of each annulus was formed by the test tube. The ID of the outer tube of each annulus was 25 mm. The annuli were connected by approximately 0.5 m long adiabatic circular tubes of 25 mm ID. The flow orientation was upward on the water/steam side and downward on the sodium side.

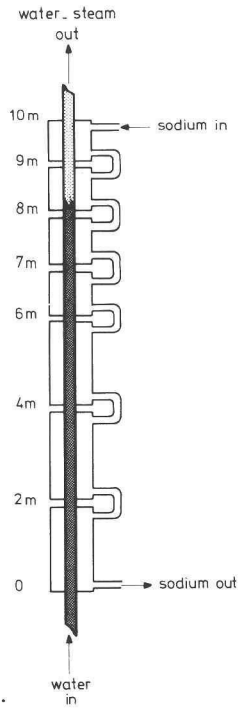

Fig. 2.2 TT1

Both on the sodium side and on the water/steam side outlet pressure, mass flow and temperature at ζ = 0, (i.e., at the inlet of the test tube) 2, 4, 6, 7, 8, 9 and 10 m (i.e., at the outlet of the test tube) were measured. The measurement of the pressure drop on the water/steam side was carried out across the successive sections given by the locations ζ = 0, 4, 6, 8, 9 and 10 m. In the last 4 m part of the tube, wall temperatures were also measured at 34 axial positions at r = 4.68 mm. The water/steam side outlet temperature was recorded on a two-channel line recorder. The throttling coefficient of the turbine flow meter at the inlet of the test tube was 10.7 in accordance with the manufacturer's specifications.

The ID of the by-pass built around the test tube was 24.3 mm.

In order to photograph the two-phase flow, two photographical test sections were used, which are referred to as FTS1 and FTS2.

FTS1 was an adiabatic, cylindrical sapphire of 8 mm ID, 25 mm OD and 20 mm height. FTS2 was an adiabatic square sapphire channel of 7.1 x 7.1 x 20 mm. The wall thickness of the channel was 3 mm. Each photographical test section was mounted just at the end of TT1 after a 20 mm long transition piece, as shown in Fig. 2.3. The cross sectional area along this piece was practically equal to the cross sectional area of the test tube and of the sapphire channel. The transition piece was perfectly insulated. The subcoolings used during the photographical tests were low. It was therefore assumed that the bubbles (or plugs) did not

become smaller along this transition piece. This assumption was verified by measuring the bubble (or plug) diameters along the photographical test section. These diameters were approximately constant.

Through FTS1 and FTS2 the pictures of boiling were taken in one dimension, i.e., perpendicular to the direction of flow.

The aim of the photographical tests was the measurement of the weighted mean velocity of the vapour phase. If this velocity is determined for some conditions, the void fraction is then known, as discussed in Chapter 3. In the literature void fraction has been usually determined with X or γ-ray absorption methods or neutron back scattering method.

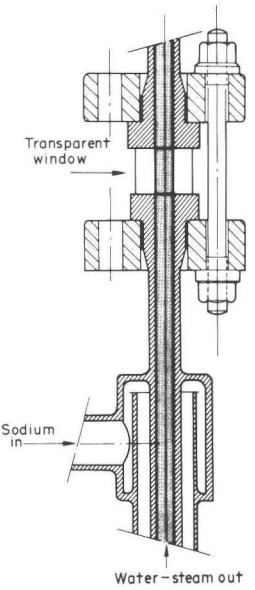

Fig. 2.3 Sketch of the top part of TT1 with FTS1

The maximum error in the determination of the above velocity was about 5% and was mainly due to optical resolution of the sapphire and the statistical method used to calcula this velocity in the bubble flow region.

For some tests (see Section 3.1.3.3), the void fraction should be known for the accurate prediction of the steam quality. For these tests, void fraction was determined by measuring the bubble and plug dimensions on the developed films using a Boscar motion analyzer and equation (3.29). For plug flow a few large plugs or a single large plug and comparatively small bubbles were seen on a developed film. In a bubble flow region for which the void fraction was determined this was low, i.e., less than 5% (see Table 3.2). The error in the determination of the void fraction was solely due to errors in measuring bubble or plug dimensions, and was estimated to be about 15%. This error, however, is of not much significance, as discussed in Section 3.1.3.3.

2.1.2.2 Test Tube 2 (TT2)

With TT1, it was not possible to carry out stability tests at low mass velocities: The static head in the by-pass determined the minimum value of mass flow in the test tube, since the total pressure drop in the by-pass pipe and in the test tube were equal. Therefore an 8.84 m long, horizontal V-shaped (corner angle = 7.25 degrees) tube of the same bore as TT1 and of 14 mm OD, and a flow control valve were added to the inlet of TT1. The flow in a part of the 8.84 m long tube was heated by sodium. For this purpose a 5.1 m long annulus similar to that described in Section 2.1.2.1 was used. The above modification of TT1 made it possible to perform stability tests at low mass velocities and to study the effect of throttling on the stability. The by-pass pipe used for TT1 was also installed around TT2.

In addition to those measured for TT1, the temperature at the new water/steam side inlet and the new sodium side outlet and the pressure drop across the flow control valve were measured. The water/steam side outlet temperature and the mass flow in the test tube were also recorded on a two-channel line recorder. By means of the flow control valve mounted at the inlet of TT2, the value of inlet throttling coefficient was adjusted.

2.1.2.3 Test Tube 3 (TT3)

This 20.45 m long test tube of 13.12 mm ID and 17.1 mm OD was manufactured from stabilised ferritic steel, 10CrMoNbNi9.10, and consisted of a 9.40 m vertical and an 11.05 m V-shaped horizontal tube. The sodium side surrounding the test tube was constructed of 4 annuli, a construction similar to that used for TT1, which is shown in Fig. 2.2. From the base, these annuli were respectively 10.25, 4, 3 and 2 m long. The inner wall of each annulus was formed by the test tube. The ID of the outer tube of each annulus was 29.7 mm. The annuli were connected by approximately 0.5 m long adiabatic circular tubes of 29.7 mm ID. A 0.80 m long piece at the inlet and a 0.40 m long piece at the outlet of the test tube were not heated. The flow orientation was upward on the water/steam side and downward on the sodium side. By means of two flow control valves mounted at the inlet of the test tube, the value of the inlet throttling coefficient was adjusted between 54.7 and 382.9. This coefficient (i.e., total of the pressure loss coefficients of the two flow control valves and a flow meter between these valves) was based on the tube diameter. For given openings of the valves, this coefficient was taken as an average of the

values obtained in all tests carried out with the same openings.

The ID of the by-pass pipe used was 49.3 mm.

Both on the sodium side and on the water/steam side mass flow, outlet pressure and temperature along the test tube at ζ = 0.80 (i.e., at the inlet of the heated part of the test tube), 11.05, 15.05, 18.05 and 20.05 m (i.e., at the end of the heated part of the test tube) were measured. Sodium side temperatures were also measured at 12 additional axial positions. The measurement of the pressure drop on the water/steam side was carried out across the successive sections given by the locations mentioned above. Outlet temperatures both on the sodium side and on the water/steam side and the inlet temperature, mass flow and outlet pressure on the water/steam side, and the pressure drop in the by-pass pipe were simultaneously recorded on a six-channel line recorder.

2.1.2.4 Test Tube 4 (TT4)

This test tube was a 44.43 m long (i.e., straightened length) helically coiled tube of 18 mm ID and 26 mm OD. It was manufactured from stainless steel-316. The test tube was placed concentrically in an other helically coiled tube of 49 mm ID. The flow on the sodium side was downward between these coils, and upward in the test tube. A 2.00 m long piece at the inlet and a 2.30 m long piece at the outlet of the test tube were not heated. The coil diameter was 1.5 m and the helix angle was 7.77 degrees.

Both on the sodium side and on the water/steam side outlet pressure, mass flow and the temperature along the test tube at ζ = 2.000 (i.e., at the inlet of the heated part of the tube), 8.838, 13.594, 18.350, 23.106, 27.862, 32.618, 34.996, 37.374, 39.752 and 42.130 m (i.e., at the outlet of the heated part of the tube) were measured. The measurement of the pressure drop on the water/steam side was carried out across the successive sections given by the locations ζ = 2.000, 13.594, 23.106, 27.862, 32.618, 37.374 and 42.130 m. In the wall of the last 9.51 m of the heated part of the test tube at the inside, top, outside and bottom, wall temperatures were also measured at 24 axial and 2 radial locations. The coordinates of the latter were r = 9.75 mm and 11.25 mm. Thus the number of measurements for the wall temperatures was 192 for one test run. For the dryout tests the mass flow and the outlet temperature on the water/steam side and the 4 wall temperatures measured at the end of the heated part

of the test tube, i.e., at ζ = 42.13 m and r = 9.75 mm were simultaneously recorded on a six-line recorder. For the stability tests, outlet temperatures both on the sodium side and on the water/steam side, and the inlet temperature, mass flow and outlet pressure on the water/steam side, and the pressure drop in the by-pass pipe were also simultaneously recorded on a six channel line recorder.

For 41% of the stability tests carried out in the test tube, the value of inlet throttling was adjusted between 223 and 665 by means of two control valves fitted at the inlet of the test tube. For the calculation of the inlet throttling coefficient the same procedure was used as described for TT3. For the rest of the tests, these valves were not mounted and in this case the throttling of the flow was solely due to the turbine flow meter at the inlet of the test tube, and K = 15 - 27.

The ID of the by-pass pipe used was 49.3 mm.

2.1.2.5 Test Tube 5 (TT5)

This 40.13 m long (i.e., straightened length) helically coiled test tube of 18 mm ID and 26 mm OD was manufactured from stainless steel-316. The coil diameter was 0.7 m and the helix angle 8.83 degrees.

The sodium side surrounding the test tube was constructed in the form of eight annuli, a construction similar to that given in Fig. 2.2. From the base their respective lengths were 8.829, 6.622, 4.403, 4.403, 4.403, 2.184, 2.184 and 2.184 m. The inner wall of each annulus was formed by the test tube. The ID of the outer tube of each annulus was 49 mm. The annuli were connected by approximately 0.5 m long, U-type, adiabatic circular tubes of 49 mm ID. The distance between the successive annuli was 36 mm. The flow orientation was upward on the water/steam side and downward on the sodium side. A 4.63 m long piece at the inlet of the test tube was not heated.

Both on the sodium side and on the water/steam side outlet pressure, mass flow and the temperature along the test tube at ζ = 4.630 (i.e., at the inlet of the heated part of the tube), 13.459, 20.117, 24.556, 28.995, 33.434, 35.654, 37.873 and 40.130 m and the pressure drop on the water/steam side across the tube sections between two successive values of the above given locations were measured. In the last 10.70 m of the heated part of the test tube measurements of the wall temperatures were carried out at

25 axial locations in a pattern similar to that described for TT4. Thus in total 200 wall temperatures were measured for one test run.

In order to photograph two-phase flow, a photographical test section (i.e., FTS3) was mounted at the end of the test tube after a 58 mm transition piece. This photographical test section was an adiabatic, square sapphire channel of 16 x 16 x 20 mm. The wall thickness of the channel was 3 mm. The cross sectional area along the whole length of the transition piece was practically equal to the cross sectional area of the test tube and of the photographical test section. This transition piece was perfectly insulated. The subcoolings used in the photographical tests were low. It was therefore assumed that the bubbles (or plugs) did not become smaller along this transition piece. This assumption was verified by measuring the bubble (or plug) diameters along the photographical test section. These diameters were approximately constant.

Through FTS3, the pictures of boiling were taken in two dimensions, as explained in Section 3.2.2.1. The aim of the photographical tests was to determine the weighted mean velocity of the vapour phase, which is related to void fraction. The error in measuring this velocity was about 5% due to reasons stated in Section 2.1.2.1.

2.1.2.6 Test Tube 6 (TT6)

This test tube was a short version of TT5, i.e., the last 26.671 m long part of TT5 was TT6. The instrumentation of the latter was identical to that of TT5. In order to photograph the two-phase flow, the photographical test section (i.e., FTS3) described in Section 2.1.2.5 was also mounted at the end of the test tube after the aforesaid 58 mm long transition piece.

2.1.3 Type of Instruments

Both on the sodium side and on the water/steam side temperatures were measured with chromel-alumel thermocouples of 0.5 mm OD in TT1 and TT2 and with a similar type of thermocouples of 1 mm OD in TT3, TT4, TT5 and TT6. For the measurement of the wall temperatures chromel-alumel thermocouples of 0.34 mm OD were used. The maximum error in measuring the above-mentioned temperatures was between 1.2 and 1.6 K.

Both the sodium side and water/steam side mass flows were measured with turbine flow meters, which had errors less than 1%. Only during the drift velocity tests (see Table 3.2) very low mass velocities (i.e., $G < 96$ kg/m^{2}s) were used on the water/steam side. Since the manufacturer provided no data for the accuracy of the turbine flow meter used for these tests for $G < 96$ kg/m^{2}s, this flow meter was calibrated with an estimated accuracy of 10% for $G < 96$ kg/m^{2}s. Beyond $G > 96$ kg/m^{2}s, the accuracy of the flow meter was 1%.

For the measurement of the water/steam side outlet pressure, a dead-weight balance manometer was used, which had a maximum error of 30 kN/m^2. The pressure drops were measured with pressure transducers, which had an error between about 4% and 10%, with the exception of pressure drops measured for a few test runs carried out at low mass velocities.

Several isothermal and single-phase flow runs were made to calibrate the wall thermocouples. This resulted in the rejection of the temperatures measured by some of the wall thermocouples.

All the measurements were collected with an on-line data acquisition system and processed by a Hewlett-Packard-2116B computer mentioned before.

2.2 50 MW-SCTF

2.2.1 The Test Unit and the Instrumentation

The test unit used was the evaporator of the 50 MWth liquid sodium heated steam generator. This steam generator was designed by Neratoom for a LMFBR, SNR-300. It was tested in the 50 MW Sodium Component Test Facility at Hengelo (O). The steam generator consists of an evaporator and a superheater. A description of the steam generator is given in [C4, L9]; data for the 50 MW Sodium Component Test Facility may be found in [B16].

In the present study it is only dealt with the stability experiments carried out in the evaporator and it should be stressed that at all operating conditions of SNR-300, the evaporator produces wet steam of qualities of 0.95 or less, and it is not susceptible to instabilities. Under extreme conditions far remote from the operating conditions of SNR-300, instabilities were observed, however, when steam with a high degree of superheating had to be produced in the evaporator.

The evaporator is a counterflow, 30 MWth unit and operates in the forced-convection mode. The water/steam flows upward in 139 straight vertical tubes of 12.6 mm ID and 17.2 mm OD, and is heated by sodium flowing downward around the tubes arranged in a shell in an equi-triangular pattern of 27.5 mm pitch. The effective (i.e., heated) tube length is 18.64 m, and the total tube length between the tube plates 19.34 m. The steam generator was manufactured from 2¼Cr1Mo stabilised ferritic steel.

The evaporator was heavily instrumented [L9]. It is considered sufficient to mention here that the values of the inlet and outlet temperatures, outlet pressure and mass flow both on the sodium side and on the water/steam side of the evaporator were measured with pre-calibrated instruments, and collected with an on-line data acquisition system and processed by a Siemens-300 computer.

In order to detect the instabilities, six thermocouples were placed on the upper tube plate at the outlets of six tubes at different radial locations, as indicated in Fig. 2.4. The temperatures measured by these thermocouples were recorded both on potentiometric multichannel recorders and on the computer. In the present work only the instabilities detected in these six tubes are dealt with; the inlet temperature and outlet pressure for these tubes were known since these quantities are equal for all the tubes in the evaporator. The pressure drop across the tubes of the evaporator is also equal for each tube. The flow at the inlet of the evaporator was

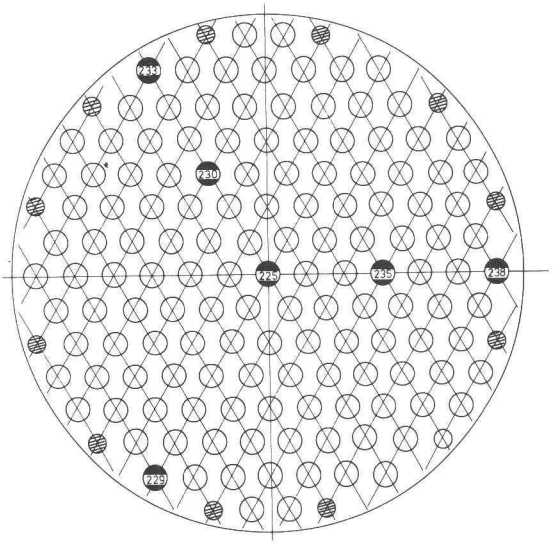

Fig. 2.4 Locations of the tubes in which instabilities were detected

not throttled.

All the temperatures were measured with inconel-sheathed, chromel-alumel thermocouples of 1 mm OD; the error in determining a temperature was 3/8%. Water/steam side mass flow was measured with an orifice meter with an accuracy of 2%. Sodium-side mass flow was measured with an electromagnetic flow meter with an accuracy of less than 4%. The pressures were measured with Barton cells with an accuracy of less than 2%.

Chapter Three

VOID FRACTION

3.1 STRAIGHT TUBES

3.1.1 Introduction

The best known equation used to determine void fraction is the so-called slip correlation, which, in fact, is a physical definition of the slip ratio,

$$S = \frac{\bar{v}_1}{\bar{v}_2} = \frac{\bar{X}}{1 - \bar{X}} \frac{1 - \bar{\alpha}}{\bar{\alpha}} \frac{\rho_L}{\rho_v} \tag{3.1}$$

where

$$\bar{v}_1 = \frac{\phi_v}{A_v} = \frac{\bar{X}\, W}{\rho_v\, A_v} \tag{3.2}$$

$$\bar{v}_2 = \frac{\phi_L}{A_L} = \frac{(1 - \bar{X})\, W}{\rho_L\, A_L} \tag{3.3}$$

$\bar{\alpha}$ is, per definition, equal to A_v/A.

An other type of equation used for the determination of void fraction is from Armand [A8]:

$$\beta/\bar{\alpha} = \frac{1}{K_A} = C \tag{3.4}$$

where

$$\beta = \frac{\phi_v}{\phi_v + \phi_L} = \frac{\bar{X}}{\bar{X} + (1 - \bar{X})(\rho_v/\rho_L)} \tag{3.5}$$

Armand has experimentally demonstrated that the flow parameter K_A in equation (3.4) is a constant for the adiabatic bubble and slug flow of air-water mixtures in a horizontal pipe at atmospheric pressure conditions for vapour volumetric rate ratios of less than 0.9 and greater than 0.3. Later Armand and Treshchev [A9] have shown indirectly that the flow parameter is a pressure dependent constant for the flow of steam/water mixtures with or without heat addition in horizontal pipes for the

pressure range of 0.98 to 17.7 MN/m^2 and for steam qualities less than 0.9. Bankoff [B2] was the first to derive equation (3.4), and evaluate theoretically the flow parameter by assuming a power-law for both distribution of velocity and void fraction for bubble flow in a circular tube. He has verified equation (3.4) using data for steam/water mixtures with or without heat addition in vertically and horizontally orientated rectangular channels and circular tubes up to 13.8 MN/m^2. He reports that the flow parameter, K_A, is a pressure dependent constant. Owing to the lack of data, however, he has not been able to show directly whether the flow parameter he evaluated theoretically is a pressure dependent constant. Bankoff has related the slip ratio to the flow parameter, as given below:

$$S = \frac{\bar{v}_1}{\bar{v}_2} = \frac{1 - \bar{\alpha}}{K_A - \bar{\alpha}} \tag{3.6}$$

Zuber and Findlay [Z2] have derived a general expression to determine the velocity field and void fraction in any two-phase flow by considering radial void- and volumetric flux density distributions and the relative velocity between the two phases in a channel: They first established a velocity field, which is useful for characterizing the flow of a two-phase mixture,

$$V = J + v_d \tag{3.7}$$

where V is the velocity of the vapour phase, J, the volumetric flux density of a two-phase mixture and v_d, the drift velocity. They considered the weighted mean value of a quantity F_w, as defined below:

$$F_w = \frac{\langle \alpha \ F \rangle}{\langle \alpha \rangle} = \frac{\frac{1}{A}\int_A \alpha \ F \ dA}{\frac{1}{A}\int_A \alpha \ dA} \tag{3.8}$$

In view of equation (3.7) and (3.8), they obtained the weighted mean velocity of the vapour phase V_v, as follows:

$$V_v = \frac{\langle \alpha \ J \rangle}{\langle \alpha \rangle} + \frac{\langle \alpha \ v_d \rangle}{\langle \alpha \rangle} \tag{3.9}$$

where

$$V_v = \frac{\langle V\ \alpha \rangle}{\langle\ \alpha\ \rangle} \tag{3.10}$$

Multiplying and dividing the first term of the RHS of equation (3.9) by <J>, they obtained

$$V_v = C\ \langle\ J\ \rangle + \frac{\langle \alpha\ v_d \rangle}{\langle\ \alpha\ \rangle} \tag{3.11}$$

or $$V_v = C\ \bar{J} + V_d \tag{3.12}$$

where the distribution parameter C, is defined by

$$C = \frac{\langle \alpha\ J \rangle}{\langle \alpha \rangle\ \langle J \rangle} = \frac{\frac{1}{A}\int_A \alpha J\ dA}{[\frac{1}{A}\int_A J dA]\ [\frac{1}{A}\int_A \alpha\ dA]} \tag{3.13}$$

and $\bar{J}$, the average volumetric flux density of a two-phase mixture, by

$$\bar{J} = \frac{\phi_L + \phi_v}{A} = G\ (\frac{\bar{X}}{\rho_v} + \frac{1 - \bar{X}}{\rho_L}) \tag{3.14}$$

Considering equations (3.5) and (3.14) and the definition of void fraction (i.e., $\bar{\alpha} = A_v/A$), and since

$$V_v = \frac{\phi_v}{A_v} \tag{3.15}$$

equation (3.12) becomes

$$\beta/\bar{\alpha} = C + V_d/\bar{J} \tag{3.16}$$

The aforesaid investigators have evaluated the distribution parameter C in equation (3.16) for a circular tube by assuming a polynominal distribution for profiles of radial void- and volumetric flux density. Zuber and Findlay [Z2], Zuber et al. [Z3] and Staub and Zuber [S13] report that, in general, this parameter is a function of flow pattern and geometry,

and that V_d, the weighted mean drift velocity in equation (3.16), is a function of flow pattern, geometry and pressure.

Zuber et al. [Z3] and Staub and Zuber [S13] have shown that equation (3.16) correlates well water and Refrigerant-22 data taken in vertical circular tubes and rectangular channels and over a large range of conditions if the effects of flow regimes and geometry are not considered and if

$$C = 1.13 \tag{3.17}$$

and

$$V_d = 1.18 \left[\sigma g \left(\rho_L - \rho_v\right)/\rho_L^2 \right]^{1/4} \tag{3.18}$$

Although Zuber et al. [Z3] have demonstrated that the distribution parameter calculated with profiles of void fraction and volumetric flux density as measured by Adorni et al. [A3] in a circular tube is about 1.14, the weighted mean drift velocity evaluated from the same data (Fig. 1 in [Z3]) differs by about 1270% from that evaluated from equation (3.18).

When the relative velocity between the two phases is zero or negligible, as in the case of the flow in horizontal channels or flow in vertical pipes at high velocities and elevated pressures (see equations (3.16) and (3.18)), the weighted mean drift velocity, or $V_d/\bar{J}$ in equation (3.16), becomes zero or negligible, and this equation reduces to equation (3.4). In this case the values of the distribution (or flow) parameter reported by Armand and Treshchev [A9], Bankoff [B2] and Zuber et al. [Z3] are in serious disagreement with each other. Furthermore the radial void distribution measured recently with an advanced technique by Inoue et al. [I1], Kobayasi [K5] and Ohba [O1] for the bubble flow regime in a circular tube and in a rectangular channel deviates considerably from that assumed by Zuber and Findlay [Z2], Zuber et al. [Z3] and Bankoff [B2] to predict the distribution (or flow) parameter.

Drift velocity is the difference between the velocity of the vapour phase and the volumetric flux density of the vapour and liquid mixture, as defined by equation (3.7). Weighting the drift velocity in accordance with equation (3.8) yields the weighted mean drift velocity. No literature exists on the adequate determination of this velocity for bubble- and plug-flow regimes during the flow boiling of water at elevated pressures. Many investigators have reported data on the motion of gas bubbles in liquids. (For references see [A10, P1, W1]). Most of these studies deal

with the motion of individual air bubbles in a stagnant water and in a turbulent water stream. However, no scaling-law has yet been established between the motion of individual gas bubbles and the motion of the flow boiling bubbles. The latter form, in fact, a population consisting of many different sizes of bubbles with different velocities. For the velocity of the vapour phase in the bubble- (or plug-) flow regime, the velocity of the whole bubble (or plug) population has to be considered. A statistical approach is therefore required to determine the velocity of a bubble (or plug) population.

It follows from the above discussion that adequate data are needed for the value of C, the distribution parameter and V_d, the weighted mean drift velocity. As indicated in [Z2], equation (3.12) gives a straight line with slope C in the $V_v/\bar{J}$-plane and the interception of this line with the V_v-axis gives V_d. (See Fig. 3.3). For the determination of equation (3.12) (or the aforesaid parameters, i.e., C and V_d) for a given flow regime and pressure, therefore, it is sufficient to measure V_v, the weighted mean velocity of the vapour phase, for at least two given sets of operating conditions (i.e., mass velocity, steam quality and subcooling) in a channel, since $\bar{J}$, the average volumetric flux density of the mixture, depends only on the operating conditions.

The aim of this part of the thesis (i.e., Section 3.1) is to demonstrate the experimental determination of equation (3.12) (or distribution parameter C and weighted mean drift velocity V_d) for bubble- and plug-flow in a vertical small diameter tube. For this purpose first C was measured accurately i.e., the operating conditions of the tests were chosen in such a way that $C >> V_d/\bar{J}$ in equation (3.12). If $C >> V_d/\bar{J}$, this equation does not permit an adequate determination of V_d. For the measurement of V_d, therefore, the operating conditions of the tests were selected such that the magnitude of $V_d/\bar{J}$ was in the same order as the magnitude of C. Having determined C and V_d, these were inserted into equation (3.16). Thereafter this equation was compared with the extensive void fraction data of various investigators taken for the subcooled nucleate flow boiling of water, the saturated bulk boiling of water and the flow of steam/water mixtures without heat addition in vertical channels.

3.1.2 Determination of the Distribution Parameter

3.1.2.1 Tests

The distribution parameter was determined in TT1. For this purpose, FTS1 (i.e., the photographical test section 1) was mounted at the end of TT1. The pictures of subcooled nucleate flow boiling were taken through the cylindrical sapphire channel with a high-speed rotating mirror camera (Dynafax, model 350) at a frequency of 5000 frames/s. During the experiments subcooling at the end of the test section was slowly decreased, while pressure, heat flux and mass velocity were kept constant. The objective of the camera could be adjusted such that the bubbles (or plugs) either in the whole cross section or in half the cross section of the cylindrical sapphire channel could be photographed. For every test run, pictures of boiling were taken from these two positions of the objective. It took half an hour to reach steady-state conditions after which photographs were taken. In total 42 runs were carried out. The operating conditions of the tests were: $P = 4.1 - 15.9$ MN/m^2; $G = 2018 - 2237$ kg/m^{2}s; $\Delta T_{sub} = 0.0 - 4.5$ K; $\bar{X} = 0 - 2.9\%$. These operating conditions are also given in detail in Table 3.1, and fulfill the requirement that $V_d/\bar{J} << 1$.

After developing the films, bubble (or plug) velocities and diameters were measured with a Boscar motion analyzer in order to determine the weighted mean velocity of the vapour phase, V_v.

3.1.2.2 Determination of the Weighted Mean Velocity of the Vapour Phase

3.1.2.2.1 Plug Flow

At pressures lower than about 7 MN/m^2, plug flow started immediately after the initial point of net vapour generation, and a few plugs (or even sometimes a single plug) and several comparatively small bubbles in a liquid continuum were visible on the developed films, as shown schematically in Fig. 3.1. The magnitudes of the length and the diameter of a plug were in the same order of magnitude as the tube diameter. The velocity of every plug and bubble appearing on the film was measured at several axial positions (between 2 and

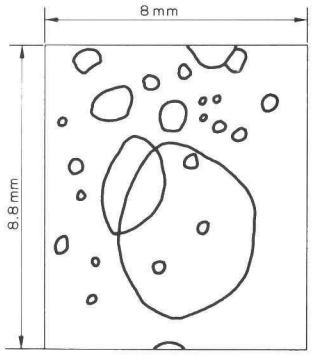

Fig. 3.1 Schematic description of plug flow at 4.1 MN/m^2.

Table 3.1 Data from TT1 for the Determination of the Distribution Parameter

No.	P MN/m^2	G kg/m^2s	ΔT_{sub} K	$\bar{X}$ %	V_v m/s
1	4.1	2202	1.9	0.00*	2.85
2	4.1	2237	0.0	1.076	3.65
3	4.1	2145	0.6	0.348	3.08
4	4.1	2092	0	1.150	3.85
5	4.1	2092	0	1.150	3.93
6	4.1	2203	1.2	0.00	3.05
7	4.1	2172	1.0	0.090	3.17
8	4.1	2185	0	1.104	3.84
9	4.1	2218	0	1.086	4.77
10	4.1	2218	0	1.086	4.64
11	4.1	2181	0.1	0.884	4.42
12	4.1	2115	0.8	0.205	2.89
13	4.1	2124	0.6	0.352	3.19
14	7.0	2162	0.9	0.039	2.87
15	7.0	2090	0.4	0.034	2.76
16	10.0	2042	1.2	0.114	3.12
17	10.0	2029	1.2	0.115	2.79
18	10.0	2028	0.9	0.249	3.13
19	10.0	2025	1.6	0.00	3.01
20	10.0	2018	0.6	0.424	2.98
21	10.0	2018	0.7	0.370	3.00
22	12.0	2203	4.5	0.00	3.29
23	12.0	2139	3.0	0.00	3.30
24	12.0	2138	2.7	0.064	3.60
25	12.0	2131	2.1	0.290	3.39
26	12.0	2131	1.8	0.420	3.43
27	12.0	2137	0.6	1.140	3.68
28	14.0	2119	3.8	0.00	3.28
29	14.0	2104	1.6	1.440	3.36
30	14.0	2076	1.0	2.140	3.82
31	14.0	2069	0.9	2.260	3.72
32	14.0	2111	0.6	2.900	3.99
33	14.0	2121	3.8	0.00	3.35
34	15.9	2110	4.1	0.00	3.67
35	15.9	2104	4.1	0.00	3.69
36	15.9	2103	3.1	0.217	3.52
37	15.9	2120	1.7	0.626	4.04
38	15.9	2138	0.3	1.870	4.19
39	15.9	2154	1.0	1.070	4.19
40	15.9	2151	1.2	0.860	3.70
41	15.9	2183	1.9	0.540	3.75
42	15.9	2183	2.0	0.510	3.52

* The steam qualities given as (0.00) were in fact negligibly small.

and 28 positions). Thus the number of velocities measured varied between 8 and 247 for each test run. The reason why the velocity of a plug or a bubble was measured at several axial positions was to determine the time-averaged value of the velocity. As shown in the paper of Warschauer [W2], the velocities of bubbles (or plugs) vary significantly with time during the bubble (or plug) flow regime.

Since all the bubbles and plugs were approximately elliptically shaped, the equivalent diameter of a plug (or bubble) was determined by averaging the measured major and minor axes of a plug (or bubble). No deformation in plug (or bubble) shape was observed during measurement of the velocity of a plug (or bubble).

In order to determine the weighted mean velocity of the vapour phase (or velocity of the centre of gravity of the vapour phase in plug flow) the following equation was used:

$$V_v \frac{\pi}{6} \rho_v \sum_{e=1}^{e} D_e^3 = \frac{\pi}{6} \rho_v \left\{ \frac{D_1^3}{m} \sum_{m=1}^{m} V_m + \frac{D_2^3}{m} \sum_{m=1}^{m} V_m + .. + \frac{D_e^3}{m} \sum_{m=1}^{m} V_m \right\} \quad (3.19)$$

where D_1, D_2,.., D_e in equation (3.19) are the measured equivalent diameters of the plugs and bubbles seen on a developed film. It was possible to determine this velocity up to a void fraction of 33%. It follows from the description of the plug flow regime that the small bubbles which could not be seen on a developed film did not substantially affect the prediction of the weighted mean velocity of the vapour phase, since the bubble volume used in equation (3.19) is proportional to the third power of the bubble diameter, which is much smaller than the diameter of a plug.

3.1.2.2.2 Bubble Flow

For pressures higher than about 10 MN/m^2, numerous small bubbles of different sizes in a continuous liquid were visible on the developed films up to high values of steam quality. The distribution of the bubble diameters was approximately a normal distribution. Since the number of bubbles on a developed film was large, the weighted mean velocity of the vapour phase for this flow regime was determined by a statistical method from the measured velocities of a sufficient number of bubbles taken randomly from the bubble population. For each test run, a sample of

4 to 10 bubbles was taken from the bubble population and the velocity and diameter (or major and minor axes when they were elliptically shaped) of each bubble in the sample were measured at several axial positions (between 1 and 19 positions). Thus the number of velocities measured varied between 15 and 140 for each test run. Analysed bubble populations were selected such that a representative bubble sample could be taken from them. For this flow regime it was possible to determine the weighted mean velocity of the vapour phase up to 18% void fraction, and this velocity could be calculated with the formula below:

$$V_v = \frac{1}{j} \sum_{j=1}^{j} \left(\frac{1}{m} \sum_{m=1}^{m} V_m\right)_j \qquad (3.20)$$

or

$$V_v \frac{\pi}{6} \rho_v \sum_{j=1}^{j} D_j^3 = \frac{\pi}{6} \rho_v \left(\frac{D_1^3}{m} \sum_{m=1}^{m} V_m + \frac{D_2^3}{m} \sum_{m=1}^{m} V_m + .. + \frac{D_j^3}{m} \sum_{m=1}^{m} V_m\right) \qquad (3.21)$$

The weighted mean velocity of the vapour phase predicted by equation (3.20) was considered for further analysis, since it was found to differ by not more than a few per cent from that predicted by equation (3.21).

3.1.2.3 Determination of Steam Quality

In order to determine $\bar{J}$ (see equation (3.14)), the steam quality has to be known.

During the tests, heat losses were compensated by installing trace heaters in the insulation material which covered the piping on the sodium side. Steam quality was therefore calculated from the following heat balance:

$$[W (\Theta_i - \Theta_o) c]_n - [W (H_o - H_i)]_w = W_w \bar{X} \lambda \qquad (3.22)$$

For this purpose the difference between the temperatures at the inlet and outlet of the test tube both on the sodium and water/steam sides were calibrated.

Since the steam quality in the subcooled boiling region is extremely low, the steam quality calculated with equation (3.22) may involve a con-

siderable error. In order to minimise this error in steam quality, the following method was adopted: During the experiments, only the subcooling at the end of the test tube was slowly decreased, while mass velocity, heat flux and pressure were kept constant. In this way first the initial point of net vapour generation was determined from the developed films, as explained in Chapter 4. At this particular point steam quality can be considered to be negligibly low, as shown in Chapter 4. Thereafter subcooling was plotted versus $\bar{X}W_w\lambda$, the heat used for vapour formation, for a given pressure and the best fitting curve was drawn through the experimental points. An example of this is shown in Fig. 3.2 for 12 MN/m^2. Then for a given subcooling $\bar{X}W_w\lambda$, the heat used for vapour formation, was determined from the figure and from this the steam quality. It is obvious that this steam quality is the true steam quality, i.e., the quality based on thermal non-equilibrium.

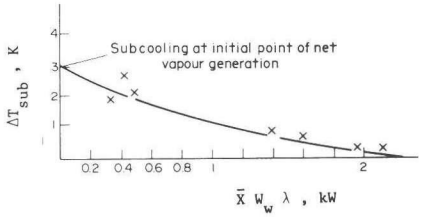

Fig. 3.2 Determination of steam quality at 12 MN/m^2.

3.1.2.4 Distribution Parameter

In order to determine the distribution parameter and the weighted mean drift velocity by the aid of equation (3.12), V_v, the measured weighted mean velocity of the vapour phase, was plotted versus $\bar{J}$, the average volumetric flux density of the steam/water mixture, for a given pressure, as shown in Fig. 3.3, for example for 4.1 MN/m^2. $\bar{J}$ was calculated from equation (3.14), using the measured steam quality. The slope of the line drawn through the experimental data gives the value

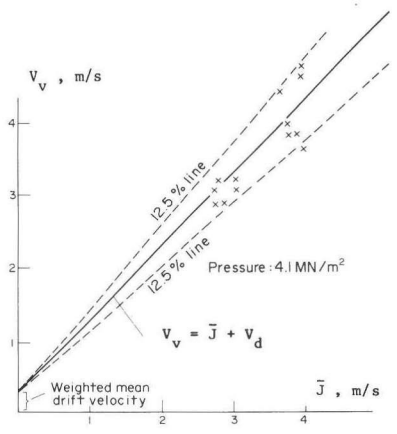

Fig. 3.3 Determination of distribution parameter and weighted mean drift velocity at 4.1 MN/m^2.

of the distribution parameter C, and the interception of this line with the V_v-axis the value of the weighted mean drift velocity V_d. As can be seen from the figure, the value of the distribution parameter is equal to 1 and that of the weighted mean drift velocity equals 0.3 m/s. The distribution parameters and weighted mean drift velocities determined by this procedure for all test runs yielded

$$C = 1 \tag{3.23}$$

and

$$V_d = 0.36\ (1 - P_r)^{0.9} \tag{3.24}$$

, as shown in Fig. 3.4. The distribution parameter given by equation (3.23) is in contradiction with that reported in [B2, Z3].

For the operating conditions of the present tests, $V_d/\bar{J} \ll 1$. It follows then from equation (3.12) that the determination of the distribution parameter seems fairly accurate but not that of the weighted mean drift velocity. The adequate determination of the latter is given below.

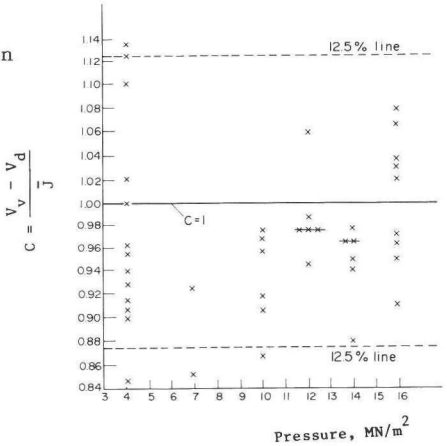

Fig. 3.4 Verifications of equations (3.23) and (3.24).

3.1.3 Determination of the Weighted Mean Drift Velocity

3.1.3.1 Tests

Drift velocities were measured in TT1. For this purpose FTS2 (i.e., photographical test section 2) was mounted at the end of TT1. The pictures of subcooled nucleate flow boiling were taken through FTS2 with a high speed rotating prism camera (Hycam Model, 120 m) at a frequency of 10000 frames/s for the following range of operating conditions: $P = 4.3 - 18$ MN/m², $G = 51 - 107$ kg/m²s, $\Delta T_{sub} = 0 - 1.3$ K, $\bar{\alpha} = 0.08 - 26\%$. The operating conditions are also given in detail in Table 3.2.

When running the experiments, it took half an hour to reach steady-state conditions, after which photographs were taken. The velocity of a

bubble (or plug) was measured by the use of a Boscar motion analyzer from the developed films.

3.1.3.2 Determination of the Weighted Mean Velocity of the Vapour Phase

For the determination of this velocity, equation (3.12) is used after inserting the value of the measured distribution parameter (see equation 3.23) into it, i.e.,

$$V_v/\bar{J} = 1 + V_d/\bar{J} \qquad (3.25)$$

Table 3.2 Data for the Drift Velocities

No.	P MN/m^2	G kg/m^2s	$\bar{\alpha}$ %	$\bar{J}$ m/s	V_d m/s	ΔT_{sub} K
1	4.25	59.5	2.51	0.081	0.159	0
2	4.25	59.5	2.51	0.081	0.169	0
3	7.25	87.6	2.87	0.128	0.212	0.1
4	7.26	72.1	0.08	0.098	0.152	0.3
5	7.26	62.5	4.55	0.097	0.181	0
6	7.26	62.5	4.55	0.097	0.190	0
7	10.10	93.6	14.57	0.182	0.163	0.5
8	10.09	73.7	4.40	0.119	0.176	0.6
9	10.09	61.3	2.74	0.095	0.134	0.8
10	12.15	106.9	0.52	0.165	0.165	1.1
11	12.15	81.2	1.08	0.126	0.124	0.8
12	12.14	55.1	1.37	0.087	0.157	0.9
13	14.08	105.9	2.88	0.178	0.154	0.9
14	14.16	83.3	0.93	0.137	0.181	0.9
15	14.17	74.5	26.00	0.199	0.154	0.8
16	16.02	106.0	1.97	0.186	0.169	1.0
17	16.03	65.9	2.91	0.118	0.151	1.0
18	16.03	53.4	0.77	0.093	0.157	0.7
19	17.97	101.1	1.34	0.186	0.139	1.3
20	17.96	51.3	0.78	0.095	0.174	1.1

In accordance with equation (3.25) it is sufficient to measure V_v, the weighted mean velocity of the vapour phase (i.e., the velocity of the centre of gravity of the vapour phase), for the determination of V_d, since $\bar{J}$ in this equation is a known function of the operating conditions. As can be deduced from Table 3.2, $V_d/\bar{J} \cong 0.75 - 2.22$ during the tests. This permitted an accurate determination of V_d since $C = 1$ in equation (3.25).

3.1.3.2.1 Plug Flow

In the plug flow regime, bubbles assumed either the shape of a plug or of a spherical cap, and $D/d > 0.6$, i.e., the magnitude of the equivalent diameter of a plug was in the same order of magnitude as the hydraulic diameter of the sapphire channel.

In order to determine the equivalent diameter of a plug, the plug was considered to be elliptically shaped, and the minor and major axes of the plug were measured with a Boscar motion analyzer. The arithmetic mean of the aforesaid axes was taken as the equivalent diameter.

Periodic variation of the volume of a plug (or bubble) was observed during the rise of the plug (or bubble). This cyclic variation of the volume became negligible at pressures higher than 14.2 MN/m^2. During the rise, a plug (or a bubble) rotated slowly and irregularly.

In order to determine the weighted mean velocity of the vapour phase in the plug flow regime, a procedure similar to that given in Section 3.1.2.2.1 was used.

3.1.3.2.2 Bubble Flow

In the bubble-flow regime, the equivalent bubble diameter varied between 0.81 and 3.87 mm and the bubble shape was ellipsoid. The equivalent bubble diameter was found by averaging the measured major and minor axes of a bubble. The number of bubbles on the developed films was between 1 and 20. In this flow regime, the weighted mean velocity of the vapour phase was determined with a procedure similar to that given in Section 3.1.2.2.2.

3.1.3.3 Determination of the Steam Quality

In order to determine $\bar{J}$ in equation (3.25), i.e., the average volumetric flux density of the water/steam mixture, the steam quality has to be known. During all the tests, the steam quality was very low. The evaluation of this from a heat balance, therefore, might involve a considerable error. For this reason, the steam quality was determined by solving the following fundamental identities, which hold for any two-phase flow,

$$\phi_v = V_v A_v = \bar{X}GA/\rho_v \tag{3.26}$$

and

$$\bar{\alpha} = A_v/(A_L + A_v) = A_v/A \tag{3.27}$$

, as given below:

$$\bar{X} = \frac{\bar{\alpha}\ \rho_v\ V_v}{G} \tag{3.28}$$

$\bar{\alpha}$, the void fraction in equation (3.28), was determined from the following equation:

$$\bar{\alpha} = \frac{\pi}{6} \sum_{e=1}^{e} D_e{}^3/B \tag{3.29}$$

3.1.3.4 The Weighted Mean Drift Velocity

Having determined the weighted mean velocity of vapour phase V_v and the true steam quality $\bar{X}$ with the aid of V_v, the weighted mean drift velocities were solved from equations (3.25) and (3.14) and tabulated in Table 3.2. It follows from equations (3.14) and (3.28) that the measurement errors in V_v influence also the average volumetric flux density $\bar{J}$ and consequently V_d. This is, however, of secondary importance, since $\bar{X}$ was very low for the tests carried out, as can be deduced from equation (3.28) and Table 3.2. In this case, errors in $\bar{X}$ are of no significance for the prediction of $\bar{J}$ for the operating conditions of the tests carried out.

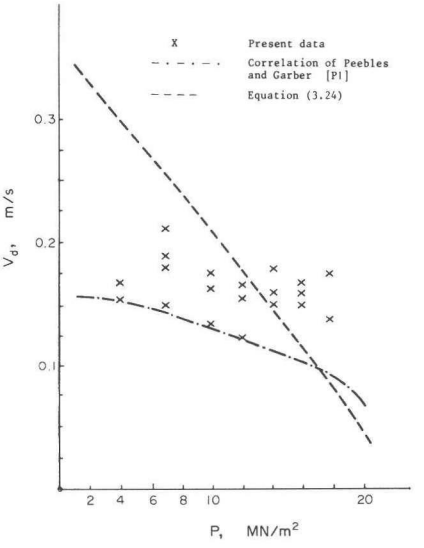

Fig. 3.5 Comparison of the data for the drift velocity with different correlations.

First the data obtained were compared with the tentative correlation established in Section 3.1.2.4 and with the well known

correlation of Peebles and Garber [P1] used by Zuber and his co-workers [Z2, Z3, S13] to predict the drift velocity for the bubble flow regime (i.e., equation (3.18)). As can be seen from Fig. 3.5, the agreement of the aforesaid correlations with the data is far from satisfactory.

As shown in Fig. 3.6, data for drift velocities were correlated with the following equation, established using the dimensional analysis:

$$V_d = 16.1 \left[\frac{(\rho_L - \rho_v) g \mu_L}{\rho_L^2}\right]^{1/3} \tag{3.30}$$

The reason why the few data do not fit the correlation well is probably due to errors in measuring mass velocities below 96 kg/m^{2}s. It follows from Figs. 3.5 and 3.6 that the drift velocity does not significantly vary with pressure.

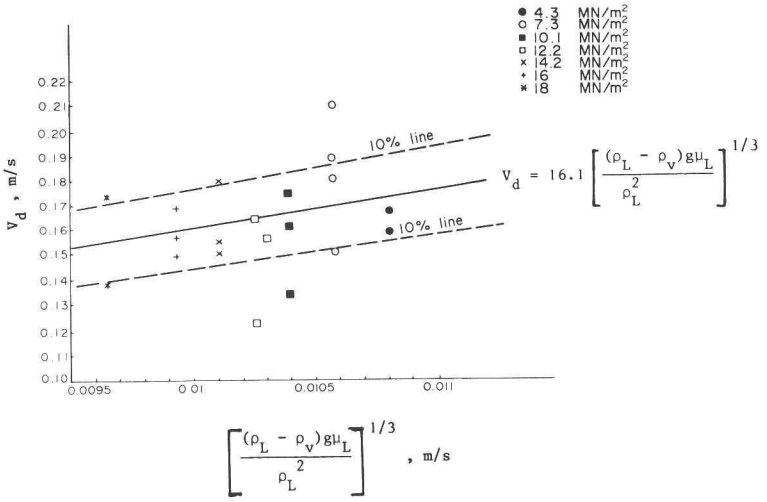

Fig. 3.6 Correlation of the data for the drift velocity.

3.1.4 Verification of Equation (3.16)

The distribution parameter C and weighted mean drift velocity V_d were determined above, as given by equations (3.23) and (3.30) respectively. If these equations are inserted into equations (3.12) and (3.16),

equation (3.12) gives a velocity field and equation (3.16) the void fraction in plug and bubble flow, since $\bar{J}$ and β are known functions of the operating conditions. C and V_d were obtained using equation (3.12) and this equation is identical to equation (3.16). The measured void fractions given in Table 3.2 were compared in Fig. 3.7 with those predicted by equation (3.16). These void fraction data were obtained during the measurement of the drift velocities. Equation (3.16) fits the data well.

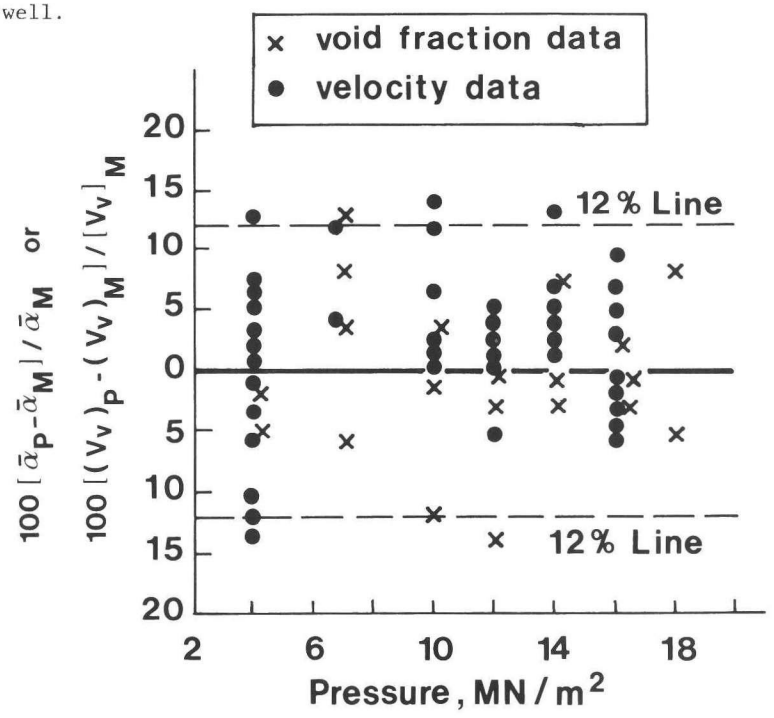

Fig. 3.7 Verification of equation (3.16).

The measured weighted mean velocity of the vapour phase given in Table 3.1 were also compared in Fig. 3.7 with those predicted by equation (3.12). When these data were produced, void fraction was not measured. An accurate determination of the drift velocity was not possible from these data either. It follows from Fig. 3.7 that equation (3.12) fits the data well, thus this equation adequately describes a velocity field in plug- and bubble flow.

3.1.5 Void Fraction Correlation for the Adiabatic and Diabatic Flow of Steam/Water Mixtures

For the present tests, void fraction was not measured extensively but a velocity field in bubble and plug flow. This velocity field is characterized by equation (3.12) in which C and V_d are given respectively by equations (3.23) and (3.30). By inserting the last mentioned two equations into equation (3.16), equation (3.16) was compared with the data of various investigators obtained for a wide range of operating conditions for the adiabatic and diabatic flow of steam/water mixtures in different types of vertical channels [A4, E2, M5, R8]. The ranges of geometries and operating conditions for these data are given in Table 3.3. In the above comparison flow regimes were not taken into account. The number of data considered was 580. Not all the data from [E2, M5, R8] could be considered. Only the data for comparatively high steam qualities, as indicated in Table 3.3, were studied since for subcooled nucleate flow boiling, in which steam qualities are low, a simple heat balance does not give the steam quality as a result of the thermal non-equilibrium existing between the phases. With the exception of the 173 low mass velocity data of [R8] taken in an annulus for P = 1 - 5 MN/m^2 and $G \cong 130$ kg/m^2s, the agreement of the data with equation (3.16) was satisfactory, considering $V_d/\bar{J} \ll 1$ for the data [U4]. In order to correlate the data of [A4, E2, M5] taken in circular tubes and rectan-

Table 3.3 Conditions for Void Fraction Experiments of Various Investigators

P (MN/m^2)	Number of data	Geometry *	d (mm)	Heat flux (MW/m^2)	G (kg/m^2s)	$\bar{X}$ (%)	$\bar{\alpha}$ (%)	Ref.
3-5	75	circular tube	9.16	adiabatic	388-3504	0-80	0-99	A4
13.8	54	rectangular channel	4.74	0.32-1.58	895-1153	10-37	42-85	E2
2-6.9	75	circular tube and annulus	7.7-10.2	adiabatic	400-3400	10-88	58-99	M5
2-9.8	11	circular tubes	15.7-34.3	0.014-2	400-1700	10-60	49-99	M5
1-5	365	annulus	13	0.60 -1.22	127-1368	5-21.9	55-87	R8

* All the test tubes used were vertical.

gular channels and the present data, equations (3.12) and (3.16) were slightly modified as follows:

$$V_v/\bar{J} = 1.03 + V_d/\bar{J} \tag{3.31}$$

and

$$\beta/\bar{\alpha} = 1.03 + V_d/\bar{J} \tag{3.32}$$

V_d in equations (3.31) and (3.32) is given by equation (3.30).

The reason why the low mass-velocity data of [R8] obtained in an annulus do not fit equation (3.16) is straightforward. For a mass velocity of about 130 kg/m^{2}s and for $P \geq 1$ MN/m^2, $V_d/\bar{J}$ is of importance for the determination of equation (3.16), and the weighted mean drift velocity in an annulus should differ from the weighted mean drift velocity in a circular tube [Z3]. In the present study this velocity was measured in a circular tube, and it is, in general, a function of flow pattern, geometry and pressure, as stated in Section 3.1.1. Comparison of equation (3.32) with the data of [R8] taken in annuli yielded the following drift velocity in an annulus, which is 2.5 bigger than that in a circular or rectangular tube for given fluid properties:

$$V_d = 40.25[(\rho_L - \rho_v)\mu_L g/\rho_L^2]^{1/3} \tag{3.33}$$

Results of the comparison of equations (3.31) and (3.32) with all the data mentioned in Table 3.3 and the present data are shown in Fig. 3.8. Since the number of data considered was large, i.e., 642, not all the data could be given in the figure. The data shown in the figure were selected such that the range of maximum error in predicting void fraction can be seen. Equations (3.31)

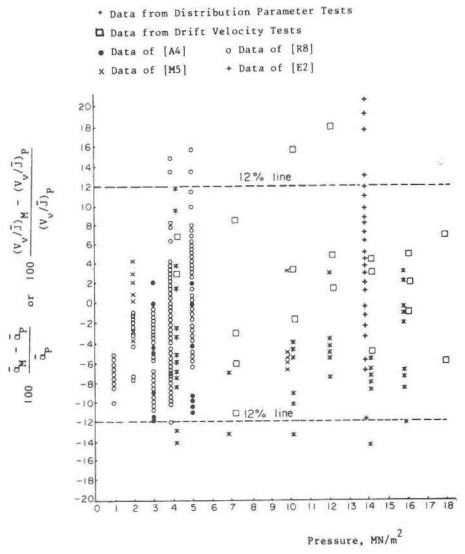

Fig. 3.8 Comparison of the void fraction data with → equations (3.31) and (3.32).

and (3.32) correlate all the data well, i.e., within about 12% accuracy with the exception of 15 data, as can be deduced from the figure. The RMS error for correlating the data is 6%.

For the 449 data out of 642 data considered, the condition, $V_d/\bar{J} << 1$, applies. It follows then from equation (3.32) that the value of the distribution parameter C is practically equal to one, that is, to the empirical value determined for the distribution parameter in the present study, as given by equation (3.23).

Equations (3.31) and (3.32) apply to small and medium size tubes. For large diameter tubes and for slug flow the distribution parameter differs substantially from unity [W1, Z2, Z3]. Collins et al. [C9] have shown theoretically and experimentally that the distribution parameter is a function of the Reynolds number for the slug flow of air/water mixtures and air/water-glycerol mixtures in a large diameter tube of 51.4 mm ID at atmospheric pressure. However, it is not yet demonstrated in the literature that slug flow exists for the diabatic flow of steam/water mixtures at medium and high pressures.

The range of operating conditions for the data used to establish equations (3.31) and (3.32) are summarized as follows: P = 1 - 18 MN/m^2; $\bar{\alpha}$ = 0.08 - 99%; d = 4.7 - 34.3 mm; G = 51 - 3504 kg/m^2s; q = adiabatic (i.e., without heat addition) and 0.01 - 2.0 MW/m^2.

3.2 HELICALLY COILED TUBES

3.2.1 Introduction

To the knowledge of the author no literature exists on void fraction for the flow boiling of water at elevated pressures in helical coils. Data for void fraction for the adiabatic flow of gas/liquid mixtures in helical coils are given in [A5, B1, B14, K2, R4]. Most of these works deal with the flow of air/water mixtures. Rippel et al. [R4] measured void fraction for the concurrent downflow of air/water, helium/water, Freon-12/water, air/2-propanal mixtures through a coil with d_c/d = 19.9. With the exception of high values of void fraction, the results of their air/water tests fit the correlation of Lockhart and Martinelli [L8] well [R4]. This correlation is based on data obtained in horizontal tubes. Banerjee et al. [B1] also report that the data for void fraction obtained for a wide range of fluids and coil diameters fit the aforesaid corre-

lation well. The air/water data of Boyce et al. [B14] taken in a coil with $d_c/d = 48$ were also correlated with the aforesaid correlation. Akagawa et al. [A5] measured void fraction for the flow of air/water mixtures in two helical coils with $d_c/d = 11$ and 22.7. They correlated the data for $0.18 \leq \beta \leq 0.95$ with the equation given below:

$$\beta/\bar{\alpha} = 1.2 \tag{3.34}$$

The data of the last mentioned authors do not fit the correlation of Lockhart and Martinelli [L8] well. Kasturi and Stepanek [K2] obtained data for void fraction for two-phase concurrent flows of different gas and liquid mixtures in a helical coil with $d_c/d = 53.2$, and compared the data with the correlation of Hughmark [H6]. The data do not fit this correlation well.

It can be shown that the void fraction data of Rippel et al. [R4], Boyce et al. [B14] and Akagawa et al. [A5] for the flow of air/water mixtures in helical coils can be correlated within 10% accuracy with the equation

$$\beta/\bar{\alpha} = C \tag{3.35}$$

where $C = 1.12$. For these data $0.18 \leq \beta \leq 0.99$ and $11 \leq d_c/d \leq 48$, and C, the distribution parameter, appears not to be affected by centrifugal forces.

It is worthwhile mentioning that for the flow of air/water mixtures in horizontal tubes the value of the distribution parameter is reported to be 1.2 [A8] and 1.27 [N2, R3] for $0.3 \leq \beta \leq 0.9$.

The above indicates that for the flow of air/water mixtures the distribution parameter in horizontal tubes is greater than the distribution parameter in helical coils.

Due to the complex nature of two-phase flow in helical coils, results of the experiments given in [A5, B1, B14, K2, R4] for the flow of gas/liquid mixtures can not be extrapolated to the flow boiling of water at elevated pressures. In the latter case, vapour velocity and radial accelerations are much lower than those in an atmospheric gas/liquid system.

It follows from Section 3.1 that for helical coils with small helix angle or for horizontal tubes, equations (3.12) and (3.16) reduce to

$$V_v/\bar{J} = C = \beta/\bar{\alpha} \qquad (3.36)$$

since V_d, the weighted mean drift velocity, is negligibly small or zero. In accordance with equation (3.36) it is sufficient to measure V_v, the weighted mean velocity of the vapour phase, for the determination of distribution parameter and consequently of the void fraction since β and $\bar{J}$ in equation (3.36) can be predicted from the known operating conditions. The aim of this part of the thesis (i.e., Section 3.2) is to present data and correlations for the determination of the distribution parameter and consequently of the void fraction in helically coiled tubes for bubble and plug flow.

3.2.2 Determination of the Distribution Parameter

3.2.2.1 Tests

The distribution parameter was determined in TT6 for $\beta < 0.12$ and in TT5 for $\beta \geq 0.12$. For this purpose, the photographical test section (i.e., FTS3), described in Section 2.1.2.5 was mounted at the end of TT5 and TT6. The pictures of boiling were taken in two dimensions perpendicular to the direction of flow through the sapphire channel with a high speed rotating prism camera (Hycam model, 120 m) at a frequency of 10,000 frames/s. The schematic description of the optical system used is given in Fig. 3.9. This system permits to follow a particle on a developed film in three dimensions, as illustrated in Fig. 3.10. A particle at the location A (x, y, z) on the (x - y) plane in the sapphire channel is shown on a developed film. The three coordinates of the particle and the (x - z) and (y - z) planes are also indicated in the figure. The position of the sapphire channel with respect to the test tube is also shown in the figure.

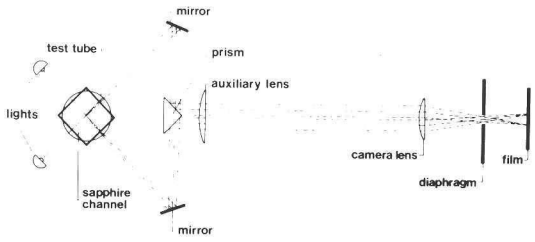

Fig. 3.9 Schematic description of the optical system used.

During the experiments, subcooling at the end of the test tube was slowly decreased, while the pressure, heat flux and mass velocity were

kept constant. It took half an hour to reach steady state conditions, after which photographs were taken.

In total 44 runs were analysed. In these runs bubble and plug flow regimes were observed and the range of operating conditions was:

$P = 4 - 18\ MN/m^2$;

$G = 429 - 1518\ kg/m^2s$;

$q = 0.013 - 0.42\ MW/m^2$ (average heat flux for last coil);

$\Delta T_{sub} = 0.3 - 12.5\ K$;

$\bar{X} = 0.000032 - 0.0753$; $\beta = 0.00018 - 0.579$; $V_v = 0.817 - 3.48\ m/s$.

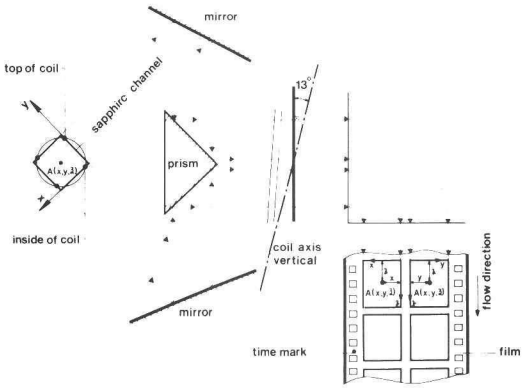

Fig. 3.10 System of coordinates.

The operating conditions of the tests are also given in detail in Table 3.4.

After developing the films, bubble (or plug) velocities and diameters were measured with a Boscar motion analyzer in order to determine V_v, the weighted mean velocity of the vapour phase.

3.2.2.2 Determination of the Weighted Mean Velocity of the Vapour Phase

3.2.2.2.1 Plug Flow

For pressures of 4 and 8.1 MN/m^2, plug flow started immediately after the initial point of net vapour generation, and one or two plugs (i.e., large bubbles) and several comparatively small bubbles in a liquid continuum were visible on the developed films, as shown schematically in Fig. 3.11. For almost all the test runs analysed,

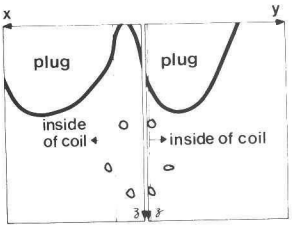

a - plug flow
($P = 8.1\ MN/m^2$; $G = 431\ kg/m^2s$; $\Delta T_{sub} = 2K$)

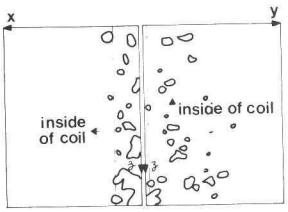

b - bubble flow
($P = 12\ MN/m^2$; $G = 1495\ kg/m^2s$; $\Delta T_{sub} = 9.3K$)

Fig. 3.11 Plug and bubble flow.

Table 3.4 Data from TT5 and TT6 for the Determination of the Distribution Parameter

No.	P MN/m^2	G kg/m^2s	ΔT_{sub} K	$\bar{X}$ %	V_v m/s
1	4.03	1518	3.9	0.088	1.75
2	4.03	1516	2.6	0.195	2.05
3	4.03	1513	1.6	0.169	2.22
4	4.04	1509	0.3	0.354	2.32
5	4.04	1509	0.3	0.354	2.53
6	4.20	1467	1.3	0.981	2.53
7	4.20	1467	1.3	0.981	2.56
8	4.24	1446	0.3	3.243	2.97
9	4.24	1446	0.3	3.243	3.18
10	4.22	1464	0.6	2.162	3.06
11	4.22	1464	0.6	2.162	3.33
12	4.22	1464	0.6	2.162	2.86
13	8.10	1457	1.5	4.835	3.47
14	8.10	1457	1.5	4.835	2.58
15	8.11	1469	1.7	4.126	3.23
16	8.11	1469	1.7	4.126	2.73
17	8.11	1493	3.0	2.669	3.48
18	8.11	1493	3.0	2.669	2.93
19	8.05	431	2.0	5.433	0.99
20	8.05	431	2.0	5.433	0.99
21	8.07	429	2.2	7.527	1.04
22	8.14	1518	9.2	0.013	1.79
23	8.14	1502	5.7	0.086	1.93
24	8.11	1508	7.3	0.020	1.70
25	8.12	1498	4.8	0.212	2.27
26	8.11	1497	3.4	0.275	2.29
27	8.10	1499	3.6	0.313	2.20
28	8.11	1487	1.7	0.482	2.60
29	8.11	1487	1.7	0.482	2.52
30	8.11	1487	1.7	0.482	2.51
31	8.11	1479	1.1	0.656	3.04
32	12.0	1465	7.7	0.044	1.80
33	12.0	1464	5.8	0.126	1.82
34	12.0	1468	5.1	0.200	1.83
35	12.0	1472	3.6	0.852	2.17
36	16.1	1454	8.3	0.036	2.24
37	16.1	1436	6.4	0.215	2.00
38	16.1	1433	5.2	0.510	2.08
39	16.0	754	4.4	0.0032	0.82
40	16.0	760	2.5	0.178	0.98
41	16.0	759	1.1	0.782	1.00
42	18.0	1461	9.6	0.0067	2.21
43	18.0	1459	8.4	0.0141	2.14
44	18.0	1461	6.8	0.134	2.44

the magnitude of the equivalent diameter of a plug was in the same order of magnitude as the hydraulic diameter of the sapphire channel. The first plugs appeared at the vicinity of the wall of the coil, somewhere between the inside (near the coil axis) and the top position. When the steam quality was increased, plugs became larger and agglomerated. Finally single plug was present in the test section. For steam qualities higher than about 7%, wavy flow was observed and the vapour phase started to occupy the whole right hand side of the cross section of the coil.

The velocity of every plug and bubble appearing on the film was measured at several axial positions (between 16 and 75 positions). Thus the number of velocities measured varied between 20 and 80 for each test run. The reason why the velocity of a plug or a bubble was measured at several axial positions was to determine the time averaged value of the velocity.

Since the plugs for low values of the outlet steam quality and all the bubbles were approximately elliptically shaped, the equivalent diameter of such a plug (or bubble) was determined by averaging the measured major and minor axes of the plug (or bubble). These axes were measured on the (y - z) plane. At higher values of the outlet steam quality, plugs assumed the shape of a cylinder or a cylinder with a spherical cap. The dimensions of these types of plugs were measured in the (x - z) and (y - z) planes, and the equivalent diameter of the plug was determined by equating the volume of the plug to that of a sphere. A cylindrical volume was approximated by the volume of a rectangular parallelepiped. No deformation in plug (or bubble) shape was observed during the measurement of the velocity of a plug (or bubble).

In order to determine the weighted mean velocity of the vapour phase (or velocity of the centre of gravity of the vapour phase in plug flow) equation (3.19) was used and it was possible to determine this velocity up to 72% void fraction. For $\beta \geq 0.12$, one large plug was present in the test section, which drastically simplified equation (3.19).

3.2.2.2.2 Bubble Flow

For pressures of 12, 16 and 18 MN/m^2, numerous small bubbles of different sizes in a continuous liquid were visible on the developed films up to a steam quality of about 1%. This flow pattern, i.e., bubble flow,

is shown schematically in Fig. 3.11. Bubbles were observed at the vicinity of the wall of the coil between the inside and top position. When the mass velocity was decreased from 1450 kg/m^{2}s to 760 kg/m^{2}s at 16 MN/m^2, it was clearly seen that bubbles climbed towards the top of the coil. When the steam quality was increased, bubbles began to coalesce, and a wavy flow was then observed.

Since the number of bubbles was large on a film, the weighted mean velocity of the vapour phase for this flow regime was determined by a statistical method from the measured velocities of a sufficient number of bubbles taken randomly from the bubble population. For each test run, a sample of three to nine bubbles was taken from the bubble population and the velocity and diameter (or major and minor axes when they were elliptically shaped) of each bubble in the sample were measured at several axial positions (between 13 and 40 positions). Thus the number of velocities measured varied between 63 and 300 for each test run. Analysed bubble populations were selected such that a representative bubble sample could be taken from them. For this flow regime, it was possible to determine the weighted mean velocity of the vapour phase up to 8.2% void fraction, and this velocity was calculated from equation (3.20).

3.2.2.3 Determination of the Steam Quality

In order to determine $\bar{J}$ (see equations (3.14) and (3.36)), the steam quality has to be known. During the tests heat losses were compensated by installing trace heaters in the insulation material which covered the piping on the sodium side. Steam quality was therefore calculated from the heat balance for the whole test tube by a procedure similar to that given in Section 3.1.2.3. The steam quality was also determined using equation (3.28). The void fraction in this equation was evaluated from equation (3.29). The arithmetic average of the steam qualities calculated by the above described procedures was considered for further analysis. $\bar{J}$, calculated by the use of this average steam quality, deviated by at most 6% from the $\bar{J}$ calculated by using the steam quality from the heat balance (or from equation (3.28)). The reason why the above mentioned averaging procedure was used for the determination of the steam quality was that flow pattern instabilities were observed at 4 and 8.1 MN/m^2. These instabilities are discussed in Chapter 7. Although the determination of

the steam quality might include some errors, these errors were of not much significance in predicting $\bar{J}$, since the steam qualities were low and the pressures were high for the data presented here (see equation (3.14)).

3.2.2.4 Distribution Parameter

Having determined V_v and $\bar{X}$, the distribution parameter was obtained from equations (3.36) and (3.14). For $0.00018 \leq \beta < 0.4$, this parameter was correlated as a function of the vapour volumetric rate ratio and the Froude number, as shown in Fig. 3.12. The correlation is

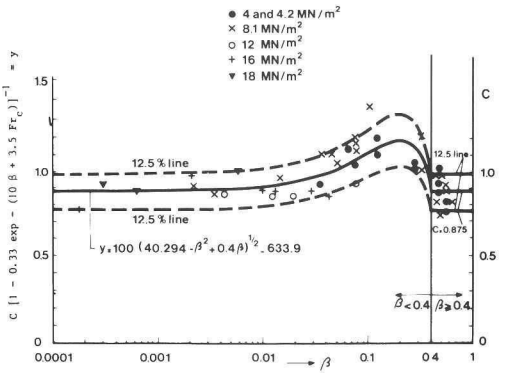

Fig. 3.12 Correlation of the data for the distribution parameter.

$$C = (100[40.294 - \beta^2 + 0.4\,\beta]^{1/2} - 633.9) \times (1 - 0.33 \exp - [10\,\beta + 3.5\,Fr_c]) \qquad (3.37)$$

For the data correlated, P = 4 - 18 MN/m^2 and G = 754 - 1518 kg/m^{2}s. The Froude number in equation (3.37) shows the ratio of centrifugal to gravity forces for the liquid phase. For $\beta < 0.4$, the centrifugal forces affect the phase distribution in the test tube and thereby the distribution parameter. For $\beta < 0.1$, the distribution parameter is found to be less than 1. It is reported in [A8, H2] that for the flow of air/water mixtures and for the diabatic flow of steam/water mixtures at elevated pressures in horizontal tubes the distribution parameter is less than 1 for $\beta < 0.3$.

For $0.4 \leq \beta \leq 0.579$, the distribution parameter is not affected by centrifugal forces, and is equal to 0.875, as shown in Fig. 3.12. For the data considered, P = 4.2 - 8.1 MN/m^2 and G = 429 - 1493 kg/m^{2}s.

The sharp transition in the value of the distribution parameter at $\beta \cong 0.4$ can not be explained satisfactorily since the experimental data for the radial void and volumetric flux density distributions in helical coils are not available at present (see equation (3.13)). It is anticipated that this phenomenon is related to the variation of flow pattern at $\beta \cong 0.4$.

For horizontal straight tubes, the Froude number on the RHS of equation (3.37) becomes zero since the coil diameter for a horizontal tube is infinite. In this case equation (3.37) predicted reasonably well the distribution parameter from the data of Haywood et al. [H2] taken in a horizontal tube for $P = 1.7 - 14.5$ MN/m^2 and $\beta < 0.40$. These data show a considerable scatter, however. For vertical tubes equation (3.37) is undefined since the coil diameter for a vertical tube equals zero.

Armand and Treshchev [A9] report the value of C as 0.98 and 0.95 for 4.2 and 8.1 MN/m^2 respectively for the diabatic flow of steam/water mixtures in horizontal tubes for $\beta = 0.3 - 0.9$. Analogous with the data for the flow of air/water mixtures, the distribution parameter for the flow of steam/water mixtures in helical coils is smaller than the distribution parameter for the flow of steam/water mixtures in horizontal tubes for $\beta > 0.4$. It has to be indicated here, however, that the void fraction data of Armand and Treshchev were obtained by an indirect method.

Chapter Four

INCIPIENT POINT OF BOILING AND INITIAL POINT OF NET VAPOUR GENERATION

4.1 INTRODUCTION

During subcooled nucleate flow boiling of a liquid in a channel there are two transition points along the channel. These are referred to as Incipient Point of Boiling (IPB) and Initial Point of Net Vapour Generation (IPNVG). The IPB is the point in the channel where the first bubble forms and gets detached from the heated surface. The IPNVG is the point in the channel where the activation of a significant number of nucleation centres takes place. At this point void fraction also rises suddenly (see Fig. 4.6). Before this point is reached, the void fraction is very low and the bubbles are attached to the heated wall at high subcoolings [G2]. The IPB and IPNVG are of importance not only for understanding boiling phenomena, but also for evaluating the void fraction [K7], instability conditions [S2] and heat transfer surfaces in steam generators.

The aim of this chapter of the thesis is to present experimental data for the IPB and IPNVG obtained in a vertical tube and two helically coiled tubes for water. The determination of these points was carried out with a high-speed photographic technique at medium and high pressures. The present data for the IPB and the experimental data for IPB for water from literature were correlated systematically. A correlation equation for the determination of the IPNVG for water and Refrigerant-22 was also given. A scaling law to predict the IPNVG for other liquids different from those mentioned above was established.

The IPB and IPNVG are closely related to the mechanism of heat transfer for the subcooled nucleate flow boiling. Therefore, before presenting the aforesaid data, a phenomenological heat transfer equation was established for this type of boiling [U12]. The dimensionless numbers which characterize the IPB and IPNVG were then derived from this equation. The equation is

$$q = Y_{41} \Delta T_{sat}^{Y_{42}} + h \Delta T_{sub} \qquad (4.1)$$

The first term on the RHS of equation (4.1) is the heat flux due to boiling and the second term is the heat flux due to suppressed forced convection.

Equation (4.1) is in fact a slightly modified version of the Rohsenow's superposition equation [R6]. Rohsenow used ΔT_{sat} instead of ΔT_{sub} in equation (4.1). Rohsenow's superposition equation, however, fails to describe heat transfer at the transition from subcooled nucleate flow boiling to fully developed boiling since at this transition the effect of liquid velocity on heat transfer should disappear and equation (4.1) should reduce to equation (4.2),

$$q = Y_{41} \Delta T_{sat}^{Y_{42}} \tag{4.2}$$

where Y_{41} is a constant for a given pressure and surface fluid combination and Y_{42} is a constant for a given fluid. It is well known that the heat transfer rate in fully developed boiling is not affected by fluid velocity and can be predicted from equation (4.2) (i.e., pool boiling equation) in accordance with the work of Borishanskii et al. [B10], Forster and Greif [F3], Kutateladze [K9] and Rohsenow [R5].

Subcooled nucleate flow boiling is a transition between the forced convection and the fully developed boiling regimes, and the heat transfer rate in this type of boiling consequently is affected by the forced convection and the boiling heat transfer modes. Therefore equation (4.1) was found convenient to describe the above type of heat transfer and to express the fact that liquid velocity has no influence on the heat transfer rate in fully developed boiling. Equation (4.1) was also verified with the experimental data of Bergles and Rohsenow [B8] using the forced convection heat transfer coefficient given by these investigators and the Y_{41} and Y_{42} values proposed by Rohsenow [R5]. (Y_{41} and Y_{42} are given by equations (5.7) and (5.8)). These data were obtained in a small diameter vertical tube for water at low pressures. Equation (4.1) was found to fit the data well [U12]. Only for a particular point in the subcooled nucleate flow boiling, i.e., for the IPB the results are shown in Fig. 4.1. Equation (4.1) predicts the wall superheat at the IPB very well. It is then concluded that equation (4.1) predicts the heat transfer rates well for the whole subcooled nucleate flow boiling region in a vertical tube of small diameter. The

wall superheat is of paramount importance for bubble dynamics. At high pressures the verification of equation (4.1) would not be adequate because the wall superheats reported in the literature for these pressures are very low. The procedure to determine the heat flux in accordance with equation (4.1) is shown in Fig. 4.2.

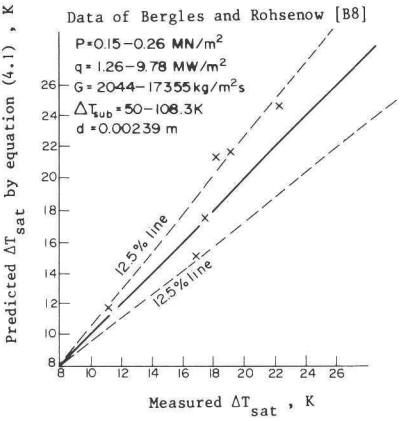

Fig. 4.1 Correlation of data of Bergles and Rohsenow [B8] for wall superheat.

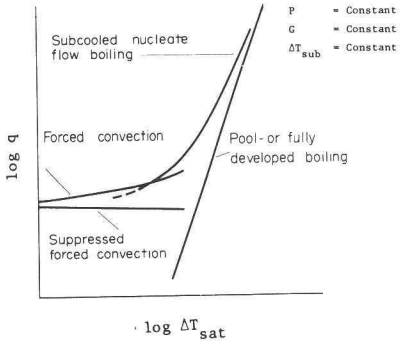

Fig. 4.2 Subcooled nucleate flow boiling curve.

When the heat flux calculated from the forced convection equation exceeds that given by equation (4.1), the latter is recommended to predict the heat flux in the subcooled nucleate flow boiling regime. The other procedures to draw the subcooled nucleate flow boiling curve are from Bergles and Rohsenow [B8], Forster and Greif [F3], Kutateladze [K9], McAdams et al. [M4] and Rohsenow [R6]. The procedure presented here is in fact a modification of the superposition method of the last mentioned author, as stated before.

The heat flux at the IPB (or IPNVG) is given by equation (4.1), i.e.,

$$q = \{Y_{41}\ \Delta T_{sat}^{Y_{42}} + h\ \Delta T_{sub}\}_{IPB\ (or\ IPNVG)} \qquad (4.3)$$

For a constant heat flux system, the following equation applies to fully developed boiling:

$$q_{IPB\ (or\ IPNVG)} = (Y_{41}\ \Delta T_{sat}^{Y_{42}})_F \qquad (4.4)$$

Equation (4.3) can be reduced to a non-dimensional form by the use of equation (4.4) for the IPB

$$\{\frac{h\ \Delta T_{sub}}{q}\}_{IPB} = \{1 - [\frac{(\Delta T_{sat})_{IPB}}{(\Delta T_{sat})_F}]^{Y_{42}}\} \qquad (4.5)$$

and for the IPNVG

$$\{\frac{h\ \Delta T_{sub}}{q}\}_{IPNVG} = \{1 - [\frac{(\Delta T_{sat})_{IPNVG}}{(\Delta T_{sat})_F}]^{Y_{42}}\} \qquad (4.6)$$

The dimensionless number on the LHS of equation (4.5) (or equation (4.6)) shows the ratio of the heat flux due to suppressed forced convection to the total heat flux and the dimensionless expression on the RHS of equation (4.5) (or equation (4.6)) the ratio of the heat flux due to boiling to the total heat flux. The IPB and IPNVG are transition points and heat transfer increases rapidly beyond these points. It is logical then to assume that the dimensionless numbers in equation (4.5) (or equation (4.6)) should characterize the transitions at the IPB and IPNVG. The verification of this with the experimental data is given in Section 4.2 for the IPB and in Section 4.3 for the IPNVG. For the above verification the dimensionless number on the LHS of equation (4.5) (or equation (4.6)) was used since this dimensionless number could be evaluated from the present data but not the dimensionless number on the RHS of equation (4.5) (or equation (4.6)).

4.2 THE IPB DURING THE SUBCOOLED NUCLEATE FLOW BOILING OF WATER IN VERTICAL AND HELICALLY COILED TUBES

4.2.1 Experimental Data

In TT1 (i.e., a vertical tube) and in TT5 and TT6 (i.e., helical coils) data for the IPB were obtained from the results of the tests

carried out to determine the distribution parameter. These tests are described in detail in Sections 3.1.2 and 3.2.2. For these tests the pictures of subcooled nucleate flow boiling were taken through the sapphire channels at constant pressure, heat flux and mass velocity, while subcooling was decreased slowly. When the first bubble was seen on a developed film, the conditions at which the film was taken were specified as those of the IPB, as given in Table 4.1. The above is an accurate and direct determination of the IPB. No direct method was reported for the experimental determination of the IPB in vertical tubes [B8, T1] and on a flat plate [T5] for water. No literature exists on data for the IPB in helical coils.

Table 4.1 Data for the IPB

	P	G	q	ΔT_{sub}	D_m
	MN/m^2	kg/m^2s	kW/m^2	K	mm
vertical tube	15.9	2134	391	7.3	0.225
	14.0	2167	336	6.9	0.255
	12.0	2208	326	5.9	0.300
	10.0	2040	138	2.6	0.313
	4.1	2189	128	2.9	0.210
helical coil	18.0	1460	390	12.5	-
	16.1	1458	323	12.0	-
	12.0	1471	263	11.8	-
	8.1	1516	226	11.7	-
	4.0	1518	148	7.3	-
	16.0	757	82	4.4	-

The heat flux at the IPB (i.e., at the end of the test tube) was calculated from the equation

$$q = (\theta_i - T_o)U \qquad (4.7)$$

where U, the overall coefficient of heat transfer, from the well-known heat exchanger formula for the last metre of the test tube for TT1 and for the last coil for TT5 and TT6. Equation (4.7) gives the peripheral average heat flux for a helical coil.

4.2.2 Correlation of the Data for the IPB for Water from Vertical Tubes and a Flat Plate

Experimental data for the IPB for water from vertical tubes are from Bergles and Rohsenow [B8] and Tarasova and Orlov [T1]. The first two investigators determined the IPB in a stainless steel circular tube of 2.39 mm ID at P = 0.15 and 0.26 MN/m^2 and the latter investigators in inner tube-, outer tube- and inner- and outer tube heated annuli at P = 4.9 - 19.6 MN/m^2. The annuli were constructed from stainless steel and nickel. Treshchev [T5] reported experimental data for the IPB obtained on a nickel flat plate for water at P = 0.5 - 5 MN/m^2. The experimental data of all the above mentioned investigators were produced with an indirect method and these investigators did only correlate their own data.

In order to correlate the aforesaid data and the present data given in Table 4.1, the value of the dimensionless number on the LHS of equation (4.5), i.e., the value of $(h\ \Delta T_{sub}/q)_{IPB}$ was calculated from these data and plotted versus pressure as shown in Fig. 4.3. The forced convection heat transfer coefficient, h, in the above dimensionless number was predicted from the well-known correlation $Nu_b = Y_{43} Re_b^{0.8} Pr_b^{0.4}$, in which Y_{43} is equal to 0.023 for circular tubes [K4], and to $0.015\ (d_2/d_1)^{0.25}$ for inner tube-, outer tube- and inner- and outer tube heated annuli [K10]. For a flat plate, the forced convection heat transfer coefficient was

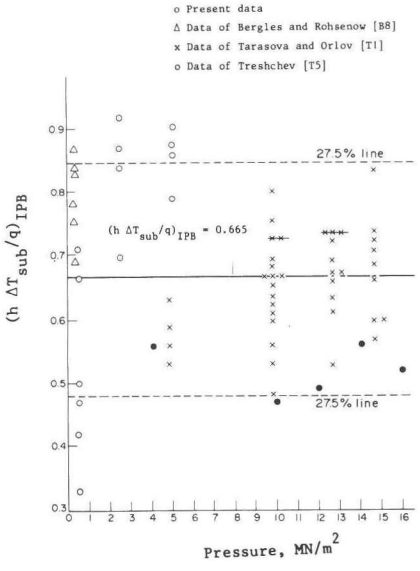

Fig. 4.3 Correlation of the IPB data from vertical tubes and a flat plate.

calculated from the formula $Nu = 0.0366\ Re^{0.8} Pr^{1/3}$, in which the fluid properties have to be determined at the temperature given below [K4].

$$T = T_b - \frac{0.1\ Pr + 40}{Pr + 72}\ (T_b - T_h) \tag{4.8}$$

As for the data of Bergles and Rohsenow [B8], the forced convection heat transfer coefficient given in their paper was used. It follows from Fig. 4.3

$$\left\{\frac{h\ \Delta T_{sub}}{q}\right\}_{IPB} = 0.665 \tag{4.9}$$

regardless of channel geometry and operating conditions. The range of operating conditions for the data considered to establish equation (4.9) is as follows: P = 0.15 - 19.6 MN/m^2; G = 470 - 17355 kg/m^2s; q = 0.13 - 9.8 MW/m^2; ΔT_{sub} = 2.6 - 108 K; d = 2.13 - 32 mm. The number of data considered was 68. The data of Tarasova and Orlov [T1] taken at P = 19.6 MN/m^2 are not shown in Fig. 4.3. These data fit the equation (4.9) well, i.e., within 10% accuracy.

As can be seen from Fig. 4.3, all the present data fall below the correlation line, y = 0.665. This is due to an indirect method used for the experimental determination of the IPB in [B8, T1, T5]. For the sake of illustration of this, the method of Tarasova and Orlov is mentioned briefly: These investigators assumed that the subcooled nucleate flow boiling begins at the point along a channel beyond which the wall surface temperature remains constant. In accordance with the recent tests of Abdelmessih et al. [A1], there is an abrupt drop in temperature from the inception of boiling to fully developed nucleate boiling. For these tests this temperature drop was of considerable magnitude. It follows from the above that the point specified as the IPB by Tarasova and Orlov is not the IPB but most probably a point before the IPB. Fig. 4.3 reveals also this fact. Nevertheless, at the present state of art, the experimental data of [B8, T1, T5] and the equation (4.9) are considered to be fairly adequate.

4.2.3 Correlation of the Data for the IPB for Water from Helical Coils

The experimental data for the IPB obtained in TT5 and TT6 (see Table 4.1) were correlated using the local values of operating conditions. Heat flux, heat transfer coefficient and temperature vary along the periphery of a helical coil. For an extensive range of conditions and for some of the present tests, the peripheral local values of the aforesaid quantities were also determined at the last 10.7 m of the heated part of the helically coiled test tubes (i.e., TT6 and TT5). This was done using the values of two temperatures measured in the wall of the test tube at known radial positions at the inside, top, outside and bottom of the test tube and using Fourier's law of conduction and Newton's law of cooling. At the inside of the coil the wall temperature is highest, and consequently the IPB and IPNVG have to be located there. Using the local operating conditions at this location, the IPB data were correlated by

$$[(h/q)_I \ \Delta T_{sub}]_{IPB} = 0.445 \qquad (4.10)$$

The data are compared with equation (4.10) in Fig. 4.4. This equation fits the data well.

$(h/q)_I$ in equation (4.10) was calculated from the following correlation established using our experimental data and the experimental data given in [S4]:

$$(h_{pa}/q_{pa}) \ / \ (h/q)_I = 3.12 \ (d/d_c)^{0.17} \qquad (4.11)$$

for Re = 11800 - 439000 and d_c/d = 17 - 104.

The results of the comparison of the equation (4.10) with the data obtained in TT1 (i.e., a vertical tube; see Table 4.1) are also shown in Fig. 4.4. All these data are below the correlation line. It follows from equation (4.10) and Fig. 4.4 that the IPB is retarded in a helical coil. This is a logical result. In the wall of a helically coiled steam generator tube, heat is conducted circumferentially and an initial superheat is necessary for the formation of the first bubble [A1]. In the wall of a vertical steam generator tube, however, circumferential heat conduction does not take place.

A design engineer deals, in general, with the average operating conditions in a helical coil. Therefore, for practical applications, the IPB data obtained in TT5 and TT6 were also correlated using the

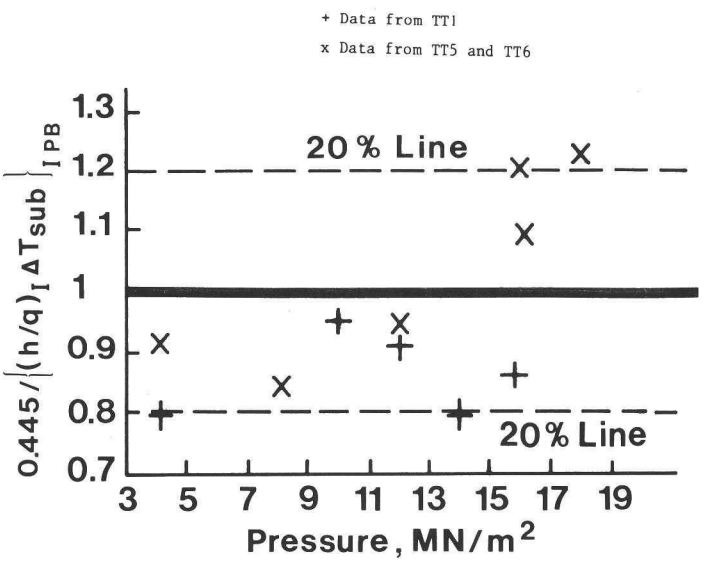

Fig. 4.4 Correlation of the IPB data from TT5 and TT6 using local values of the operating conditions.

average values of the operating conditions, as given below:

$$(h_{pa}\ \Delta T_{sub} Pr_b^{0.78}/q_{pa})_{IPB} = 0.762 \qquad (4.12)$$

h_{pa}, the peripheral average heat transfer coefficient for single phase flow in equation (4.12), was evaluated from the correlation given in [P3].

$$Nu_b = 0.0225\ Re_b^{0.8} Pr_b^{0.4}\ (1 + 3.4\ d/d_c) \qquad (4.13)$$

This correlation fitted our heat transfer data well.

Equation (4.12) is compared with the data for the IPB in Fig. 4.5. This equation fits the data very well.

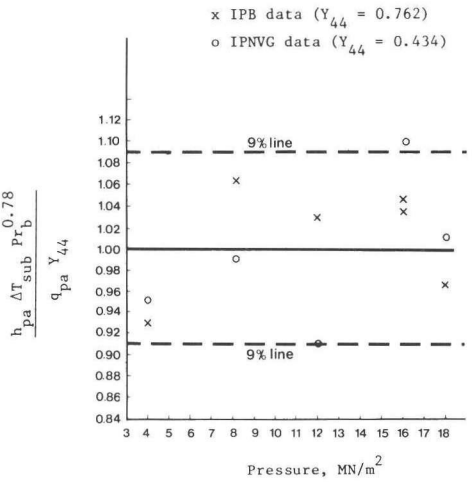

Fig. 4.5 Correlation of the IPB and IPNVG data from TT5 and TT6 using average values of the operating conditions.

4.3 THE IPNVG DURING THE SUBCOOLED NUCLEATE FLOW BOILING OF LIQUIDS IN VERTICAL AND HELICALLY COILED TUBES

4.3.1 Experimental Data

In TT1 (i.e., a vertical tube) and in TT5 and TT6 (i.e., helical coils), the data for the IPNVG were obtained from the results of the tests carried out to determine the distribution parameter. (See Sections 3.1.2 and 3.2.2). For these tests the pictures of subcooled nucleate flow boiling were taken through the sapphire channels at constant pressure, heat flux and mass velocity while subcooling was decreased slowly.

For the determination of the IPNVG in TT1 the following procedure was used. Per definition, void fraction increases sharply at the IPNVG. Therefore, the number of bubbles appearing on the developed films was counted for different subcoolings at a constant heat flux, pressure and mass velocity. When the number of bubbles was found to increase suddenly, the conditions at which the film was taken were specified as those of the IPNVG, as given in Table 4.2. For instance there were about 30 bubbles on the film at ΔT_{sub} = 5.9 K, q = 0.38 MW/m^2, P = 13.9 MN/m^2 and G = 2121 kg/m^{2}s. When the subcooling was decreased to 4.3 K, with heat flux, pressure and

Table 4.2 Data for the IPNVG

	No.	P MN/m^2	G kg/m^2s	ΔT_{sub} K	q_{pa} MW/m^2
vertical tube	1	13.9	2121	4.3	0.380
	2	15.8	2121	4.1	0.450
	3	17.8	2184	3.7	0.515
	4	12.0	2139	3.0	0.331
	5	10.0	2025	1.6	0.137
	6	4.1	2203	1.2	0.128
helical coil	7	18.0	1454	7.3	0.413
	8	16.1	1435	7.3	0.350
	9	12.0	1470	6.2	0.289
	10	8.1	1499	6.4	0.236
	11	4.0	1517	4.5	0.157

mass velocity kept constant, the number of bubbles on the film was 170. Therefore the conditions at which the film was taken were specified as those of the IPNVG. When the subcooling was decreased further, the number of bubbles increased sharply. Before the IPNVG was reached, for the case of very small numbers of bubbles present in the test section (say, about 30), not all the bubbles were attached to the wall of the test section, but some were already in the bulk of the water.

In order to determine the IPNVG in TT5 and TT6, the volume of all the bubbles on a developed film was measured and plotted versus subcooling, as shown in Fig. 4.6 for 16 MN/m^2 for example. The best fitting curve was drawn through the experimental points. The interception of the tangent drawn to this curve with the subcooling axis gave the subcooling at the IPNVG, as illustrated in Fig. 4.6. The experimental data for the IPNVG from TT5 and

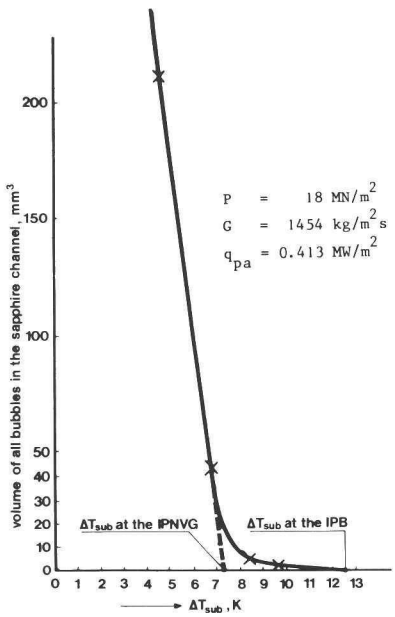

Fig. 4.6 Determination of the IPNVG.

TT6 are summarized in Table 4.2.

The heat flux at the IPNVG was calculated from equation (4.7).

4.3.2 Correlation of the Data

The existing correlations for the prediction of the IPNVG are from Griffith et al. [G1], Bowring [B13], Rouhani [R9, R10], Levy [L6] and Staub [S12]. The last two workers have extensively investigated the IPNVG, and each of them has given a semi-empirical correlation to evaluate the subcooling at this point, considering a force balance on a departing bubble from the heated surface and the temperature and velocity profiles in a channel. These workers assumed that the IPNVG is situated there where the first bubble departs from the heated surface. As observed visually in this study, the above assumption is not correct at least for low subcoolings. Recently there appeared two more correlations. One of them does not fit the experimental data obtained in annuli well [S1, S5]. The other one was derived from a theoretical analysis [S5]. This correlation predicts the subcooling at the IPNVG for water reasonably well (i.e., within 30% accuracy) but it is not suitable for other liquids than water.

Since the correlations presented in the literature are either applicable to a limited range of conditions or cumbersome to use in practical calculations, the available experimental data for the IPNVG for water and Refrigerant-22 from literature and the present data were correlated. For this purpose the experimental data of Egen et al. [E2]; Maurer [M2], as reported by Bowring [B13]; Ferrell [F2]; Rouhani [R7], as reported by Levy [L6]; Cook [C5] as reported by Kroeger and Zuber [K7]; Evangelisti and Lupoli [E3], and Staub et al. [S14] were considered. The ranges of operating conditions and geometries for these data are summarized in Table 4.3. Six water tests of Staub et al. [S14] were conducted with small amounts of additives.

For the correlation of the data for the IPNVG, the following procedure was used. First the value of the dimensionless number on the LHS of equation (4.6) was calculated from the aforesaid data and from the present data obtained during the early stage of the tests (i.e., the data numbered as 1 and 2 in Table 4.2). The forced convection heat transfer coefficient in this dimensionless number was evaluated from the well-known correlation, $Nu_b = Y_{45} Re_b^{0.8}$ in which Y_{45} is equal to $0.023\ Pr_b^{0.4}$ for circular and

rectangular tubes and to 0.020 $(d_2/d_1)^{0.53}$ $Pr_b^{0.333}$ for annuli [K4].

Table 4.3 Range of Data for the IPNVG from Literature

Parameter	Water	Refrigerant-22
Geometry	Circular tubes, rectangular channels, annuli	Circular tube
Pressure, MN/m^2	0.1 - 13.7	1.2 - 3.3
Mass velocity, kg/m^2s	132 - 2818	180 - 1391
Hydraulic diameter, mm	4.1 - 19.8	10.2
Subcooling at the IPNVG, K	3.7 - 42	3.2 - 7.3
Heat flux at the IPNVG, MW/m^2	0.15 - 1.92	0.02 - 0.06
Number of data	73	13

Analysis of the calculated dimensionless numbers yielded the following results.

For a given liquid, regardless of channel geometry, pressure, heat flux, subcooling and mass velocity, there are two velocity regions in which

$$\left\{\frac{h\ \Delta T_{sub}}{q}\right\}_{IPNVG} = Y_{46} = \text{constant} \qquad (4.14)$$

These two velocity regions are sharply separated by a given value of velocity, u = 0.45 m/s. This velocity is connected to bubble growth and is close to the velocity at which condensation due to forced convection ceases to affect the bubble growth rate in subcooled nucleate flow boiling, as shown experimentally by Snyder and Robin [S9] and semi-theoretically in the next chapter of this thesis.

For water, $Y_{46} = 0.24$ for $u \geq 0.45$ m/s and $Y_{46} = 0.11$ for $u < 0.45$ m/s.

For Refrigerant-22, $Y_{46} = 0.18$ for $u \geq 0.45$ m/s and $Y_{46} = 0.11$ for $u < 0.45$ m/s.

Since the forced convection effect due to condensation disappears for $u < 0.45$ m/s, the value of the dimensionless number given by equation (4.14) should differ for the aforesaid two velocity regions. This is due to the fact that this dimensionless number accounts for the ratio of the heat flux due to forced convection to the total heat flux. The expression, $Y_{46}/(h\ \Delta T_{sub}/q)_{IPNVG}$, is shown versus reduced pressure in Fig. 4.7.

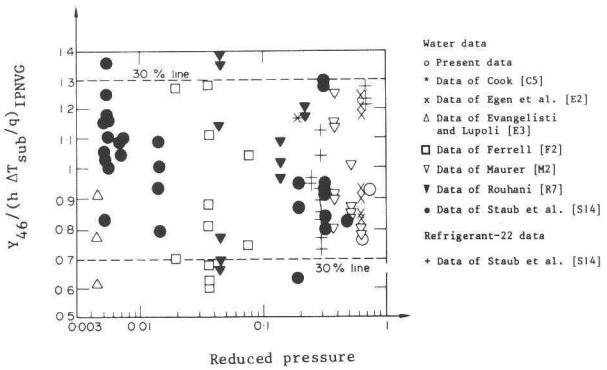

Fig. 4.7 Correlation of the IPNVG data.

Correlation of the data appears quite feasible, taking into account that the experimental determination of ΔT_{sub} may involve some errors, and that there are some inconsistencies in the test results, as indicated by Levy [L6]. For instance the data of Egen et al. [E2] and Ferrell [F2] show that an increase in mass velocity at constant heat flux and pressure increases subcooling at the IPNVG. The data of Evangelisti and Lupoli [E3], Maurer [M2], Rouhani [R7] and Staub et al. [S14] show the reverse trend, however.

For all the data correlated, the RMS error was 19%, and it appears that nearly all the correlated data are within a 30% error band, with the exception of a few low pressure data, as shown in Fig. 4.7. The results of the correlation given by equation (4.14) were also compared with the results of the correlations of Bowring [B13] and of Levy [L6] with the aid of the experimental data of Evangelisti and Lupoli [E3] and with the experimental data used by these workers to establish their correlations. Equation (4.14) correlated the data better than the correlations of Levy and Bowring by 24% and 56% respectively. These percentages were based on the RMS error.

With two exceptions, the data given in Table 4.2 from TT1, TT5 and TT6 (i.e., from a vertical tube and two helically coiled tubes) were not used to establish equation (4.14). The results of the comparison of this equation with these data are given in Fig. 4.8. Equation (4.14) fits the data well.

For the data obtained in the helically coiled test tubes the values of the local operating conditions at the inside of the tube were used to

evaluate the LHS of equation (4.14). These operating conditions were determined with the procedure given in Section 4.2.3.

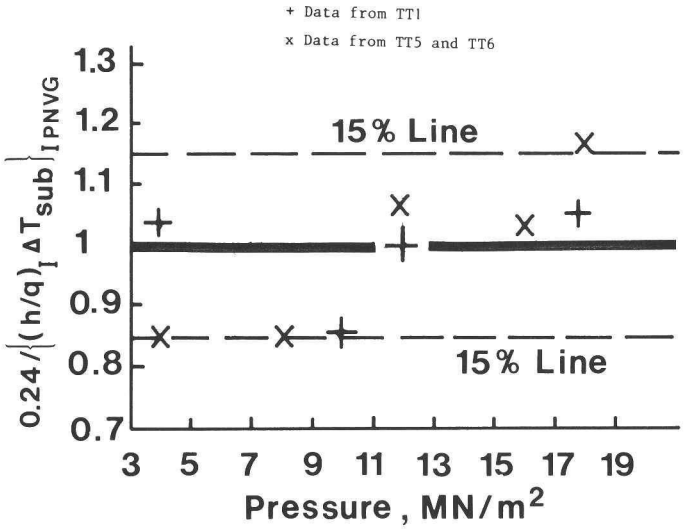

Fig. 4.8 Comparison of equation (4.14) with the data for the IPNVG given in Table 4.2.

The ranges of the geometries, operating conditions and fluids for the experimental data used to derive equation (4.14) are summarized as follows: Geometry: vertical circular and rectangular tubes, vertical annuli and helical coils; d = 4.1 - 19.8 mm; d_c/d = 38.9; P = 0.1 - 18.0 MN/m^2; G = 132 - 2818 kg/m^{2}s; ΔT_{sub} = 1.2 - 42 K; q = 0.02 - 1.92 MW/m^2; type of fluid: water and Refrigerant-22. The number of data considered was 97.

Equation (4.14) was derived from equation (4.1), a phenomenological heat transfer equation for subcooled nucleate flow boiling. This probably indicates that the above phenomenological heat transfer equation applies to both vertical tubes and helical coils after the activation of a significant number of nucleation centres (i.e., after the IPNVG), provided that the local operating conditions are considered in the helical coils.

Using the average values of the operating conditions, the data for the IPNVG from TT5 and TT6 were also correlated. For this purpose, the constant on the RHS of equation (4.12) was taken equal to 0.434. The results are shown in Fig. 4.5. The agreement of the data with the correlation is very good.

In order to predict the subcooling at the IPB and IPNVG for a given channel and known operating conditions by the use of the present correlations, it is clear that an iterative method has to be used since the RHS's of the correlations are equal to the numerical constants and the LHS's of the correlations depend on temperature and pressure.

4.3.3 A Scaling Law for the IPNVG

When the pool boiling curve of a liquid is known, the IPNVG for this liquid can be determined. This will now be shown.

For water Y_{42} in equation (4.2) is reported to be $Y_{42} = 3$ by Rohsenow [R5] and Borishanskii et al. [B10]. For the pool boiling of Refrigerant-22, Ratiani and Avaliani [R1] report $Y_{42} = 3$, based on rather limited data. For fully developed boiling of this liquid Y_{42} can be taken equal to approximately $Y_{42} = 2.65$, as suggested by Zuber et al. [Z4], based on fairly extensive data; therefore this Y_{42}-value was considered here.

Using $Y_{42} = 3$ for water and $Y_{42} = 2.65$ for Refrigerant-22 and the expression given by equation (4.14), the dimensionless number on the RHS of equation (4.6) was calculated for both water and Refrigerant-22.

$$\left\{\frac{(\Delta T_{sat})_{IPNVG}}{(\Delta T_{sat})_F}\right\}_w \cong \left\{\frac{(\Delta T_{sat})_{IPNVG}}{(\Delta T_{sat})_F}\right\}_{R\text{-}22} \cong 0.92 \text{ for } u \geq 0.45 \text{ m/s} \quad (4.15)$$

$$\left\{\frac{(\Delta T_{sat})_{IPNVG}}{(\Delta T_{sat})_F}\right\}_w \cong \left\{\frac{(\Delta T_{sat})_{IPNVG}}{(\Delta T_{sat})_F}\right\}_{R\text{-}22} \cong 0.96 \text{ for } u < 0.45 \text{ m/s} \quad (4.16)$$

It follows from equations (4.15) and (4.16) that the dimensionless number on the RHS of equation (4.6), $(\Delta T_{sat})_{IPNVG}/(\Delta T_{sat})_F$, is a constant depending only on one particular value of velocity, u = 0.45 m/s, regardless of the type of liquid, channel geometry and operating conditions in a channel. The constant on the RHS of equation (4.14) can therefore be predicted for any liquid using the RHS of equation (4.6) and equation (4.15) if $u \geq 0.45$ m/s (or equation (4.16) if $u < 0.45$ m/s), provided that the pool boiling or fully developed boiling equation of the liquid is known.

Chapter Five

BUBBLE DYNAMICS DURING THE SUBCOOLED NUCLEATE FLOW BOILING OF WATER

5.1 INTRODUCTION

Determination of bubble growth rate, maximum bubble diameter and maximum bubble growth time for the subcooled nucleate flow boiling of water is of interest for a basic understanding of the phenomenon of subcooled boiling. The maximum bubble diameter and maximum bubble growth time are closely related to void fraction and heat transfer rate [T3]. So far no predictive equations of broad generality for bubble dynamics during the subcooled nucleate flow boiling of water have appeared in literature, although experimental data have been presented by Griffith et al. [G1], Gunther [G2], Tolubinsky and Kostanchuk [T3] and Treshchev [T5]. S.J.D. van Stralen from Technological University of Eindhoven has extensively studied bubble dynamics, however, mostly for superheated binary mixtures. Therefore his work is not mentioned here.

The aim of this chapter of the thesis is to present experimental data for the maximum bubble diameter obtained with the aid of a high-speed photographic technique at medium and high pressures during the subcooled nucleate flow boiling of water. For this type of boiling, a heat transfer controlled bubble model was also established to derive a correlation for the maximum bubble diameter, maximum bubble growth time and bubble growth rate.

The model was based on the assumption that a spherical or an ellipsoidal bubble grows on a very thin, partially dried liquid film which is formed between the bubble and the heated surface. During growth, the bubble was assumed to take up heat by the evaporation of the very thin liquid film while it dissipates heat by condensation to the surrounding liquid at its upper half. Since difficulties were anticipated with a closed form solution of the multi-dimensional formulation, a spatially lumped formulation of the model was used.

The data obtained and the experimental data for the maximum bubble diameter, maximum bubble growth time and bubble growth rate from literature were in good agreement with the results of the established model.

Experimental data and a correlation are also presented for the drag

coefficient for the motion of a bubble or plug in a turbulent water stream.

5.2 MAXIMUM BUBBLE DIAMETER, MAXIMUM BUBBLE GROWTH TIME AND BUBBLE GROWTH RATE

5.2.1 Experimental Data

The experimental data for the maximum bubble diameter were obtained from the results of tests carried out to determine the distribution parameter in TT1. These tests are described in detail in Section 3.1.2.

The maximum bubble diameter at the IPB and the maximum bubble diameter beyond the IPB were measured. The latter is in fact the maximum diameter of the average bubble of a bubble population consisting of numerous bubbles. The reason why a distinction was made between these two maximum bubble diameters is due to the following fact. At the IPB a single bubble or a few bubbles exist and the growth of a bubble is thus not affected by liquid agitation caused by movement of the numerous bubbles, contrary to the growth of a bubble in a bubble population.

In subcooled nucleate flow boiling numerous bubbles are produced beyond the IPB and these bubbles have different diameters. Therefore, in order to determine the maximum bubble diameter beyond the IPB, the photographs obtained from the developed films were enlarged up to 18 times and the diameters of bubbles appearing on the photographs were measured. The films dealt with were taken at high pressures, i.e., $P = 13.9 - 17.7$ MN/m^2. This is probably the reason why the bubbles on the photographs were mostly spherically shaped. For every photograph analysed the measured bubble diameters were averaged by weighting them with the number of bubbles. This average value was then considered as the maximum bubble diameter in accordance with the definition given in paragraph (j) of Section 5.2.2.1 and tabulated in Table 5.1. The bubble diameters were also measured at several axial locations along the photographical test section. These diameters were approximately constant. The heat flux given in Table 5.1 was calculated from equation (4.7). The bubble population varied per photograph between 65 and 450. The distribution of the measured bubble diameters approximated a normal distribution, thus making the averaging procedure easier.

At the IPB, two or three bubbles were visible on a developed film

Table 5.1 Data for the Maximum Bubble Diameter Beyond the IPB

P	ΔT_{sub}	u	q	D_m
MN/m^2	K	m/s	MW/m^2	mm
13.9	3.7	3.27	0.38	0.15
13.9	4.3	3.27	0.39	0.14
13.9	3.7	3.27	0.42	0.18
13.9	5.9	3.27	0.39	0.11
15.8	4.1	3.57	0.45	0.15
15.8	4.1	3.57	0.45	0.13
17.7	3	3.75	0.55	0.13

and they were either spherically or elliptically shaped. The films dealt with were taken at medium and high pressures, i.e., P = 4.1 - 15.9 MN/m^2. Bubble diameters were measured on a developed film with a Boscar motion analyzer and averaged over the number of bubbles on the film. This average value was then considered as the maximum bubble diameter and tabulated in Table 4.1. When a bubble was elliptically shaped, the bubble diameter was determined by averaging the measured major and minor axes of the bubble. The heat flux at the IPB was calculated from equation (4.7).

Examination of Tables 4.1 and 5.1 yields the conclusion that for practically the same operating conditions the maximum bubble diameter at the IPB is considerably bigger than the maximum bubble diameter of the average bubble of a bubble population. This is probably due to the fact that bubble growing at the IPB will not dissipate heat due to liquid agitation caused by movement of the numerous bubbles, contrary to the growth of a bubble in a bubble population, thus heat available will be used for the growth of the bubble.

5.2.2 A Bubble Model for the Subcooled Nucleate Flow Boiling

5.2.2.1 Assumptions

In order to derive a correlation for maximum bubble diameter, maximum bubble growth time and bubble growth rate during the subcooled nucleate flow boiling of water, a bubble model was established using the following assumptions.

a. For a given geometry and constant operating conditions (i.e., constant subcooling, velocity, heat flux and pressure) the numerous bubbles produced in the subcooled nucleate flow boiling beyond the IPB have different maximum diameters and growth times. A statistical approach is therefore required, and these quantities have to be calculated by averaging them for the whole bubble population. This statistical approach was first suggested by Gunther [G2] and was used later by Tolubinsky and Kostanchuk [T3] and Treshchev [T5]. The terms "maximum bubble diameter" and "maximum bubble growth time" used here refer to average values for the whole bubble population. At the IPB, there exists a single bubble or a few bubbles. Therefore, for these bubbles, the averaging procedures are drastically simplified.

b. A spherical or an ellipsoidal bubble grows on a very thin partially dried liquid film which is formed between the bubble and the heated surface, as schematized in Fig. 5.1. The formation of a thin liquid

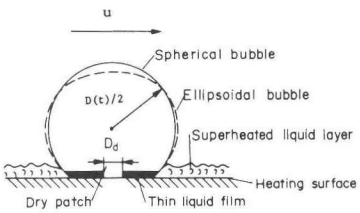

Fig 5.1 Schematic bubble description.

film between the bubble and the heating surface was first postulated by Snyder [S9]. Later this postulate was verified experimentally by Torikai et al. [T4], Cooper [C6], Cooper and Lloyd [C7] and Van Ouwerkerk [O2]. The evidence for the existence of a dry area in the thin liquid film on the heating surface was presented for atmospheric pressure conditions by Torikai et al. [T4] and Van Ouwerkerk [O2].

c. The instantaneous bubble volume is equal to the volume of a sphere of diameter D(t).

d. The dry area under the bubble is of a circular shape, as experimentally verified by Torikai et al. [T4].

e. During its growth, the bubble takes up heat by the evaporation of the very thin liquid film over the area

$\pi\ (D_p(t))^2(1 - D_d^2/(D_p(t))^2)/4$, in which $D_d/D_p(t)$ is assumed to be a constant for a given pressure in accordance with the experimental data of Torikai et al. [T4]. Here $D_p(t)$ is the diameter of the total contact part of the bubble with the heating surface. Assuming that the bubble remains semi-spherical or semi-ellipsoidal during most of its growth period, $D_p(t)$ in the above expression was replaced by the bubble diameter D(t).

f. Inertia controlled bubble growth is neglected since its duration is very short, as experimentally determined by Sernas and Hooper [S6].

g. Bubble growth within the superheated liquid layer is neglected since the ratio of the maximum bubble diameter to the thickness of this layer varies between 11 and 25 at atmospheric pressure conditions [U13]. This also justifies the assumption that the heat input to the bubble from the superheated layer can be neglected in comparison with the heat from the thin liquid film since $D_d/D(t)$ is anticipated not to be large.

h. The bubble loses heat to the surrounding liquid by condensation at its upper-half surface. In subcooled nucleate flow boiling numerous bubbles cover the heating surface. The bottom-half of the bubble therefore will probably not face the cold liquid stream, thus being ineffective in losing heat from the bubble. Abdelmessih et al. [A2] also report that a bubble forming at the IPB loses heat at its top.

i. Bubble growth is an isobaric process.

j. In subcooled nucleate flow boiling, there are two types of bubbles in so far the departure from the heated surface is concerned. The bubbles formed at high subcoolings do not leave the heated surface, although they attain their maximum diameter. They slide along the heated surface or collapse, as observed visually by Gunther [G2]. The bubbles formed at medium or low subcoolings leave the heating surface upon reaching their maximum diameters. The condition for departure from the heated surface can thus be expressed as $dD(t)/dt = 0$. The work reported therefore covers the above two types of bubbles.

k. The very thin liquid layer under the bubble is fed continuously by the liquid surrounding the bubble.

l. A spatially lumped formulation of the model is considered.

The above assumptions will lead a simple bubble model. This can be justified, however, as quoted from Dwyer [D8]:

"Forced-convection boiling is a complicated process, and it is impossible to write the usual differential equations of motion and energy for realistic models, and establish the appropriate boundary conditions. For this reason, all theoretical equations which have been proposed are based on mechanistic postulates, rather than rigorous mathematical analysis".

Even the models proposed for one-phase flow include sometimes unrealistic assumptions. In order to illustrate this, the well-known model of Lyon [K4] established to derive heat transfer coefficient and friction factor for one-phase flow using the analogy between momentum and heat transfer can be mentioned. The model predicts heat transfer coefficients very well, especially for liquid metals. However, the assumptions used to established the model imply that the model applies only to the limiting case of no heat transfer [K4].

5.2.2.2 Mathematical Formulation of the Model and Solution

Using the above given assumptions, the energy balance for the bubble yields

$$q_h \frac{\pi (D(t))^2}{4} \{1 - \frac{D_d^2}{(D(t))^2}\} = h_c \Delta T_{sub} \frac{\pi (D(t))^2}{2} + \frac{\pi}{6} \rho_v \lambda \frac{d(D(t))^3}{dt} \quad (5.1)$$

with the initial condition

$$t = 0 \qquad D(t) = 0 \quad (5.2)$$

The unknowns in equation (5.1) are, q_h, the heat flux to the bubble from the very thin liquid film under it, h_c, the heat transfer coefficient for the loss of heat from the bubble to the surrounding liquid and $D_d/D(t)$, the ratio of the diameter of the dry area under the bubble to the bubble diameter.

q_h, the heat flux to the bubble from the very thin liquid film under it, is given by Sernas and Hooper [S6] as follows:

$$q_h = \frac{\overline{\Delta T}_{sat}\ Y_{51}\ k_l}{(\pi\ Y_{52}\ t)^{\frac{1}{2}}} \tag{5.3}$$

where

$$Y_{51} = \left\{\frac{(k\ \rho\ c)_h}{(k\ \rho\ c)_l}\right\}^{\frac{1}{2}} \tag{5.4}$$

$$Y_{52} = \left\{\frac{k}{\rho\ c}\right\}_l \tag{5.5}$$

$\overline{\Delta T}_{sat}$ in equation (5.3), the initial superheat of the very thin liquid layer under the bubble, is estimated from the equation (4.1), the phenomenological heat transfer equation established in the preceding chapter,

$$\overline{\Delta T}_{sat} = \left\{\frac{q_h - h\ \Delta T_{sub}}{Y_{41}}\right\}^{(1/Y_{42})} \tag{5.6}$$

where

$$Y_{41} = \frac{\lambda\ \mu_l \left\{\frac{c}{0.013\ \lambda\ Pr^{1.7}}\right\}^3_l}{[\sigma/(\rho_l - \rho_v)g]^{\frac{1}{2}}} \tag{5.7}$$

$$Y_{42} = 3 \tag{5.8}$$

and h, the single phase forced convection heat transfer coefficient, follows from the well-known relation $Nu_b Re_b^{-0.8} Pr_b^{-1/3}$ = constant, where the constant equals 0.0366 for flat plates and 0.023 for circular tubes. The above relation in fact differs slightly from that given in [K4]. (See also Section 4.2.2 for the correct form of the relation). However, this difference is of no practical importance for the conditions considered in this study.

h_c in equation (5.1), the heat transfer coefficient for the loss of heat from the bubble to the surrounding liquid, is derived in Appendix 1 with a method analogous to that given by Levenspiel [L5], and is equal to

$$h_c = \frac{Y_{53}\ Y_{54}\ \lambda\ D(t)}{2(1/\rho_v - 1/\rho_l)} \tag{5.9}$$

where

$$Y_{53} = \left(\frac{u}{u_o}\right)^{0.47} \quad \text{for } u > 0.61 \text{ m/s} \tag{5.10}$$

$$Y_{53} = 1 \quad \text{for } u \leq 0.61 \text{ m/s} \tag{5.11}$$

$$u_o = 0.61 \text{ m/s} \tag{5.12}$$

Y_{54} in equation (5.9) is a function of fluid properties at the state of saturation, that is, a pressure dependent constant, and is equal to 61 $(Ks)^{-1}$ at 0.17 MN/m^2 for the average bubble of a bubble population consisting of numerous bubbles, as given in Appendix 1. It follows also from this appendix that the value of Y_{54} for the average bubble of a bubble population should differ from that for a bubble forming at the IPB.

Substituting equations (5.3) and (5.9) into equation (5.1) and differentiating the second term on its RHS yields

$$\frac{dD(t)}{dt} = Y_{55}\, Y_{56}\, t^{-\frac{1}{2}} - Y_{53}\, Y_{54}\, Y_{57}\, D(t) \tag{5.13}$$

where

$$Y_{55} = \frac{(q_h - h\, \Delta T_{sub})^{1/3}\, k_1\, Y_{51}}{2\, Y_{41}^{1/3}\, \rho_v\, \lambda(\pi\, Y_{52})^{\frac{1}{2}}} \tag{5.14}$$

$$Y_{56} = \{1 - D_d^2/(D(t))^2\} \tag{5.15}$$

$$Y_{57} = \frac{\Delta T_{sub}}{2(1 - \rho_v/\rho_1)} \tag{5.16}$$

The solution of equation (5.13) which is presented below gives the bubble diameter as a function of time or bubble growth.

Equation (5.13) is a linear first order differential equation, and its solution may be written straightforwardly if it is considered that Y_{53}, Y_{54}, Y_{55}, Y_{56} and Y_{57} in the equation are not time dependent.

$$D(t) = e^{-Y_{58}t}\left[Y_{55}\, Y_{56} \int t^{-\frac{1}{2}}\, e^{Y_{58}t}\, dt + Y_{59}\right] \tag{5.17}$$

where

$$Y_{58} = Y_{53}\ Y_{54}\ Y_{57} \tag{5.18}$$

$e^{Y_{58}t}$ and $e^{-Y_{58}t}$ may be replaced by their identities given in series.

$$D(t) = \frac{Y_{55}\ Y_{56}[\int[t^{-\frac{1}{2}}\ (1 + Y_{58}\ t + Y_{58}^2\ t^2/2! + Y_{58}^3\ t^3/3! + \ldots)]\ dt] + Y_{59}}{(1 + Y_{58}\ t + Y_{58}^2\ t^2/2! + Y_{58}^3\ t^3/3! + \ldots\ldots)} \tag{5.19}$$

After integration of the nominator, equation (5.19) becomes

$$D(t) = \frac{2\ Y_{55}\ Y_{56}\ t^{\frac{1}{2}}\ (1 + Y_{58}\ t/3 + Y_{58}^2\ t^2/10 + \ldots\ldots) + Y_{59}}{(1 + Y_{58}\ t + Y_{58}^2\ t^2/2! + \ldots\ldots)} \tag{5.20}$$

By the use of the initial condition, i.e., $D(t) = 0$ for $t = 0$, Y_{59}, the integration constant in equation (5.20), is found to be equal to zero. Experimental data of Gunther [G2] and Tolubinsky and Kostanchuk [T3] show that $Y_{58}\ t_m < 1$ at 0.1 MN/m^2. (In the calculation of $Y_{58}\ t_m$, the value of Y_{54} (see equation (5.18)) determined for 0.17 MN/m^2 is used, since Y_{54} is only a function of the fluid properties at the state of saturation and its value at 0.1 MN/m^2 will therefore not differ much from that at 0.17 MN/m^2). Thus, when the high-order terms in equation (5.20) are neglected, it becomes

$$D(t) = \frac{2\ Y_{55}\ Y_{56}\ t^{\frac{1}{2}}\ (1 + Y_{58}\ t/3)}{1 + Y_{58}\ t} = \frac{2\ Y_{55}\ Y_{56}\ t^{\frac{1}{2}}\ (1 + Y_{53}\ Y_{54}\ Y_{57}\ t/3)}{1 + Y_{53}\ Y_{54}\ Y_{57}\ t} \tag{5.21}$$

Equation (5.21) gives the bubble growth or the time dependent bubble diameter.

When the bubble reaches its maximum (or departure) diameter, equations (5.13) and (5.21) give

$$t_m^{\frac{1}{2}} = \frac{Y_{55}\ Y_{56}}{Y_{53}\ Y_{54}\ Y_{57}\ D_m} \tag{5.22}$$

$$D_m = \frac{2\ Y_{55}\ Y_{56}\ t_m^{\frac{1}{2}}\ [1 + 1/3\ Y_{53}\ Y_{54}\ Y_{57}\ t_m]}{1 + Y_{53}\ Y_{54}\ Y_{57}\ t_m} \tag{5.23}$$

since

$$\frac{dD(t_m)}{dt} = 0 \text{ and } D(t_m) = D_m \text{ when } t = t_m \ . \tag{5.24}$$

D_m, the maximum bubble diameter, and t_m, the maximum bubble growth time, can be found then from the solution of the above two equations.

$$D_m = 1.21 \frac{Y_{55}\ Y_{56}}{(Y_{53}\ Y_{54}\ Y_{57})^{\frac{1}{2}}} \tag{5.25}$$

$$t_m = \frac{1}{1.46\ Y_{53}\ Y_{54}\ Y_{57}} \tag{5.26}$$

In order to calculate D(t), bubble growth, D_m, maximum bubble diameter, and t_m, maximum bubble growth time, with the aid of equations (5.21), (5.25) and (5.26), two quantities, i.e., Y_{54} and Y_{56} have to be known since Y_{53}, Y_{55}, Y_{57} in these equations depend on the operating conditions, geometry and the material, thus known. These equations are in general form, that is, they apply both to a bubble at the IPB and to the average bubble of a bubble population consisting of numerous bubbles. At the IPB, there exists a single bubble or a few bubbles, and the growth of a bubble is thus not affected by the liquid agitation caused by movement of the numerous bubbles, in contradiction with the growth of a bubble in a bubble population. Therefore the values of the two unknowns, i.e., the values of Y_{54} and Y_{56}, should differ for these two types of bubbles.

5.2.2.3 Maximum Bubble Diameter

5.2.2.3.1 The Maximum Diameter of the Average Bubble of a Bubble Population

In order to determine the maximum diameter of the average bubble of a bubble population consisting of numerous bubbles using equation (5.25), the expression, $(Y_{56}/Y_{54}^{\frac{1}{2}})$, in this equation has to be known. Y_{54} is a pressure dependent constant, as derived in Appendix 1 and Y_{56} was assumed to depend on pressure alone, (see paragraph (e) of Section 5.2.2.1). Therefore the above expression should depend also on pressure alone. For the

verification of this and for the determination of the expression, the following procedure was used.

Equation (5.25) was written in an open form.

$$\frac{D_m \, (Y_{53} \, \Delta T_{sub})^{\frac{1}{2}}}{(q_h - h \, \Delta T_{sub})^{1/3} \, (k \, \rho \, c)_h^{\frac{1}{2}}} = \frac{0.605 \, Y_{56} \, [2(1 - \rho_v/\rho_l)]^{\frac{1}{2}} \, k_l}{Y_{54}^{\frac{1}{2}} \, \rho_v \, \lambda \, Y_{41}^{1/3} \, (\pi \, Y_{52})^{\frac{1}{2}} \, (k \, \rho \, c)_l^{\frac{1}{2}}} \qquad (5.27)$$

The RHS of equation (5.27) contains only pressure dependent variables; it should therefore be a constant for a given pressure. In order to verify this, the LHS of the equation was used since $(Y_{56}/Y_{54}^{\frac{1}{2}})$ on the RHS of the equation is not known. The LHS of the equation, however, contains only quantities that can be measured (D_m, ΔT_{sub}, q, u) or predictable quantities (h, k_h, ρ_h and c_h).

The LHS of equation (5.27) was calculated from the present data given in Table 5.1 and from the experimental data of Griffith et al. [G1], Gunther [G2], Tolubinsky and Kostanchuk [T3] and Treshchev [T5] given in Table 5.2, and plotted versus pressure in Fig. 5.2. From this figure it is concluded that the LHS of equation (5.27) is a constant within reasonable accuracy limits for a given pressure. Consequently the RHS of this equation should depend also on pressure alone. Furthermore Fig. 5.2 shows that the LHS (or RHS) of the equation is a constant for the whole pressure range between 1 and 17.7 MN/m^2 regardless of operating conditions and of geometry and maximum bubble diameter.

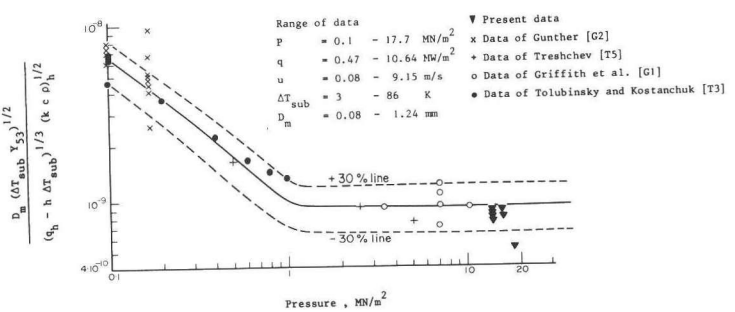

Fig. 5.2 Verification of equation (5.27).

Table 5.2 Experimental Data for Maximum Bubble Diameter and Maximum Bubble Growth Time According to Various Investigators.

Bubble number	Pressure	Max. bubble diameter	Subcooling	Velocity	Max. bubble growth time	Heat flux	Type and dimension of the heating surface	Investigator
-	MN/m^2	mm	K	m/s	µs	MW/m^2	mm	-
1	0.1	1.24	5	0.20	-	0.47	stainless steel plate 55 x 2.5**	Tolubinsky and Kostanchuk [T3
2	"	0.9	20	"	1200	"	"	"
3	"	0.56	40	"	-	"	"	"
4	"	0.47	60	"	-	"	"	"
5	"	0.76	72	3.05	175	4.50	stainless steel plate 63.5 x 4.8**	Gunther [G2]
6	"	0.88	50	"	250	"	"	"
7	"	1.02	33	"	300	"	"	"
8	"	0.55	85	"	-	"	"	"
9	0.17	0.62	83	1.50	200*	6.14	"	"
10	"	0.50	"	3.05	125*	6.14	"	"
11	"	0.36	"	6.10	67*	6.14	"	"
12	"	0.58	86	3.05	-	2.30	"	"
13	"	0.58	"	"	-	4.50	"	"
14	"	0.51	"	"	-	6.14	"	"
15	"	0.44	"	"	-	8.06	"	"
16	"	0.32	"	"	-	10.64	"	"
17	0.2	0.5	20	0.08	-	0.47	same as given for bubble number 1	same as given for bubble number 1
18	0.4	0.3	20	0.08	1200	0.47	"	"
19	0.5	0.26	30	1.9	-	1.40	nickel plate 32 x 5.1***	Treshchev [T5

Table 5.2: continued

Bubble number	Pressure	Max. bubble diameter	Subcooling	Velocity	Max. bubble growth time	Heat flux	Type and dimension of the heating surface	Investigator
-	MN/m^2	mm	K	m/s	µs	MW/m^2	mm	-
20	0.6	0.23	20	0.08	-	0.47	same as given for bubble number 1	same as given for bubble number 1
21	0.8	0.20	"	"	-	0.47	"	"
22	1.0	0.19	"	"	5000	0.47	"	"
23	2.5	0.14	54	1.9	-	2.03	same as given for bubble number 19	same as given for bubble number 19
24	3.45	0.095	51	6.1	-	6.38	stainless steel plate 12.7 x 9.5**	Griffith et al. [G1]
25	5.0	0.12	62	1.9	-	2.90	same as given for bubble number 19	same as given for bubble number 19
26	6.9	0.106	39	6.1	-	3.95	same as given for bubble number 24	same as given for bubble number 24
27	6.9	0.146	11	6.1	-	3.25	"	"
28	6.9	0.082	53	9.15	-	7.01	"	"
29	6.9	0.088	54	9.15	-	5.75	"	"
30	10.3	0.081	80	6.1	-	8.53	"	"

* The value given is not the bubble-growth time but the half of the bubble-life time.

** In order to evaluate the physical properties of stainless steel, stainless steel, type 304 (austenitic) 18-8S, is considered.

*** In order to evaluate the physical properties of nickel, nickel of 99.97% purity is considered.

Having verified that the expression, $(Y_{56}/Y_{54}^{\frac{1}{2}})$, is a pressure dependent constant, the value of this was then determined from equation (5.25) and from the aforesaid data given in Tables 5.1 and 5.2, as shown in Fig. 5.3. In accordance with Fig. 5.3

$$Y_{56}/Y_{54}^{\frac{1}{2}} = 2.10^{-5}\ P^{0.709} \tag{5.28}$$

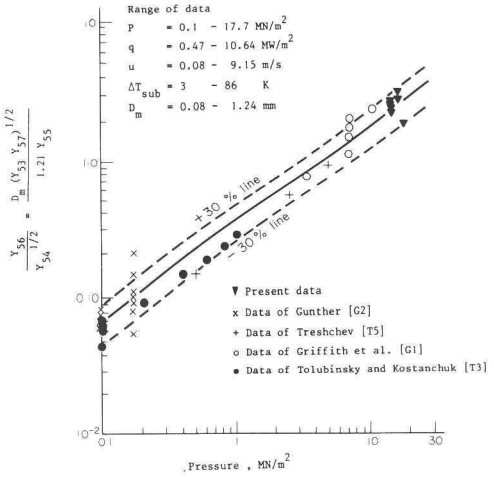

Fig. 5.3 Correlation of the data for the maximum diameter of the average bubble of a bubble population.

Substitution of equation (5.28) into equation (5.25) yielded the maximum bubble diameter of the average bubble of a bubble population.

$$D_m = \frac{2.42\ 10^{-5}\ P^{0.709}\ Y_{55}}{(Y_{53}\ Y_{57})^{\frac{1}{2}}} \tag{5.29}$$

As can be deduced from Fig. 5.3, equation (5.29) predicts reasonably well the maximum diameter of the average bubble of a bubble population.

Recently Serizawa [S5] reported also a correlation for the maximum bubble diameter. He states that the results of his correlation are "quite consistent" with the results of equation (5.29).

The ranges of geometries and operating conditions for the data used to establish equation (5.29) is as follows: Geometry: stainless steel plates, a nickel plate and a circular tube; $P = 0.1 - 17.7$ MN/m^2; $q = 0.47 - 10.64$ MW/m^2; $u = 0.08 - 9.15$ m/s; $\Delta T_{sub} = 3 - 86$ K; $D_m = 0.08 - 1.24$ mm. The number of data considered was 37.

All the above data were obtained from the bubble populations consisting of numerous bubbles; equation (5.29) therefore gives the maximum bubble diameter of the average bubble of a bubble population consisting of numerous bubbles, but not the maximum bubble diameter at the IPB. The latter is presented below.

5.2.2.3.2 Maximum Bubble Diameter at the IPB

In order to determine this diameter, a method similar to that given in the above section was followed and $Y_{56}/Y_{54}^{\frac{1}{2}}$ was determined first. For this purpose the data presented in Table 4.1 and low-pressure data of Abdelmessih et al. [A2] taken on an artifical nucleation site manufactured from stainless steel were used. For the data of the above investigators, the wall superheat given in their paper was used instead of predicting this superheat from equation (5.6). The evaluation of the properties of the stainless steel carried out in accordance with the footnote in Table 5.2.

The relation obtained for $Y_{56}/Y_{54}^{\frac{1}{2}}$ was

$$Y_{56}/Y_{54}^{\frac{1}{2}} = 1.426.10^{-7}\ P^{1.072} \tag{5.30}$$

Substitution of equation (5.30) into equation (5.25) then yielded the maximum bubble diameter at the IPB,

$$D_m = \frac{1.725.10^{-7}\ P^{1.072}\ Y_{55}}{(Y_{53}\ Y_{57})^{\frac{1}{2}}} \tag{5.31}$$

The results of the comparison of equation (5.31) with the present data and data of Abdelmessih et al. [A2] are shown in Fig. 5.4. This equation predicts the maximum bubble diameter at the IPB well.

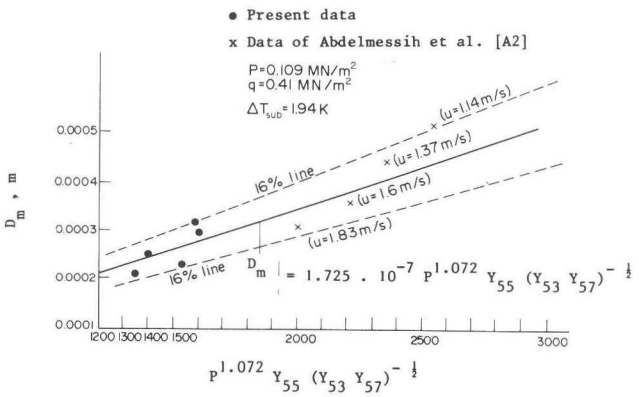

Fig. 5.4 Correlation of the data for maximum bubble diameter at the IPB.

The range of operating conditions of the data used to establish equation (5.31) is summarized below: P = 0.11 - 15.9 MN/m^2; G = 1094 - 2208 kg/m^2s; ΔT_{sub} = 1.9 - 7.3 K; q = 0.128 - 0.410 MW/m^2. The number of data considered was 9 and D_m varied between 0.21 and 0.51 mm.

5.2.2.4 Maximum Bubble Growth Time

5.2.2.4.1 Maximum Growth Time of the Average Bubble of a Bubble Population

In order to determine maximum bubble growth time using equation (5.26), Y_{54} in this equation has to be known. Although $Y_{56}/Y_{54}^{\frac{1}{2}}$ was determined, Y_{56} and Y_{54} could not be found since no other relation between them could be established. Therefore to predict Y_{54} and consequently Y_{56}, the following procedure was adopted. Fig. 5.2 shows that there is an essential variation in the mechanism of bubble growth at about 1 MN/m^2. For this pressure the value of Y_{54} was first determined using equation (5.26) and the data of Tolubinsky and Kostanchuk given in Table 5.2, and the value of Y_{54} was found to be equal to 13.7 $(Ks)^{-1}$. With the aid of this value and equations (5.15) and (5.25), $D_d(t_m)$, the diameter of the dry area under the bubble, was found to be $D_d(t_m) = 0.04\ D_m$.

The average value of $D_d(t_m)$ was also calculated for 0.17 MN/m^2 as $D_d(t_m) = 0.53\ D_m$ using equations (5.15) and (5.25) and the data of

Gunther [G2] for eight bubbles presented in Table 5.2. Y_{54} is known for this pressure, as given in Appendix 1. Comparison of these two $D_d(t_m)$ values shows that the dry area under the bubble disappears at about 1 MN/m^2. Therefore

$$Y_{56} = \{1 - D_d^2/(D(t))^2\} \cong 1 \text{ for } P = 1 - 17.7 \text{ MN/m}^2 \tag{5.32}$$

For the above given pressure range, Y_{54} was then calculated from equation (5.28) using $Y_{56} = 1$ in this equation.

$$Y_{54} = 0.25.10^{+10}\ P^{-1.418} \text{ for } P = 1 - 17.7 \text{ MN/m}^2 \tag{5.33}$$

Up to 1 MN/m^2, due to lack of experimental data, Y_{54} was determined by linear interpolation and extrapolation using the values of Y_{54} found for 0.17 and 1 MN/m^2.

$$Y_{54} = 65 - 5.69.10^{-5}\ (P - 10^5) \text{ for } P = 0.1 - 1 \text{ MN/m}^2 \tag{5.34}$$

For the above given pressure range, Y_{56} was found from equation (5.28), substituting equation (5.34) into it.

$$Y_{56} = 2.10^{-5}\ P^{0.709}\ [65 - 5.69.10^{-5}\ (P - 10^5)]^{\frac{1}{2}}$$

$$\text{for } P = 0.1 - 1 \text{ MN/m}^2 \tag{5.35}$$

The above given Y_{54} and Y_{56} values have to be substituted into equations (5.13), (5.21) and (5.26) to determine the rate of bubble growth, instantaneous bubble diameter and maximum bubble growth time, respectively.

Having determined the value of Y_{54}, the experimental data of Gunther [G2] and Tolubinsky and Kostanchuk [T3] for maximum bubble growth times given in Table 5.2 were compared with those predicted by equation (5.26), as shown in Fig. 5.5. Equation (5.26) predicts the maximum bubble growth time well, i.e., within 20% accuracy.

The range of the data used to establish equation (5.26) is summarized below: P = 0.1 - 1 MN/m^2; q = 0.47 - 4.5 MW/m^2; ΔT_{sub} = 20 - 72 K; u = 0.08 - 3.05 m/s; t_m = 175 - 5000 μs; D_m = 0.19 - 0.9 mm. The number of data considered was 6.

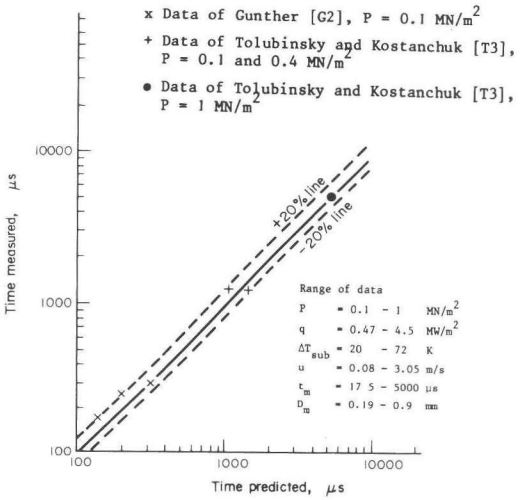

Fig. 5.5 Comparison of experimental and predicted maximum bubble growth times for the average bubble of a bubble population.

5.2.2.4.2 Maximum Growth Time of a Bubble at the IPB

In the above section it is shown that the dry area under the bubble disappears at about 1 MN/m^2 for the average bubble of a bubble population. This is anticipated due to low wall superheats for the high pressures. It is logical then to assume that the dry area under a bubble growing at the IPB should also disappear at about 1 MN/m^2. In this case,

$$Y_{56} = 1 \text{ for } P = 1 - 17.7 \text{ MN/m}^2 \tag{5.36}$$

The value of Y_{54} could then be evaluated from equation (5.30) as given below:

$$Y_{54} = 4.92.10^{13}\ P^{-2.144} \text{ for } P = 1 - 17.7 \text{ MN/m}^2 \tag{5.37}$$

Since Y_{54} and Y_{56} are known, bubble growth, the bubble growth rate and maximum bubble growth time can be predicted by equations (5.13),

(5.21) and (5.26) respectively for P = 1 - 17.7 MN/m^2. However, due to lack of experimental data, neither the above equations could be verified, nor the values of Y_{54} and Y_{56} could be determined for a bubble at the IPB for pressures lower than 1 MN/m^2.

5.2.2.5 The Growth of the Average Bubble of a Bubble Population

The growth of a average bubble of a bubble population is expressed by equation (5.21), and Y_{54} and Y_{56} in this equation are known, as given in Section 5.2.2.4. The bubble growth (or the instantaneous bubble diameter) predicted by this equation was compared with the data of Gunther [G2], as shown in Fig. 5.6. It appears that the predicted growth of the average bubble fits the data quite well. The average maximum diameter of the bubble population, D_m in Fig. 5.6, was given by Gunther in his paper.

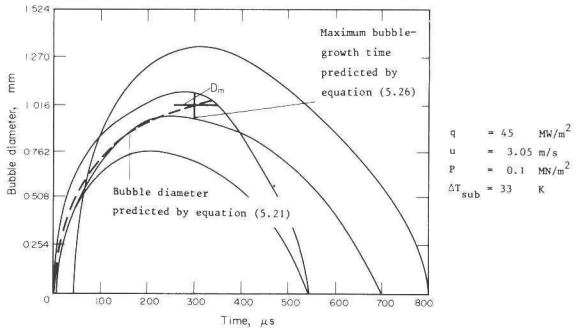

Fig. 5.6 Comparison of experimental and predicted bubble growth.

5.3 DRAG COEFFICIENTS FOR THE BUBBLE AND PLUG FLOWS

The drag coefficient is the ratio of buoyancy forces to drag forces acting on a bubble or a plug, and is given by the following equation for the steady motion of a bubble or a plug:

$$C_d = \frac{4}{3} \frac{\rho_L - \rho_v}{\rho_L} \frac{gD}{\Delta u^2} \qquad (5.38)$$

where Δu is the difference between the time averaged bubble velocity and

the local liquid velocity. This coefficient could be determined from the results of the analysis of the tests carried out in TT1 to measure the drift velocity. These tests and the results of the tests are described in detail in Section 3.1.3. In order to determine the drift velocity, the diameters and the time averaged values of the velocities of the bubbles and plugs seen on a film were measured. These data and the data for the operating conditions were sufficient to evaluate the drag coefficients for a reasonable range of conditions, which is presented in Table 5.3.

Table 5.3 The Range of Data used for the Evaluation of the Drag Coefficients

P (MN/m^2)	G (kg/m^2s)	D (mm)	$\bar{V}_a$ (m/s)
10.1	93.6	3.33 - 5.73	0.32 - 0.35
14.2	74.5	1.10 - 5.90	0.29 - 0.355
4.3	59.5	3.19 - 3.56	0.24 - 0.25
7.3	62.5 - 87.6	1.08 - 3.67	0.25 - 0.34
10.1	61.3 - 73.7	1.23 - 3:87	0.22 - 0.33
12.2	55.1 - 106.9	1.27 - 2.11	0.19 - 0.34
14.2	83.3 - 105.9	0.94 - 1.82	0.20 - 0.36
16	53.4 - 106	1.05 - 1.59	0.16 - 0.41
18	51.3 - 101.1	0.81 - 1.26	0.19 - 0.37

In order to determine C_d for bubble flow, the local liquid velocity was taken equal to the average liquid velocity based on total mass flow and the cross sectional area of the sapphire channel for the following two reasons: Firstly, for the bubble flow region the measured void fraction was very low, i.e., between 0.08% and 4.55% (see Table 3.2). Secondly, owing to the transition piece between the sapphire channel and the test tube, the velocity profile in the sapphire channel could be assumed to be uniform except in the boundary layer near the channel wall.

For plug flow, the local liquid velocity was taken equal to the average liquid velocity based on total mass flow and the cross sectional area of the sapphire channel. The bubble or the plug velocity was determined from the equation

$$\bar{V}_a = \frac{1}{m} \sum_{m=1}^{m} V_m \tag{5.39}$$

Data for the drag coefficients were correlated with the following equation:

$$C_d = \frac{\exp\ (18.967 + 2.74\ Y_{510} - 28.35\ Y_{510}^2 + 48.75\ Y_{510}^3 - 32.82\ Y_{510}^4)}{Re^2} \tag{5.40}$$

where

$$Y_{510} = (1 - D/d) \tag{5.41}$$

$$Re = \frac{D\ \rho_L\ \Delta u}{\mu_L} \tag{5.42}$$

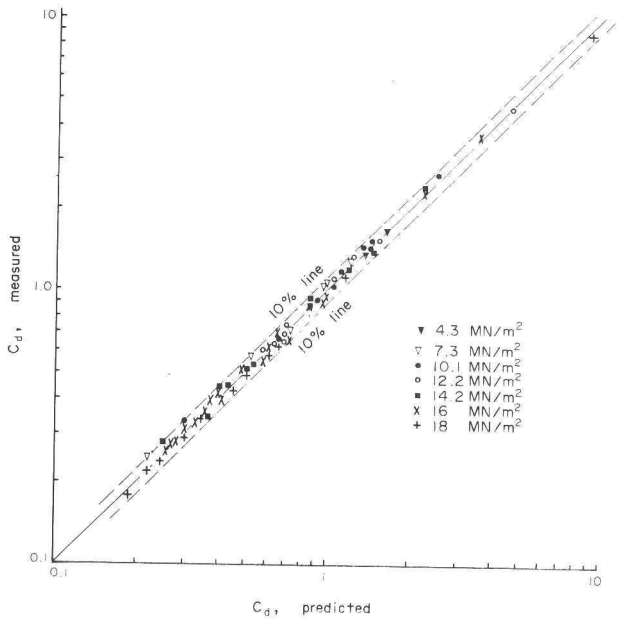

Fig. 5.7 Comparison of the data for drag coefficient with equation (5.40).

The accuracy of equation (5.40) is 10%, as shown in Fig. 5.7, and the RMS error in correlating the data was 4.4%. The number of data considered was 77. The bubble or the plug Reynolds number varied between 372 and 11256.

Chapter Six

DRYOUT AND TWO-PHASE FLOW PRESSURE DROP IN SODIUM HEATED HELICALLY COILED STEAM GENERATOR TUBES AT ELEVATED PRESSURES

6.1 INTRODUCTION

Sodium heated helically coiled tube steam generators are used in the LMFBR cooling system. Very little literature exists for the dryout and two-phase flow pressure drop in helically coiled tubes. In what follows only the work reported in the literature for elevated pressures is mentioned. A literature review deals with the studies made at low pressures [H4].

The first systematic analysis of the dryout (or Departure of Nucleate Boiling, DNB) in electrically heated coiled tubes for $P = 17.2\ MN/m^2$ is given in [C3]. Correlations are reported in [D5, N1, R11] to determine the dryout heat flux and two-phase flow pressure drop in sodium and electrically heated helically coiled tubes at medium and high pressures. The correlations given in [R11] apply to only two dryout locations and those of [D5, N1] to one dryout location, probably to the termination of the dryout. As quoted from [C3], "the DNB in coiled tubes occurs at different steam qualities for different positions around the circumference of the tube, whereas, for vertical straight tubes DNB occurs around the complete circumference of the tube at one steam quality." In [A7], two-phase flow pressure drop data obtained in three electrically heated helically coiled tubes of $d_c/d = 46$, 104 and 186 at $P = 17.9\ MN/m^2$ are compared with the results of six correlations and of these the correlation of [B17] gives the best overall agreement.

It is logical to assume that a dryout correlation based on data obtained in vertical tubes should apply to a helical coil provided that the effect on the dryout heat flux of centrifugal forces is taken into account. This statement will be verified later on in Section 6.2.2.2. In a sodium heated helically coiled steam generator tube, the heat flux along the axis of the tube is not uniform. It is therefore considered relevant here to mention briefly the state of art for the prediction of the dryout heat flux in non-uniformly heated vertical circular steam generator tubes at elevated pressures. Dryout/burnout has been extensively studied in the literature. It is not possible to review all of these

studies in this thesis. The reader is referred to books published recently [B18, H5]. The well known dryout correlations for uniformly heated vertical circular steam generator tubes and for elevated pressures are collected in [C2].

In so far as the application of the dryout correlations based on the data obtained in uniformly heated steam generator tubes (i.e., electrically heated tubes) to non-uniformly heated steam generator tubes is concerned, unjustified and harmful speculations in the literature have been found. For example it is stated in [L4] that the correlations of Peskov et al. [P2], Becker [B7] and Lee [L3] are adequate for non-uniformly heated steam generator tubes and for elevated pressures. These correlations are based on the data obtained in uniformly heated vertical circular steam generator tubes, and are well accepted in the literature [C2]. Above three correlations were compared with the data of De Munk et al. [M7] obtained in a non-uniformly heated vertical circular steam generator tube (i.e., in TT1). The correlations predict the dryout heat flux from these data very poorly, i.e., with a RMS error of 39.8%, 59.8% and 111.5%, respectively. The results of the correlations of Konkov [K6] and Tippets [T2] yielded a similar RMS error, i.e., 78.9% and 103.4%, respectively. It thus seems justified to draw the conclusion that no adequate correlation has appeared in the literature as yet for non-uniformly heated vertical circular steam generator tubes.

The aim of this chapter of the thesis is to report the results of the tests carried out to determine the dryout conditions in three sodium heated circular helically coiled tubes, i.e., in TT4, TT5 and TT6. A correlation was also established to predict the dryout heat flux for uniformly and non-uniformly heated helically coiled- and vertical circular steam generator tubes.

Dryout conditions were measured only at the inside (i.e., the side of the tube nearest to the helix axis), top, outside (i.e., the tube surface furthest from the helix axis) and bottom of each test tube. The operating conditions of the tests were: $P = 14.7 - 20.2$ MN/m^2; $G = 112 - 1829$ kg/m^{2}s; $\Delta T_{sub} = 35.6 - 156.8$ K; $X_o = 0.15 - 1.61$. The 203 data obtained for the first and last detected dryout and the 674 data taken for $P = 4.3 - 20.2$ MN/m^2 in long and short, uniformly heated vertical circular tubes, i.e., electrically heated tubes [P2, C1], and in a 10 m long, non-uniformly heated vertical circular tube, i.e., in TT1 [M7]

, were correlated to predict the dryout heat flux within 20% accuracy for 98% of the time. The RMS error for all the 877 data was 9.01%.

In the above coils the two-phase flow pressure drop was also measured for the following range of conditions: P = 14.9 - 20.1 MN/m^2; G = 296 - 1829 kg/m^2s; X_{bt} = 0.15 - 1.0; ΔP_{tp} = 3.0 - 88 kN/m^2. The 70 data obtained and the 299 data from a 10 m long, sodium heated vertical circular tube for P = 14.3 - 19.9 MN/m^2 [M7] (i.e., from TT1) were correlated to predict the two-phase flow pressure drop within 20% accuracy for 98% of the time. The RMS error for all the 369 data was 9.87%.

6.2 DRYOUT IN SODIUM HEATED HELICALLY COILED STEAM GENERATOR TUBES AT ELEVATED PRESSURES

6.2.1 Tests

6.2.1.1 Test Procedure

Dryout conditions were measured in TT4, TT5 and TT6. In order to determine these conditions, two types of tests were carried out. In the first type of tests (i.e., the preliminary tests) the steam quality at the outlet of a test tube was slowly increased to about 1 or higher than 1 by increasing the sodium side inlet temperature. After reaching the steady-state conditions all the measurements were collected. In the second type of tests (i.e., the detailed tests), which were only performed in TT4, the outlet steam quality was increased by very small increments by increasing the sodium side inlet temperature. After each increment and after the steady-state conditions had been reached, all the measurements were collected. By observing the fluctuations in the wall temperatures registered on the multi-channel recorder, the occurrence of the dryout along the circumference of the test tube (i.e., at the inside, top, outside and bottom positions) was followed.

Tests were carried out systematically. For a given mass flow and inlet subcooling measurements were made at three pressure levels, mostly at 15, 17.5 and 20 MN/m^2.

The operating conditions of the tests are summarized in Table 6.1. These conditions are also given in detail in Table A2.1 in Appendix 2.

Table 6.1 Dryout Data from TT4, TT5 and TT6

Test tube → / Operating conditions ↓	TT4	TT5	TT6
First detected dryout			
P [MN/m²]	14.7 - 20.2	14.9 - 20.1	16.8 - 18.5
G [kg/m²s]	112 - 1558	116 - 1829	387 - 1505
q_d [kW/m²]	41 - 712	84 - 612	195 - 367
X_d	0.08 - 0.64	0.24 - 0.79	0.40 - 0.43
ΔT_{sub} [K]	41.2 - 146.9	69.1 - 156.8	35.6 - 79.6
L_e/d	329 - 1293	342 - 989	418 - 620
n	61	36	2
Last detected dryout			
P [MN/m²]	14.7 - 20.2	14.9 - 20.1	16.8 - 18.5
G [kg/m²s]	112 - 1558	116 - 1829	387 - 1505
q_d [kW/m²]	69 - 691	113 - 731	265 - 445
X_d	0.46 - 1	0.73 - 1.0	0.76 - 1.0
ΔT_{sub} [K]	41.2 - 146.9	69.1 - 156.8	35.6 - 79.6
L_e/d	357 - 1123	395 - 939	500 - 717
n	65	36	3

6.2.1.2 Data Reduction

All the measurements made were first transformed into a graphical form by plotting the steam quality, peripheral average heat flux and sodium and water/steam side temperatures versus the length of a test tube. Smooth curves were drawn through the measured or calculated values. In a graph the wall temperatures were also plotted for the tests carried out in TT4 and the wall surface temperatures at the water/steam side for the tests carried out in TT5 and TT6. For one test run four graphs were then obtained for the inside, top, outside and bottom positions. An example is

given in Fig. 6.1.

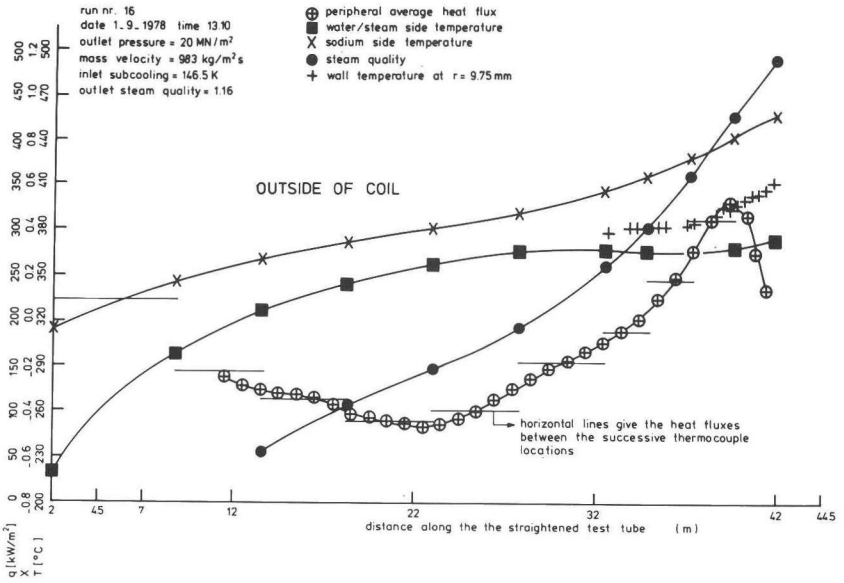

Fig. 6.1 Plot of measurements.

The steam quality was calculated with a heat balance. For the determination of the peripheral average heat flux, the power developed along a test tube was approximated by a 9th or 10th degree polynomial. This power was referenced to the inlet of the test tube. Thereafter the peripheral average heat flux was determined from this polynomial for each successive meter of the test tube with the following formula:

$$q = [Q(\zeta + 1) - Q(\zeta)]/(1 \cdot \pi d) \qquad (6.1)$$

The value thus determined was then assumed to be valid for the location $(\zeta + 0.5)$ m. The results obtained were also checked with the average heat fluxes calculated for the tube sections between two successive thermocouple locations. Wall surface temperatures at the water/steam side for the tests carried out in TT5 and TT6 were calculated with the

well-known heat conduction formula.

For the first type of tests, the location of the dryout was determined as follows: Before reaching the dryout, the wall temperatures at r = 9.75 mm (or wall surface temperatures at the water/steam side) in the nucleate boiling region were practically constant. After the dryout these temperatures rose. Therefore two wall temperature profiles were drawn in a graph, one before the dryout and the other after the dryout. The axial coordinate of the intersection of these two temperature profiles was assumed to be the location of the dryout. The values of the steam quality and the peripheral average heat flux were then taken from the graph for the aforesaid location.

For the second type of tests, which were carried out only in TT4, dryout took always place at the end of the test tube. When temperature fluctuations were observed on the multi-channel recorder during a run, the run taken before was considered as the dryout run. The graphs made by a procedure similar to that explained above for several runs after and before the dryout run were also consulted to ascertain the determination of the dryout. The peripheral average heat flux at the end of the test tube was predicted with the method explained above.

In both types of tests dryout was only measured at the inside, top, outside and bottom of the test tube.

The methods used to predict the location of dryout appeared to practically eliminate the errors due to mounting the wall thermocouples at the desired coordinates, i.e., r = 9.75 mm and 11.25 mm.

6.2.2 Discussion of Results

6.2.2.1 Observations

Dryout always took place in the last quarter length of a test tube. The distance between the locations of the first and last detected dryout varied between 0.2 and 5.1 m. This distance was a small fraction of the length of a test tube, i.e., up to 15%. The above suggests that the location of the first detected dryout nearly coincides with the location where the dryout actually takes place first and the location of the last detected dryout with the location where the dryout in fact terminates. This result is of importance for practical applications.

At mass velocities higher than about 850 kg/m^{2}s, the dryout was first detected at the inside of a test tube. The last detected dryout was at the outside of the tube. At mass velocities lower than 850 kg/m^{2}s, the first and last detected dryouts were at the top and bottom of the tube respectively. As indicated in [C3], the location of the dryout appears to depend on, among other things, the centrifugal and gravitational forces.

At high mass velocities wall temperature fluctuations at r = 9.75 mm were very small at the first detected dryout location and these fluctuations became larger at the last detected dryout location. Decreasing the mass flow yielded larger temperature fluctuations.

6.2.2.2 Correlation of the Dryout Data

Only the data taken for the first and last detected dryouts were considered.

The operating conditions for these data are summarized in Table 6.1.

The present data, the 215 data of De Munk et al. [M7] obtained in a 10 m long, sodium heated vertical circular tube for P = 14.8 - 20.2 MN/m^2 (i.e., in TT1) and the 127 data taken in electrically heated vertical circular tubes of 11 different L_h/d ratios for P = 15.7 - 19.6 MN/m^2 [P2] were correlated with the equation

$$Bo = 0.97\ Y_{61}\ Y_{62}\ Y_{63}\ Y_{64}\ Y_{65}/(Y_{66}\ Y_{67}) \tag{6.2}$$

where

$$Y_{61} = 1 + 3.8\ \Delta H \tag{6.3}$$

$$Y_{62} = 0.114 - 0.041\ \ln(1 - P_r) \tag{6.4}$$

$$Y_{63} = 1 + 4.59\ (L_e/d)^{-1.2} \tag{6.5}$$

$$Y_{64} = 1 + 0.44\ [\exp(-0.056\ d_c/d) - \exp(-3\ d_c/d)] \tag{6.6}$$

for the first detected dryout,

$$Y_{64} = 1 + 0.56\ [\exp(-0.011\ d_c/d) - \exp(-3\ d_c/d)] \tag{6.7}$$

for the last detected dryout,

$$Y_{65} = (2\ \delta/d)^{0.32} \tag{6.8}$$

$$Y_{66} = L_e/d + 28\ Fr^{0.22} \tag{6.9}$$

$$Y_{67} = 1 \tag{6.10}$$

The boiling and Froude numbers in equations (6.2) and (6.9) are given by

$$Bo = q_d/(\lambda\ G) \tag{6.11}$$

$$Fr = G^2/(g\ \rho_l^2\ d) \tag{6.12}$$

The equivalent length L_e in equations (6.5) and (6.9) is per definition

$$L_e\ \pi\ d\ q_d = A\ G\ (H_l - H_i + \lambda\ X_d) \tag{6.13}$$

The equivalent length was used in the past by some investigators to take into account the effect on the dryout of the axial non-uniform heat flux distribution and is based on the following hypothesis: The power developed up to the dryout/burnout point in a non-uniformly heated tube is the same as that of a uniformly heated tube of the same bore and of a hypothetical length found from the condition that in both tubes the local heat fluxes are equal at the dryout/burnout location [B3, L2].

Equation (6.2) is in fact a modification of the correlation of Becker [B7] for electrically heated vertical circular tubes. This correlation is

$$q_d = 10^4\ G\ [450 + 10^{-3}\ (H_l - H_i)][1.02 - (P_r - 0.54)^2]/(40\ L_h/d + 156\ G^{0.445} \tag{6.14}$$

and fits the data obtained at elevated pressures well [B7, C2].

For the purpose of this study the above correlation was made non-dimensional and modified by taking the effects on the dryout of coil diameter, wall thickness and axial heat flux distribution: In an

electrically heated vertical tube the heat flux is in general uniform along the tube, while in a sodium heated helically coiled or vertical tube the heat flux is not uniform along the tube. In a helical coil, dryout appears to be affected by conduction in the tube wall, as observed in [C3] and in the present study, and the heat flux varies peripherally. Therefore this effect was taken into account in equation (6.2) with the parameter given by equation (6.8). Since the bubble formation or the evaporation of a liquid layer on a heated wall is affected by conduction in the wall, (see equation (5.3)), the use of this parameter seems also justified for the correlation of data obtained in vertical tubes. To the knowledge of the author this parameter has not been used in any of the numerous empirical dryout correlations presented in the literature so far.

In order to determine the dryout heat flux and the equivalent length by the use of equations (6.2) and (6.13), a simultaneous solution of these equations is not permitted. A kind of iterative method has to be followed. First the equivalent length has to be solved from equation (6.13) for a given axial position in a tube. Thereafter this equivalent length has to be inserted into equation (6.2) to determine the dryout heat flux. This procedure has to be repeated till the calculated dryout heat flux equals the heat flux at the axial location considered.

In the experiments carried out with short electrically heated vertical tubes dryout took place at the end of the tube [P2]. For these tubes $L_e = L_h$, and therefore equation (6.2) alone is sufficient to determine the dryout heat flux. However, for a sodium heated vertical tube [M7] or a long, electrically heated vertical tube [C1] dryout does not take place at the end of the tube but somewhere before the end. Therefore for these types of tubes equations (6.2) and (6.13) have to be used together for the determination of the dryout heat flux.

With three exceptions, equation (6.2) predicts the dryout heat flux within 20% accuracy from the present data, the data of [M7] and the data of [P2] taken for P = 15.7 - 19.6 MN/m^2. The RMS error for all the 545 data considered is 8.56%. The ranges of the operating conditions and geometries for the data of [M7, P2] are summarized in Table 6.2. The methods used to obtain the data of [M7] are given in [M6].

For the derivation of equation (6.2) the 137 data of [P2] obtained in short electrically heated vertical circular tubes of 21 different

Table 6.2 Dryout Data from Several Investigators*

P [MN/m²]	G [kg/m²s]	q_d [kW/m²]	X_d [-]	ΔT_{sub} [K]	L_h [m]	d [mm]	$\frac{d}{2\delta}$ [-]	$\frac{L_e}{d}$ [-]	n [-]	Ref.
14.8-20.2	399-3491	131- 919	0.25 -0.69	18.6-121	10	7.86	1.90	257- 759	215	[M7]
15.7-19.6	594-5444	613-3582	0** -0.334	7.2-163.3	0.52-1.65	10	5- 6.67	52- 165	127	[P2]
9.8-13.7	492-5542	698-4931	0** -0.431	8 -273	0.25-2.1	8-10	4- 6.67	25- 250	114	[P2]
4.3- 9.5	1151-2529	184- 480	0.433-0.772	29.2- 90.2	22	11.8	2.27	1320-1771	99	[C1]
9.7-16.0	1111-2495	155- 418	0.296-0.512	67 -135.5	22	11.8	2.27	1500-1827	119	[C1]

* All the test tubes used were vertical circular tubes.

** True steam quality.

L_h/d ratios for P = 9.8 - 13.7 MN/m^2 and 218 data of [C1] taken in a long, electrically heated vertical circular tube for P = 4.3 - 16 MN/m^2 were not used. With the exception of those taken for low boiling numbers (i.e., 23 data), the aforesaid data of [P2] fitted the correlation within the experimental accuracy of the data, i.e., 25% for 95% of the time. In order to restrict the application of the correlation to the above mentioned 114 data taken for high boiling numbers, the following criteria were established:

$$P_r \geq 0.437 \tag{6.15}$$

$$Bo\ (L_e/d)^{0.25}\ [1 + 0.3\ (10^{-3}\ L_e/d)^{4.28}] \geq 3.46\ .\ 10^{-3}\ (1 - P_r)^{1.11} \tag{6.16}$$

Thus equation (6.2) is only valid for the conditions given by equations (6.15) and (6.16). The ranges of operating conditions and geometries of the 114 data of [P2] taken for P = 9.8 - 13.7 MN/m^2 are given in Table 6.2. These data, the present data and data of [P2] taken for P = 15.7 - 19.6 MN/m^2 and the data of [M7] satisfy the conditions expressed by equations (6.15) and (6.16).

The 218 data of [C1] fitted the correlation within 30% accuracy, with 6 exceptions. However, all the errors for the data obtained for $P \geq 9.66$ MN/m^2 were positive, and almost all the errors for the data obtained for $P < 9.66$ MN/m^2 were negative. In order to correlate these data properly, equation (6.2) was slightly modified. For this purpose the term Y_{67} given by equation (6.10) was transformed into the following form:

$$Y_{67} = 1 + 0.049\ (1 - P_r)^{1.27}\ (10^{-3}\ L_e/d)^{4.28} \tag{6.17}$$

for

$$P_r \geq 0.437 \tag{6.18}$$

$$Y_{67} = [1 + 0.049\ (1 - P_r)^{1.27}\ (10^{-3}\ L_e/d)^{4.28}]/[1.82 - 1.24\ P_r] \tag{6.19}$$

for

$$P_r < 0.437 \tag{6.20}$$

In the past several investigators correlated also the dryout data obtained at medium and high pressures for two separate pressure regions, as specified roughly by equations (6.18) and (6.20) [B4, B7, C2]. At $P_r \cong 0.414$, the ratio of the enthalpy of water at the state of saturation to the latent heat of evaporation is unity. This ratio is greater than unity for $P_r > 0.414$ and smaller than unity for $P_r < 0.414$. This is probably why the effect on the dryout heat flux of pressure differs in the vicinity of a particular pressure.

The expressions which include L_e/d in equations (6.17) and (6.19) become practically zero for $L_e/d \leq 759$, that is, $Y_{67} \cong 1$ for the present data and the data of [M7, P2].

After the above mentioned modification, the 218 data of [C1] fitted the correlation well, i.e., within 19% accuracy for 99% of the time with a RMS error of 8%. These data satisfy the conditions given by equations (6.15) and (6.16). The ranges of operating conditions and geometries for these data are given in Table 6.2.

The errors in predicting the dryout heat flux in accordance with the final form of equation (6.2) are shown versus reduced pressure in Figs. 6.2 through 6.8 for the present data and the data of [C1, M7, P2]. The correlation fits the data well, i.e., within 20% accuracy for 98% of the time. The RMS error for all the 877 data was 9.01%.

This accuracy is considered satisfactory. In order to ascertain this, the 215 data of [M7] obtained in a sodium heated vertical circular tube were compared with the correlations of [B7, K6, L3, P2, T2] which were derived from the data taken in uniformly heated (i.e., electrically heated) vertical circular tubes at high pressures. The correlation of [B7] is given by equation (6.14). This correlation fitted the data poorly, i.e., the RMS error in predicting the dryout heat flux was 59.8%. When using L_e/d instead of L_h/d in the correlation, the correlation yielded a RMS error of 10.7%. However, with 5 exceptions the error was between +8.4% and -29.2%. The correlations of [P2, K6, T2, L3] also fitted the data poorly, i.e., with a RMS error of 39.8%, 78.9%, 103.4% and 111.5%, respectively. For the last mentioned correlations it was not possible to check the effect of the equivalent length since these correlations do not include the tube length as a correlating parameter. From the above it is quite clear that the correlations based on data obtained in uniformly heated tubes yield very inaccurate results for non-uniformly heated tubes.

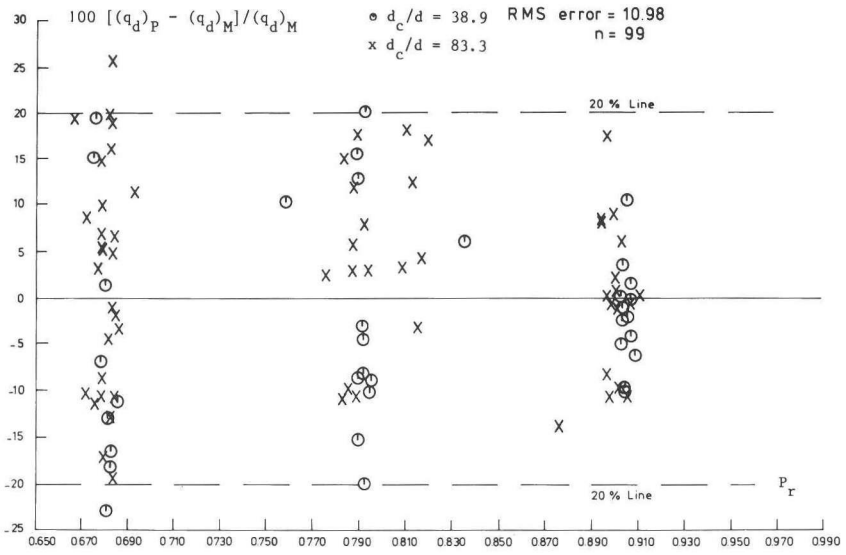

Fig. 6.2 Errors in predicting the heat flux for the first detected dryout.

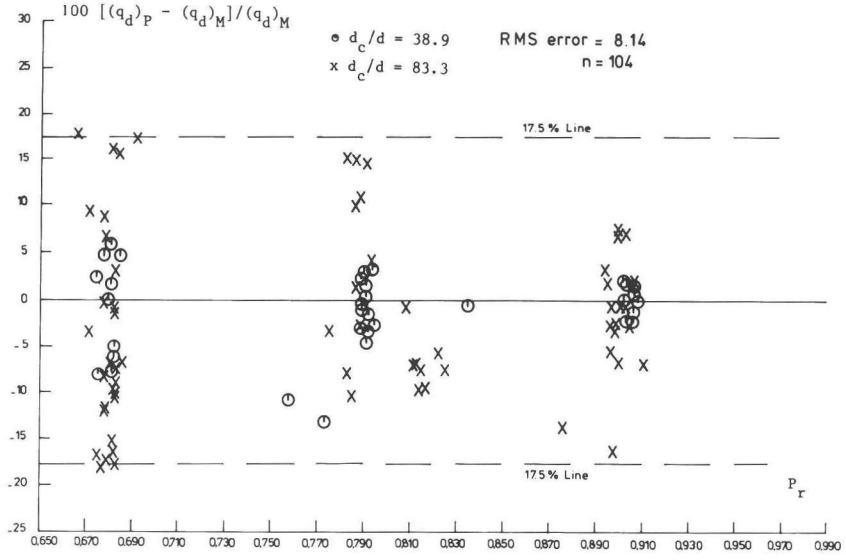

Fig. 6.3 Errors in predicting the heat flux for the last detected dryout.

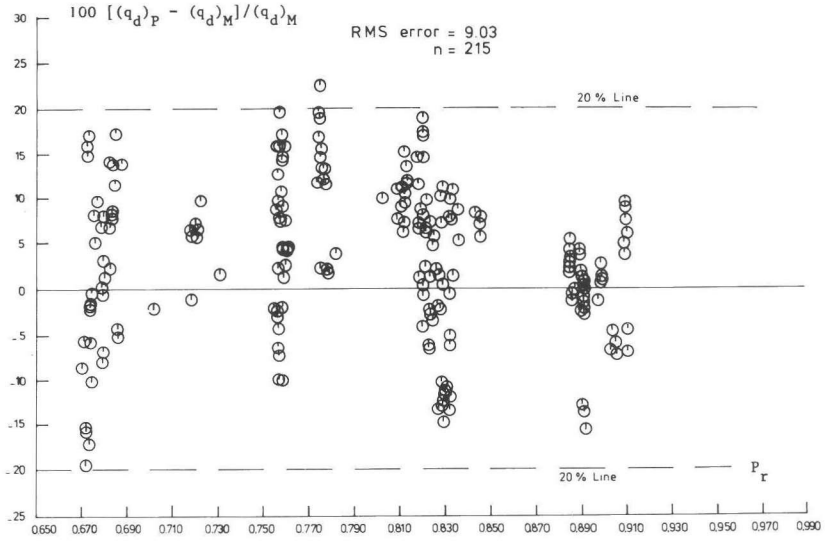

Fig. 6.4 Errors in predicting the dryout heat flux from the data of [M7].

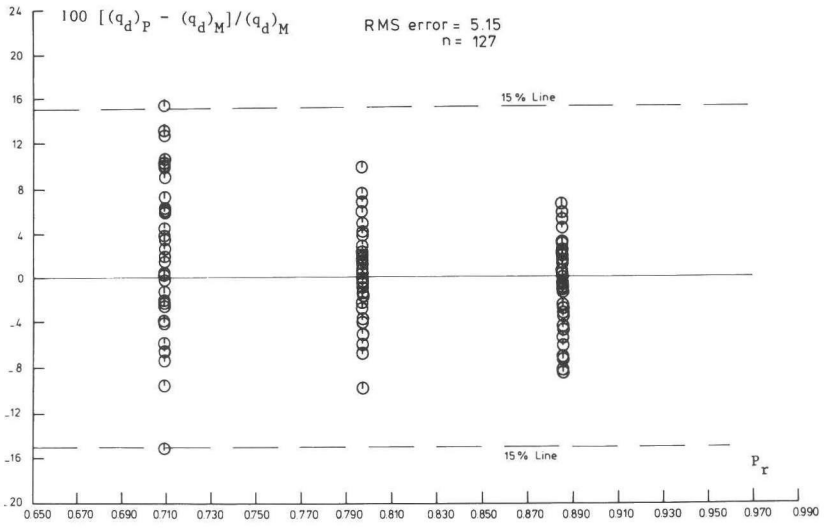

Fig. 6.5 Errors in predicting the dryout heat flux from the data of [P2] obtained for P = 15.7 - 19.6 MN/m^2.

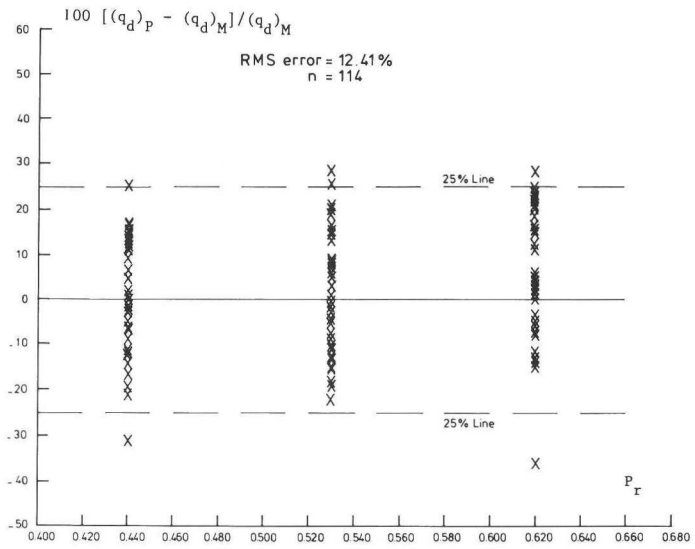

Fig. 6.6 Errors in predicting the dryout heat flux from the data of [P2] obtained for P = 9.8 - 13.7 MN/m^2.

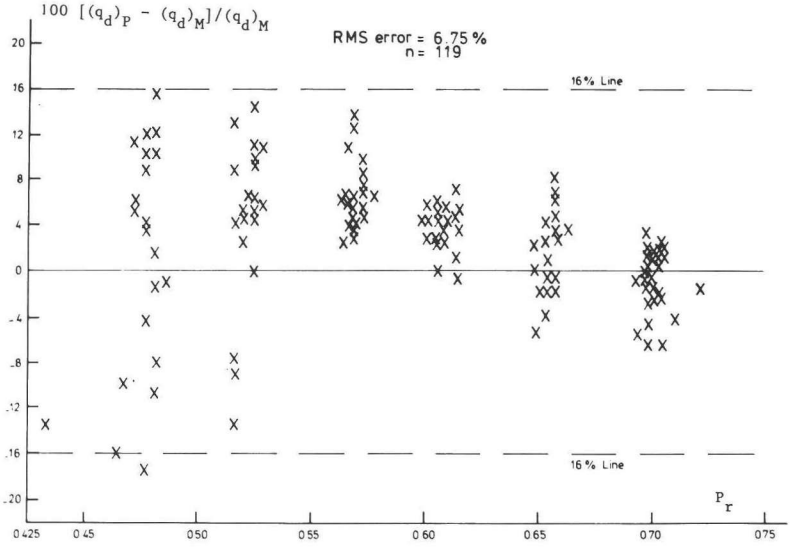

Fig. 6.7 Errors in predicting the dryout heat flux from the data of [C1] obtained for P = 9.7 - 16 MN/m^2.

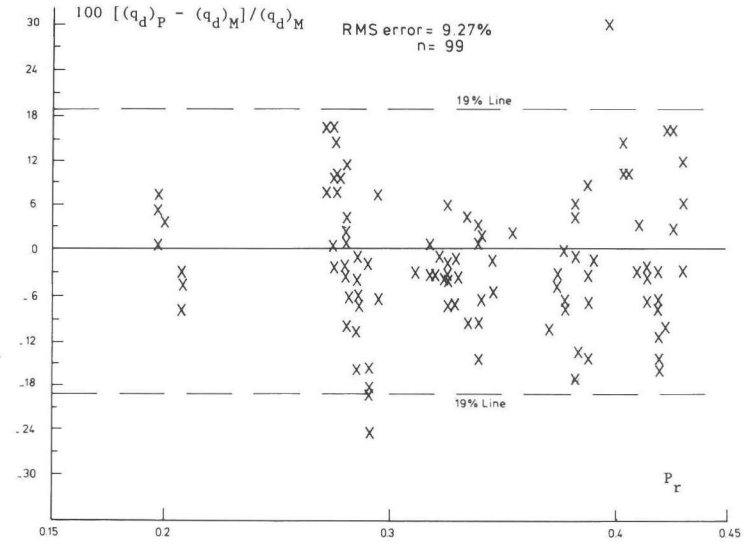

Fig. 6.8 Errors in predicting the dryout heat flux from the data of [C1] obtained for P = 4.3 - 9.5 MN/m^2.

The ranges of geometries and operating conditions of the data used to establish equation (6.2) are recapitulated as follows: Geometries and heating conditions: sodium heated helically coiled circular tubes, a sodium heated vertical circular tube and short and long, electrically heated vertical circular tubes; L_h = 0.25 - 40.13 m; $d/(2\ \delta)$ = 1.90 - 6.67; P = 4.3 - 20.2 MN/m^2; G = 112 - 5542 kg/m^2s; ΔT_{sub} = 8 - 273 K; X_d = 0 - 1; q_d = 41 - 4931 kW/m^2.

Equation (6.2) is not recommended for short tubes for pressures lower than 9.7 MN/m^2 since it has not been verified with the data obtained in these tubes for P < 9.7 MN/m^2.

In equation (6.2) d_c = 0 for vertical tubes and d_c = ∞ for horizontal tubes. The equation was not verified, however, with data from the latter.

6.2.2.3 Interpretation of Equation (6.2)

Equations (6.2) and (6.6) suggest that the effect on the heat flux for the first detected dryout of d_c/d is quite negligible beyond d_c/d = 38.9

The above ratio clearly affects the heat flux for the last detected dryout, as deduced from equations (6.2) and (6.7). This seems a logical result since before the last detected dryout most of the tube wall is not wetted by the liquid and the peripheral distribution of the liquid along the wall would, among other things, be a function of d_c/d. Before reaching the first detected dryout, the whole tube surface is wetted by liquid. It seems therefore that beyond $d_c/d = 38.9$, the mechanism of dryout in vertical tubes is similar to that in helical coils.

Equations (6.2) and (6.13) also suggest that the so-called equivalent length hypothesis is of physical importance for the mechanism of dryout.

6.2.2.4 The Length Between the First and Last Detected Dryouts

In order to determine this length for the sodium heated helically coiled tubes the well-known heat exchanger formulas will do. The required overall heat transfer coefficient is obtained as the average of the overall heat transfer coefficients predicted just before the first detected dryout and just after the last detected dryout. With the above procedure the aforesaid length could be predicted within 1.5% accuracy for the data presented. This accuracy was based on the total tube length.

6.3 TWO-PHASE FLOW PRESSURE DROP IN SODIUM HEATED STEAM GENERATOR TUBES AT ELEVATED PRESSURES

6.3.1 Experimental Data

Two-phase flow pressure drop was measured in three sodium heated helically coiled test tubes, i.e., in TT4, TT5 and TT6. For the determination of this pressure drop from the results of tests, the measured values were plotted versus the length of a test tube. A smooth curve was drawn through these values. The two-phase flow pressure drop was then obtained from this curve by assuming that $X = 0$ at the start of boiling and $X = 1$ at the termination of boiling if $X_o > 1$. In total 70 data were obtained. The range of operating conditions for these data is: $P = 14.9 - 20.1$ MN/m^2; $G = 296 - 1829$ kg/m^{2}s; $X_{bt} = 0.15 - 1.0$; $\Delta P_{tp} = 3.0 - 88$ kN/m^2. These operating conditions are also given in detail in Table A2.1 in Appendix 2.

6.3.2 Correlation of the Data

The two-phase flow pressure drop in a steam generator tube is the sum of the two-phase flow acceleration, gravitational and frictional pressure drop, i.e.,

$$\Delta P_{tp} = \Delta P_a + \Delta P_g + \Delta P_f \tag{6.21}$$

The two-phase flow acceleration pressure drop is due to the change in specific volume of the water/steam mixture along the steam generator tube. At elevated pressures, both water and steam can be assumed to be incompressible along the tube. For such a case, this pressure drop is given in [M1].

$$\Delta P_a = \frac{G^2}{\rho_l} \left\{ \frac{(1 - X_{bt})^2}{1 - \bar{\alpha}_{bt}} + \frac{X_{bt}^2 \rho_l}{\bar{\alpha}_{bt} \rho_v} - 1 \right\} \tag{6.22}$$

The two-phase flow gravitational pressure drop is due to the weight of the water/steam mixture in the steam generator tube. This pressure drop is per definition,

$$\Delta P_g = g \int_0^{\bar{\alpha}_{bt}} [(1 - \bar{\alpha}) \rho_l + \bar{\alpha} \rho_v] \, d\zeta \tag{6.23}$$

In order to evaluate equations (6.22) and (6.23), a proper void fraction correlation (i.e., a slip correlation) has to be used and the variation of the steam quality along the steam generator tube has to be known.

The two-phase flow frictional pressure drop is due to shear stresses in the water/steam mixture in the steam generator tube. This pressure drop is usually given by the following equation in the literature:

$$\Delta P_f = \Delta P_{lo} \frac{\Delta P_f}{\Delta P_{lo}} \tag{6.24}$$

where ΔP_{lo} is the frictional pressure drop if water with total mass flow flows in the steam generator tube, i.e.,

$$\Delta P_{lo} = 2 f l_B G^2/(d \rho_l) \qquad (6.25)$$

$\Delta P_f/\Delta P_{lo}$ in equation (6.24) is usually referred to as "two-phase flow friction multiplier". f in equation (6.25) is the single-phase flow friction factor, which should be evaluated at the state of saturation.

In the literature two models appear in principle to establish two-phase flow pressure drop correlations, the homogeneous flow model and the slip model. In the homogeneous flow model, the steam and water mixture flowing in the steam generator tube is accepted as a homogeneous mixture with a single velocity (i.e., slip ratio equals 1), while in the latter slip is considered between the two phases (i.e., slip ratio differs from unity). Both models use equation (6.21).

Before an attempt was made to correlate the present data, they were first compared with the well-known slip model of Martinelli and Nelson [M1] and the homogeneous flow model of Owens [O3]. Martinelli and Nelson have given the two-phase flow friction multiplier in equation (6.24) in a graphical form to be a function of the outlet steam quality and pressure. In accordance with Owens, this multiplier is

$$\Delta P_f/\Delta P_{lo} = [1 + (X_i + X_{bt}) (\rho_l/\rho_v - 1) / 2] \qquad (6.26)$$

Martinelli and Nelson, and Owens assumed a linear variation of steam quality along a steam generator tube. Martinelli and Nelson have not evaluated ΔP_g in equation (6.21); this can be done, however, straightforwardly using equation (6.23) and the void fraction correlation presented by these investigators.

Throughout this study, f, the single-phase flow friction factor in equation (6.25), is evaluated from Moody's correlation given in [K4] for straight tubes and from Ito's correlation for helical coils [I3]. The latter is

$$f = 0.079 \, Re^{-0.25} \, [Re \, (d/d_c)^2]^{0.05} \qquad (6.27)$$

and applies to the condition $Re \, (d/d_c)^2 > 6$.

The slip model of Martinelli and Nelson fitted the data rather well, i.e., between -14.6% and 28.9% accuracy with a RMS error of 14.5%. The homogeneous flow model of Owens fitted the data fairly well, i.e., between -22.8% and 11.4% with a RMS error of 7.5%. The above mentioned models were also checked with the 299 data of De Munk et al. [M7] obtained in a 10 m long, sodium heated vertical circular tube (i.e., in TT1). The operating conditions for these data were: P = 14.3 - 19.9 MN/m^2; G = 399 - 3498 kg/m^2s; X_{bt} = 0.06 - 1; ΔP = 8 - 226 kN/m^2. Both models fitted these data very poorly. The accuracy of the slip model was between -19% and 115% and that of the homogeneous flow model between -23% and 85%. The RMS errors were 38.7% and 25.9% respectively. Therefore the data presented and the data of [M7] were properly correlated using equation (6.21). For this purpose, the following two-phase flow friction multiplier was established:

$$\Delta P_f/\Delta P_{lo} = (1 + Y_{68}\ Y_{69}) \tag{6.28}$$

where

$$Y_{68} = 3850\ X_{bt}^{0.2}\ P_r^{-1.515}\ Re_l^{-0.758} \tag{6.29}$$

$$Y_{69} = 1 + Re_l^{0.1}\ (3.67 - 3.04\ P_r)\ [\exp\ (-\ 0.014\ d_c/d) - \exp\ (-\ 2\ d_c/d)] \tag{6.30}$$

For the present data void fraction was evaluated from the correlations presented in Section 3.2. Beyond a vapour volumetric rate ratio of 0.57, the flow was assumed to be homogeneous. For the data of [M7] void fraction was evaluated from the correlations given in Section 3.1.5. Beyond a vapour volumetric rate ratio of 0.9, the flow was assumed to be homogeneous. Thus, both for the present data and for the data of [M7], the flow patterns along the test tube were not considered.

In order to determine equation (6.23), it was assumed that the steam quality is a linear function of the axial coordinate and that the pressure is constant in the tube. For the present data equation (6.23) had to be determined with a numerical integration method up to a vapour volumetric rate ratio of 0.4. For this purpose, the trapezoidal rule was used.

The error in predicting the two-phase flow pressure drop is shown versus reduced pressure in Figs. 6.9 and 6.10 for the present data and the data of [M7]. The correlation predicts the two-phase flow pressure drop within 20% accuracy for 98% of the time. The RMS error for all the 369 data is 9.87%.

In equation (6.21) $d_c = 0$ for vertical tubes and $d_c = \infty$ for horizontal tubes. The equation was not verified, however, with the data from the latter.

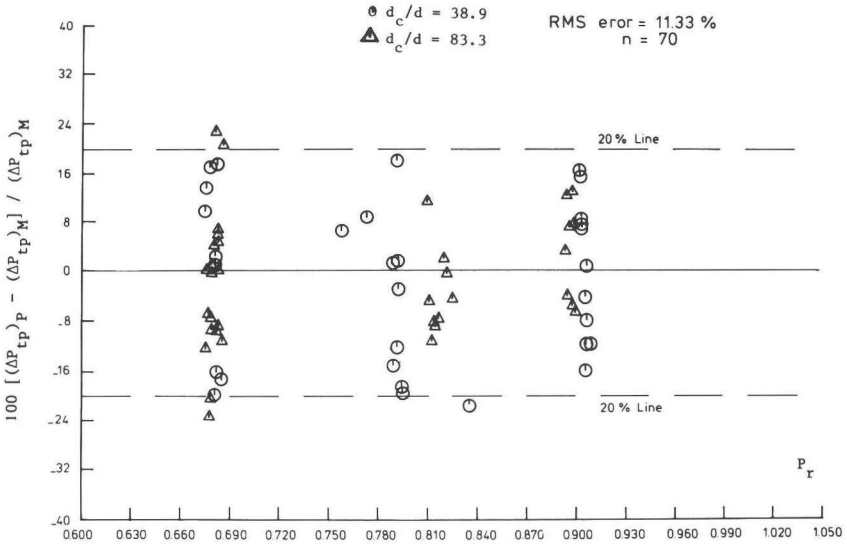

Fig. 6.9 Errors in predicting the two-phase flow pressure drop from the present data.

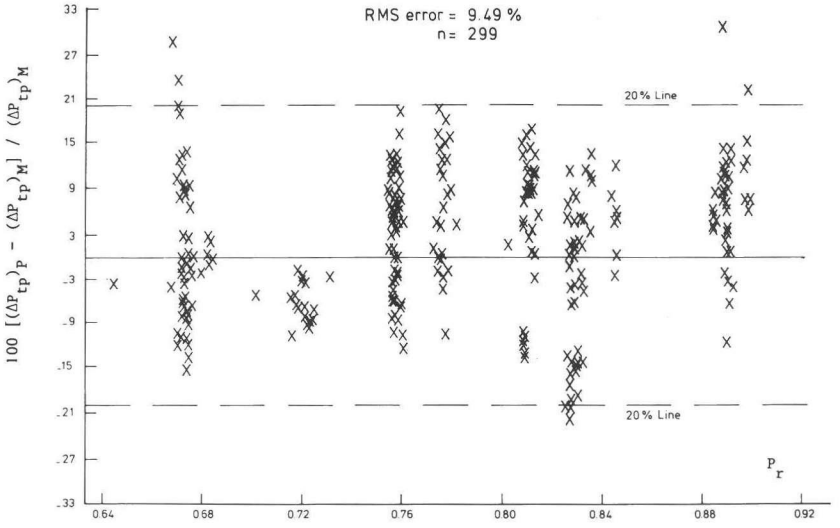

Fig. 6.10 Errors in predicting the two-phase flow pressure drop from the data of [M7].

Chapter Seven

TWO-PHASE FLOW INSTABILITIES IN STEAM GENERATOR TUBES

7.1 INTRODUCTION

7.1.1 The Phenomena

Two-phase flow instabilities jeopardize the safety of a steam generator since they cause flow maldistribution among the tubes or inside the tubes, and thermal cycling at the upper tube plate and at the dryout location.

For any single steam generator tube the pressure drop across the tube is practically constant. For such a tube a pressure drop-versus-mass flow curve of the shape indicated by (a) in Fig. 7.1 would obviously imply that three mass flows are possible for a given pressure drop. In the AB-region, where $d(\Delta P)/dW$ is negative, the flow is unstable. If the tube operates with a mass flow in this region, the mass flow will take a steady-state value in the DA- or BC-region after a small disturbance of the flow and will not return to its original state. A sudden decrease to the DA-region may cause serious damage to the tube because of inadequate cooling. This type of instability is referred to in the literature as static, aperiodic or Ledinegg instability [L1], or sometimes also as flow excursion. The Ledinegg instability can be prevented by installing a flow resistance such as an orifice at the inlet of the tube. In that case, curve (a) in Fig. 7.1 will be modified to curve (b).

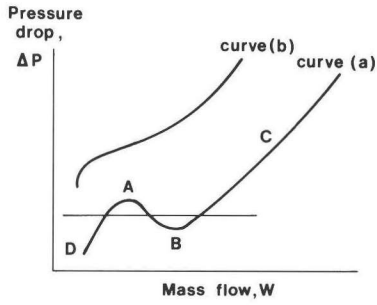

Fig. 7.1 Pressure drop characteristic of a steam generator tube.

Even if the pressure drop versus mass flow is like curve (b) in Fig. 7.1, the steam generator tube is still susceptible to dynamic instabilities, i.e., periodic flow or/and temperature oscillations. Many types of dynamic instabilities can occur in a steam generator tube, which can be ascribed to a number of different causes, i.e., propagation of

pressure or density waves [P4], variation of flow patterns [J1] and thermodynamic non-equilibrium between the phases in the superheated steam region [R2]. However, sufficient evidence has been presented in the literature that the main type of dynamic instability of interest to the design of steam generators is that caused by the propagation of density waves. This type of instability is referred to as density-wave [S15], time-delay [B11] or mass flow-void feedback [N3] instability or oscillations. In the text the words "oscillation" and "instability" are used indiscriminately, though strictly speaking an oscillation would have to diverge to become unstable. In the present study observed Density Wave Oscillations (DWO) always began with small amplitudes and thereafter reached a so-called limit cycle, i.e., they became sustained, as shown in Figs. 7.2, 7.3 and 7.4.

DWO are due to multiple regenerative feedback between the flow rate, the vapour generation rate and pressure drop [N3], and are well explained by Vriesema [V1] for an evaporator tube with uniform and constant heat supply:

"An increase in feedwater mass flow rate leads to an opposite variation in mixture quality: the same amount of steam (constant heat supply) is, as it were, mixed with a larger amount of water. This quality variation propagates through the evaporator at approximately the speed of the mixture. The dynamic storage of water, caused by the decrease in average void fraction, delays the response of the velocities and hence of the pressure drops further down-stream in the evaporator. As the frictional pressure drop is concentrated near the end of the evaporator tube where velocities are highest, the pressure drop response of the entire tube will be delayed. Under unfavourable conditions this time delay between disturbance (feedwater flow variation) and reaction (opposing pressure drop variation) may result in a positive feedback causing a diverging oscillation."

DWO have been extensively studied during the last two decades. For a detailed literature survey on the subject, the reader is referred to [B12]. In the following only the literature data found pertinent to the present study are briefly reviewed.

7.1.2 Previous Investigations on DWO in Steam Generator Tubes and in Freon Systems

7.1.2.1 Experimental Evidence

The sources of available experimental DWO data may be classified according to

- heated fluid
- forced circulation versus natural circulation system
- exit quality
- heat supply: electric, i.e., imposed heat flux (with or without axial variations) versus heating fluid
- arrangement: single versus multi tubes, with versus without by-pass.

The DWO data from steam generator tubes are given in [B5, B6, B15, D2, D4, F1, K8, L7, N3, Q1, S3, S11, V1, W3] and the DWO data from Freon systems in [C8, K1, S2, S15]. These data were obtained either from forced circulation systems [B15, C8, D2, F1, K1, K8, Q1, S2, S3, S15, V1, W3] or natural circulation systems [B5, B6, D4, L7, N3, S11]. In the works of [B15, D2, F1, K8, S3, V1, W3], the thermodynamic steam quality at the outlet of the test section was larger than 1 (i.e., once-through operation) and in the works of [B5, B6, C8, D4, K1, L7, N3, Q1, S2, S11, S15] smaller than 1. The test sections used in these investigations were heated either electrically [B5, B6, C8, D2, D4, L7, K1, N3, Q1, S2, S11, S15] or by a fluid, i.e., by sodium [B15, K8, S3, W3], a molten salt [V1] and a gas [F1]. In the works of [B5, B6, D4, L7, N3, Q1, S2, S11, S15, V1], a single tube was used and in those of [B15, C8, D2, F1, K1, K8, S3, W3] multi tubes consisting of 2 up to 139 tubes. In the investigations reported by [C8, Q1, S2], a large by-pass pipe was built around the test tube in order to maintain the pressure drop in the tube constant. The conclusions of the the above mentioned studies on which most theoretical investigations also agree are summarized below.

DWO are low frequency flow oscillations, the period of which is of the same order of magnitude as the transit time of a fluid particle in the steam generator tube. There is a "rule of thumb" in the literature that the period of the DWO is approximately one or two times the transit time of a fluid particle in a tube [B12, K3], though Yadigaroglu and Bergles [Y1] have reported that it may be only a small fraction of the transit time in the higher mode region.

The variables affecting the DWO are geometry, pressure, inlet subcooling, heat flux, thermal conductivity and specific heat of the tube

material, and axial pressure and heat flux distributions in the tube. The other parameters being constant, the stability of a steam generator tube may be increased by decreasing the heat flux [Q1], the exit pressure drop [B6] (i.e., outlet throttling), the heated length [C8] and the inlet subcooling at low subcoolings [B6, C8, S11], and by increasing the flow [Q1], the pressure [B6, S11], the inlet pressure drop [B6, L7] (i.e., inlet throttling), the inlet subcooling at high and medium subcoolings [B6, C8, S11] and the tube diameter [S11]. A non-uniform heat flux distribution stabilizes the flow [D4]. All the above conclusions were based on data obtained in steam generator tubes, in which no superheated steam was produced. Some of these were the result of one investigation only.

7.1.2.2 Methods for Predicting the Inception Conditions of DWO

In the literature, two entirely different methods, i.e., a stability model or a purely empirical relation is used to predict the inception conditions of the DWO.

7.1.2.2.1 Stability Models

A stability model for a steam generator tube is a simultaneous solution of one dimensional non-steady state, linearized or non-linearized continuity, momentum and energy conservation equations with appropriate boundary conditions and subsidiary equations [B6, B9, B11, B12, D1, D2, D4, J2, K3, N3, P4, Q1, S7, S10, S11, V1, Z1]. The last mentioned equations are correlations for the properties of water and steam, empirical correlations for void fraction, heat transfer and pressure drop for different flow regimes in a steam generator tube, and a correlation for the thermal non-equilibrium condition in subcooled nucleate flow boiling. Almost all the stability models given in the literature are computer programs.

Three main approaches have been used in the literature for the solution of the three conservation equations:

a. Non-linear approach: In this approach, the non-linear conservation equations and the subsidiary equations are solved simultaneously with a numerical or an analog method for a given large or small disturbance

The solution is capable of supplying information about inception conditions, frequency and amplitude of the DWO. A large computer is needed to perform such an analysis. An example of this type of solution is the model of Solberg and Bakstad [S10].

b. Linear approach: In this approach, the highly non-linear conservation equations are first linearized. The simultaneous solution of these linearized equations and the subsidiary equations is carried out in such a way that the solution yields the transfer function of the steam generator. Thereafter this transfer function is analyzed with the methods of well-known feed-back theory. A computer is needed for the solution. From this type of solution, only the inception conditions of the DWO but not the amplitude and frequency of the DWO can be obtained, since the three conservation equations are highly non-linear. An example of this type of solution is the model of Vriesema [V1, V2] which is applicable to a broad range of geometries and conditions. One of the most interesting aspects of the model is that it also permits a detailed sensitivity analysis. This type of solution is justified to determine the inception conditions of the DWO, since these oscillations always begin with small amplitudes and therefore non-linearities in the three conservation equations need not be considered.

c. Analytical approach: In this approach linearized conservation equations and the subsidiary equations are solved with an analytical method. For this purpose, these equations have to be significantly simplified. The example is the model of Zuber [Z1]. This type of solution may be suitable for the phenomenological analysis of the DWO.

For a detailed analysis of the stability models, the reader is referred to the works of Neal and Zivi [N3] and Bjørlo et al. [B9], and the thesis of Vriesema [V1].

It is well known that neither do the one-dimensional continuity, momentum and energy equations completely describe two-phase flow [K3, P4] nor have the heat transfer, void and pressure drop correlations used in the stability models presented in the literature have been developed or even verified for non-steady state conditions [B9, K3, N3, P4]. Furthermore, because of error margins in the aforesaid correlations and errors in the measurement of the inception conditions of the DWO, a

stability model can not, in general, predict the power at the inception of the DWO closer than about 10% accuracy. This margin may be much larger for some of the stability models given in the literature, as demonstrated by Neal and Zivi [N3] and Bjørlo et al. [B9]. Neal and Zivi have compared 6 selected stability models with some or all of the 52 data of various investigators taken in forced and natural circulation steam generator tubes for a wide range of operating conditions and geometries. These models apply to the condition $X_o < 1$, and appear to predict the power at the start of the DWO deviating by more than 95% from the measured value [N3]. The authors obtained the best results with the model of [J2], which predicts the power at the start of the DWO deviating by not more than about 20% from the measured value for "about 70% of the time" [N3]. For the rest of the time the model, however, gives the power with accuracies varying from 20% to 95%. Stability models which can be applied to a once-through steam generator tube are scarce in the literature [D1, D2, E1, V1, W3]. It is reported in [D2, F1] that the model given in [D1] does not fit the data well. A similar conclusion can also be drawn for the models of [V1, W3].

7.1.2.2.2 Empirical Relations

The work of Shotkin [S7, S8] and Kuboto et al. [K8] can be mentioned. Shotkin suggested that the data for the DWO can be correlated in the q/G versus $(H_l - H_i)$ plane, provided that systematic tests are carried out for the determination of the so-called crucial boiling length. If the length of the boiling region in a tube is less than this length, then DWO will occur.

Very recently, following the approach used in [F1, U6], Kuboto et al. [K8] correlated very well the data for the DWO obtained in sodium heated helically coiled once-through steam generator tubes. For this purpose they established simple equations. They did not, however, explain why these simple equations should fit well the data for the DWO despite the complexity of this phenomenon.

7.1.3 Chapter Objectives

It is concluded from the above section and from the literature not

discussed here for the sake of brevity, that there exists no adequate and general criterion to determine the inception conditions of the DWO for a wide range of conditions, especially for once-through steam generator tubes. One of the reasons of this is the lack of systematic experimental data for the inception conditions of the DWO, as already indicated by Saha et al. [S2].

The aim of this chapter of the thesis is to report the results of experiments carried out to determine the inception conditions of the DWO in 4 sodium heated, forced circulation once-through steam generator tubes, (TT1, TT2, TT3 and TT4), and in the evaporator of Neratoom's 50 MW steam generator. The present data and the data of various investigators taken in sodium and electrically heated, forced circulation once-through steam generator tubes were correlated accurately. Two different correlations were obtained to predict the power at the inception of the DWO. One of them was based on the geometrical parameters and a few operating conditions and the other on the geometrical parameters and all the operating conditions. Both correlations were closely related to the physical mechanism of the DWO. An empirical relation was established for the multiple regenerative feedback mechanism, which caused the DWO in the test tubes.

The data given in the literature for the inception conditions of the DWO in natural circulation steam generator tubes were also correlated.

In this chapter data are also presented for flow pattern instabilities observed in TT1, TT5 and TT6 and for the instabilities due to thermodynamic non-equilibrium between the phases in the superheated steam region.

7.2 DENSITY WAVE OSCILLATIONS (DWO)

7.2.1 Forced Circulation Systems

7.2.1.1 Tests

7.2.1.1.1 Overview of Test Program

The inception conditions of the DWO were measured in TT1, TT2, TT3 and TT4 and in the evaporator of the Neratoom's 50 MW steam generator. A by-pass pipe was used for each test tube in order to keep the total pressure drop in the tube constant. The tests were carried out in such a way that the effects of all operating conditions and inlet throttling on the stability could be determined. For this purpose, the outlet steam

quality at the inception of the DWO was measured within about 2.5% accuracy for most of the tests carried out in TT3 and within 6% accuracy for the remaining tests. In total 351 data for the inception conditions of the DWO were obtained (i.e., 11, 1, 160, 146 and 33 data from TT1, TT2, TT3 and TT4 and the evaporator respectively). The ranges of geometries and operating conditions of these tests are summarized in Table 7.1.

In the early stage of the study tests were only carried out in TT1, TT2 and in the evaporator. The results of these tests revealed that the outlet steam quality at the start of the DWO was practically constant for a given pressure, geometry and inlet throttling. These tests were carried out at low and medium subcoolings (i.e., $\Delta H = 0.096 - 0.38$) and for $P = 5.3 - 17$ MN/m^2. During the tests, the test tubes and the evaporator operated in the once-through and forced circulation modes. Quandt [Q1] has also drawn a similar conclusion from the results of his own tests carried out in a very short rectangular tube at low and medium subcoolings for $P = 4.1 - 11$ MN/m^2. For these tests, superheated steam was not produced in the test tube and the tube operated in the forced circulation mode. Although the above phenomenon could not be explained, the 44 data from TT1 and the evaporator and the 62 data of various investigators taken in sodium and electrically heated, forced circulation steam generator tubes [B15, D2, D3, Q1, S3, W3] were correlated accurately with a simple equation. Using the data from TT3 and TT4, this equation was modified later for the effect on the DWO of inlet throttling. The established correlation predicted the power at the start of the DWO within 8% accuracy for 87% of the time with a RMS error of 5.97% from all the 413 data considered.

In a later stage of the study, extensive and systematic tests were carried out in TT3 and TT4 at medium and high pressures in order to be able to explain the above mentioned phenomenon related to the outlet steam quality at the start of the DWO. During the tests the test tubes operated in once-through and forced convection modes. In total 306 data were obtained for the inception conditions of the DWO. From the results of these tests, it was also concluded that the outlet steam quality at the inception of the DWO is a function of pressure for a given inlet throttling in each test tube, whereas the effects of all the other operating conditions on this steam quality are of secondary importance. This phenomenon as well as the mechanism of the DWO observed in the test tubes were clari-

Table 7.1 The Ranges of Geometries and Operating Conditions of the Present Data for the Inception Conditions of the DWO

Test tube/component *	P	G	X_{IC}	ΔT_{sub}	W_n/W_w	By-pass	K	ψ
	MN/m^2	kg/m^2s		K		ratio		s
TT1 (a vertical tube); d = 7.86 mm; L_t = 10 m	6.2-14.1	706-1365	1.14-1.34	27 -81.6	10.3-18	7.2-14	10.7	1 - 2.6
TT2 (a tube comprised of a 10 m vertical and an 8.84 m V-shaped horizontal tube); d = 7.86 mm	14.1	353	1.40	78.2	11.4	11.6	713	2
TT3 (a tube comprised of a 9.40 m vertical and an 11.05 m V-shaped horizontal tube); d = 13.12 mm	7.6-19	439-1020	1.37-2.20	23 -166.3	8.8-19.9	0.1-13	54.7-382.9	1.3- 7
TT4 (a helical coil, d_c/d = 83.3); d^c= 18 mm; L_t = 44.43 m	6 -19.1	187- 768	1.15-2.38	3.2-168	8.6-29.5	2.2-12	15 -665	2.8-13.5
Evaporator consisting of 139 tubes; d = 12.6 mm; L_t = 19.34 m	5.3-17	-	1.10-1.59	23.9-111	-	$\simeq$ 139	0	4 - 7.6

* The test tubes and the evaporator operated in once-through and forced convection modes during the tests, and were heated by sodium.

fied. An empirical relation was established for the multiple regenerative feedback mechanism, which caused the DWO in the test tubes. The present data and the data of various investigators taken in sodium and electrically heated forced circulation, once-through steam generator tubes, thus in total 380 data were correlated accurately. The established correlating equation predicted the power at the start of the DWO within 7.5% accuracy for 98% of the time with a RMS error of 3.33%. All of the above 380 data were obtained in once-through steam generator tubes.

7.2.1.1.2 Tests in TT3 and TT4

The inception conditions of the DWO are defined here as the operating conditions of the stable run made just before the run in which the DWO appear. In order to generate the DWO during most of the tests the steam quality at the outlet of each test tube was increased by very small increments by raising the sodium side inlet temperature. For a few tests the DWO were created by decreasing only the water/steam side pressure. The DWO were detected by observing the recordings of the water/steam side mass flow on the six-channel recorder. When the limit-cycle mass-flow oscillations appeared on the recorder, as shown in Fig. 7.2, the operating conditions of the previous stable run were specified as the inception conditions of the DWO. It was also ensured that the observed oscillations fulfilled the three conditions: a. That they stay sustained. b. That they disappear when the sodium-side inlet temperature is decreased or when the water/steam-side pressure is increased. c. That their period is of about the same order of magnitude as the transit time of a fluid particle in the test tube.

For 82% of the tests carried out in TT3 and 45% of the tests carried out in TT4, the sodium side inlet temperature was increased in steps of 5 K or the water/steam side outlet pressure was decreased in steps of 0.25 MN/m^2. For the rest of the tests, the increment or the decrement in the aforesaid temperature and pressure was in 10 K and 0.56 MN/m^2 steps, respectively.

A typical example of the DWO detected in the TT4 is shown in Fig. 7.2. Just after the operating conditions were measured at the time t_1 the sodium side inlet temperature was increased by a step of 5 K. The time axis shown

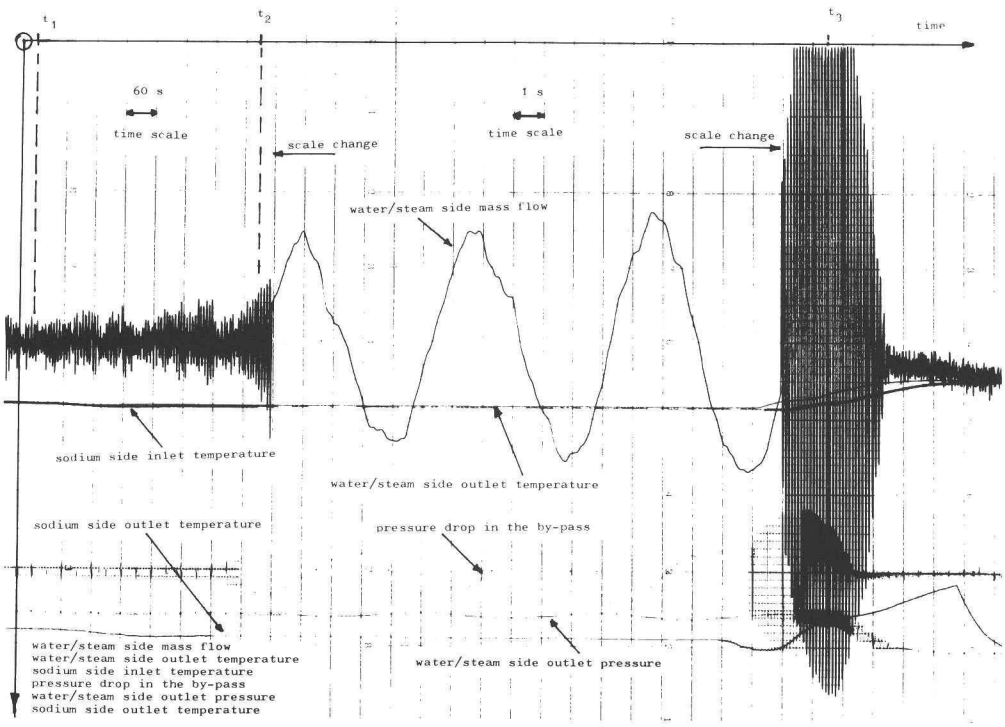

Fig. 7.2 DWO in TT4

in the figure applies only to the measurement of the mass velocity. The vertical axis is linear. At the origin of the coordinate system, all the measured quantities were equal to zero. Limit cyle oscillations began to develop at about the time t_2. These oscillations reached their maximum amplitude at the time t_3. The peak-to-peak amplitude of these oscillations was then 200% of the value of the mass flow measured at the time t_1. Thereafter the sodium side inlet temperature was decreased and the water/steam side pressure was increased. The oscillations then disappeared. The operating conditions taken at the time t_1 were considered as the inception conditions of the DWO, and they were: $P = 15.05\ MN/m^2$; $G = 598\ kg/m^2s$; $T_o = 609.9°C$; $\theta_i = 610.1°C$; $T_i = 301.0°C$; $W_n/W_w = 8.81$; by-pass ratio: 3.55. The sodium side inlet temperature was constant and practically equal to the water/steam side outlet temperature during the oscillations.

Most of the tests were carried out systematically; in other words the effects on outlet steam quality, at the inception of the DWO, of water/steam side inlet subcooling, mass velocity, outlet pressure and inlet throttling, and the ratio of the mass flow in the sodium side to that in the water/steam side were investigated at several pressure levels (i.e., P = 14, 16 and 18 MN/m^2). For this purpose, the outlet steam quality at the inception of the DWO was measured for several values of one of the aforesaid parameters, while the other parameters were kept constant and the measurements were repeated at several pressure levels.

A total of 2240 tests were carried out. In 160 tests with TT3 and in 146 tests with TT4, DWO were observed. The range of operating conditions for the data obtained for the inception conditions of the DWO are given in Table 7.1. These operating conditions are presented in detail in Tables A3.1 and A3.2 in Appendix 3. (The tables are quite lengthy; therefore they are placed in Appendix 3).

The period of the observed mass flow oscillations was between 1.3 and 7 s in TT3 and between 2.8 and 13.5 s in TT4. Peak-to-peak amplitudes of these oscillations varied from 30% to 200% of the mass flow recorded at the last stable test run. The water/steam side outlet temperature did not oscillate.

In the tests carried out in TT3 with high inlet subcoolings, the outlet pressure also oscillated. The peak-to-peak amplitude of these oscillations was up to a few percent of the outlet pressure and their period was equal to that of the mass flow oscillations. There was a phase difference between these two oscillations. During the tests carried out with low inlet subcoolings, no pressure oscillations were observed, nor during the tests carried out with high inlet subcoolings and very small by-pass ratios. The tests carried out in TT4 were less susceptible to pressure oscillations than those carried out in TT3. The generation of pressure oscillations is explained as follows: The amount of highly superheated steam produced in the test tube varies periodically. This superheated steam condenses completely in the cold water in the upper header coming from the by-pass. This causes variations in pressure, since the volume of the high pressure part of the loop is small, as mentioned before.

During all the stable test runs for which $X_o > 0$, mass flow oscillations with small irregular periods and amplitudes were always present

in both test tubes. These irregular mass flow oscillations were assumed to be caused by boiling noise and the noise created by the flow in the rather small diameter by-pass pipe. Because of these irregular mass flow oscillations mass flow in the water/steam side was measured at one-second intervals for 10 seconds and the arithmetic average of the measurements was considered.

7.2.1.1.3 Tests in TT1 and TT2

In order to produce DWO in these test tubes the steam quality at the outlet of each test tube was increased by very small increments, either by increasing the sodium side mass flow or/and the inlet temperature and keeping the water/steam side mass flow constant or by decreasing the water/steam side mass flow and keeping the sodium side inlet temperature and mass flow constant for a constant inlet subcooling and pressure at the water/steam side. The DWO were detected by recording water/steam side outlet temperature (for all the tests) and flow (only in TT2) on a two-channel line recorder. When the first diverging temperature oscillations in TT1 and temperature and flow oscillations in TT2 appeared on the recorder, the operating conditions of the previous stable run were specified as the inception conditions of the DWO. It was also checked whether the requirement was fulfilled that the temperature oscillations in TT1 and the temperature and flow oscillations in TT2 reached a limit cycle and thereafter were sustained in the test run for which the DWO were detected.

A total of 59 tests were carried out. The operating conditions of these tests were given in detail in [U5]. For 11 tests with TT1 and for 1 test with TT2 DWO were detected. The operating conditions for the data obtained for the inception conditions of the DWO are summarized in Table 7.1 and given in detail in Table 7.2. The throttling coefficient K of the flow meter at the inlet was not measured for TT1. The value of 10.7 listed in the table derives from the manufacturer's specifications.

Peak-to-peak amplitudes of the observed DWO varied between 14 and 50 K and the periods between 1 and 2.6 s. An example of these oscillations is shown in Fig. 7.3.

Table 7.2 DWO Data from TT1 and TT2

Test tube	P MN/m^2	K	G kg/m^2s	ΔT_{sub} K	X_{IC}	$\frac{W_n}{W_w}$	θ_i °C	ψ s
TT1	12.1	10.7	1105	36.0	1.22	11.7	471.2	2.0
"	12.1	10.7	1129	35.1	1.20	11.5	470.5	2.0
"	12.1	10.7	1094	29.7	1.24	11.9	472.7	2.0
"	6.3	10.7	1365	74.0	1.19	12.7	466.2	1.0
"	6.2	10.7	1179	29.2	1.21	12.1	450	2.0
"	6.2	10.7	1199	33.3	1.14	11.4	444.8	2.0
"	14.1	10.7	737	79.6	1.31	18.0	436.8	2.0
"	14.1	10.7	728	79.9	1.32	15.2	445.8	2.0
"	14.1	10.7	724	81.5	1.29	12.6	454.9	2.0
"	14.1	10.7	706	81.6	1.34	10.3	475.6	2.6
"	12.2	10.7	980	27.0	1.28	13.4	464.3	2.0
TT2	14.1	713	353	78.2	1.40	11.4	455.9	2.0

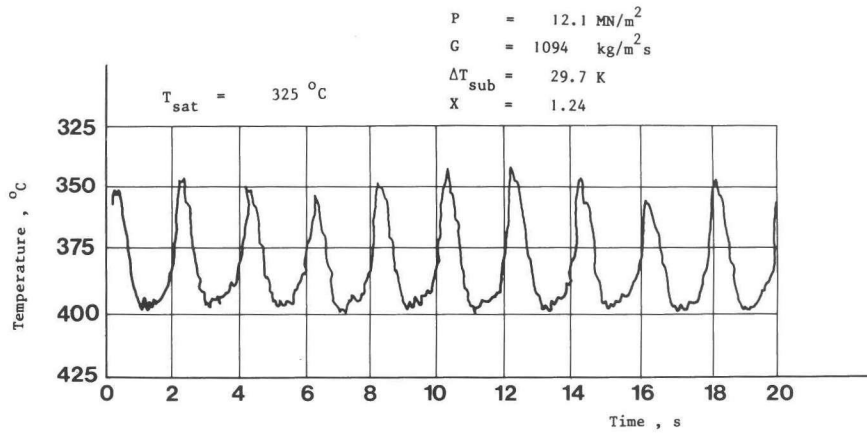

Fig. 7.3 A typical example of density wave oscillations in TT1.

7.2.1.1.4 Tests in the Evaporator of the 50 MW Steam Generator

At all operating conditions of SNR-300, the evaporator produces wet

steam of qualities of 0.95 or less, and it is not susceptible to instabilities. Under extreme conditions far remote from the operating conditions of SNR-300, instabilities were observed, however, when steam with a high degree of superheating had to be produced in the evaporator; in other words the evaporator operated as a once-through steam generator for the test runs for which the instabilities were detected.

In order to produce the DWO in the evaporator, the steam quality at the outlet of the evaporator was increased by very small increments by decreasing water/steam side mass flow while keeping the other operating conditions constant both at the water/steam and sodium side. Detection equipment for DWO in the form of thermocouples was installed for the 6 tubes indicated in Fig. 2.4, by recording the temperatures at the outlets of these tubes. The inception conditions of the DWO were determined with a procedure similar to that described in Section 7.2.1.1.2. The difference between the water/steam-side outlet temperatures of two successive test runs did not exceed 10 K. During a test run, the total mass flow in the unit and the temperature and pressure at the outlet and inlet of the unit were kept constant.

For almost all the test runs, instabilities were first detected in the tubes located at the outer tube bundle region; i.e., for the tubes numbered 233 and 238 in Fig. 2.4. If the mass flow was decreased further, the tubes in the inner tube bundle region also became unstable. The operating conditions for the data obtained for the inception conditions of the DWO in the aforesaid 6 tubes are summarized in Table 7.1 and given in detail in Tables 7.3 and 7.4.

The peak-to-peak amplitudes of the observed DWO varied between 9 and 60 K and the periods between 4 and 7.6 s. An example of these oscillations is shown in Fig. 7.4.

The flow at the inlet of the evaporator was not throttled.

During some test runs, outlet temperature oscillations with small irregular periods and amplitudes of a few degrees Kelvin were observed. These were probably caused by multiple irregular interactions between flow rate, pressure drop and vapour generation rate due to mode of operation, viz. by decreasing the mass flow in the unit in small steps; these instabilities disappeared after some minutes.

Table 7.3 Data for the Inception Conditions of the DWO in the Tubes of the Evaporator

Run No.	Location 233 T_o (°C)	Location 233 ψ (s)	Location 238 T_o (°C)	Location 238 ψ (s)	Location 229 T_o (°C)	Location 229 ψ (s)	Location 235 or 225 T_o (°C)	Location 235 or 225 ψ (s)
1.3*	437+	-	433+	7	-	-	-	-
2.4	428+	-	-	-	-	-	-	-
2.5	-	-	428	6.7	-	-	-	-
3.7	408+	-	405+	7.5	405	7	-	-
4.4	399+	-	399+	6.7	-	-	-	-
13.2	430+	-	427+	5	427	5.5	-	-
13.4	-	-	-	-	-	-	430/431‡	6/6‡
14.0	418+	-	-	-	-	-	-	-
14.2	-	-	429	7.6	-	-	-	-
14.3	-	-	-	-	434	6	-	-
14.4	-	-	-	-	-	-	423‡	6.6‡
14.5	-	-	-	-	-	-	430	7.5
15.0	418+	-	-	-	-	-	-	-
15.4	-	-	431	6.6	431	7	-	-
19.7	382+	5	-	-	-	-	-	-
19.8	-	-	-	-	372	6	-	-
20.3	386+	4	-	-	-	-	-	-
21.3	367+	4	-	-	-	-	-	-
21.8	-	-	-	-	389	5	-	-
22.1	380+	4	-	-	-	-	-	-
26.2	424+	6.6	-	-	-	-	-	-
26.5	-	-	427	6	-	-	-	-
26.9	433	6	-	-	-	-	-	-
28.9	374+	4	-	-	-	-	-	-
33.0	-	-	315	5	-	-	-	-

* For the values of P and T_i, see the corresponding run in Table 7.4.

\+ Hot channel, in which the instabilities occur first.

‡ Location 225.

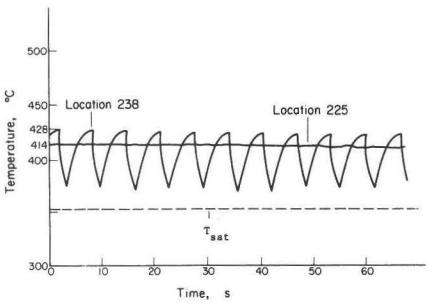

Fig. 7.4 Typical example of density wave oscillations in the evaporator.

Table 7.4 Operating Conditions for the Evaporator

	Sodium side				Water/steam side		
Run No.	W_n (kg/s)	θ_i (°C)	Q (MW)	W_w (kg/s)	T_i (°C)	T_o (°C)	P (MN/m^2)
1.3	170	452	21.2	13.0	286	394	16.7
2.4	170	442	18.9	11.5	286	396	16.7
2.5	170	442	18.1	10.7	286	409	17.0
3.7	174	421	14.8	8.6	286	395	17.0
4.4	179	403	8.7	4.7	286	400	16.7
13.2	174	440	18.1	11.5	302	404	16.7
13.4	173	443	15.1	9.2	301	418	16.6
14.0	183	440	22.3	13.9	260	364	16.8
14.2	182	442	20.0	10.8	260	410	16.7
14.3	186	442	19.5	10.0	260	419	16.7
14.4	186	441	18.1	9.2	259	418	16.5
14.5	179	441	16.1	8.7	259	414	16.8
15.0	172	439	21.8	12.8	240	374	16.8
15.4	173	441	18.8	9.8	240	416	16.7
19.7	122	408	10.4	6.2	300	337	12.8
19.8	121	408	10.1	5.5	300	359	12.2
20.3	125	411	12.5	7.4	280	330	12.3
21.3	123	408	12.2	6.8	260	330	12.3
21.8	120	412	10.5	5.7	260	356	13.4
22.1	124	409	11.9	6.5	240	337	13.4
26.2	126	434	12.1	6.7	301	422	16.2
26.5	126	436	12.9	7.4	301	418	16.3
26.9	127	441	14.5	8.4	300	411	16.2
28.9	121	386	11.3	5.9	281	324	9.2
33.0	62	351	6.6	2.5	214	305	5.3

7.2.1.2 Data Reduction

The outlet steam quality at the inception of the DWO was determined from the measured outlet temperature and pressure in TT3, TT4 and in the evaporator since $X_o > 1$, and by means of a heat balance in TT1 and TT2 due to thermodynamic non-equilibrium between the phases at the outlet of these test tubes.

Throughout this chapter the measured outlet pressure is used for the evaluation of the properties of water and steam since $P >> \Delta P$ for the data obtained.

In TT3 and TT4, the lengths of the superheated steam, boiling and preheat regions were determined by plotting the steam quality versus tube length and assuming $X = 1$ and $X = 0$ at the beginning of the super-

heated steam and boiling regions, respectively. The steam quality was calculated from a heat balance. The variation of the steam quality was assumed to be linear between the calculated two values. The steam quality was calculated at 17 locations in TT3 and at 11 locations in TT4.

In order to predict the transit time of a fluid particle in a heat transfer region, the average density in the region has to be known, (see equation (7.4)). For the superheated steam region the average density was determined using the arithmetic mean temperature in the region. For the preheat region, the transit time was calculated as the sum of the transit times in the adiabatic and heated parts of the region. In the boiling region, the average density has been calculated with the following formula,

$$\rho_B = \frac{1}{l_B} \int_0^{l_B} [(1 - \bar{\alpha})\ \rho_l + \bar{\alpha}\ \rho_v]\ d\ \zeta \qquad (7.1)$$

, assuming a linear axial variation of the steam quality. In TT3 boiling took always place in the horizontal part of the tube. Void fraction in equation (7.1) was therefore evaluated for TT3 and TT4 with the correlation given in [A9] for horizontal tubes up to a vapour volumetric rate ratio of 0.9. Thereafter the flow was assumed to be homogeneous. For the data of [Q1], void fraction was evaluated from equation (3.32).

K, the inlet throttling coefficient, was determined from the equation below,

$$\Delta P = K \frac{G^2}{2\ \rho_i} \qquad (7.2)$$

where ΔP is the pressure drop across an orifice or a flow control valve installed at the inlet of a test tube, G, mass velocity in the test tube, and ρ_i, the density of the fluid at the inlet of the test tube.

7.2.1.3 Discussion of the Results of the Tests carried out in TT3 and TT4

In these test tubes extensive tests were carried out and 306 data for the inception conditions of the DWO were obtained. The analysis of the

results of these tests yielded the basic mechanism of the DWO in once-through steam generator tubes, which are discussed in the following sections.

7.2.1.3.1 The Mechanism of the DWO

As discussed in Section 7.1.1, the observed DWO in both test tubes are time delay oscillations. The length of the superheated steam region and the transit time in this region are of vital importance for the mechanism of the DWO. This can be shown as follows: In Fig. 7.5, the relationship at the inception of the DWO between the reduced outlet pressure P_r, the inlet throttling coefficient K, and the ratio of the length of the superheated steam region to the total tube length l_s/L_t, is shown for TT3. This figure shows that (l_s/L_t) at the inception of the DWO

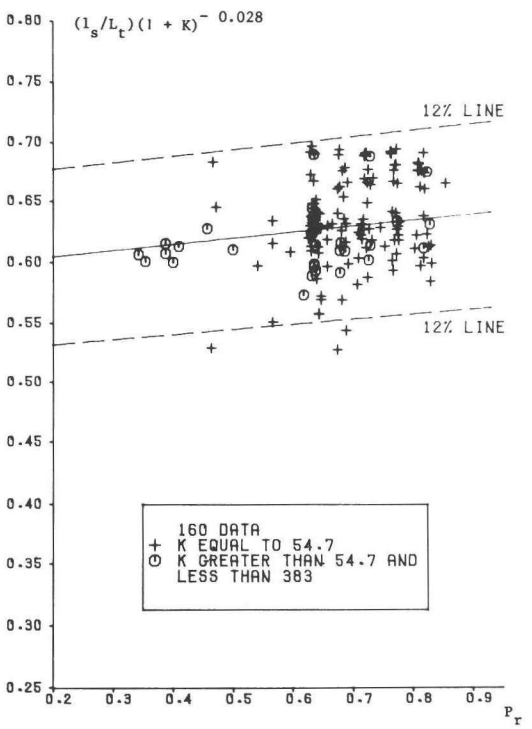

Fig. 7.5 Determination of the length of the superheated steam region at the inception of the DWO in TT3.

is described within about 12% accuracy by equation

$$l_s/L_t = Y_{71} (1 + K)^{0.028} (0.95 + 0.079 P_r) \qquad (7.3)$$

where $Y_{71} = 0.626$. So the length of the superheated steam region in TT3 at the inception of the DWO is approximately constant for a given outlet pressure and inlet throttling. The effect of the outlet pressure on this length is minute and that of inlet throttling is considerable but not of paramount importance. A similar result is also obtained from TT4 tests with the value of Y_{71} in equation (7.3) equal to 0.688. With the exception of 17 data taken mostly at low pressures when the irregular mass flow oscillations were comparatively large, equation (7.3) predicts the length of the superheated steam region at the inception of the DWO also within 12% accuracy for the data obtained in TT4. The aforesaid length is considerable. For example for $P = 14$ MN/m^2, it is equal to about 35.6 m if $K = 223$ and to 33.3 m if $K = 20$ in TT4 and to 14.3 m if $K = 54.7$ in TT3. Y_{71} in equation (7.3) appears to be dependent on tube length and can be expressed as ($Y_{71} = 0.52 + 6.82 \cdot 10^{-5} L_t/d$) for once-through steam generator tubes of $1559 \leq L_t/d \leq 2468$.

In all the tests at the inception of the DWO, $(\theta(\zeta) - T(\zeta))$, the difference between the sodium and water/steam side temperatures decreased approximately exponentially along the superheated steam region. This is illustrated in Fig. 7.6 for a few tests carried out in TT3. For this purpose, $(\theta(\zeta) - T(\zeta))/(\theta_s - T_s)$, the ratio of this temperature difference to the temperature difference between the sodium and water/steam side at the beginning of the superheated steam region was plotted along this region. The exponential decrease of the difference between the sodium and water/steam side temperatures along the superheated steam region is due to the behaviour of the specific heat of steam in the vicinity of the saturation temperature at high pressures, as shown for instance for $P = 14$ MN/m^2 in Fig. 7.7. $Q_s(\zeta)/(Q_t)_s$, the ratio of the power transferred along the superheated steam region to the total power transferred in this region is also given in Fig. 7.6, which shows that in the last 50% of this region or beyond the about 15 m point along the test tube almost no heat is transferred to the water/steam side. During most of the tests only the sodium side inlet temperature was increased by small increments. This resulted in a gradual increase in the length of the superheated steam

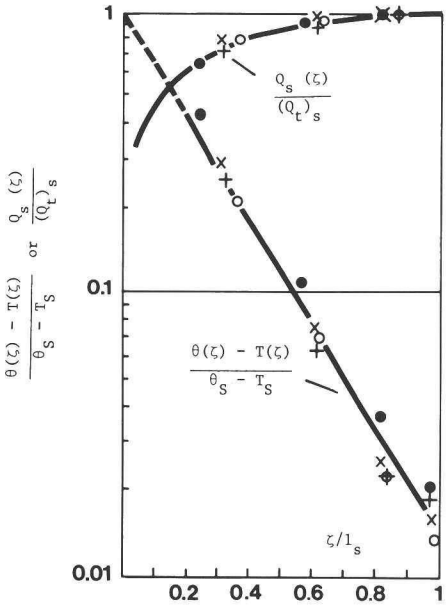

Range of data:
P=14-14.3 MN/m^2
G=544-910 kg/m^{2}s
ΔT_{sub}=101-157 K
W_n/W_w=8.9-17.9
K=54.7

Fig. 7.6 Profiles of the dimensionless temperature difference between the sodium and water/steam side and the dimensionless power along the superheated steam region.

region and a decrease in the lengths of the preheat and boiling regions. From the above the significance of the length of the superheated steam region for the mechanism of the DWO is obvious: In order to trigger the multiple regenerative feedback mechanism which generates the DWO in a test tube when outlet pressure and inlet throttling are kept constant, the length of the superheated steam region has to reach a constant value. Thereafter the DWO appear and the multiple regenerative feedback mechanism begins to operate. Inlet throttling delays this mechanism in accordance with equation (7.3) i.e., the length of the superheated steam region increases with increasing throttling coefficient.

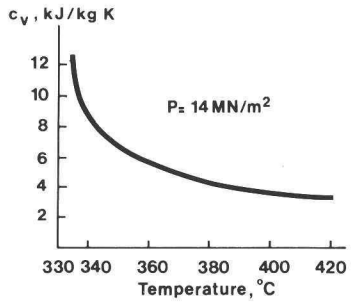

Fig. 7.7 Specific heat of steam versus temperature at P = 14 MN/m^2.

7.2.1.3.2 The Relation for the Mechanism of the DWO

In order to determine this relation, the transit times of a fluid particle in all the different heat transfer regions in a steam generator tube have to be considered. The transit time of a fluid particle in a heat transfer region is

$$\tau = 1\ \bar{\rho}/G \tag{7.4}$$

This transit time is transformed into a non-dimensional form as follows:

$$\tau^{+} = (g\ \tau^{2}/1)^{\frac{1}{2}} = (1\ \bar{\rho}^{2}\ g/G^{2})^{\frac{1}{2}} \tag{7.5}$$

The term in parentheses in equation (7.5) is the reciprocal of the Froude number and shows the ratio of gravity to inertia force.

With tha data taken in TT3 the following empirical relation has been established between inlet throttling coefficient, outlet pressure and transit times at the inception of the DWO in the preheat, boiling and superheated steam regions:

$$\frac{(1/\tau_s^{+}) + (1/\tau_p^{+})}{(1/\tau_s^{+}) + (1/\tau_p^{+}) + (1/\tau_B^{+})} = Y_{72}\ (1 + K)^{-\ 0.028}\ \ (0.855 - 0.15\ P_r) \tag{7.6}$$

where $Y_{72} = 1$. Equation (7.6) is shown in Fig. 7.8 for the data from TT3. This figure shows that the LHS of equation (7.6) is practically constant at the inception of the DWO for a given outlet pressure and inlet throttling. Inlet throttling delays the DWO in accordance with equation (7.6) i.e., the length of the superheated steam region increases with increasing inlet throttling coefficient. This is demonstrated below. The second term both in the numerator and in the denominator of equation (7.6) need not to be considered for this demonstration since they are of second order of importance. In this case, equation (7.6) is written in an open form for a given pressure as follows:

$$\frac{1}{1 + [1_s\ \bar{\rho}_s^{2}/(1_B\ \bar{\rho}_B^{2})]^{\frac{1}{2}}} = \text{constant x } (1 + K)^{-\ 0.028} \tag{7.7}$$

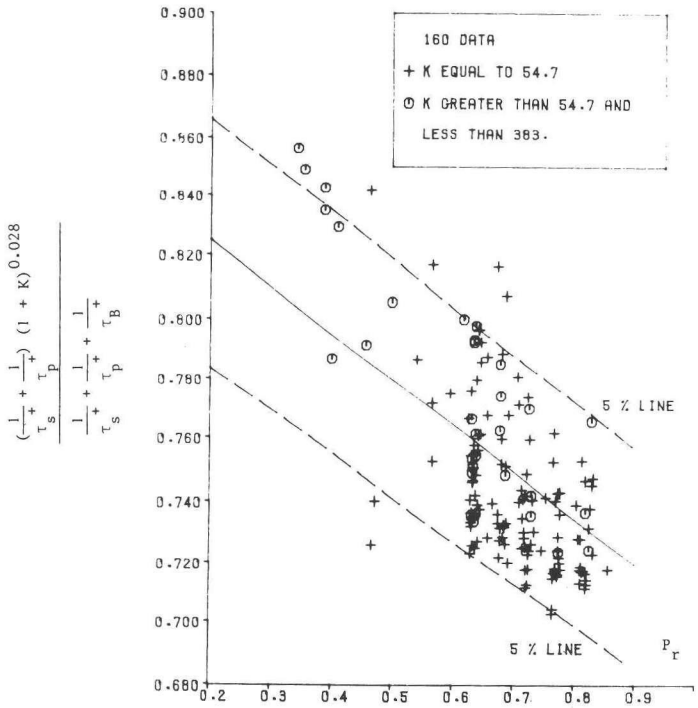

Fig. 7.8 Verification of the mechanism of the DWO in accordance with equation (7.6).

During most of the tests carried out in TT3 the inlet temperature of the sodium side was increased. This caused an increase in the length of the superheated steam region and a decrease in the length of boiling and preheat regions. $\bar{\rho}_s$ decreases if the inlet temperature at the sodium side increases. $\bar{\rho}_B$ is constant if it is assumed that the steam quality along the boiling region varies linearly and the pressure in the test tube is constant. The RHS of equation (7.7) decreases with increasing inlet throttling. Thus follows from this equation that the length of the superheated steam region has to be increased if the inlet throttling coefficient increases.

Equation (7.6) was only checked with 16 data taken in TT4 for the pressure range P = 13.9 - 14.3 MN/m^2. For these data G = 262 - 675 kg/m^{2}s;

ΔT_{sub} = 20.4 - 168 K; X_{IC} = 1.49 - 1.96. If the value of Y_{72} in equation (7.6) is taken as 0.92, this equation fits the data within 6% accuracy. It is obvious that this value is only for TT4 and Y_{72} = 1 for TT3.

The above confirms that the observed DWO are "time delay oscillations", that inlet throttling delays the mechanism of the DWO, and that Y_{72} in equation (7.6) is a weak function of (L_t/d).

Equation (7.6) gives the mechanism of the DWO in TT3 and in TT4 if these tubes operate in the once-through mode. It then follows in order to initiate DWO in these tubes, the condition expressed by equation (7.6) has to be fulfilled.

For a steam generator tube for which $X_o \leq 1$, τ_s^+ vanishes from equation (7.6). In this case, this equation was checked with the 8 data reported in [Q1] for a very short electrically heated tube of L_t/d = 153. These data were taken for ΔH = 0.087 - 0.131 and P = 4.1 - 8.3 MN/m^2. The value of Y_{72} in equation (7.6) for these data was 0.44 with an accuracy of 10%.

Provided that the RHS of equation (7.6) is determined for a reasonable amount of data taken in tubes of different geometries, the equation may serve a stability model since it includes the mechanism of the DWO. Y_{72} in this equation is a weak function of (L_t/d) and can be expressed as $(Y_{72} = 1.135 - 8.7 \cdot 10^{-5} L_t/d)$ for once-through steam generator tubes of $1559 \leq L_t/d \leq 2468$.

7.2.1.3.3 The Outlet Steam Quality at the Inception of the DWO

This steam quality appears to be almost solely a function of outlet pressure for a given inlet throttling in both test tubes. The effects of all other operating conditions on the aforesaid steam quality seem to be of secondary importance. This conclusion was also drawn from the results of the tests carried out in TT1 and the evaporator, as demonstrated in Section 7.2.1.4.1. Quandt [Q1] reported a similar conclusion obtained from the data taken in a very short steam generator tube in which no superheated steam was produced.

The fact that the outlet steam quality at the inception of the DWO is constant, can be explained as follows: Average density in the superheated steam region at the inception of the DWO was solved from equation (7.6) and correlated within about 12% accuracy for 129 data taken in TT3, for which K = 54.7, with the equation below,

$$\bar{\rho}_s = 3.62 + 82.76\ P_r \qquad (7.8)$$

, as shown in Fig. 7.9. Y_{72} in equation (7.6) is equal to 1 for TT3.

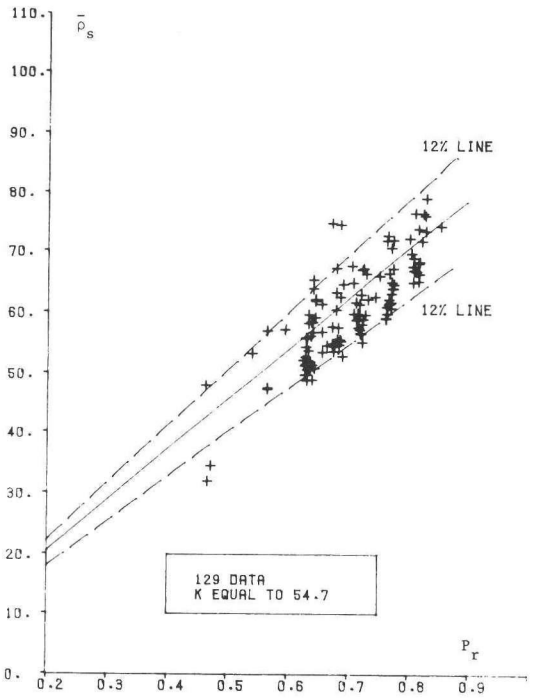

Fig. 7.9 Average density in the superheated steam region of TT3 at the inception of the DWO.

Assuming that this density is equal to that calculated from the average temperature in the superheated steam region, the outlet steam quality at the inception of the DWO was determined within 0.4% accuracy by the use of equation (7.8) and a Steam Table [A6], as given below:

$$X_{IC} = 0.721 - 0.764\ \ln\left[(1 - P_r)\ P_r^{0.3}\right] \qquad (7.9)$$

With four exceptions, equation (7.9) fits the aforesaid data within 8% accuracy. The RMS error for all the data is 4.2%. From this it is concluded

that outlet steam quality (or temperature) at the inception of the DWO is practically a function of pressure for a given inlet throttling and geometry, and that the effects on the inception of the DWO of other operating conditions are of secondary importance. It was found in Section 7.2.1.3.1 that the length of the superheated steam region at the inception of the DWO was also practically a function of pressure, inlet throttling and geometry. It follows from the above that the superheated steam region dominates the mechanism of the DWO in both the test tubes and equation (7.6) seems to give this mechanism well.

7.2.1.4 Correlation of the Data

Having established the physical mechanism of the DWO, the data for the inception conditions of the DWO can be correlated straightforwardly and in different ways, as already demonstrated in Section 7.2.1.3.

Equation (7.3), in fact, correlates the data obtained in TT3 and TT4 very well if it is considered that only a small part of the total power is developed in a large proportion of the superheated steam region. The above suggests also that equation (7.3) can be used safely for the prediction of the inception conditions of the DWO for once-through steam generator tubes without considering that the equation was based on data obtained for $1559 \leq L_h/d \leq 2468$.

Below, the present data and the data available from the literature are correlated using the results given in Section 7.2.1.3 in two different ways for practical applications. For this purpose, dimensional analysis is used. As stated on page 1.6, the dimensionless numbers which fully characterise the dynamics of two-phase flow are numerous and it is practically impossible to take all of them into account when correlating the data [I2]. Furthermore, as indicated in [K4], the use of the Buckingham and Rayleigh methods of dimensional analysis will yield dimensionless groups, but their physical significance is not evident. The use of differential equations allows one to interpret physically the dimensionless groups thus derived, but still provides no information on the fundemental mechanism of the process [K4]. Thus, the experiment is the only safe basis for the selection of the dimensional variables for the correlation of the DWO data. As concluded from [M3], the logical grouping of these variables into dimensionless groups can then be accepted without hesitation. In this case howev

the physical significance of these dimensionless groups may not be evident [K4].

The present experiments clearly demonstrate that the most significant dimensional variables for the inception of the DWO in a once-through steam generator tube are total or heated tube length, outlet temperature, outlet pressure and pressure drop due to inlet throttling. For the present experiments $L_h \cong L_t$. These variables are transformed into dimensionless numbers such as L/d, the ratio of tube length to tube diameter, X, outlet steam quality, P_r, reduced pressure and K, inlet throttling coefficient. The importance of the first mentioned three dimensionless numbers on the mechanism of the DWO is due to fact that they characterise the length of the superheated steam region and the transit time of a fluid particle in this region. As demonstrated in the preceding section, these are of vital importance for the mechanism of the DWO in a once-through steam generator tube. The importance of the inlet throttling coefficient on this mechanism is due to distribution of the pressure losses along the tube: The total of these pressure losses is constant and the DWO are time-delay oscillations. The experiments of Quandt [Q1] carried out in a steam generator tube in which no superheated steam is produced show that the inlet subcooling also influences the inception conditions of the DWO. This is logical, since subcooling characterises the length of the boiling (or preheat) region in this tube. The inlet subcooling can be non-dimensionalised as ΔH, the dimensionless inlet subcooling enthalpy.

It follows from the above that it seems sufficient to consider five dimensionless numbers, i.e., L/d, X, P_r, K and ΔH for the correlation of the DWO data. Therefore, a correlation (i.e., equation (7.18)) was first established using the above dimensionless numbers. This equation applies both to a steam generator tube in which no superheated steam is produced and to a once-through steam generator tube. This correlation should be very useful for many practical applications since it includes a few operating conditions. It is also an accurate correlation.

For some special applications in engineering practice, improvements in the accuracy are considered very useful for predicting the inception conditions of the DWO, especially for a once-through steam generator tube producing superheated steam only. This can be achieved if the second-order variables are also considered for the correlation of the DWO data. These variables, in their non-dimensional form, are W_n/W_w, the ratio of sodium-side

mass flow to water/steam side mass flow and Re_v, the Reynolds number for flow in the superheated steam region. The first dimensionless number influences the length of the superheated steam region and the latter accounts for the variation of water/steam-side mass flow. Thus a second correlation (i.e., equation (7.21)) was established considering the aforesaid five dimensionless numbers, i.e., L/d, X, P_r, ΔH, K, and W_n/W_w and Re_v. The correlation thus obtained is indeed more accurate than the first correlation, but applies to once-through steam generator tubes producing superheated steam only.

7.2.1.4.1 Correlation of the Data Using a Few Operating Conditions

As stated before, the first part of the present DWO study comprised tests in TT1, TT2 and in the evaporator. For the tubes of the latter the inlet and outlet temperatures and the pressure were measured, but not water/steam side mass flow nor the operating conditions on the sodium side with the exception of the inlet temperature. Any correlation of having to include the data obtained in the evaporator had to be related to three operating conditions only, i.e., inlet and outlet temperatures and pressure, and geometry. As stated in the above section, however, the use of these parameters is justified and sufficient for the correlation of data.

The data of TT1, the evaporator and the literature [B15, D2, D3, Q1, S3, W3] were considered. The ranges of operating conditions and geometries for these data are summarized in Table 7.5. These operating conditions are the inception conditions of the DWO, i.e., they were measured for the last stable test run before the DWO occurred in the test tube.

In the tests of [B15] the total pressure drop in the test tube, which was one of the 139 tubes of a large capacity sodium heated steam generator, was constant. In these tests, the flow at the inlet of the test tube was not throttled and the mass velocity in the test tube was not measured. In the work reported by [D2, D3] three identical serpentines were arranged in parallel. Each serpentine used consisted of three tubes of different inside diameters. For this serpentine L_h/d is determined as the arithmetic sum of L_h/d for each tube. The flows at the inlet of the serpentines were throttled. In experiments reported by [S3] two and by [W3] three test tubes were arranged in parallel; [Q1] reports a large by-pass pipe built

Table 7.5 The Range of the Data Used to Establish Equation (7.11)

Geometry and dimensions of the test tube and type of heating	L_h/d -	P MN/m^2	X_{IC} -	G kg/m^2s	ΔT_{sub} K	Y_{74} Y_{75} Y_{76}
Electrically heated rectangular channel; d = 4.49 mm; L = 0.686 m; n = 18 [Q1].	153	4.1-11.0	0.273-0.726	436-2088	2.8- 86.1	0.297 - 0.146 0
Present tests from TT1; n = 11.	1272	6.2-14.1	1.14 -1.34	706-1365	27 - 81.6	1.029 - 0.358 0
Sodium heated vertical tube of 11.4 mm ID.; L_h = 14.58 m; n = 8 [B15].	1279	16 -17.3	1.51 -1.62	-	87.3- 93.7	1.030 - 0.360 0
Present tests from evaporator; n = 33.	1535	5.3-17.0	1.10 -1.59	-	23.9-111.3	0.956 - 0.390 0
Sodium heated coil of 17 mm ID., d_c/d = 47.4; L_h = 43 m; n = 2 [S3].	2529	9.9	1.44 -1.46	835	104.2	-
Sodium heated serpentine of 9.4 mm ID., L_h = 39.65 m; n = 1 [W3].	4220	16.7	1.85	-	127.6	-
Electrically heated serpentine consisting of three tubes of 18.2 mm, 21.8 mm and 29.9 mm ID., tubes with lengths of 24.1 m, 158.9 m and 26.6 m respectively; n = 33 [D2, D3].	9502	4.3-14.4	1.01 -1.69	118- 362 (at the inlet)	118.4-245.9	1.809 - 1.242 1.47

around the test tube. Thus a constant pressure drop is maintained in the test tube. For the tests carried out in TT1 and the tests of [S3, W3], throttling of the flow at the inlet of the test tube was solely due to a flow measuring device (i.e., a turbine flow meter or an orifice) and was assumed to be negligible small for a long tube. In the work of [Q1], a venturi was used to measure the flow at the inlet of the test tube, of which inlet throttling was also considered negligible.

For correlation of the data, the exit steam quality at the start of the DWO was first plotted versus pressure, subcooling being a parameter. This resulted in the following relation:

$$X_{IC} = [Y_{74} + Y_{75} \ln (1 - P_r)][1 + 1.7 \exp (- 50 \Delta H)]/[1 + Y_{76} \Delta H] \quad (7.10)$$

where Y_{74}, Y_{75} and Y_{76} are numerical constants for a given (L_h/d) and tabulated in Table 7.5.

For the data of [B15, D2, D3, S3, W3], the outlet steam quality was calculated from the measured outlet temperature and pressure, using a Steam Table [A6] and for those of [Q1] with a heat balance, assuming thermodynamic equilibrium between the phases. From the data of [D2, D3] it was not possible to deduce where the pressure was measured, at the inlet or at the outlet of the test tube. It seems most probable that the above mentioned pressure is the outlet pressure. For the data of [D2, D3] the outlet steam quality was therefore calculated using the pressure reported, without considering whether it was measured at the inlet or at the outlet of the test tube. This may introduce errors in the evaluation of the outlet steam quality, though of only a few percent, since for these data $P >> \Delta P$, a condition which also applies to all the data considered. For the evaluation of H_i and H_l in ΔH in equation (7.10), the value of the outlet pressure was used.

The results of the comparison of equation (7.10) with the data obtained in once-through steam generator tubes, i.e., in TT1, the evaporator and with the data of [B15, D2, D3] are shown in Fig. 7.10. From this figure it was concluded that the outlet steam quality at the start of the DWO was practically constant for a given pressure for the tests carried out in TT1, the evaporator and for the tests of [B15], and for a given pressure and inlet subcooling for the tests of [D2, D3], since (exp. -50 ΔH) in equation (7.10) is negligible for all the data considered.

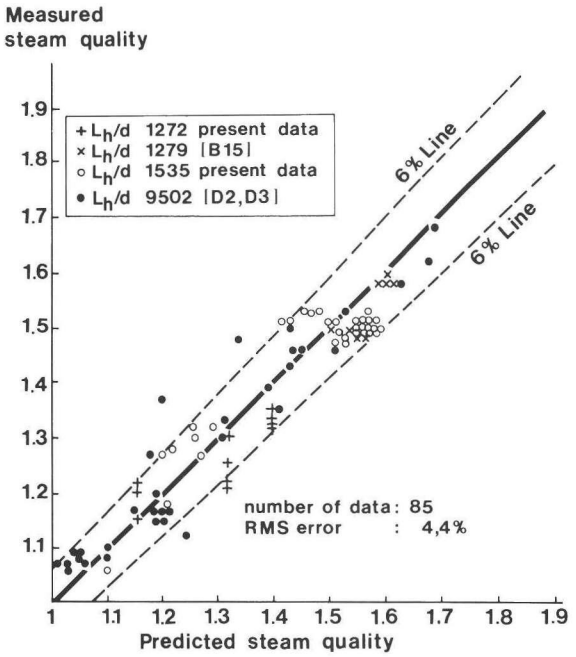

Fig. 7.10 Verification of equation (7.10).

For the latter mentioned data, however, the effect of inlet subcooling was not significant. These data were obtained in very long electrically heated serpentines and the length of preheat region in each serpentine was very long due to large subcoolings used. For the rest of the test tubes considered, the preheat region was comparatively short. This is probably the reason why inlet subcooling slightly affects the inception of the DWO in these serpentines, as equation (7.6) may imply.

Equation (7.10) applies equally to a tube around which a by-pass pipe is built and to multitubes [B15, D2, D3], i.e., the effect of a by-pass pipe could not be discerned.

It followed then from equation (7.10) that the data could be correlated straightforwardly if the Y_{74}, Y_{75} and Y_{76} in this equation were expressed as a function of (L_h/d). This has been done, considering also the data of [Q1] taken in a very short steam generator tube in which no superheated steam was produced and the data of [S3, W3] obtained in

once-through steam generator tubes. The correlation obtained is

$$X_{IC} = Y_{77}\, Y_{78}\, [Y_{79} + Y_{710} \ln (1 - P_r)]/Y_{711} \tag{7.11}$$

where

$$Y_{77} = 1 + 1.8 \exp \{- 11.4\, (1- P_r)[1 + 3.83 \cdot 10^{-5} \times \exp (1.11 \cdot 10^{-3}\, L_h/d)]\} \tag{7.12}$$

$$Y_{78} = 1 + 3.3 \exp (- 4.5 \cdot 10^{-3}\, L_h/d) \exp (- 50\, \Delta H) \tag{7.13}$$

$$Y_{79} = (0.98 + 0.088 \cdot 10^{-3}\, L_h/d)/[1 + 5.1 \times \exp (- 5.3 \cdot 10^{-3}\, L_h/d)] \tag{7.14}$$

$$Y_{710} = - 0.14 \exp (0.23 \cdot 10^{-3}\, L_h/d) \tag{7.15}$$

$$Y_{711} = 1 + 2.9 \cdot 10^{-3}\, (10^{-3}\, L_h/d)^{2.77}\, \Delta H \tag{7.16}$$

If the steam quality at the outlet of a steam generator tube exceeds the outlet steam quality predicted by equation (7.11) the DWO will occur in the tube. In accordance with this equation, it is sufficient to know only two operating conditions, namely inlet temperature and outlet pressure in order to determine the outlet steam quality at the start of the DWO in a steam generator tube of known dimensions. The outlet temperature is then also known for a once-through steam generator tube.

Quandt [Q1] showed that for a short steam generator tube in which no superheated steam was produced, very low inlet subcoolings substantially affect the outlet steam quality at the start of the DWO. From the data obtained in TT3 and TT4 it is concluded, however, that the effect of very low subcoolings on the steam quality at the start of the DWO is negligible for once-through steam generator tubes. This is borne out by Fig. 7.8 and has led to the reduction of equation (7.6) to equation (7.7), that is, the dimensionless transit time in the preheat region is of secondary importance for the mechanism of the DWO. The data from short steam generator tubes in which no superheated steam was produced are very scarce in the literature. The aforesaid subcooling effect could be taken into account in equation (7.11) only by the use of the few data (i.e.,

five data) of [Q1] for which $\Delta H = 0.0119 - 0.0238$ and $L_h/d = 153$, and was expressed with the parameter Y_{78} given by equation (7.13). (For the rest of the data of [Q1], ΔH varies between 0.087 - 0.31). Equation (7.11) is therefore not recommended for very low subcoolings (i.e., $\Delta H < 0.087$) if $L_h/d < 1272$. Note that $Y_{78} \cong 1$ if $L_h/d \geq 1272$ and $\Delta H \geq 0$ or if $153 \leq L_h/d \leq 1272$ and $\Delta H \geq 0.087$.

The power at the start of the DWO is expressed by equation

$$Q = W_w \, (H_1 - H_i + \lambda \, X_{IC}) \tag{7.17}$$

where X_{IC} is given by equation (7.11). The results of the comparison of the data with equation (7.17) are shown in Fig. 7.11. This equation

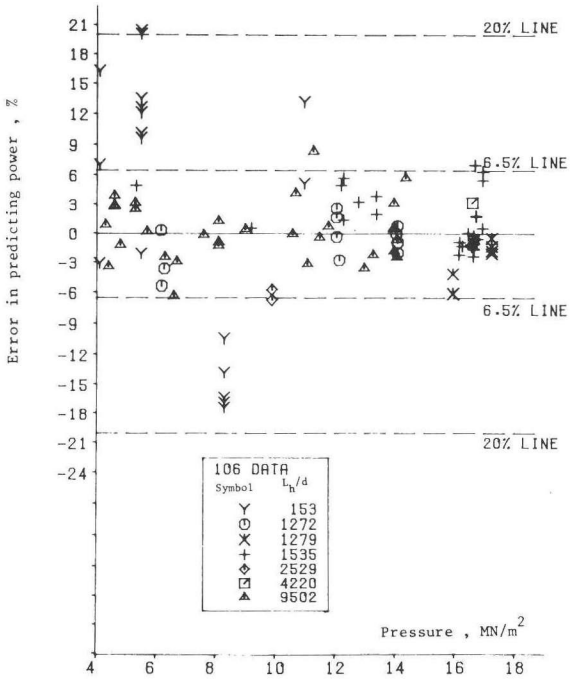

Fig. 7.11 Error in predicting power at the start of the DWO in accordance with equations (7.11) and (7.17).

predicts the power at the start of the DWO accurately within about 6.5% with a RMS error of 3.3% for the 88 data from once-through steam generator tubes of $1272 \leq L_h/d \leq 9502$, and accurate within 20% with a RMS error of 13.3% for the 18 data from a steam generator tube of $L_h/d = 153$, in which no superheated steam was produced. The RMS error for all the data was 6.2%.

In Section 7.2.1.3.2 it was shown that the effect of inlet throttling is to increase the length of the superheated steam region at the inception of DWO. While a full discussion of its effect on outlet steam quality will be given later in this section when presenting the final form of equation (7.11) (i.e., equation (7.18)) it may already be stated on the basis of the data from [D2, D3] obtained in a very long once-through steam generator tube of $L_h/d = 9502$ that the effect on the outlet steam quality at the inception of the DWO of inlet throttling is negligible for very

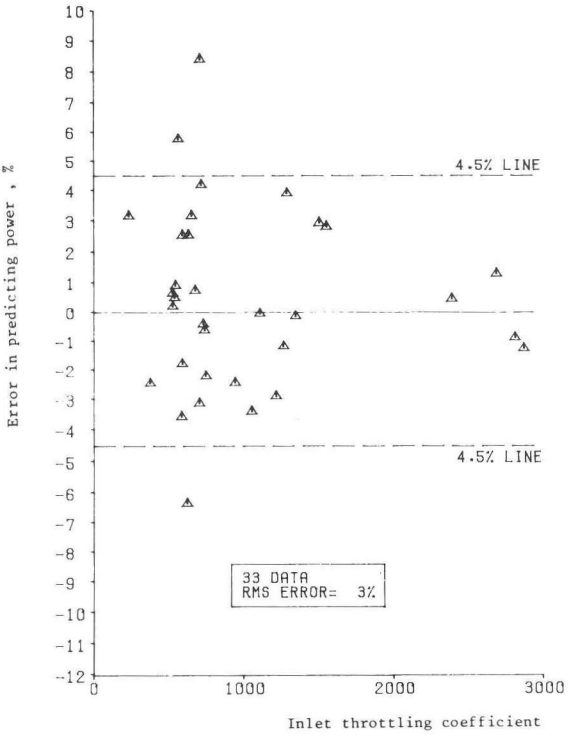

Fig. 7.12 Effect of inlet throttling on the inception conditions of DWO for a very long steam generator tube of $L_h/d = 9502$.

long tubes: For these data, the error in predicting the power at the start of the DWO in accordance with equations (7.11) and (7.17) is shown versus the inlet throttling coefficient in Fig. 7.12. The conclusion drawn from the figure is that this effect seems negligible for very long steam generator tubes, in other words, this effect is within the experimental accuracy. It will be shown later in this section and Section 7.2.1.4.2, that this effect is negligible beyond $L_h/d > 4118$ or $L_t/d > 4167$. It then follows from the above that equation (7.11) does not apply to a steam generator tube of $L_h/d \leq 4118$ or $L_t/d \leq 4167$, if the flow is throttled at the inlet of the tube.

Equation (7.11) implies that the heat input per unit mass of fluid flowing in a steam generator tube of known dimensions (i.e., L_h and d) is constant at the start of the DWO for a given pressure and inlet subcooling. (See also equation (7.17)). This result agrees with the physical mechanism of the DWO established from the data obtained in TT3 and TT4 after equation (7.11) had been derived. In accordance with this mechanism (see Section 7.2.1.3.3) the outlet steam quality at the start of the DWO in a once-through steam generator tube of known dimensions is practically a function of pressure for a given inlet throttling. Therefore, at the start of the DWO, the heat input per unit mass of fluid flowing in a once-through steam generator tube of known dimensions should depend on pressure, subcooling and inlet throttling for $L_h/d \leq 4118$ and on pressure and subcooling for $L_h/d > 4118$, as can be deduced from equation (7.17).

Using the data obtained in TT3 and TT4, equation (7.11) was modified for the effect on the outlet steam quality at the start of the DWO of inlet throttling i.e., this equation was multiplied by $[1 + K]^{Y_{712}}$. The final form of the equation is

$$X_{IC} = Y_{77}\, Y_{78}\, [Y_{79} + Y_{710} \ln (1 - P_r)][1 + K]^{Y_{712}/Y_{711}} \qquad (7.18)$$

where

$$Y_{712} = 0.07 - 0.017 \cdot 10^{-3} L_h/d \text{ for } L_h/d \leq 4118 \qquad (7.19)$$

$$Y_{712} = 0 \qquad \text{for } L_h/d > 4118 \qquad (7.20)$$

The effects of various parameters included in Y factors on the outlet

steam quality at the inception of the DWO in accordance with equation (7.18) are summarized in Table 7.6.

Table 7.6 Effects of Various Parameters included in Y Factors on the Outlet Steam Quality at the Inception of the DWO in accordance with Equations (7.18) and (7.21)

	Factor	Effect
equation (7.18)	Y_{77}	reduced pressure and length-to-diameter ratio
	Y_{78} and Y_{711}	dimensionless inlet subcooling enthalpy and length-to-diameter ratio
	Y_{79} and Y_{710}	length-to-diameter ratio
	Y_{712}	inlet throttling coefficient and length-to-diameter ratio
equation (7.21)	Y_{713}	reduced pressure
	Y_{714}	ratio of sodium to water/steam side-mass flow
	Y_{715}	dimensionless inlet subcooling enthalpy
	Y_{716}	dimensionless mass velocity (i.e., Reynolds number)
	Y_{717}	inlet throttling and length-to-diameter ratio
	Y_{719}	distribution of the pressure drop due to surface friction and bends along a tube

Inserting equation (7.18) into equation (7.17), the results of the latter were compared with the 306 data from TT3 and TT4 and 11 data from TT1 and 1 data from TT2. The throttling coefficient of the flow meter at the inlet of TT1 was also considered. This equation predicted the power at the start of the DWO for these data well, i.e., within 8% accuracy for 88% of the time. The RMS error for all the 318 data is 5.78%.

The ranges of geometries and operating conditions used to establish equation (7.18) are recapitulated below: Geometry: circular straight tubes, circular serpentines, circular helical coils; tubes, each comprised of

a circular vertical and a circular V-shaped horizontal tube, and a rectangular straight tube; type of heating: sodium and electrical heating; L_h = 0.686 - 200 m; L_h/d = 153 - 9502; d = 4.49 - 29.9 mm; X_{IC} = 0.27 - 2.38; P = 4.1 - 19.1 MN/m^2; G = 118 - 2088 kg/m^2s; ΔT_{sub} = 2.8 - 245.9 K; K = 0 - 2882. The number of data considered was 413. The correlation applies both to a once-through steam generator tube and to a steam generator tube in which no superheated steam is produced. The correlation predicts the power at the start of the density wave oscillations from these 413 data within 8% accuracy for 87% of the time with a RMS error of 5.97%.

7.2.1.4.2 Correlation of the Data Using All the Operating Conditions

For this purpose the data obtained in TT1, TT2, TT3, TT4 and the evaporator, and all the literature data mentioned in Table 7.5 relevant to once-through steam generator tubes [B15, D2, D3, S3] with the exception of those from [W3] were considered. The data of [W3] were disregarded since all the operating conditions were not available from these data.

As stated before, no separate mass flows were measured in the evaporator tests for test tubes in which the DWO were detected. These were assumed to be equal to the average values in the evaporator. In some of these tests the average water/steam side mass flow was measured with a considerable error (i.e., from 10 to 35%), as can be deduced from Table 7.4. These tests were disregarded. The above applies also to the tests of [B15].

In the work reported by [D2, D3] three identical serpentines were arranged in parallel. Each serpentine consisted of three tubes of different inside diameters. For this serpentine L_t/d was determined as the arithmetic sum of (L_t/d) for each tube. The average diameter for the serpentine was then determined from L_t/d = 10150 and L_t = 223.3.

In the tests reported by [S3] two test tubes were arranged in parallel. For these tests the throttling of the flow at the inlet of the test tube was assumed to be negligible, since it was solely due to a turbine meter of which the throttling coefficient was not reported, and the test tube was fairly long (i.e., L_t/d = 2529).

For the tests carried out in TT1, the throttling coefficient of the turbine flow meter at the inlet of the tube was considered, as given in Table 7.1.

For the correlation of the data, the effects on the outlet steam quality at the inception of the DWO of inlet throttling and each of the operating conditions, namely, mass flow both on the sodium side and on the water/steam side, outlet pressure and inlet subcooling on the water/steam side, were determined separately as expressed by equations (7.22) to (7.27) with the aid of the very accurate data obtained in TT3. (These data are the first 127 and the last 4 data in Table A3.1; TT3 was the test tube consisting of a vertical and a V-shaped horizontal tube). For this purpose these operating conditions were used in dimensionless form, i.e., W_n/W_w, the ratio of sodium side mass flow to water/steam side mass flow, Re_v, the Reynolds number for flow in the superheated steam region, P_r, the reduced pressure and ΔH, the dimensionless inlet subcooling enthalpy. Thereafter a correlation was established for all the data obtained in TT3. By comparing this correlation with the data from TT4 (i.e., a helical coil), TT1, TT2, the evaporator and data reported in [B15, D2, D3, S3], the effect of inlet throttling on the tube length and the effect of the friction factor on the outlet steam quality at the inception of the DWO were determined by expressions given by equations (7.28) to (7.30). The term in the denominator of equation (7.30) is practically identical to Blasius's friction factor for straight tubes and the sum of the first two terms in the numerator is the friction factor for helical coils [I3]. The last term in the numerator represents loss coefficients of the bends along a straight tube or a serpentine. The final correlation obtained is

$$X_{IC} = Y_{713}\, Y_{714}\, Y_{715}\, Y_{716}\, Y_{717}\, Y_{719} \tag{7.21}$$

where

$$Y_{713} = 0.131 - 0.135 \ln [(1 - P_r)\, P_r^{0.2}] \tag{7.22}$$

$$Y_{714} = 1 - 0.005\, W_n/W_w \tag{7.23}$$

$$Y_{715} = 1 + 0.13\, \Delta H \tag{7.24}$$

$$Y_{716} = Re_v^{0.125} \tag{7.25}$$

$$Y_{717} = [1 + K/(L_t/d)^{0.37}]^{Y_{718}} \quad (7.26)$$

$$Y_{718} = 0.11 \quad \text{for the TT3} \quad (7.27)$$

$$Y_{718} = 0.175 - 4.2 \cdot 10^{-5} (L_t/d) \quad \text{for } L_t/d \leq 4167 \quad (7.28)$$

$$Y_{718} = 0 \quad \text{for } L_t/d > 4167 \quad (7.29)$$

$$Y_{719} = \{[Y_{720} + 0.029 (d/d_c)^{0.5} + (Nd/L_t)^{1.18}]/Y_{720}\}^{0.79} \quad (7.30)$$

$$Y_{720} = 0.304 \, Re_v^{-0.25} \quad (7.31)$$

Equations (7.23), (7.24) and (7.25) clearly indicate that the effects on the outlet steam quality at the inception of the DWO of the ratio of the sodium-side mass flow to the water/steam-side mass flow, the inlet subcooling enthalpy and the water/steam-side mass flow are of secondary importance. The effects of various parameters included in Y factors on the outlet steam quality at the inception of the DWO in accordance with equation (7.21) are summarized in Table 7.6.

If the steam quality at the outlet of a once-through steam generator tube exceeds the outlet steam quality predicted by equation (7.21), DWO appear in the tube. The power at the inception of the DWO is again expressed by equation (7.17), where X_{IC} is now given by equation (7.21). The results of comparison of the data from TT3, and data from TT1, TT2, the evaporator and the data reported in [B15, D2, D3, S3] are given in Figs. 7.13 and 7.14 respectively. Equation (7.17) predicted the power at the inception of the DWO within 7.5% accuracy for 98% of the time. The RMS error for all the 380 data was 3.33%.

The effect of inlet throttling on X_{IC} seems to decrease with increasing (L_t/d) and disappears beyond $L_t/d > 4167$; in other words this effect stays within the experimental accuracy for $L_t/d > 4167$. For the data reported in [D2, D3] from a very long tube of $L_t/d = 10150$, the inlet throttling coefficient varies between 237 and 2882. These data are shown in Fig. 7.14.

The ranges of geometries and operating conditions of the data used to establish equation (7.21) are recapitulated below: Geometry: circular

straight tubes, circular coils, a circular serpentine and tubes, each comprised of a circular vertical and a circular V-shaped horizontal tube; type of heating: sodium and electrical heating; L_t = 10 - 223.3 m; L_t/d = 1272 - 10150; d = 7.86 - 22 mm; d_c/d = 47.4 - 83.3; P = 4.3 - 19.1 MN/m^2; G = 118 - 1365 kg/m^{2}s; ΔT_{sub} = 3.2 - 245.9 K; X_{IC} = 1.01 - 2.38; K = 0 - 2882. The number of data considered was 380. The correlation applies only to once-through steam generator tubes producing superheated steam only.

As discussed in Section 7.1.2.2.1, a stability model in the form of a long computer program can not, in general, predict the power at the inception of the DWO better than to about 10%. It is known that the accuracy of stability models presented so far in the literature can be much less than 10%. It must be remembered, however, that an empirical

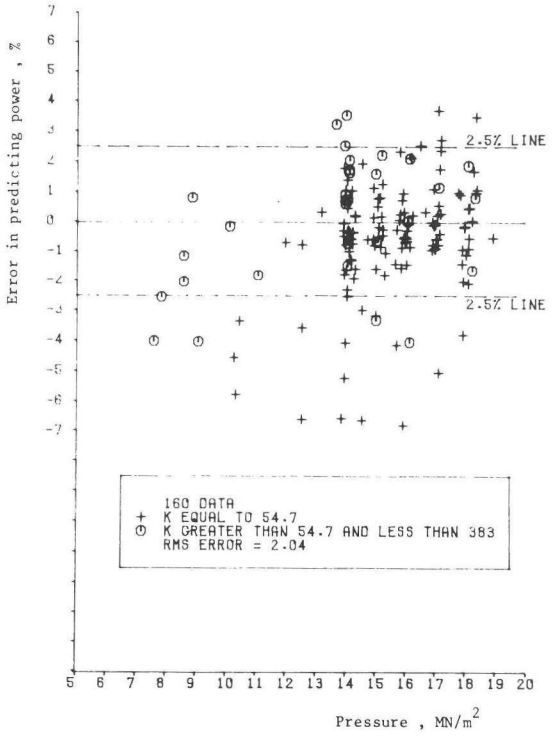

Fig. 7.13 Errors in predicting the power in accordance with equations (7.17) and (7.21) for the data taken in TT3.

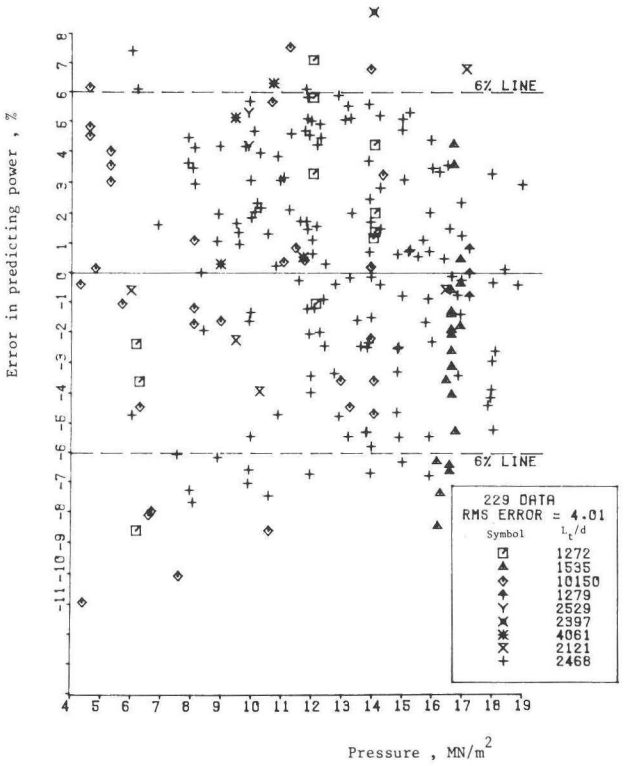

Fig. 7.14 Errors in predicting power in accordance with equations (7.17) and (7.21) for the data taken in TT1, TT2, TT4 and the evaporator and the data of [B15, D2, D3, S3].

correlation lacks generality and is as a rule, invalid outside its range. Nevertheless, if the mechanism of the DWO described before is considered, it seems that the correlations presented in this section and in Section 7.2.1.4.1 are not much susceptible to this invalidity.

Figs. 7.6 and 7.8 demonstrate also the fact that accurate and systematic tests can enlighten even the physical mechanism of a complicated phenomenon such as DWO in once-through steam generator tubes without consulting time consuming theoretical models.

7.2.1.4.3 The Period of the DWO in Steam Generator Tubes

A rather approximate correlation was found in the literature [B12] indicating that the ratio of the period of the DWO to the transit time of a fluid particle in a tube varies between 1 and 2. This correlation appears to have been based on the early tests performed mostly in natural circulation tubes in which no superheated steam was produced. In the early stage of the present study, this ratio was calculated for the tests carried out in TT1, TT2 and the evaporator, and for the data of [Q1], and was found to vary between 0.1 and 1.5 [U6]. However, these calculations were rather rough. In [U6], a correlation for the period of the DWO was also established. This correlation did not fit at all the accurate data from TT3.

In order to correlate these data and data taken in TT4 for $P = 13.9 - 14.3$ MN/m^2 and $G = 262 - 675$ kg/m^{2}s, the following equation was established.

$$\psi = \tau_t \, (1 + K)^{-0.32} \left(1.7 + \frac{1}{1 + 2.45\ 10^8\ e^{-0.57\ K}}\right) \qquad (7.32)$$

The results of the comparison of equation (7.32) with the data are shown in Fig. 7.15. The correlation predicts the period of the DWO within about 30% accuracy for 98% of the time with a RMS error of 14.3% from these data. The inlet throttling appears to affect the period of the DWO.

After the derivation of the correlation it was also checked with the data of [Q1] obtained for $P = 4.1 - 8.3$ MN/m^2 and $G = 436 - 2088$ kg/m^{2}s in a very short steam generator tube in which no superheated steam was produced. With one exception the correlation predicts the period of the DWO within about 22% accuracy from these 12 data.

For the range of throttling coefficients considered, ψ given by equation (7.32) varies between $0.81\ \tau_t$ and $0.38\ \tau_t$. This does not seem to contradict the results of the experiments reported in the late 50's and early 60's [B5, B6, L7, Q1, S11]. These experiments yielded a rough indication that the period of the DWO is approximately one or two times the transit time of a fluid particle in a tube. However, in these experiments the inlet throttling coefficient was either zero or negligible, and the experiments were carried out in natural circulation systems, with the exception of those from [Q1]. The results of the experiments of [Q1]

were considered in establishing equation (7.32), which equation clearly indicates that the inlet throttling influences the period of the DWO. This is logical since DWO are time-delay oscillations and the inlet throttling influences the mechanism of DWO, as discussed previously.

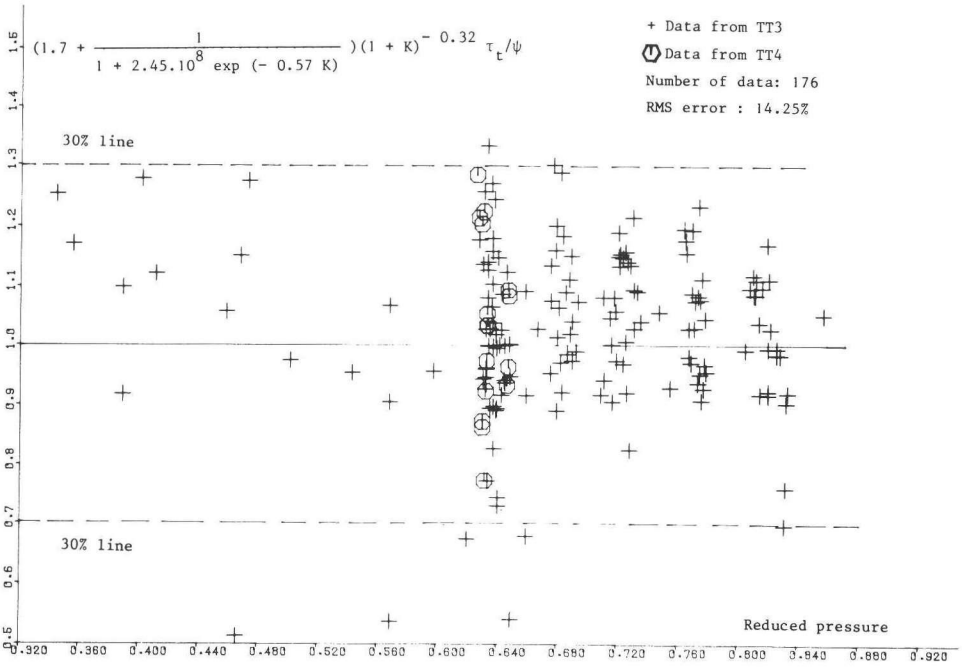

Fig. 7.15 Correlation of the data for the period of the DWO from TT3 and TT4.

The ranges of geometries and operating conditions of the data used to establish and to check equation (7.32) are summarized below: Geometry: a tube consisting of a vertical and a horizontal V-shaped circular tube, a circular helical coil and a rectangular tube; L_t = 0.68 - 44.43 m; d = 4.49 - 18 mm; P = 4.1 - 19 MN/m^2; G = 262 - 2088 kg/m^{2}s; X_{IC} = 0.27 - 2.20; ΔT_{sub} = 2.8 - 168 K; τ = 0.345 - 12.5 s; K = 0 - 450. The number of data considered was 188. RMS error for the correlation of the data was 15.1%.

7.2.2 Correlation of the DWO Data from Natural Circulation Steam Generator Tubes (NCSGT's)

In this section, it is demonstrated that the data for the inception conditions of the DWO from NCSGT's can also be correlated accurately with simple equations. For this purpose, the data of [B5, B6, L7, S11] and those of Anderson as quoted from [N3] are considered. The ranges of operating conditions and geometries of these 110 data are summarized in Table 7.7 and are as follows: Geometry and heating conditions: electrically heated vertical circular tubes and vertical annuli; d = 8.51 - 36 mm; L_h = 0.91 - 4.89 m; L_h/d = 34 - 489; P = 0.2 - 7.1 MN/m^2; X_{IC} = 0.04 - 0.62; G = 529 - 1230 kg/m^{2}s; ΔT_{sub} = 0 - 244 K. These data were obtained in steam generator tubes in which no superheated steam was produced.

The aforesaid data are correlated by equations (7.33) and (7.34) for circular tubes and annuli, respectively.

$$X_{IC} = 8\, Y_{721}\, (L_h/d)^{0.22}\, P_r^{1.64}/(Y_{722}\, Y_{723}\, Y_{724}) \tag{7.33}$$

$$X_{IC} = 480\, Y_{721}\, P_r^{0.93}\, Y_{725}\, Y_{726}\, Y_{727} \tag{7.34}$$

where

$$Y_{721} = Fr^{-\,1.88\, P_r^{0.5}} \tag{7.35}$$

$$Y_{722} = 2.13 - 1.13 \exp\,(-\,586\, \Delta H^3\, Fr) \tag{7.36}$$

$$Y_{723} = 1 + 0.12 \exp\,[-\,2.76\, (A_o/A - 1)\, Fr^{0.7}] \tag{7.37}$$

$$Y_{724} = 1 + 2.03 \quad 10^4\, [(L_h/d)\, Fr^{-\,0.5}]^{-\,3.25} \tag{7.38}$$

$$Y_{725} = (d_1/d_2)^{2.53/(1\, +\, 4\, P_r^{2.52})} \tag{7.39}$$

Table 7.7 Data for the Inception Conditions of the DWO from NCSGT's

Geometry of the test channel	L_h/d	d mm	P MN/m^2	X_{IC} %	G kg/m^2s	(ΔT_{sub}) K	n
circular tube [N3]	34	26.6	2.10-4.19	4.75-12.1	668- 800	8.6- 25.7	3
circular tube [N3]	58	15.8	2.82-3.51	6.00- 7.37	742- 763	16.9- 19.9	2
annulus [S11]	96	25.0	0.20-1.56	4.00- 8.60	773- 993	0.4- 21.0	5
circular tube [B6]	136	36.0	1.08-3.04	9.50-39.70	760- 940	7.9- 8.0	3
circular tube [B6]	147	30.0	1.08-5.00	4.30-49.40	875-1230	10.0	4
annulus [S11]	149	16.2	0.20-3.00	4.70-19.90	519- 785	0 - 43.0	10
annulus [L7]	216	12.7	6.16-7.09	8.30-26.9	671-1009	23.7-174.5 (in KJ/kg)	36
circular tube [B6]	245	20.0	1.08-6.96	9.60-62.3	529-1140	1.9- 16.0	19
annulus [L7]	305	8.5	6.55-6.97	10.6 -41.3	675-1117	60.7-290.5 (in KJ/kg)	26
circular tube [B5]	489	10.0	5.0	18.7 -35.1	549- 624	164 -244	2

$$Y_{726} = (L_h/d)^{-\ 0.93/(1\ +\ 60.4\ P_r^{3.55})} \tag{7.40}$$

$$Y_{727} = 1 + 1.69\ (1 - P_r)^{13.7}\ \exp\ (-\ 38\ \Delta H) \tag{7.41}$$

Correlation of the DWO data from NCSGT's using two equations different from those given for forced circulation steam generator tubes seems justified in accordance with the work presented in Section 7.2.1. In that section it was shown that the DWO observed in two forced circulation once-through steam generator tubes are time delay oscillations and that the transit time of a fluid particle in the different heat transfer regimes in the tubes, especially the transit time in the superheated steam region, is of vital importance for the mechanism of the observed DWO. An empirical relationship, i.e., equation (7.6) was also established for the mechanism of the DWO using 176 data taken for a fairly wide range of conditions. The pressure drops between the inlet and outlet both of the aforesaid tubes were constant. In a natural circulation loop, the sum of the pressure drops along the loop equals zero; it is logical then to assume that the transit time of a fluid particle in every part of the loop has to be considered for the mechanism of the DWO. Nevertheless the above mentioned empirical relationship, i.e., equation (7.6) suggests that the transit time in the two-phase flow region in a natural circulation loop for which $X_o < 1$ is most significant for the mechanism of the DWO. This transit time strongly depends on void fraction and the void fraction in a vertical circular tube differs from that in a vertical annulus, as shown in Chapter 3 (see equations (3.30) and (3.33)). Shotkin [S8] has drawn an analogous conclusion from the results of the data obtained in steam generator tubes in which no superheated steam was produced, that is, the DWO starts in a steam generator tube if the length of the boiling region in the tube is smaller than the so-called crucial boiling length.

The Froude number is used in equations (7.33) and (7.34) in order to take into account the mass velocity in a non-dimensional form. This number in a modified form is also used for correlating the void fraction data [N2, Z3]. It is anticipated therefore that equations (7.33) and (7.34) are not applicable to horizontal NCSGT's. It follows also from the above paragraph that the effect of the Froude number on the outlet steam quality at the inception of the DWO should be different for vertical circular

tubes and vertical annuli, as given by equations (7.33) and (7.34).

In accordance with both equation (7.33) and equation (7.34) the effect of very small inlet subcoolings on the outlet steam quality at the inception of the DWO is very significant, while the effect of high subcoolings on this steam quality is negligible. This is in agreement with the results of the tests considered. In these tests inlet subcoolings varied between 0 and 244 K. (See Table 7.7).

If the steam quality at the outlet of a NCSGT exceeds the outlet steam quality predicted by equation (7.33) (i.e., for a circular tube) or by equation (7.34) (i.e., for an annulus) DWO will occur in the NCSGT. The power at the start of the DWO is given by equation (7.17) in which X_{IC} is expressed by equation (7.33) for circular tubes and by equation (7.34) for annuli.

The error in predicting power at the start of the DWO for the data of [B5, B6, L7, S11] and those of Anderson as quoted from [N3] is shown versus pressure in Fig. 7.16. With 5 exceptions, the errors are within 20%. The RMS error for all the data is 10.6%.

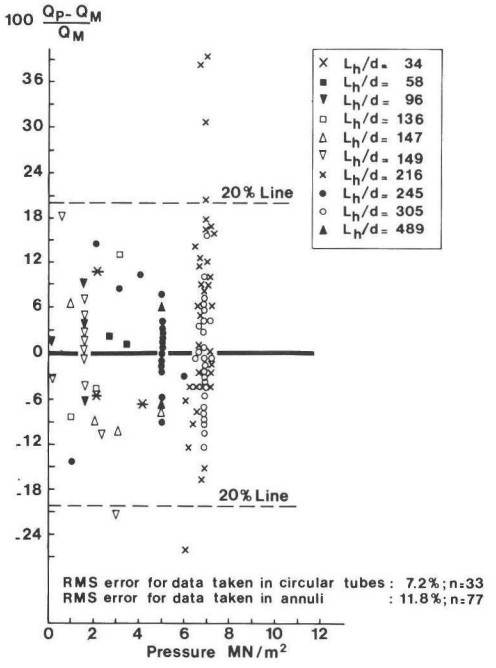

Fig. 7.16 Error in predicting power at the start of the DWO for NCSGT's.

In Figs. 7.16 and 7.11 all the data considered by Neal and Zivi [N3] (i.e., some data of [B6, S11] from NCSGT's and all the data of [Q1] from a short forced circulation steam generator tube) to check 6 stability models are included. The correlations given here predict the power at the start of the DWO with 20% accuracy for 95% of the time for all the data considered by Neal and Zivi [N3]. It should be remembered, however, that an empirical correlation lacks generality and usually can not be used outside its range.

For the data of [B6], the inlet throttling coefficient varies between 0.55 and 6.75. Although for 13 of the 62 tests of [L7] the flow at the inlet of the test tube was throttled, the throttling coefficients are not reported and are assumed to be as small as those of [B6].When correlating the data, the effect of this coefficient on the inception conditions of the DWO was not apparent and therefore it was not considered as a parameter in equations (7.33) and (7.34). It seems that these conditions are not affected substantially if the flow at the inlet of a NCSGT is slightly throttled. In a NCSGT it is not possible to measure directly the effect of inlet throttling on stability since inlet throttling affects mass velocity and thereby the pressure distribution in the tube. Furthermore the data obtained from NCSGT's in early experiments were not sufficient to form a general conclusion on the effect of inlet throttling on stability. In spite of this, it has been concluded long before in the literature that inlet throttling affects the stability of a NCSGT. Therefore, following the general conclusion given in the literature, equations (7.33) and (7.34) are not recommended if the flow at the inlet of a NCSGT is throttled.

In three tests reported in [B6], the flow at the outlet of the riser was throttled in a circular steam generator tube of $L_h/d = 216$. For two of these tests, the pressure, inlet subcooling and mass velocity were kept approximately constant while the ratio of the outlet area of riser to the test section area was changed from 0.655 to 0.328. The power at the start of the DWO for these tests varied from 118.1 kW to 32.7 kW. From the above it is concluded that the outlet throttling has a substantial effect on the inception conditions of the DWO. This effect is taken into account in equation (7.33) by the use of the term Y_{723} given by equation (7.37).

7.3 FLOW PATTERN INSTABILITIES

During the analysis of the developed films made for the measurement of the void fraction, a flow pattern instability was observed in TT1 (i.e., a vertical test tube; see Section 3.1.3: Determination of the Weighted Mean Drift Velocity) and in TT5 and TT6 (i.e., helical coils; see Section 3.2). The flow regime varied from bubble flow to plug flow with a frequency between 10 and 50 Hz for P = 4.3 - 14.2 MN/m^2 and G = 51 - 107 kg/m^2s in TT1 and for P = 4 - 8.1 MN/m^2 and G = 429 - 1518 kg/m^2s in TT5 and TT6. An example of this type of instability is shown in Fig. 7.17. The film shown in the figure was taken with a frequency of about 500 frames/s at 4 MN/m^2 in TT6 (i.e., a helical coil); zero on the film marks the beginning of the time. The time increases proportionally to the numbers given on the film.

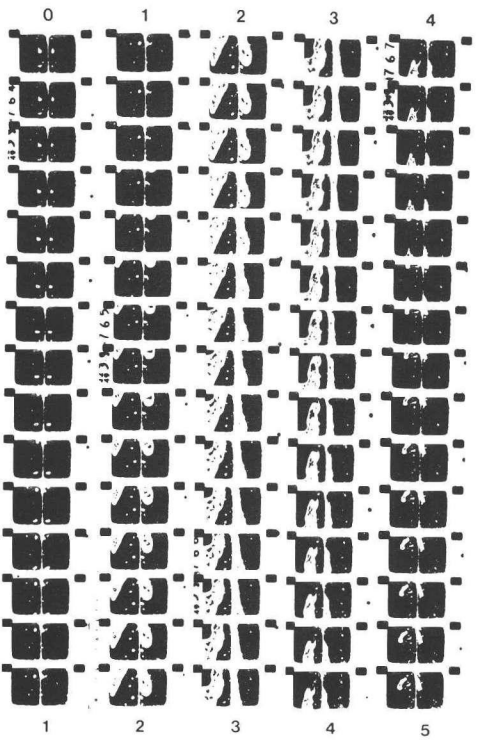

Fig. 7.17 Flow pattern instabilities at 4 MN/m^2 in TT6.

Jeclic and Yang [J1] detected analogous instabilities in an electrically heated vertical tube. In the literature the cause of this type of instability is related to the difference in pressure drop between the bubble slug flow and annular flow regimes [B12]. Since the present test tubes were very long, the variation in pressure drop in different flow regimes could not be the cause of the observed instabilities. Moreover, during these instabilities neither annular flow was observed in TT1 nor annular (or wavy or stratified flow) in TT5 and TT6. The cause of these instabilities is assumed to be the suppression of bubble growth.

The mechanism of the suppression of bubble growth in a vertical tube can then be explained as follows. Bubbles grow at the heated wall, depart from the wall, coalesce, and form a plug. The volume of the plug varies periodically and the plug rotates irregularly and, therefore, destroys the superheated liquid layer on the heated wall. The destruction of this layer delays the growth of bubbles. In the test tube the bubble flow regime exists for the time interval in which enough bubbles are produced to form a plug, and the plug flow regime thereafter. This mechanism is partly in agreement with the motion of a plug seen on developed films, as described in the penultimate paragraph of Section 3.1.3.2.1.

A similar mechanism should apply to the suppression of bubble growth in a helical coil. Bubbles grow at the inside wall of the test tube, depart from the heated surface, coalesce, and form a plug. Under the influence of centrifugal forces this plug glides along the inside wall of the test tube, presses against the thin superheated liquid layer adjacent to the tube wall, and destroys this layer. This again delays the growth of bubbles. In the test tube the bubble flow regime exists for the time interval in which enough bubbles are produced to form a plug and the plug flow regime thereafter.

7.4 INSTABILITIES DUE TO THERMODYNAMIC NON-EQUILIBRIUM BETWEEN THE PHASES

There is a kind of dynamic instability always present in a once-through steam generator tube. The temperature at any point in a cross section in the superheated region of such a steam generator tube may oscillate irregularly up to thermodynamic steam qualities of about 2 [R2]. A typical example is shown in Fig. 7.18. The temperature shown in this figure was measured in TT2 with a 0.5 OD transverse thermocouple

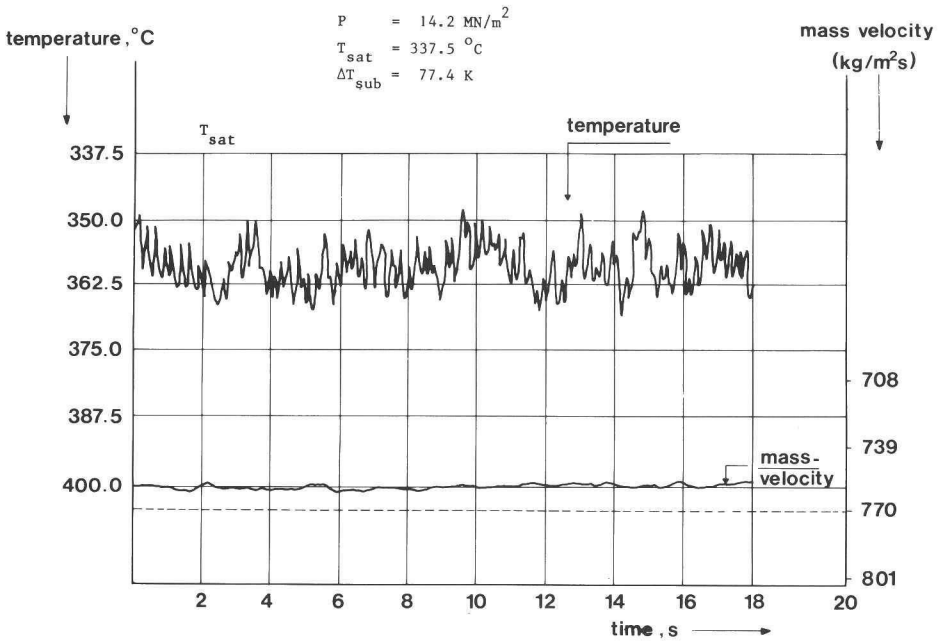

Fig. 7.18 Oscillations due to thermodynamic non-equilibrium between the phases.

located at 2.34 mm distance from the tube wall for P = 14.2 MN/m^2 (T_{sat} = 337.5°C) and ΔT_{sub} = 77.4 K. In the mass flow shown in the figure, there is no substantial variation. For P = 6.2 - 18.2 MN/m^2 and X_o = 1.02 - 1.51, the peak-to-peak amplitudes of the irregular temperature oscillations observed in TT1 and TT2 varied from 4 up to 25 K, and decreased with increasing pressure and outlet temperature. Their periods were small. These oscillations faded away at 20 MN/m^2.

The observed irregular temperature oscillations were due to the thermodynamic non-equilibrium between the phases in superheated steam region, as demonstrated also by Remisov et al. [R2]. The water droplets at the saturation temperature present in the superheated steam should wet irregularly the tip of the thermocouple. The amount of water droplets in any part of the cross-section of the tube can be assumed to vary randomly. Consequently the tip of the thermocouple would be heated up and cooled down irregularly.

The thermodynamic non-equilibrium between the phases, and the thereby resulting temperature oscillations in the superheated steam region of a once-through steam generator tube, can have serious consequences in practice: Firstly a temperature at any point in a cross-section in the superheated steam region of the tube can not be accurately measured by a conventional method, and secondly, in the case of the presence of water droplets in the superheated steam, the degree of superheating is higher than that calculated by a simple heat balance, since the heat needed for the evaporation of water droplets is used for superheating. The above is similar to the thermodynamic non-equilibrium between the phases in the subcooled nucleate boiling region of a boiling channel. However, in the latter, the bulk temperature of the liquid is lower than that calculated from a simple heat balance since a part of heat is lost in the evaporation of bubbles instead of raising the temperature of the liquid.

Chapter Eight

SUMMARY AND CONCLUSIONS

8.1 THIRD CHAPTER

a - A method, i.e., a high-speed photographic technique, was developed to measure a velocity field in a two-phase flow. The measured velocity field was used to evaluate the void fraction.

8.1.1 Vertical Tubes

a - The theoretical model of Zuber and Findlay [Z2] for the evaluation of the void fraction was verified first by experiments carried out in a small diameter vertical steam generator tube for $P = 4.1 - 18$ MN/m^2 and $G = 51 - 2237$ kg/m^{2}s. This verification gave the accurate values of the parameters used in the model. These values differed substantially from those given by Zuber and Findlay and by other investigators [B2, K7, S13, Z3]. Thereafter the results obtained were shown to apply to predict the void fraction accurately for the adiabatic and diabatic flow of steam/water mixtures in small and medium size vertical circular and rectangular tubes and vertical annuli for $d = 4.74 - 34.3$ mm; $P = 1 - 18$ MN/m^2; $G = 51 - 3504$ kg/m^{2}s and $\bar{\alpha} = 0.08 - 99\%$. For this purpose 642 data were used. 62 of these data were obtained during the present study.

b - For the conditions mentioned in paragraph (a) the value of the distribution parameter is almost equal to unity. This implies that for these conditions the radial void and volumetric flux density distributions are of no importance to predict the distribution parameter and that the difference between the cross sectional average velocity of the steam phase and the average volumetric flux density of a steam/water mixture is practically equal to the cross sectional average drift velocity. The above results simplify significantly the well known two theories, i.e., theories of Zuber and Findlay [Z2] and Bankoff [B2] for the evaluation of the void fraction and a velocity field in two-phase flow in medium and small size vertical tubes.

c - For the conditions given in paragraph (a) the weighted mean drift velocity appears to be a weak function of pressure.

8.1.2 Helical Coils

a - Experimental data and correlations were presented for void fraction in coiled steam generator tubes for d = 18 mm; d_c/d = 38.9; P = 4 - 18 MN/m^2; G = 429 - 1518 kg/m^{2}s and β = 0.00018 - 0.58. For the above given pressure range, no data for void fraction are reported in the literature for water. The total number of data obtained was 44. The accuracy of the correlations is about 12.5%.

b - For the flow of steam/water mixtures in helical coils and for β = 0.4 - 0.58; P = 4.2 - 8.1 MN/m^2; G = 429 - 1493 kg/m^{2}s and d_c/d = 38.9, the distribution parameter is not affected by centrifugal forces. It is constant and equal to 0.875. For the flow of air/water mixtures in helical coils the value of the aforesaid parameter is also constant and equal to 1.1 for β = 0.18 - 0.99 and d_c/d = 11 - 48.

c - At elevated pressures and for β = 0.4 - 0.58, the distribution parameter for the flow of steam/water mixtures in helical coils is smaller than the distribution parameter for the flow of steam/water mixtures in horizontal tubes. This conclusion also applies to the flow of air/water mixtures for β = 0.3 - 0.9.

d - For the flow of steam/water mixtures in helical coils the distribution parameter is affected by centrifugal forces and vapour volumetric rate ratio for β = 0.00018 - 0.4; P = 4 - 18 MN/m^2; G = 754 - 1518 kg/m^{2}s and d_c/d = 38.9.

8.2 FOURTH CHAPTER

a - In vertical and helically coiled circular steam generator tubes, the incipient point of boiling was measured for P = 4 - 18 MN/m^2 and G = 757 - 2208 kg/m^{2}s and the initial point of net vapour generation for P = 4 - 18 MN/m^2 and G = 1435 - 2203 kg/m^{2}s. For the measurements a direct method, i.e., a high-speed photographic technique, was used. The present 22 data and 143 data from the literature were analysed.

b - Both the IPB and IPNVG are closely related to the heat transfer mechanism for the subcooled nucleate flow boiling. Therefore a dimensionless number which characterizes these points was derived from a phenomenological heat transfer equation. This dimensionless number gives the ratio of the heat flux due to suppressed forced convection to the total heat flux at the IPB and IPNVG. For water, the value of this dimensionless number is constant and equal

b1- to 0.665 for the IPB in vertical circular tubes and annuli and on a flat plate for P = 0.15 - 19.6 MN/m^2; G = 470 - 17355 kg/m^2s; q = 0.13 - 9.8 MW/m^2; ΔT_{sub} = 2.6 - 108 K and d = 2.13 - 32 mm, and

b2- to 0.445 for the IPB in helical coils for P = 4 - 18 MN/m^2; G = 757 - 1518 kg/m^2s; q = 0.082 - 0.39 MW/m^2; ΔT_{sub} = 4.4 - 12.5 K and d = 18 mm, and

b3- to 0.24 if $u \geq 0.45$ m/s and to 0.11 if $u < 0.45$ for the IPNVG in vertical circular and rectangular tubes, vertical annuli and in helical coils for P = 0.1 - 18 MN/m^2; G = 132 - 2818 kg/m^2s; q = 0.128 - 1.92 MW/m^2; ΔT_{sub} = 1.2 - 42 K and d = 4.1 - 19.8 mm.

b4- For the IPNVG in vertical tubes and for Refrigerant-22 the value of the above dimensionless number is equal to 0.18 if $u \geq 0.45$ m/s and to 0.11 if $u < 0.45$ for P = 1.2 - 3.3 MN/m^2; G = 180 - 1391 kg/m^2s; q = 0.02 - 0.06 MW/m^2; ΔT_{sub} = 3.2 - 7.3 K and d = 10.2 mm.

c - The IPB in helical coils seems retarded in comparison with the IPB in vertical tubes. This is probably due to the peripheral conduction of heat in the wall of a helically coiled steam generator tube.

d - A scaling law to predict the IPNVG for liquids different from water and Refrigerant-22 was also established using the aforesaid phenomenological heat transfer equation for the subcooled nucleate flow boiling.

8.3 FIFTH CHAPTER

a - A heat transfer controlled bubble model yielded three semi-empirical correlations to predict bubble growth rate, maximum bubble diameter and maximum bubble growth time for the subcooled nucleate flow boiling of water. The model was verified with the data obtained for P = 0.1 - 17.7 MN/m^2; u = 0.08 - 9.15 m/s; q = 0.47 - 10.64 MW/m^2;

ΔT_{sub} = 3 - 86 K; d_m = 0.08 - 1.24 mm and t_m = 0.175 - 5 ms. For this purpose 60 data were used, 12 of which were obtained in the present study. The model fitted the experiment well.

b - The model reveals the fact that the dry area under a bubble growing in the subcooled nucleate flow boiling region of a steam generator tube disappears beyond about 1 MN/m^2.

c - The behaviour of a bubble formed at the IPB differs from the behaviour of the average bubble of a bubble population consisting of numerous bubbles. Both types of bubbles were considered in the present study.

8.4 SIXTH CHAPTER

8.4.1 Dryout

a - The dryout conditions were determined in three sodium heated helically coiled circular tubes of 18 mm ID. The heated straightened lengths of these coils were 40.13, 35.50 and 26.67 m and the coil diameters 1.5, 0.7 and 0.7 m respectively. The tests were carried out for the following range of operating conditions: P = 14.7 - 20.2 MN/m^2; G ≐ 112 - 1829 kg/m^2s; ΔT_{sub} = 35.6 - 156.8 K; X_d = 0.08 - 1; q_d = 41 - 731 kW/m^2.

b - Dryout always took place in the last quarter length of a test tube, and was detected only at the inside, top, outside and bottom positions. The distance between the locations of the first and the last detected dryout varied between 0.2 and 5.1 m. This distance was a small fraction of the length of a test tube, i.e., up to 15%. The above suggests that the location of the first detected dryout nearly coincides with the location where the dryout actually takes place first and the location of the last detected dryout with the location where the dryout in fact terminates. This result is of importance for practical applications.

c - At mass velocities higher than about 850 kg/m^2s, the dryout was first detected at the inside of a test tube. The last detected dryout was at the outside of the tube. At mass velocities lower than 850 kg/m^2s, the first and the last detected dryouts were at the top and bottom of the tube respectively. The location of the dryout appear

to depend on, among other things, the centrifugal and gravitational forces.

d - At high mass velocities wall temperature fluctuations at r = 9.75 mm were very small at the first detected dryout location and these fluctuations became larger at the last detected dryout location. Decreasing the mass flow yielded larger temperature fluctuations.

e - The 203 data obtained in the present study for the first and the last detected dryouts, the 674 data of various investigators taken in short and long electrically heated vertical circular tubes and in a long sodium heated vertical circular tube were correlated to predict the dryout heat flux within 20% accuracy for 98% of the time. The RMS error for all the 877 data is 9.01%. The ranges of geometries and operating conditions of the data used to establish the the correlation are as follows: L_h = 0.25 - 40.13 m; d = 7.86 - 18 mm; $d/(2\ \delta)$ = 1.90 - 6.67; d_c/d = 38.9 - 83.3; P = 4.3 - 20.2 MN/m^2; G = 112 - 5542 kg/m^2s; ΔT_{sub} = 8 - 273 K; X_d = 0 - 1; q_d = 41 - 4931 kW/m^2. The correlation is not recommended for short tubes for P < 9.7 MN/m^2.

f - The so-called equivalent length hypothesis would have a physical significance for the mechanism of dryout.

g - The dryout correlations based on data obtained in uniformly heated (i.e., electrically heated) tubes are not recommended for non-uniformly heated tubes.

8.4.2 Two-Phase Flow Pressure Drop

a - In the above coils two-phase flow pressure drop was also measured. The 70 data obtained and the 299 data taken in a 10 m long sodium heated vertical circular tube of 7.86 mm ID were correlated within 20% accuracy for 98% of the time. The RMS error for all the 369 data was 9.87%. The range of operating conditions for the data used to establish the correlation is: P = 14.3 - 20.1 MN/m^2; G = 296 - 3498 kg/m^2s; X_{bt} = 0.06 - 1; ΔP = 3.0 - 226 kN/m^2.

8.5 SEVENTH CHAPTER

8.5.1 DWO

a - The DWO were studied in four once-through steam generator tubes of L_t/d = 1272 - 2468 and a large scale model evaporator of L_t/d = 1535 for P = 5.3 - 19.1 MN/m^2; G = 187 - 1365 kg/m^2s; X_{IC} = 1.10 - 2.38; ΔT_{sub} = 3.2 - 168 K and K = 0 - 713. All the test tubes and the evaporator operated in the forced convection mode and were heated by sodium.

b - The DWO in once-through forced convection steam generator tubes are time-delay oscillations. The length of the superheated steam region and the transit time in this region are of vital importance for the mechanism of the DWO. In order to trigger the multiple regenerative feedback mechanism which generates the DWO in a once-through forced convection steam generator tube when outlet pressure and inlet throttling are kept constant, the length of the superheated steam region has to reach a constant value. Thereafter the DWO appear and the multiple regenerative feedback mechanism begins to operate. Inlet throttling delays this mechanism.

c - For the mechanism of the DWO in a once-through forced convection steam generator tube, a dimensionless empirical relation was established using the dimensionless transit times in different heat transfer regimes of the tube. The relation is in fact a stability model and was verified with 176 data obtained in a 44.43 m long helical coil and a 20.45 m long tube, comprised of a vertical and a horizontal V-shaped tube for P = 7.6 - 19 MN/m^2; G = 262 - 1020 kg/m^2s; ΔT_{sub} = 20.4 - 168 K and X_{IC} = 1.37 - 2.20.

d - The steam quality at the outlet of a once-through forced convection steam generator tube at the inception of the DWO is practically a function of pressure for a given inlet throttling whereas the effects of all the other operating conditions on this steam quality are of secondary importance. This was demonstrated also using the relation for the mechanism of the DWO mentioned in the above paragraph.

e - Paragraphs (b) to (d) suggest that the data for the DWO obtained in once-through forced convection steam generator tubes for the DWO can be accurately correlated in different ways. Two correlations were established for wide ranges of operating conditions and geometries.

f - The correlating parameters used in the first correlation were the dimensionless inlet subcooling enthalpy, reduced pressure, inlet throttling coefficient and the ratio of the heated length to the tube diameter. The ranges of geometries and operating conditions used to establish the correlation were: Geometry: circular straight tubes, circular serpentines, circular helical coils, tubes, each comprised of a circular vertical and a circular V-shaped horizontal tube, and a rectangular straight tube; type of heating: sodium and electrical heating; L_h/d = 153 - 9502; d = 4.49 - 29.9 mm; X_{IC} = 0.27 - 2.38; P = 4.1 - 19.1 MN/m^2; G = 118 - 2088 kg/m^{2}s; ΔT_{sub} = 2.8 - 245.9 K and K = 0 - 2882. The number of data considered was 413. The correlation applies both to a once-through forced convection steam generator tube and to a forced convection steam generator tube in which no superheated steam was produced. The correlation predicts the power at the start of the density wave oscillations from these 413 data within 8% accuracy for 87% of the time with a RMS error of 5.97%.

g - The correlating parameters in the second correlation included practically all the operational and geometrical conditions in dimensionless forms. The ranges of geometries and operating conditions of the data used to establish this correlation were: Geometry: circular straight tubes, circular coils, a circular serpentine and tubes, each comprised of a circular vertical and a circular V-shaped horizontal tube; type of heating: sodium and electrical heating; L_t = 10 - 223.3 m; L_t/d = 1272 - 10150; d = 7.86 - 22 mm; d_c/d = 47.4 - 83.3; P = 4.3 - 19.1 MN/m^2; G = 118 - 1365 kg/m^{2}s; ΔT_{sub} = 3.2 - 245.9 K; X_{IC} = 1.01 - 2.38 and K = 0 - 2882. The number of data considered was 380. The correlation applies only to once-through steam generator tubes producing superheated steam only, and predicts the power at the inception of the DWO from these data within 7.5% accuracy for 98% of the time with a RMS error of 3.33%.

h - For once-through steam generator tubes of $L_t/d > 4167$, the effect of inlet throttling on the outlet steam quality or on power at the inception conditions of the DWO disappears.

i - A correlation to predict the period of the DWO in once-through forced convection steam generator tubes and in a forced convection steam generator tube in which no superheated steam was produced was also established for L_t = 0.68 - 44.43 m; d = 4.49 - 18 mm;

$P = 4.1 - 19$ MN/m^2; $G = 262 - 2088$ kg/m^{2}s; $X_{IC} = 0.27 - 2.20$; $\Delta T_{sub} = 2.8 - 168$ K; $\psi = 0.345 - 12.5$ s and $K = 0 - 450$. The number of data considered was 188. The correlation predicts the period from these data within about 30% for 95% of the time with a RMS error of 15.1%.

j - Inlet throttling appears to affect the period of the DWO.

k - It is considered justified to conclude that the inception conditions of the DWO in once-through forced convection steam generator tubes can be predicted with simple equations, thus eliminating the use of time consuming complicated stability correlations in the form of a computer program at least for the ranges of geometries and operating conditions used in the present study. It should be stressed here that the present correlations were derived from the physical mechanism of the DWO in once-through forced convection steam generator tubes.

l - In order to support the conclusion given in paragraph (k), the 110 data obtained by different investigators in natural circulation steam generator tubes for the inception conditions of the DWO were also correlated with simple equations. The ranges of geometries and operating conditions for these data were: Geometry: vertical circular tubes and vertical annuli; $d = 8.51 - 36$ mm; $L_h = 0.91 - 4.89$ m; $L_h/d = 34 - 489$; $P = 0.2 - 7.1$ MN/m^2; $X_{IC} = 0.04 - 0.62$; $G = 529 - 1230$ kg/m^{2}s and $\Delta T_{sub} = 0 - 244$ K. The established correlatic predicts the power at the inception of the DWO from these data within 20% accuracy for 95% of the time with a RMS error of 10.6%.

m - A small amount of inlet throttling does not affect the inception conditions of the DWO in natural circulation steam generator tubes.

8.5.2 Flow Pattern Instabilities

a - The cause of the flow pattern instabilities observed in two long steam generator tubes of different geometries seems due to the suppression of bubble growth but not to the difference in pressure drop between the bubble slug flow and annular flow regimes.

8.5.3 Instabilities Due to Thermodynamic Non-Equilibrium Between the Phases

a - In the presence of these instabilities, neither the true steam quality nor the temperature of steam along the length of a once-through steam generator tube can be measured accurately with conventional methods beyond the location where the thermodynamic steam quality reaches 1. This implies that the above quantities should be evaluated theoretically at the present state of art.

ACKNOWLEDGEMENTS

a - The works reported in Chapter 2 to Chapter 8.

These works were carried out in the "Department of Reactor Technology" (KRT) of "MT-TNO", and were sponsored by the Ministry of Economic Affairs of The Netherlands. The authority between the sponsor and KRT was the "Project Group for Nuclear Energy - TNO" (PgK). The manager/director of this Group was first Mr. A.H. de Haas van Dorsser, and was succeeded by Mr. A.R. Braun. The project engineer between PgK and KRT was Mr. G.J.A.M. Meijer.

The author is indebted to Mr. K.A. Warschauer, one of the directors of MT-TNO, for his permission to write this thesis as well as for his comments on his papers. Mr. Max van Gasselt was the head of KRT where the author worked, and many thanks are due to him for his encouragements and all the contributing discussions. Mr. L.M. Rappoldt assisted in the design of the Swish rig and the test tubes used in this rig. The rig and test tubes were constructed by the "Department of Physical Measuring Techniques" under the leadership of Mr. P.H. Engelmann, head of this department. The photographical test sections were designed by Mr. W. van Deelen. Messrs. B.L. Falet, H. Slotboom, U.G. Vincent also contributed to the design and construction activities.

The Swish rig was maintained and operated by Messrs. P. van 't Verlaat, A.R. Brand, C. van Huffelen and A.J.C. Spierings. The stability and distribution parameter tests in TT1 and TT2 were carried out by Mr. P.J. de Munk. Mr. C. van Huffelen analysed all the films. The on- and off-line computer works were carried out by Messrs. G.A.C. Boersen, C. van Huffelen, B.J. Stam, R. Vogelzang and G. Wentink.

The paper which deals with Neratoom's evaporator was published with the kind permission of Neratoom. The tests reported in that paper were carried out by Mr. N.A. Doets.

The manuscript was typed by Mrs. H. Uitslag-van Amersfoort and corrected by Mr. J.D. Duyvensz. Mr. R. van den Haak drafted the figures.

b - The work reported in Appendix 4.

This work was sponsored by the "Atomic Energy Commission of Turkey". Thanks are due to Prof. Dr. S. Akpınar, Mr. İ. Deriner and Prof. Dr. F. Domaniç.

REFERENCES

[A1] A.H. Abdelmessih, S.T. Yin and A. Fakhri, Hysteresis effects and hydrodynamic oscillations in incipient boiling of Freon-11, Proceedings of International Meeting on Reactor Heat Transfer, Karlsruhe, October 9-11, 1973, pp. 331-350.

[A2] A.H. Abdelmessih, F.C. Hooper and S. Nangia, Flow effects on bubble growth and collapse in surface boiling, Int. J. Heat Mass Transfer 15, 115-125 (1972).

[A3] N. Adorni, G. Peterlongo, R. Ravetta and F.A. Tacconi, Large scale experiments on heat transfer and hydrodynamics with steam-water mixtures: Phase and velocity distribution measurements in a round vertical tube, CISE - R - 91 (1964).

[A4] G. Agostini, A. Era and A. Premoli, Density measurements of steam-water mixtures flowing in a tubular channel under adiabatic and heated conditions, Energia Nucl., Milano 18, 295-310 (1971).

[A5] K. Akagawa, T. Sakaguchi and M. Ueda, Study on a gas-liquid two-phase flow in helically coiled tubes, Bulletin of the JSME 14, 564-571 (1971).

[A6] The American Society of Mechanical Engineers, 1967 ASME Steam Tables, New York (1967).

[A7] W.T. Anglease, D.J.B. Chambers and R.C. Jeffrey, Measurement of water/steam pressure drop in helical coils, paper presented at "Multi-Phase Flow Meeting" in Glasgow (1974).

[A8] A.A. Armand, The resistance during the movement of a two-phase system in horizontal pipes, AERE - TRANS 828 (1959).

[A9] A.A. Armand and G.G. Treshchev, Investigation of the resistance during the movement of steam-water mixtures in a heated boiler pipe at high pressures, AERE Lib/Trans 816 (1959).

[A10] N.M. Aybers, Transport of gas bubbles through a stagnant liquid and turbulent liquid stream, paper presented at "Nato Advanced Study Institute on Two-Phase Flows and Heat Transfer", August 16-27, 1976, Istanbul, Turkey.

[B1] S. Banerjee, E. Rhodes and D.S. Scott, Pressure drops, flow patterns and hold-up for concurrent gas-liquid flow in helically coiled tubes, paper presented at AIChE Meeting, Tampa, Florida (May 1968).

[B2] S.G. Bankoff, A variable density single-fluid model for two-phase flow with particular reference to steam-water flow, J. Heat Transfer 82, 265-272 (1960).

[B3] P.G. Barnett, The prediction of burnout in non-uniformly heated rod clusters from burnout data for uniformly heated round tubes, AEEW-R 362 (1964).

[B4] K.M. Becker and P. Persson, An analysis of burnout conditions for flow of boiling water in vertical round ducts, Journal of Heat Transfer 86, 515-530 (1964).

[B5] K.M. Becker, R.P. Mathisen, O. Eklind and B. Norman, Measurements of hydrodynamic instabilities, flow oscillations and burnout in a natural circulation loop, AE-131, 1964, Aktiebolaget Atomenergi, Sweden.

[B6] K.M. Becker, S. Jahnberg, I. Haga, P.T. Hansson and R.P. Mathisen, Hydrodynamic instability and dynamic burnout in natural circulation two-phase flow - An experimental and theoretical study, AE-156 (1964).

[B7] K.M. Becker, Burnout conditions for round tubes at elevated pressures, paper presented at "International Symposium on Two-Phase Flow Systems", Technion City - Haifa - Israel (1971).

[B8] A.E. Bergles and W.M. Rohsenow, The determination of forced convection surface-boiling heat transfer, J. Heat Transfer 86, 365-372 (1964).
[B9] T. Bjørlo, T. Eurola, R. Grumbach, P. Hansson, A. Olson, J. Rasmussen and K. Romslo, Comparative studies of mathematical hydrodynamic models applied to selected boiling channel experiments, Proceedings of the Symposium on Two-Phase Flow Dynamics, EUR-4288e, Vol. I, pp. 981-1057 (1969).
[B10] V.M. Borishanskii, A.P. Kozyrev, L.S. Svetlova, Heat transfer during nucleate boiling of liquids, in "Convective Heat Transfer in Two-Phase and One-Phase Flows", edited by V.M. Borishanskii and I.I. Paleev, Israel Program for Scientific Translations, Jerusalem 1969, pp. 57-84.
[B11] J.A. Bouré, The oscillatory behaviour of heated channels - An analysis of the density effects - Part I: The Mechanism (non linear analysis); Part II: The oscillations thresholds (linearised analysis), CEA R 3049 (1966).
[B12] J.A. Bouré, A.E. Bergles and L.S. Tong, Review of two-phase flow instability, Nuclear Engineering and Design 25, 165-192 (1973).
[B13] R.W. Bowring, Physical model, based on bubble detachment, and calculation of steam voidage in the subcooled region of a heated channel, HPR 29, Institute for Atomenergi, Halden, Norway (1962).
[B14] B.E. Boyce, J.G. Collier and J. Levy, Hold-up and pressure drop measurements in the two-phase flow of air-water mixtures in helical coils, Proc. Int. Symp. on Research in Concurrent Gas-Liquid Flow, hel at the University of Waterloo, Sept. 18-19, 1968, pp. 203-231. Edited by E. Rhodes and D.S. Scott, Plenum Press, New York (1969).
[B15] J. Brasz, Hydrodynamic instability and performance degradation of a straight-tube sodium heated steam generator, Proceeding of Condensed Papers of the Meeting - "Two-Phase Flow and Heat Transfer Symposium-Workshop", Ft. Lauderdale - Florida, October 18-20, 1976, edited by T.N. Veziroglu, University of Miami, 1976, pp. 183-189.
[B16] A.R. Braun, Sodium test facilities available at TNO, Proceedings of the Information Meeting-TNO Contribution to LMFBR Development, May 10-11, 1973, Utrecht, The Netherlands, pp. 56-67.
[B17] C.J. Baroczy, A systematic correlation for two-phase pressure drop, Chem. Engng. Progr.Symp. Ser. 62 (64), 232-249 (1966).
[B18] D. Butterworth and G.W. Hewitt, editors, Two-Phase Flow and Heat Transfer, Oxford University Press (1977).

[C1] F. Campolunghi, M. Cumo, G. Ferrari, R. Leo and G. Vaccaro, An experimental study on heat transfer in long, subcritical once-through steam generators, Proceedings of International Meeting on Reactor Heat Transfer, Karlsruhe, pp. 373-403 (9-11 October 1973).
[C2] F. Campolunghi, M. Cumo, G. Ferrari and G. Vaccaro, A burnout correlation for once-through L.M.F.B.R. steam generators, CNEN Report - RT/ING (74) 8 (1974).
[C3] J.R. Carver, C.R. Kakarala and J.S. Slotnik, Heat transfer in coiled tubes with two-phase flow, the Babcock-Wilcox Company Research Center Report, Report No. 4438 (1964).
[C4] W.J.C. de Clercq and N.J. van Waveren, Steam-generator and intermediat heat-exchanger development, in "Sodium-Cooled Fast Reactor Engineering Proceedings of a Symposium, Monaco, 23-27 March 1970, pp. 433-451, IAE (1970).
[C5] W.H. Cook, Boiling density in vertical rectangular multichannel sections with natural circulation, ANL-5621 (1956).
[C6] M.G. Cooper, The microlayer and bubble growth in nucleate pool boiling Int. J. Heat Mass Transfer 12, 915-934 (1969).

[C7] M.G. Cooper and A.J.P. Lloyd, Transient local heat flux in nucleate boiling, Proceedings of Third International Heat Transfer Conference, Vol. III, pp. 193-203 (1966).
[C8] J.D. Crowley, C. Deane, S.W. Gouse, Two-phase flow oscillations in vertical, parallel, heated channels, Proceedings of the Symposium on Two-Phase Flow Dynamics, EUR-4288e, Vol. II, pp. 1131-1171 (1969).
[C9] R. Collins et al., J. Fluid Mech. 89, 497-514 (1978).

[D1] A.L. Davies and R. Potter, Hydraulic stability - An analysis of the causes of unstable flow in parallel channels, AEWW-R446 (1966).
[D2] R. Deam and J. Murray, The prediction of dynamic stability limits in once-through boilers using DYMEL, paper presented at "European Two-Phase Group Meeting", Erlangen, 31st May - 4th June 1976.
[D3] R. Deam, Personal communication.
[D4] F.J.M. Dijkman, Some hydrodynamic aspects of a boiling water channel, Ph.D. Thesis, Technical University of Eindhoven, The Netherlands (1969).
[D5] L. Duchatelle, L. de Nucheze and M.G. Robin, Heat transfer in helical tube sodium heated steam generators, paper presented at "1975 International Seminar-Future Energy Production-Heat and Mass Transfer Problems", Dubrovnik, August 25-30 (1975).
[D6] Du Pont de Nemours Int. S.A., Geneva, Switzerland, Thermodynamic properties of "Freon-22" refrigerant, Technical Bulletin T-22 (1964).
[D7] M.E. Durham, The thermodynamic and transport properties of liquid sodium, CEGB - Report - RD/B/M2479 (Revised) - CFR/THWP/P(72) 28 (1974).
[D8] O.E. Dwyer, Atomic Energy Review 4 (1), 3-92 (1966).

[E1] L.E. Efferding, DYNAM - A digital computer program for study of the dynamic stability of once-through boiling flow with steam superheat, GAMD-8656 (1968).
[E2] R.A. Egen, D.A. Dingee and J.W. Chastain, Vapor formation and behaviour in boiling heat transfer, BMI 1163 (1957).
[E3] R. Evangelisti and P. Lupoli, The void fraction in an annular channel at atmospheric pressure, Int. J. Heat Mass Transfer 12, 699-711 (1969).

[F1] T. Fallows, J.A. Hitchcook, R.C. Jones, J. Lis and E.W. Northover, A study of oscillatory instabilities in the parallel channels of a high pressure once-through boiler rig, Proceedings of the International Conference - Boiler Dynamics and Control in Nuclear Power Stations, The British Nuclear Energy Society, pp. 14.1-14.8 (1973).
[F2] J.K. Ferrell, A study of convection boiling inside channels, North Carolina State University, Raleigh, North Carolina (1964).
[F3] K.E. Forster and R. Greif, Heat transfer to a boiling liquid-Mechanism and correlations, J. Heat Transfer 81, 43-53 (1959).

[G1] P. Griffith, J.A. Clark and W.M. Rohsenow, Void volumes in subcooled boiling systems, ASME Paper No. 58-HT-19 (1958).
[G2] F.C. Gunther, Photographic study of surface-boiling heat transfer to water with forced convection, Trans. of ASME 73, 115-123 (1951).

[H1] A.H. de Haas van Dorsser, Introduction in Fast Reactor Technology - TNO, a brochure issued by Project Group for Nuclear Energy-TNO, Apeldoorn - The Netherlands (1973).
[H2] R.W. Haywood, G.A. Knights, G.E. Middleton and J.R.S. Thom, Experimental study of the flow conditions and pressure drop of steam/water mixtures at high pressures in heated and unheated tubes, Proc. Instn. Mech. Engrs., Vol. 175, 1961, pp. 669-748, Instn. Mech. Engrs., London.
[H3] H.G. Hirschberg, Kältemittel, pp.72-74 and 27. C.F. Müller, Karlsruhe (1966).

[H4] R.F. Hopwood, Pressure drop, heat transfer and flow phenomena for forced convection boiling in helical coils - A literature survey, AEEW-R-757 (1972).
[H5] Y.Y. Hsu, R.W. Graham, Transport Processes in Boiling and Two-Phase Systems, Hemisphere Publishing Corporation (1976).
[H6] G.A. Hughmark, Hold-up in gas-liquid flow, Chemical Engineering Progress 58, 62-65 (1962).

[I1] A. Inoue, S. Aoki and T. Koga, On the void and the velocity profiles of two-phase bubble flow in a vertical pipe, Presentation made at the Round Table Discussion on Momentum and Heat Transfer Mechanism in Two-Phase Flow, Fifth International Heat Transfer Conference, September 3-7, 1974, Tokyo.
[I2] M. Ishii, O.C. Jones, Jr., Derivation and application of scaling criteria for two-phase flows in "Two-Phase Flows and Heat Transfer", edited by S. Kakaç and F. Mayinger, Vol. 1, pp. 163-185, Hemisphere Publishing Corporation (1977).
[I3] H. Ito, Friction factors for turbulent flow in curved pipes, Journal of Basic Engineering 81, 123-134 (1959).

[J1] F.A. Jeclic and K.T. Yang, The incipience of flow oscillations in forced-flow subcooled boiling, NASA TM X-52081 (1965).
[J2] A.B. Jones and A.G. Dight, Hydrodynamic stability of a boiling channel Part II, KAPL-2208 (1962).

[K1] S. Kakaç , T.N. Veziroglu, H.B. Aksu, Y. Alp, Boiling flow instabilities in a four parallel-channel upflow system, Proceedings of International Meeting on Reactor Heat Transfer, Karlsruhe, October 9-11, 1973, pp. 404-420.
[K2] G. Kasturi and J.B. Stepanek, Two-phase flow-I. Pressure drop and void fraction measurements in cocurrent gas-liquid flow in a coil, Chemical Engineering Science 27, 1871-1880 (1972).
[K3] A. Kirchenmayer, H.E. Scholz, Stability problems of boiling water reactors, Proceedings of the Symposium on Two-Phase Flow Dynamics, EUR-4288e, Vol. I, pp. 1059-1070 (1969).
[K4] J.G. Knudsen and D.L. Katz, Fluid Dynamics and Heat Transfer, pp. 129-145, 176, 394, 403, 405, 431 and 488, McGraw Hill, New York (1958).
[K5] K. Kobayasi, Measuring method of local phase velocities and void fraction in bubble and slug flows, Presentation made at the Round Table Discussion on Momentum and Heat Transfer Mechanism in Two-Phase Flow, Fifth International Heat Transfer Conference, September 3-7, 1974, Tokyo.
[K6] A.S. Konkov, Experimental study of the conditions under which heat exchange deteriorates when a steam water mixture flows in heated tubes, Teploenergetika 13 (12), 53-57 (1966).
[K7] P.G. Kroeger and N. Zuber, An analysis of the effects of various parameters on the average void fractions in subcooled boiling, Int. J. Heat Mass Transfer 11, 211-233 (1968).
[K8] J. Kubota, T. Tsuchiya, T. Iwashita and K. Monta, Hydrodynamic stability tests and analytical model development for once-through sodium heated steam generator, paper presented at BNES Meeting - Boiler Dynamics and Control in Nuclear Power Stations, Bournemouth, October 1979.
[K9] S.S. Kutateladze, Boiling heat transfer, Int. J. Heat Mass Transfer 4, 31-45 (1961).
[K10] S.S. Kutateladze and V.M. Borishanskii, A Concise Encyclopedia of Heat Transfer, p. 114. Pergamon Press, Oxford (1966).

[L1] M. Ledinegg, "Unstabilität der Strömung bei Naturlichem und Zwangsumlauf", Die Wärme 61, 891-898 (1938).
[L2] D.H. Lee, An experimental investigation of forced convection burnout in high pressure water - Part III - Long tubes with uniform and non-uniform axial heating, AEEW-R 355 (1965).
[L3] D.H. Lee, Studies of heat transfer and pressure drop relevant to sub-critical once-through evaporators, paper presented at "IAEA Symposium on Progress in Sodium-Cooled Fast Reactor Engineering", Monaco, 23rd-27th March 1970.
[L4] D.H. Lee, Prediction of burnout, in "Two-Phase Flow and Heat Transfer", edited by D. Butterworth and G.W. Hewitt, pp. 295-322, Oxford University Press (1977).
[L5] O. Levenspiel, Collapse of steam bubbles in water, Industrial and Engineering Chemistry 51, 787-790 (1959).
[L6] S. Levy, Forced convection subcooled boiling-Prediction of vapor volumetric fraction, Int. J. Heat Mass Transfer 10, 951-965 (1967).
[L7] S. Levy, E.S. Beckjord, Hydraulic instability in a natural circulation loop with net steam generation at 1000 psia, GEAP-3215 (1959).
[L8] R.W. Lockhart and R.C. Martinelli, Proposed correlation of data for isothermal two-phase, two-component flow in pipes, Chemical Engineering Progress 45, 39-48 (1949).
[L9] P.W.P.H. Ludwig, B.M. Hus, Some results of the 50 MW straight tube steamgenerator test in the TNO 50 MW SCTF at Hengelo, paper presented at "IAEA Study Group Meeting on Steam Generators for LMFBR's", Bensberg, October 14-17 (1974).

[M1] R.C. Martinelli and D.B. Nelson, Prediction of pressure drop during forced-circulation boiling of water, Transactions of the ASME 70 (6), 695-702 (1948).
[M2] G.W. Maurer, A method of predicting steady-state boiling vapor fractions in reactor coolant channels, Bettis Technical Review, WAPD-BT-19, pp. 59-70 (1960).
[M3] W.H. McAdams, Heat Transmission, p. 135, McGraw Hill, New York (1954).
[M4] W.H. McAdams, W.E. Kennel, C.S. Minden, R. Carl, P.M. Picornell and J.E. Dew, Heat transfer at high rates to water with surface boiling, Ind. Engng. Chem. 41, 1945-1953 (1949).
[M5] Z.L. Miropolskiy, R.I. Shneyerova and A.I. Karamysheva, Vapor void fraction in steam-fluid mixtures flowing in heated and unheated channels, Heat Transfer 1970, Preprints of papers presented at the Fourth International Heat Transfer Conference, Paris-Versailles 1970, Vol. 5, Paper No. B4.7.
[M6] P.J. de Munk, Two-phase flow experiments in a 10 m long sodium heated steam generator test section, Proceedings of International Meeting on Reactor Heat Transfer, Karlsruhe, October 9-11, pp. 504-518 (1973).
[M7] P.J. de Munk, A.D. Koppenol, B.J. Stam, Warmte-overdracht- en drukvalmetingen in een natriumverhitte stoomgenerator testsectie in het drukbereik van 150 tot 200 bar, een compilatie van metingen, TNO-Report Report No. 74-0839 (1974) [Confidential].

[N1] M. Naitoh, A. Nakamura and H. Ogasawara, Dryout in helically coiled tube of sodium heated steam generator, ASME paper - 74-WA/HT-48 (1975).
[N2] L.G. Neal, An analysis of slip in gas-liquid flow applicable to the bubble and slug flow regimes, KR - Report, KR - 62 (1963).
[N3] L.G. Neal and S.M. Zivi, Hydrodynamic stability of natural circulation boiling systems, Vol. I, STL- 372-14(1) (1965).

[O1] K. Ohba, Simultaneous measurement of local flow velocity and void fraction in bubble flows using a gas laser, Presentation made at the Round Table Discussion on Momentum and Heat Transfer Mechanism in Two-Phase Flow, Fifth International Heat Transfer Conference, September 3-7, 1974, Tokyo.

[O2] H.J. van Ouwerkerk, The role of the evaporating microlayer and dry surface areas in boiling, Ph.D. Thesis, Technical University of Eindhoven, The Netherlands (1970).

[O3] W.L. Owens Jr., Two-phase pressure gradient, International Developments in Heat Transfer, Part 2, 363-368, ASME (1961).

[P1] F.N. Peebles and H.J. Garber, Studies on the motion of gas bubbles in liquids, Chemical Engineering Progress 49, 88-97 (1953).

[P2] O.L. Peskov, V.I. Subbotin, B.A. Zenkevich and N.D. Sergeyev, The critical heat flux for the flow of steam-water mixtures through pipes, in "Problems of Heat Transfer and Hydraulics of Two-Phase Media" edited by S.S. Kutateladze, pp. 48-62, Pergamon Press (1969).

[P3] N.H. Pratt, The heat transfer in a reaction tank cooled by means of a coil, Trans. Instn. Chem. Engrs. 25, 163-180 (1947).

[P4] Proceedings of the Symposium on Two-Phase Flow Dynamics, EUR-4288e, Vol I and Vol. II (1969).

[Q1] E.R. Quandt, Analysis and measurements of flow oscillations, Chem. Eng Progress Symposium Series 57 (32), 111-126 (1961).

[R1] G.V. Ratiani and D.I. Avaliani, Correlation of experimental data on heat transfer during boiling of Freon-12 and Freon-22, in Convective Heat Transfer in Two-Phase and One-Phase Flows, edited by V.M. Borishanskii and I.I. Paleev, pp. 170-173. Israel Program for Scientific Translations, Jerusalem (1969).

[R2] O.V. Remisov, V.A. Vorobyev, Yu.I. Gribanov, V.V. Sergeev, Statistical characteristics of temperature pulsations within post-burnout region, Proceedings of the Fifth International Heat Transfer Conference, Tokyo 1974, Vol. IV, pp. 215-219.

[R3] B.L. Richardson, Some problems in horizontal two-phase two-component flow, ANL-5949 (1958).

[R4] G.R. Rippel, C.M. Eidt. Jr., and H.B. Jordan. Jr., Two-phase flow in a coiled tube-Pressure drop, hold-up and liquid phase axial mixing, Ind. Engng. Chem. Process Design and Development 5, 32-39, (1966).

[R5] W.M. Rohsenow, A method of correlating heat-transfer data for surface boiling of liquids, Trans. Am. Mech. Engrs 74, 969-976 (1952).

[R6] W.M. Rohsenow, Heat transfer with evaporation, University of Michigan Press (1953).

[R7] S.Z. Rouhani, Void measurements in the region subcooled and low quality boiling, Proceedings of Symposium on Two-Phase Flow, Exeter, 21-23 June 1965, Vol. 2, pp. E501-E600 (1965).

[R8] S.Z. Rouhani, Void measurements in the regions of subcooled and low-quality boiling. AE-239, Aktiebolaget Atomenergi, Stockholm, Sweden (1966).

[R9] S.Z. Rouhani, Calculation of steam volume fraction in subcooled boiling Journal of Heat Transfer 90, 158-164 (1968).

[R10] S.Z. Rouhani and E. Axelsson, Calculation of void volume fraction in the subcooled and quality boiling regions, Int. J. Heat Mass Transfer 13, 383-393 (1970).

[R11] A.E. Ruffell, The application of heat transfer and pressure drop data to the design of helical coil once-through boilers, paper presented at "Multi-Phase Flow Meeting" in Glasgow (1974).

[S1] P. Saha and N. Zuber, Point of net vapor generation and vapor void fraction in subcooled boiling, Proceedings of the Fifth International Heat Transfer Conference, Tokyo-1974, Vol. 4, pp. 175-179, JSME-AIChE, Tokyo (1974).

[S2] P. Saha, M. Ishii, N. Zuber, An experimental investigation of the thermally induced flow oscillations in two-phase systems, J. Heat Transfer 98, 616-622 (1976).

[S3] A. Sano, A. Kanamori and T. Tsuchiya, Operating experiences with 1 MW steam generator, paper presented at "IAEA Study Group Meeting on Steam Generators for LMFBR's", Bensberg, October 14-17 (1974).

[S4] R.A. Seban and E.F. McLaughlin, Heat transfer in tube coils with laminar and turbulent flow, Int. J. Heat Mass Transfer 6, 387-395 (1963).

[S5] A. Serizawa, A study of forced convective subcooled flow boiling, paper presented at 1978 International Seminar- Momentum, Heat and Mass Transfer in Two-Phase Energy and Chemical Systems, Dubrovnik, September 4-9, (1978).

[S6] V. Sernas and F.C. Hooper, The initial vapor bubble growth on a heated wall during nucleate boiling, Int. J. Heat Mass Transfer 12, 1627-1639 (1969).

[S7] L.M. Shotkin, The flow of boiling water in heated pipes, Nuclear Science and Engineering 26, 293-304 (1966).

[S8] L.M. Shotkin, Stability considerations in two-phase flow, Nuclear Science and Engineering 28, 317-324 (1967).

[S9] N.W. Snyder and T.T. Robin, Mass-transfer model in subcooled nucleate boiling, J. Heat Transfer 91, 404-412 (1969).

[S10] K.O. Solberg, P. Bakstad, A model for the dynamics of nuclear reactors with boiling coolant with a new approach to the vapour generation process, Proceedings of the Symposium on Two-Phase Flow Dynamics, EUR-4288e, Vol. I, pp. 871-933 (1969).

[S11] C.L. Spigt, On the hydraulic characteristics of a boiling water channel with natural circulation, Ph.D. Thesis, Technical University of Eindhoven, The Netherlands (1966).

[S12] F.W. Staub, The void fraction in subcooled boiling - Prediction of the initial point of net vapor generation, J. Heat Transfer 90, 151-157 (1968).

[S13] F.W. Staub and N. Zuber, Void fraction profiles, flow mechanisms and heat transfer coefficients for Refrigerant-22 evaporating in a vertical tube, ASHRAE Transactions, Vol. 72, Part I, pp. 130-146 (1966), ASHRAE New York.

[S14] F.W. Staub, G.E. Walmet and R.O. Niemi, Heat transfer and hydraulics - The effects of subcooled voids, NYO-3679-8 (1969).

[S15] A.H. Stenning and T.N. Veziroglu, Flow oscillation modes in forced-convection boiling, Proceedings of the 1965 Heat Transfer and Fluid Mechanics Institute, Stanford University Press, pp. 301-316 (1965).

[T1] N.V. Tarasova and V.M. Orlov, Heat transfer and hydraulic resistance during surface boiling of water in annular channels, in "Convective Heat Transfer in Two-Phase and One-Phase Flows", edited by V.M. Borishanskii and I.I. Paleev, pp. 135-156. Israel Program for Scientific Translations, Jerusalem (1969).

[T2] F.E. Tippets, Analysis of the critical heat flux conditions in high pressure boiling water flows, Journal of Heat Transfer 86, 23-38 (1964).

[T3] V.I. Tolubinsky and D.M. Kostanchuk, Vapour bubbles growth rate and heat transfer intensity at subcooled water boiling, Heat Transfer 1970, Preprints of papers presented at the Fourth International Heat Transfer Conference, Paris-Versailles 1970, Vol. 5, Paper No. B 2.8.

[T4] K. Torikai, M. Hori, M. Akiyama, T. Kobori and H. Adachi, Boiling heat transfer and burnout mechanism in boiling-water cooled reactor, Third United Nations International Conference on the Peaceful Uses of Atomic Energy, Paper No. 28/P/580 (1964).

[T5] G.G. Treshchev, The number of vapor formation centers in surface boiling, in "Convective Heat Transfer in Two-Phase and One-Phase Flows" edited by V.M. Borishanskii and I.I. Paleev, pp. 97-105. Israel Program for Scientific Translations, Jerusalem (1969).

[U1] H.C. Ünal, Economic aspects of nuclear power in Turkey, in Nuclear Energy Costs and Economic Development, Proceedings of a Symposium, Istanbul, 20-24 October 1969, IAEA, pp. 673-696.

[U2] H.C. Ünal, Determination of the initial point of net vapor generation in flow boiling systems, Int. J. Heat Mass Transfer 18, 1095-1099 (1975).

[U3] H.C. Ünal, Maximum bubble diameter, maximum bubble-growth time and bubble-growth rate during the subcooled nucleate flow boiling of water up to 17.7 MN/m^2, Int. J. Heat Mass Transfer 19, 643-649 (1976).

[U4] H.C. Ünal, Void fraction and incipient point of boiling during the subcooled nucleate flow boiling of water, Int. J. Heat Mass Transfer 20, 409-419 (1977).

[U5] H.C. Ünal, An investigation of the inception conditions of dynamic instabilities in sodium heated steam generator pipes, in "Two-Phase Flows and Heat Transfer", edited by Kakac S., and Veziroglu, T.N., Vol. 3, pp. 1425-1443. Hemisphere Publishing Corporation (1977).

[U6] H.C. Ünal, M.L.G. van Gasselt and P.W.P.H. Ludwig, Dynamic instabilities in tubes of a large capacity, straight-tube, once-through sodium heated steam generator, Int. J. Heat Mass Transfer 20, 1389-1399 (1977)

[U7] H.C. Ünal, Determination of void fraction, incipient point of boiling and initial point of net vapor generation in sodium heated helically coiled steam generator tubes, J. Heat Transfer 100, 268-274 (1978).

[U8] H.C. Ünal, Determination of the drift velocity and the void fraction for the bubble and plug-flow regimes during the flow boiling of water at elevated pressures, Int. J. Heat Mass Transfer 21, 1049-1056 (1978).

[U9] H.C. Ünal, Correlations for the determination of the inception conditions of density wave oscillations for forced and natural circulation steam generator tubes, J. Heat Transfer 102, 14-19 (1980).

[U10] H.C. Ünal, Density-wave oscillations in sodium heated once-through steam generator tubes, submitted for publication in "Journal of Heat Transfer".

[U11] H.C. Ünal, M.L.G. van Gasselt and P.M. van 't Verlaat, Dry out and two-phase flow pressure drop in sodium heated helically coiled steam generator tubes at elevated pressures, accepted for publication in "Int. J. Heat Mass Transfer".

[U12] H.C. Ünal, Heat transfer to a subcooled boiling liquid and initial point of net vapour generation in forced convection systems, TNO report Ref.No. 71-03605, Central Technical Institute TNO, P.O. Box 342, Apeldoorn, The Netherlands (1971) [Confidential].

[U13] H.C. Ünal, Bubble-departure diameter, bubble-growth time and bubble-growth rate during the subcooled nucleate flow boiling of water up to 17.7 MN/m^2, TNO report, Ref.No. 73-02829, Central Technical Institute TNO, P.O. Box 342, Apeldoorn, The Netherlands (1973).

[V1] B. Vriesema, Aspects of molten fluorides as heat transfer agents for power generation, Ph.D. Thesis, Technical University of Delft, The Netherlands (1979).

[V2] B. Vriesema and D.G.H. Latzko, Void-flow instability: Prediction and verification of operating limits, paper presented at BNES Meeting - Boiler Dynamics and Control in Nuclear Power Stations, Bournemouth, October 1979.

[W1] G.B. Wallis, One-dimensional Two-Phase Flow, McGraw Hill, New York (1969).

[W2] K.A. Warschauer, Model testing and heat transfer research at TNO for the design and development of sodium cooled steam generators and other heat extraction equipment, Proceedings of the Information Meeting - TNO Contribution to LMFBR Development, May 10-11, 1973, Utrecht, The Netherlands, pp. 68-78.

[W3] R.P. Waszink and L.E. Efferding, Hydrodynamic stability and thermal performance test of a 1-MWt sodium-heated once-through steam generator model, Journal of Engineering For Power 96, 189-200 (1974).

[Y1] G. Yadigaroglu, A.E. Bergles, Fundamental and higher-mode density-wave oscillations in two-phase flow, J. Heat Transfer 94, 189-195 (1972).

[Z1] N. Zuber, Flow excursions and oscillations in boiling, two-phase flow systems with heat addition, Proceedings of the Symposium on Two-Phase Flow Dynamics, EUR-4288e, Vol. I, pp. 1071-1089 (1969).

[Z2] N. Zuber and J.A. Findlay, Average volumetric concentration in two-phase flow systems, J. Heat Transfer 87, 453-468 (1965).

[Z3] N. Zuber, F.W. Staub and G. Bijwaard, Vapor void fraction in subcooled boiling and in saturated boiling systems, Proceedings of the Third International Heat Transfer Conference, 7-12 August, 1966, Chicago, Illinois, Vol. 5, pp. 24-38, AIChE, New York (1966).

[Z4] N. Zuber, F.W. Staub, G. Bijwaard and P.G. Kroeger, Steady-state and transient void fraction in two-phase flow systems, GEAP-5417 (1967).

APPENDIX 1

DERIVATION OF THE HEAT TRANSFER COEFFICIENT FOR THE LOSS OF HEAT FROM A BUBBLE TO THE SURROUNDING LIQUID*

During subcooled nucleate flow boiling, a bubble growing on a heated surface loses heat to the surrounding liquid as a result of the temperature difference between the bubble and the liquid.

In order to determine the rate of heat transfer from the bubble, a method analogous to that given by Levenspiel [L5] will be used. First Levenspiel's method will be outlined.

Levenspiel derived the bubble heat transfer coefficient from the heat balance for a collapsing bubble as follows:

$$h_c = \frac{q_c}{\Delta} = \frac{\lambda}{2\,\Delta\,(1/\rho_v - 1/\rho_l)} \cdot \frac{dD(t)}{dt} \qquad (A.1)$$

where q_c is the rate of heat transfer from the bubble per unit area in W/m^2 and Δ instability temperature difference in K.

Equation (A.1) relates the bubble collapse rate to the bubble heat transfer coefficient.

He established experimentally that ln D(t) versus t results in a straight-line relationship of slope Y_{A1}, i.e.,:

$$\frac{d \ln D(t)}{dt} = \frac{1}{D(t)} \frac{dD(t)}{dt} = Y_{A1} \qquad (A.2)$$

Y_{A1} shows the measure of rate of change of bubble size during collapse.

Furthermore, he also determined from his own experimental data

$$Y_{A1} = 12.74\,\Delta \qquad (A.3)$$

From the equations (A.1), (A.2) and (A.3), Levenspiel finally obtained the bubble heat transfer coefficient,

$$h_c = \frac{6.37\,D(t)\,\lambda}{1/\rho_v - 1/\rho_l} \qquad (A.4)$$

* This heat transfer coefficient will be referred to as "bubble heat transfer coefficient" throughout Appendix 1.

Due to the nature of the experiments he carried out to verify equations (A.2) and (A.3), equation (A.4) can not be used for subcooled nucleate flow boiling. Levenspiel's experiments can be described as quoted from his paper:

> "Demineralized tap water was boiled vigorously for at least 15 minutes under reduced pressure in a glass container to eliminate most of the dissolved gases. The vacuum was broken; steam bubbles became unstable and imploded. Data recorded were pressure in the system and bubble size versus time".

From the above it is clear that Levenspiel calculated the bubble heat transfer coefficient, in which the influence of the liquid motion around the bubble due to bubble collapse is predominant. It can not be applied therefore to subcooled nucleate flow boiling since the bubble heat transfer coefficient in the latter case is affected not only by the influence of liquid motion caused by bubble collapse but also by velocity and agitation of the liquid around the bubble, as caused by motions of the neighbouring bubbles, and it is anticipated that the last two effects are more important than the first.

The bubble heat transfer coefficient will be calculated now for the collapsing subcooled nucleate flow boiling bubbles by a method analogous to that of Levenspiel.

Equation (A.1) relates the bubble heat transfer coefficient to the liquid motion due to bubble collapse for an isolated bubble in a subcooled stagnant liquid. Since Δ is identical to ΔT_{sub}, it may be written as follows:

$$h_c = \frac{\lambda}{2\ \Delta T_{sub}(1/\rho_v - 1/\rho_l)} \cdot \frac{dD(t)}{dt} \qquad (A.5)$$

For subcooled nucleate flow boiling, the effect of liquid velocity and liquid agitation around the bubble has also to be taken into account. Analytical derivation of these effects on the bubble heat transfer coefficient seems rather difficult; therefore use will be made of experimental data to calculate them. As a first step verification of the condition expressed by equation (A.2) has been carried out using the

experimental data of Abdelmessih et al. [A2] (isolated bubbles) and of Gunther [G2] (bubble populations), as shown in Figs. A1, A2, A3 and A4.

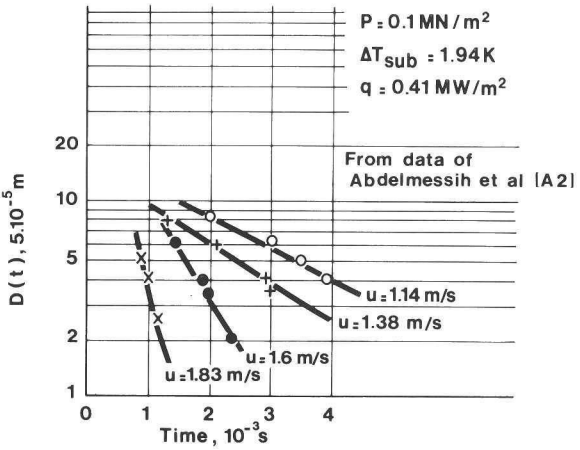

Fig. A1 Verification of equation (A.2).

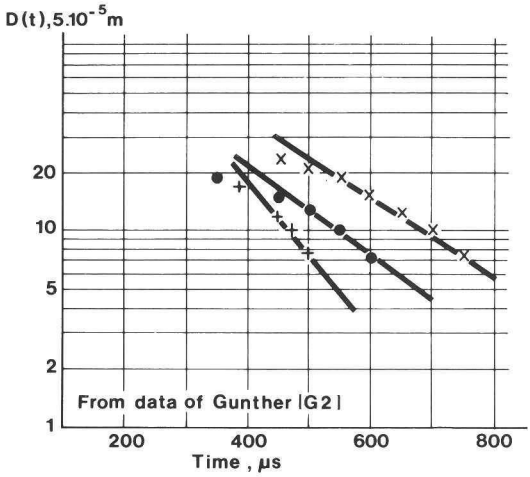

Fig. A2 Verification of equation (A.2).

From these figures it is clear that ln D(t) versus t results in a straight-line relationship of slope Y_{A1}.

As a second step, a linear empirical relation has been searched for, similar to the one given by equation, (A.3) i.e.,

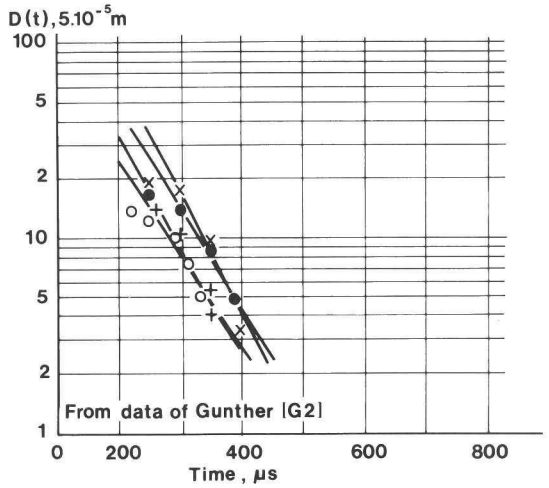

Fig. A3 Verification of equation (A.2).

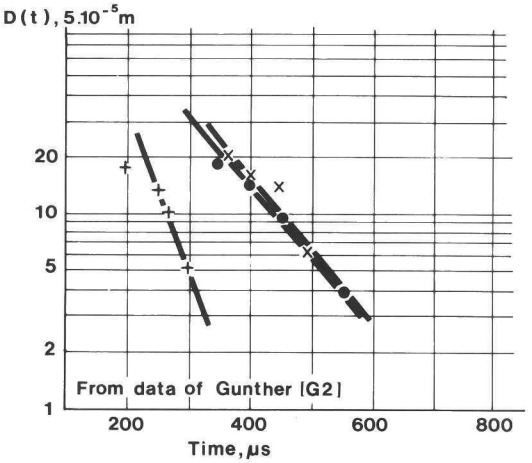

Fig. A4 Verification of equation (A.2).

$$Y_{A1} \left(\frac{u_o}{u}\right)^{Y_{A2}} = Y_{54}\Delta T_{sub} \qquad (A.6)$$

u_o in equation (A.6) shows the particular velocity at which the effect of liquid velocity on the bubble heat transfer coefficient diminishes. Snyder and Robin [S9] report u_o = 0.61 m/s for atmospheric pressure for isolated bubbles. Here the u_o value reported by these investigators will be used. The velocity at which the effect of liquid velocity on bubble

departure ceases to be dominant was found to be 0.45 m/s for a wide range of pressure conditions in Chapter 4, so that the two values are in fair agreement. Y_{A2} in equation (A.6) was assumed constant.

Equation (A.6) has been verified with the experimental data of Gunther [G2], as shown in Figs. A5 and A6. From these figures it is

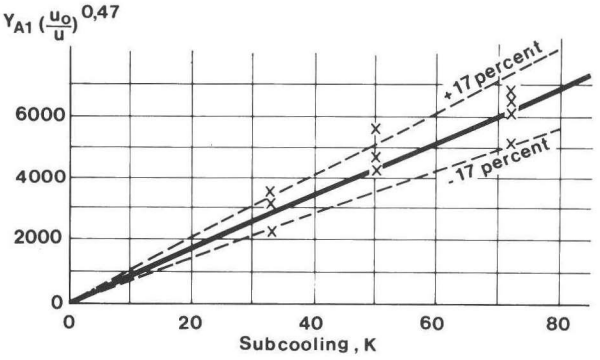

Fig. A5 Verification of equation (A.6).

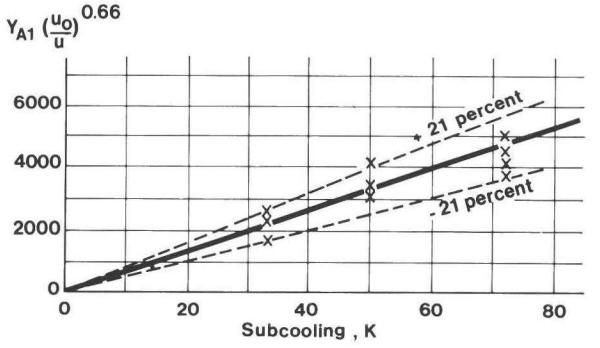

Fig. A6 Verification of equation (A.6).

clear that $Y_{A1}(\frac{u_o}{u})^{Y_{A2}}$ versus ΔT_{sub} results in a straight-line relationship (i.e., Y_{54} = constant) for different values of Y_{A2}. Therefore, combining equations (A.2), (A.5) and (A.6) yields the bubble heat transfer coefficient,

$$h_c = \frac{\lambda\, Y_{54}\, (\frac{u}{u_o})^{Y_{A2}}\, D(t)}{2(1/\rho_v - 1/\rho_l)} \qquad (A.7)$$

Equation (A.7) gives the instantaneous bubble heat transfer coefficient, and in order to use it, Y_{54} in it have to be known. Y_{54}, which is found to be constant, can only be a function of fluid properties at the state of saturation and therefore it may be taken to be a pressure dependent constant.

Now Y_{54} and Y_{A2} will be determined from the experimental data of Gunther, who measured heat transfer controlled bubble life times for three different flow velocities at 0.17 MN/m^2 (bubbles given as nos. 9, 10 and 11 in Table 5.2). From the data presented by the aforesaid author at 0.1 MN/m^2 (i.e., bubble collapse and growth curves are quite symmetrical with respect to bubble-growth time at high subcoolings) it is concluded that half the bubble life time can be taken equal to the bubble collapse time with a good approximation. The aforesaid data can be used to determine Y_{54} and Y_{A2} if the bubble diameter during collapse is known. The latter can be derived from equation (5.1) in Chapter 5, provided that $q_h = 0$ (the bubble gaining no heat during condensation) and the area for the loss of heat is equal to the total bubble area. In these circumstances, equation (5.1) becomes

$$-h_c\, \pi\, (D(t))^2\, \Delta T_{sub} = \frac{d}{dt}\, (\frac{\pi}{6}\, (D(t))^3\, \rho_v\, \lambda) \qquad (A.8)$$

Initial condition:

$$t = t_m \qquad D(t_m) = D_m$$

By substituting equation (A.7) into equation (A.8) and differentiating the RHS of the latter, this becomes after rearranging

$$\frac{-Y_{54}\, (\frac{u}{u_o})^{Y_{A2}}\, \Delta T_{sub}}{(1 - \rho_v/\rho_l)}\, D(t) = \frac{dD(t)}{dt} \qquad (A.9)$$

Solution of equation (A.9) which satisfies the initial condition is

$$D(t) = D_m e^{-\frac{Y_{54}\,(\frac{u}{u_o})^{Y_{A2}}\,\Delta T_{sub}}{(1 - \rho_v/\rho_l)}\,(t - t_m)} \qquad (A.10)$$

If a bubble life time as calculated by an averaging procedure is substituted into equation (A.10) it will not become zero, but yield a particular value. This condition can be expressed as

$$t_t - t_m = t_c \qquad D(t_t) = D_c \qquad (A.11)$$

where t_t is the bubble life time in s, t_c, the bubble collapse time in s and D_c, a fraction of maximum bubble diameter in m.

Now for the aforesaid three bubbles, equation (A.10) may be written as follows, using the data given in Table 5.2 and the condition expressed by equation (A.11):

$$(D_c)_1 \cong 0.62.10^{-3} e^{-83 \times 2.10^{-4} (\frac{1.5}{0.61})^{Y_{A2}} Y_{54}} \qquad (A.12)$$

$$(D_c)_2 \cong 0.50.10^{-3} e^{-83 \times 1.25.10^{-4} (\frac{3.05}{0.61})^{Y_{A2}} Y_{54}} \qquad (A.13)$$

$$(D_c)_3 \cong 0.36.10^{-3} e^{-83 \times 0.67.10^{-4} (\frac{6.1}{0.61})^{Y_{A2}} Y_{54}} \qquad (A.14)$$

In order to solve the above given three equations to obtain $(D_c)_1$, $(D_c)_2$, $(D_c)_3$, Y_{54} and Y_{A2}, one approximation has to be made, since the number of unknowns exceeds the number of equations: The approximation that $D_c = (D_c)_1 = (D_c)_2 = (D_c)_3$ seems quite reasonable, since D_c is a small fraction of the maximum bubble diameter and the above given equations are exponential. Then, after replacing $(D_c)_1$, $(D_c)_2$ and $(D_c)_3$ by D_c in equations (A.12), (A.13) and (A.14) these equations have been solved, yielding $Y_{A2} = 0.47$ and $Y_{54} = 61\ (Ks)^{-1}$. According to the experimental data of Snyder and Robin [S9] the bubble heat transfer

coefficient is affected by the square root of velocity. This is in fair agreement with the Y_{A2} value found here.

When the Y_{A2} value found is substituted into equation (A.7) the bubble heat transfer coefficient during the collapse of the subcooled flow boiling bubbles is found to be

$$h_c = \frac{Y_{53}\, Y_{54}\, \lambda\, D(t)}{2(1/\rho_v - 1/\rho_l)} \qquad (A.15)$$

where

$$Y_{53} = \left(\frac{u}{u_o}\right)^{0.47} \qquad u_o > 0.61 \text{ m/s} \qquad (A.16)$$

$$Y_{53} = 1 \qquad u_o \leq 0.61 \text{ m/s} \qquad (A.17)$$

Now the question arises whether equation (A.15) can be applied to bubble growth. It can be, since:

a. Equation (A.15) gives the instantaneous bubble heat transfer coefficient and is related to the time dependent bubble diameter. Therefore, as far as the effect of bubble growth alone on the bubble heat transfer coefficient is considered, it must be identical to that of bubble collapse.

b. Y_{53} and Y_{54} are predicted from the data obtained from bubbles that are formed before the initial point of net vapour generation is reached. They are bubbles which stay on the heating surface, or slide on it. Therefore, for these bubbles, the effects of liquid velocity and motion of the neighbouring bubbles on the bubble heat transfer coefficient can not be much different for the bubble collapse and the bubble growth case. At 1.7 MN/m^2, Y_{54} is equal to 61 $(Ks)^{-1}$ for the average bubble of a bubble population. The determination of Y_{54} is discussed in detail in Chapter 5.

APPENDIX 2
DRYOUT AND TWO-PHASE FLOW PRESSURE
DROP DATA FROM TT4, TT5 AND TT6

No.	P	G	ΔT_{sub}	First dryout		Last dryout		ΔP	X_{bt}	Test tube
				X_d	q_d	X_d	q_d			
	MN/m^2	kg/m^2s	K		kW/m^2		kW/m^2	10^{-1} MN/m^2		
1	15.00	1475	41.3	0.42	358	0.54	465	-	-	TT4
2	17.88	1531	56.6	0.41	361	0.65	480	-	-	"
3	20.15	1558	64.0	0.34	312	0.70	463	-	-	"
4	15.13	1469	72.2	0.41	433	0.51	513	-	-	"
5	17.42	1497	83.3	0.32	386	0.49	497	-	-	"
6	19.98	1529	94.6	0.21	332	0.46	470	-	-	"
7	19.91	1291	105.3	0.31	265	0.61	385	-	-	"
8	17.41	1264	94.3	0.41	320	0.56	403	-	-	"
9	15.11	1224	82.8	0.49	372	0.65	467	-	-	"
10	15.32	1258	125.1	0.37	380	0.53	492	-	-	"
11	17.52	1272	135.7	0.32	358	0.50	450	-	-	"
12	20.05	1299	146.9	0.20	289	0.50	420	-	-	"
13	20.02	983	146.5	0.41	214	0.64	276	-	-	"
14	17.45	937	135	0.60	290	0.77	388	-	-	"
15	14.86	996	121.8	0.64	375	0.81	410	-	-	"
16	14.86	844	45.8	0.41	225	0.55	303	-	-	"
17	17.37	847	52.4	0.56	258	0.78	332	-	-	"
18	15.00	887	80.4	0.60	315	0.80	370	-	-	"
19	15.09	316	122.9	0.35	140	0.56	205	-	-	"
20	17.32	892	90.3	0.59	288	0.81	356	-	-	"
21	15.12	867	79.2	0.60	306	0.81	353	-	-	"
22	19.83	925	101.1	0.45	202	0.72	284	-	-	"
23	19.84	613	99.6	0.33	132	0.67	218	-	-	"
24	17.41	584	88.8	0.40	164	0.68	233	-	-	"
25	15.00	595	76.7	0.43	195	0.69	290	-	-	"
26	15.02	628	120.9	0.45	227	0.67	310	-	-	"
27	17.56	628	133.9	0.40	182	0.67	248	-	-	"
28	19.95	632	144.5	0.42	166	0.62	201	-	-	"
29	17.33	342	133.5	0.28	115	0.52	185	-	-	"
30	19.92	337	145.2	0.21	90	0.46	141	-	-	"
31	14.74	318	120.5	0.33	139	0.55	195	-	-	"
32	17.46	305	83.1	0.30	97	0.56	160	-	-	"
33	19.92	308	94.9	0.32	97	0.52	125	-	-	"
34	19.86	120	95.3	0.53	41	0.99	69	-	-	"
35	17.15	117	82.1	0.46	50	0.76	77	-	-	"
36	15.13	112	72.7	0.52	63	0.84	83	-	-	"
37	15.10	122	122.9	0.48	60	0.96	97	-	-	"
38	19.38	120	146	0.60	46	1.00	73	-	-	"
39	15.00	1333	81.1	0.34	462	0.83	627	0.74	0.88	"
40	19.91	1347	104.9	0.15	349	0.70	480	0.26	0.77	"
41	19.79	1015	104.6	0.14	397	0.50	476	0.10	0.62	"
42	15.17	998	82.6	0.46	625	0.73	675	0.29	0.81	"

APPENDIX 2: continued

No.	P	G	ΔT_{sub}	First dryout		Last dryout		ΔP	X_{bt}	Test tube
				X_d	q_d	X_d	q_d			
	MN/m^2	kg/m^2s	K		kW/m^2		kW/m^2	10^{-1} MN/m^2		
43	15.10	617	82.7	0.31	287	0.69	375	0.15	0.76	TT4
44	19.85	638	104.9	0.08	182	0.61	270	0.07	0.76	"
45	15.10	635	42.1	0.29	270	0.67	394	0.18	0.74	"
46	18.19	608	57.4	-	-	0.71	311	0.10	0.78	"
47	15.09	974	41.9	0.52	585	0.75	654	0.33	0.83	"
48	15.11	1009	42.2	0.60	558	0.80	517	0.44	0.89	"
49	18.03	1043	56.6	0.44	430	0.72	480	0.27	0.84	"
50	14.94	1192	41.2	0.51	624	0.77	630	0.52	0.82	"
51	18.07	1205	56.6	0.36	474	0.74	555	0.29	0.79	"
52	17.98	1337	55.8	0.29	517	0.69	629	0.33	0.76	"
53	15.01	1379	81.5	0.34	712	-	-	0.21	0.34	"
54	19.88	1409	105.3	0.30	302	-	-	0.12	0.30	"
55	19.80	1070	105.5	0.15	382	-	-	0.03	0.15	"
56	14.96	1029	81.6	0.41	560	-	-	0.17	0.41	"
57	15.08	639	81.9	0.31	272	-	-	0.08	0.31	"
58	15.07	1019	42.2	0.45	554	-	-	0.21	0.45	"
59	15.02	1022	41.9	0.58	527	-	-	0.32	0.58	"
60	17.93	1074	56.1	0.29	285	-	-	0.11	0.29	"
61	15.01	1222	42.1	0.50	545	-	-	0.34	0.50	"
62	18.14	1236	58.1	0.28	346	-	-	0.13	0.28	"
63	15.02	1340	81.5	-	-	0.83	620	0.69	0.83	"
64	19.88	1355	104.9	-	-	0.65	420	0.23	0.65	"
65	19.81	1051	105.3	-	-	0.51	522	0.10	0.51	"
66	15.06	1002	82.1	-	-	0.73	688	-	-	"
67	15.10	618	82.8	-	-	0.69	395	0.14	0.69	"
68	19.89	643	105.1	-	-	0.63	293	0.13	0.63	"
69	15.11	633	42	-	-	0.69	425	0.16	0.69	"
70	18.26	611	57.6	-	-	0.73	327	0.10	0.73	"
71	15.08	1015	41.8	-	-	0.73	691	0.32	0.73	"
72	14.98	1020	41.4	-	-	0.79	578	0.42	0.79	"
73	17.95	1050	56.3	-	-	0.71	480	0.23	0.71	"
74	15.03	1198	41.4	-	-	0.77	680	0.50	0.77	"
75	18.02	1202	56.5	-	-	0.75	533	0.28	0.75	"
76	20.04	1829	69.1	0.24	472	0.75	731	0.69	1.00	TT5
77	17.59	1503	90.3	0.57	612	0.85	693	0.77	0.97	"
78	20.06	1498	97.8	0.33	393	0.78	532	0.46	0.90	"
79	20.11	1500	96.5	0.43	385	0.77	474	0.56	1.00	"
80	20.07	1491	143.1	0.33	401	0.76	522	0.49	0.96	"
81	15.09	1200	71.5	0.71	548	0.87	573	0.88	0.92	"
82	20.07	1227	95.6	0.31	340	0.73	463	0.31	0.95	"
83	17.46	1239	96.6	0.59	468	0.86	506	0.60	0.92	"
84	15.07	1167	119.6	0.72	528	0.88	545	0.88	1.00	"
85	17.51	1224	136.5	0.60	487	0.88	519	0.54	0.94	"
86	17.57	1196	134.3	0.64	436	0.85	469	0.62	1.00	"
87	20.04	1236	150.9	0.29	341	0.74	455	0.33	0.95	"
88	15.16	1206	128.2	0.70	554	0.85	559	0.82	0.94	"

APPENDIX 2: continued

No.	P	G	ΔT_{sub}	First dryout		Last dryout		ΔP	X_{bt}	Test tube
				X_d	q_d	X_d	q_d			
	MN/m^2	kg/m^2s	K		kW/m^2		kW/m^2	10^{-1} MN/m^2		
89	15.07	918	69.6	0.79	501	0.89	480	0.52	1.00	TT5
90	17.52	908	86.5	0.75	474	0.86	505	0.29	0.90	"
91	20.00	900	95.6	0.51	284	0.83	338	0.22	1.00	"
92	19.99	898	96.4	0.38	294	0.78	384	0.18	0.92	"
93	15.07	918	122.9	0.79	558	0.81	571	0.43	0.90	"
94	17.46	910	131.9	0.72	467	0.85	495	0.28	0.90	"
95	19.99	922	141.1	0.48	288	0.82	342	0.22	1.00	"
96	19.97	935	144.1	0.36	323	0.74	404	0.17	0.88	"
97	15.10	612	79.5	0.72	311	0.90	311	0.27	1.00	"
98	17.51	636	94.9	0.55	257	0.94	294	0.19	1.00	"
99	19.99	616	106.5	0.28	216	0.74	308	0.09	0.91	"
100	19.97	623	105.9	0.35	186	0.80	264	0.12	1.00	"
101	15.00	617	133.5	0.66	319	0.88	332	0.26	1.00	"
102	17.50	630	143.5	0.54	259	0.94	292	-	-	"
103	17.49	629	143.2	0.44	297	0.85	416	-	-	"
104	19.97	618	156.8	0.28	226	0.75	311	-	-	"
105	19.98	616	154.8	0.30	187	0.83	276	-	-	"
106	14.95	297	88.9	0.37	137	0.99	177	0.13	1.00	"
107	17.45	304	103.6	0.34	118	0.95	159	0.10	1.00	"
108	14.93	298	139.7	0.41	148	0.95	178	0.13	1.00	"
109	17.53	296	153.1	0.25	107	1.00	188	0.09	1.00	"
110	15.04	118	143.2	0.56	114	0.99	131	-	-	"
111	17.46	116	155.3	0.33	84	0.99	113	-	-	"
112	18.48	1505	35.6	0.43	367	0.76	445	0.78	0.79	TT6
113	17.11	710	61.4	-	-	0.99	344	0.23	1.00	"
114	16.77	387	79.6	0.40	195	1.00	265	0.11	1.00	"
115	15.18	636	47	-	-	-	-	0.08	0.23	TT4

APPENDIX 3
EXPERIMENTAL DATA FOR THE DWO
FROM TT3 AND TT4

TABLE A3.1: Data for the DWO from TT3

No.	P 10^{-1} MN/m^2	G kg/m^{2}s	$\frac{W_n}{W_w}$	K	H_i kJ/kg	X_{IC}	ψ s
1	140.9	567.5	14.2	54.73	1049.9	1.59	4.50
2	141.3	585.3	13.7	54.73	1045.2	1.60	5.00
3	142.1	568.5	14.5	54.73	1044.3	1.62	5.00
4	157.3	593.6	13.7	54.73	1063.3	1.75	5.00
5	172.1	614.6	13.0	54.73	1078.5	1.93	5.00
6	182.7	628.2	12.6	54.73	1088.4	2.11	5.00
7	183.9	673.2	12.0	54.73	826.3	2.17	7.00
8	141.4	568.5	14.2	54.73	1049.0	1.60	4.50
9	147.5	569.6	13.8	54.73	1055.7	1.65	4.50
10	158.2	592.6	13.5	54.73	1056.3	1.75	4.50
11	139.7	576.9	17.9	54.73	1013.2	1.51	5.00
12	145.8	586.3	17.7	54.73	1020.2	1.56	5.00
13	158.4	597.8	17.1	54.73	1032.4	1.68	4.70
14	165.4	612.5	16.7	54.73	1032.6	1.76	4.50
15	172.3	621.9	16.4	54.73	1039.1	1.84	5.00
16	184.1	654.4	15.5	54.73	1039.9	2.02	5.50
17	139.4	567.5	14.8	54.73	1028.5	1.57	4.80
18	150.9	589.4	14.1	54.73	1043.0	1.67	4.80
19	169.8	618.8	13.1	54.73	1044.3	1.88	4.80
20	178.1	631.3	13.0	54.73	1045.8	2.01	5.00
21	184.3	644.9	12.4	54.73	1046.0	2.13	5.50
22	102.8	1019.7	10.4	54.73	897.7	1.59	5.00
23	156.8	854.3	12.0	54.73	1048.2	1.88	3.80
24	171.4	746.5	14.0	54.73	1073.8	1.87	4.30
25	142.6	909.8	11.6	54.73	990.5	1.74	3.50
26	152.6	904.6	11.5	54.73	1024.5	1.83	3.50
27	143.4	878.4	12.0	54.73	995.6	1.72	3.50
28	142.1	566.4	14.2	54.73	980.1	1.61	4.50
29	152.6	588.4	13.5	54.73	994.1	1.71	4.50
30	160.1	604.1	13.0	54.73	996.6	1.81	5.00
31	170.1	618.8	12.5	54.73	996.8	1.95	5.20
32	180.2	642.8	12.0	54.73	997.1	2.10	5.50
33	140.8	528.7	15.3	54.73	1358.5	1.51	3.50
34	152.2	542.3	14.7	54.73	1354.8	1.62	3.60
35	162.7	558.0	14.2	54.73	1357.2	1.74	4.00
36	170.8	566.4	14.1	54.73	1358.7	1.86	3.90
37	179.4	577.9	13.8	54.73	1358.3	2.01	3.90
38	139.4	486.8	17.7	54.73	1415.3	1.47	3.50
39	150.2	492.1	17.2	54.73	1439.9	1.61	3.50
40	159.5	493.1	16.8	54.73	1474.9	1.78	3.50
41	171.4	507.8	16.0	54.73	1471.1	1.91	3.50
42	181.4	525.6	15.3	54.73	1472.2	2.01	3.80
43	140.8	531.9	16.2	54.73	1285.7	1.50	4.00
44	151.7	544.4	15.6	54.73	1284.5	1.61	4.00
45	161.7	552.8	15.1	54.73	1286.0	1.75	4.00

TABLE A3.1: continued

No.	P 10^{-1} MN/m^2	G kg/m^{2}s	$\frac{W_n}{W_w}$	K	H_i kJ/kg	X_{IC}	ψ s
46	171.8	567.5	14.7	54.73	1285.1	1.88	4.00
47	181.8	584.2	14.1	54.73	1285.6	2.02	4.50
48	142.3	563.3	15.7	54.73	1133.0	1.55	4.20
49	152.5	581.1	14.9	54.73	1134.4	1.64	4.00
50	162.2	599.9	14.5	54.73	1086.8	1.74	4.30
51	172.2	618.8	14.0	54.73	1133.9	1.86	4.50
52	183.2	634.5	13.6	54.73	1134.9	2.06	5.00
53	171.5	614.6	14.1	54.73	1043.3	1.91	4.50
54	178.8	627.1	13.9	54.73	1039.6	2.01	4.50
55	120.0	579.0	15.2	54.73	1236.2	1.42	4.00
56	132.1	606.2	14.4	54.73	1257.0	1.50	4.00
57	143.3	620.9	13.8	54.73	1256.5	1.59	3.80
58	151.0	638.7	13.5	54.73	1255.1	1.66	3.00
59	161.2	649.1	13.1	54.73	1257.7	1.79	3.50
60	140.8	513.0	15.4	54.73	1174.7	1.54	4.50
61	140.7	504.6	12.7	54.73	1174.7	1.60	4.50
62	140.4	571.6	13.9	54.73	1041.9	1.62	4.40
63	158.8	602.0	13.1	54.73	1044.1	1.81	4.30
64	170.6	620.9	12.5	54.73	1044.7	1.94	4.70
65	140.2	525.6	15.5	54.73	1333.8	1.50	4.20
66	149.5	535.0	14.9	54.73	1343.8	1.58	3.70
67	159.5	546.5	14.5	54.73	1345.2	1.69	3.70
68	170.4	560.1	14.0	54.73	1343.7	1.85	3.60
69	141.6	513.0	14.6	54.73	1358.3	1.53	3.70
70	151.3	524.5	14.1	54.73	1358.3	1.62	3.50
71	160.8	539.2	13.6	54.73	1356.7	1.73	3.70
72	171.2	548.6	13.5	54.73	1355.3	1.87	4.00
73	180.6	569.6	12.8	54.73	1354.4	2.04	4.00
74	140.8	502.5	17.2	68.80	1415.7	1.54	3.00
75	161.6	500.5	17.3	70.80	1411.9	1.80	3.20
76	182.7	537.1	16.0	68.16	1411.3	2.07	4.30
77	139.9	560.1	17.6	67.61	1013.6	1.52	4.60
78	152.3	583.2	17.0	64.96	1011.6	1.64	4.50
79	161.7	596.8	16.4	65.69	1013.2	1.75	4.50
80	171.6	599.9	16.2	69.89	1012.9	1.91	5.00
81	181.4	624.0	15.5	67.34	1013.6	2.05	4.80
82	140.1	514.1	17.8	117.15	1015.0	1.63	3.50
83	150.4	524.5	17.2	115.60	1015.7	1.82	4.20
84	140.1	485.8	18.9	122.90	1188.0	1.59	3.20
85	150.6	498.4	18.2	121.99	1189.3	1.73	3.70
86	139.6	508.8	19.0	54.73	1385.7	1.47	3.20
87	160.1	529.8	17.9	54.73	1384.3	1.68	3.60
88	169.2	537.1	17.6	54.73	1385.9	1.80	3.60
89	179.3	552.8	16.9	54.73	1384.2	1.97	4.00
90	159.7	528.7	18.1	54.73	1383.7	1.66	3.60
91	169.4	543.4	17.6	54.73	1384.2	1.78	3.60
92	141.1	507.8	18.2	54.73	1410.2	1.49	3.10
93	149.9	528.7	17.2	54.73	1409.5	1.59	3.00

TABLE A3.1: continued

No.	P 10^{-1} MN/m^2	G kg/m^{2}s	$\frac{W_n}{W_w}$	K	H_i kJ/kg	X_{IC}	ψ s
94	159.6	548.6	16.7	54.73	1407.5	1.69	3.50
95	169.5	560.1	15.9	54.73	1407.3	1.82	3.50
96	179.7	572.7	15.3	54.73	1405.9	2.01	3.80
97	149.5	595.7	15.2	54.73	1128.7	1.64	4.00
98	141.3	590.5	16.3	54.73	1039.1	1.60	4.30
99	151.9	608.3	15.8	54.73	1039.2	1.70	4.50
100	160.5	603.1	16.0	54.73	1038.5	1.78	4.50
101	171.1	624.0	15.1	54.73	1040.1	1.90	5.00
102	181.4	642.8	14.7	54.73	1041.2	2.07	5.20
103	141.8	849.1	12.2	54.73	1039.1	1.72	3.30
104	151.1	874.2	11.8	54.73	1040.6	1.80	3.70
105	160.6	889.9	11.5	54.73	1040.3	1.94	3.70
106	141.4	625.0	16.7	105.66	1043.8	1.65	3.80
107	150.3	641.8	16.0	105.38	1044.8	1.74	3.90
108	161.0	659.6	15.4	106.93	1045.5	1.91	4.30
109	140.0	642.8	16.1	101.92	767.7	1.69	5.00
110	183.7	682.6	14.6	107.94	1390.4	2.20	4.50
111	140.9	606.2	17.4	196.62	1039.1	1.79	3.50
112	101.3	601.0	17.2	201.00	1038.9	1.51	2.10
113	110.8	618.8	16.5	200.09	1039.5	1.60	2.40
114	140.1	584.2	18.1	54.73	1040.5	1.57	4.10
115	159.1	624.0	16.7	54.73	1032.0	1.73	4.70
116	171.9	648.1	16.2	54.73	1032.7	1.87	5.00
117	140.7	529.8	16.3	54.73	1282.6	1.57	3.20
118	150.3	547.6	15.6	54.73	1282.5	1.64	3.50
119	160.5	562.2	15.1	54.73	1284.5	1.74	3.70
120	170.3	579.0	14.5	54.73	1283.0	1.87	4.00
121	180.1	595.7	14.1	54.73	1281.5	2.01	4.30
122	90.8	559.1	18.3	273.45	1038.3	1.55	1.80
123	140.1	492.1	18.4	54.73	1408.0	1.54	2.90
124	179.6	559.1	15.8	54.73	1403.6	2.04	4.00
125	139.8	574.8	15.8	54.73	1040.5	1.60	4.30
126	159.0	611.4	14.7	54.73	1043.2	1.78	4.30
127	169.8	628.2	14.4	54.73	1043.3	1.90	4.70
128	88.7	438.7	19.9	204.38	948.3	1.37	2.70
129	138.8	488.9	8.8	54.73	1012.7	1.73	4.50
130	158.5	591.5	12.3	54.73	980.1	1.77	5.50
131	104.6	496.3	15.0	54.73	940.2	1.40	3.50
132	103.4	454.4	16.1	54.73	1140.6	1.38	3.50
133	153.2	539.2	14.9	54.73	1207.6	1.69	4.50
134	145.7	637.6	12.3	54.73	1096.2	1.72	6.00
135	125.6	620.9	12.9	54.73	1192.9	1.61	3.30
136	141.5	562.2	14.2	105.57	1052.7	1.64	5.00
137	140.4	559.1	14.1	155.84	1040.0	1.66	3.50
138	140.9	591.5	13.3	158.49	1057.9	1.75	3.50
139	141.5	654.4	12.0	162.59	1072.9	1.77	3.80
140	137.0	675.3	11.9	162.77	848.8	1.73	4.50
141	139.8	544.4	8.9	54.73	1086.1	1.72	5.00

TABLE A3.1: continued

No.	P 10^{-1} MN/m^2	G kg/m^{2}s	$\frac{W_n}{W_w}$	K	H_i kJ/kg	X_{IC}	ψ s
142	145.7	547.6	8.8	54.73	1057.0	1.82	4.50
143	181.4	639.7	10.6	54.73	1006.3	2.16	5.50
144	153.5	586.3	11.4	54.73	1034.7	1.75	4.50
145	142.5	571.6	11.9	54.73	1030.8	1.63	5.00
146	157.2	584.2	10.1	54.73	1042.2	1.88	4.50
147	125.6	926.6	11.1	54.73	1005.9	1.68	5.50
148	143.4	901.4	11.4	54.73	993.8	1.77	6.00
149	142.6	834.4	12.4	54.73	1047.6	1.70	3.50
150	139.8	685.8	15.3	54.73	1047.1	1.59	4.00
151	149.4	950.6	11.0	54.73	990.4	1.82	3.50
152	125.6	559.1	17.0	54.73	943.5	1.48	5.00
153	167.0	613.5	14.7	54.73	981.3	1.86	5.30
154	142.9	551.8	12.8	54.73	1044.7	1.65	4.10
155	181.6	574.8	13.4	54.73	1343.9	2.04	4.00
156	189.6	576.9	16.1	54.73	1384.2	2.16	4.40
157	85.9	552.8	18.2	382.94	1036.8	1.54	1.60
158	85.9	598.9	17.2	378.74	1039.2	1.55	1.80
159	75.9	563.3	17.7	381.48	1040.0	1.54	1.30
160	78.4	588.4	17.2	361.86	942.6	1.54	1.50

TABLE A3.2: Data for the DWO from TT4

No.	P 10^{-1} MN/m^2	G kg/m^{2}s	$\frac{W_n}{W_w}$	K	H_i kJ/kg	X_{IC}	ψ s
1	105.90	303.00	13.70	223.00	1234.70	1.663	3.5
2	96.10	518.00	8.90	223.00	1085.80	1.660	5.5
3	95.10	517.00	9.00	223.00	1085.80	1.640	6.0
4	99.40	515.00	8.60	223.00	1087.30	1.730	5.5
5	101.20	544.00	9.73	223.00	1085.90	1.674	5.5
6	116.00	567.00	9.50	223.00	1086.90	1.828	5.5
7	118.50	575.00	10.62	223.00	1086.90	1.796	5.5
8	124.90	593.00	10.50	223.00	1086.00	1.886	5.5
9	118.40	536.00	16.55	223.00	1084.00	1.635	5.5
10	129.40	509.00	17.20	223.00	1084.10	1.925	5.3
11	116.50	501.00	17.60	223.00	1083.50	1.678	4.8
12	80.60	454.00	17.97	223.00	855.50	1.679	3.0
13	108.90	644.00	12.99	223.00	862.10	1.731	5.5
14	118.90	291.00	28.29	223.00	853.70	1.488	12.0
15	127.80	287.00	28.52	223.00	853.60	1.643	8.0
16	138.30	290.00	27.45	223.00	854.10	1.786	8.5
17	148.60	302.00	26.44	223.00	855.40	1.887	8.0
18	159.50	302.00	26.06	223.00	856.60	2.038	8.0
19	123.00	284.00	29.47	223.00	853.80	1.569	9.5
20	118.90	295.00	16.22	223.00	854.50	1.510	3.1
21	118.10	293.00	16.30	223.00	854.10	1.525	3.1
22	118.80	294.00	16.27	223.00	854.10	1.522	3.2
23	128.20	289.00	15.79	223.00	854.50	1.698	9.5
24	138.80	294.00	16.02	223.00	855.00	1.957	8.0
25	148.80	303.00	15.49	223.00	855.90	1.949	10.0
26	123.30	297.00	16.49	223.00	854.30	1.562	2.8
27	118.80	301.00	26.75	223.00	718.00	1.584	9.0
28	139.60	325.00	24.35	223.00	719.60	1.685	12.5
29	108.30	285.00	16.57	223.00	669.10	1.573	9.0
30	120.60	286.00	16.29	223.00	856.40	1.616	8.5
31	105.70	274.00	17.15	223.00	856.60	1.498	9.0
32	88.60	256.00	18.83	223.00	852.80	1.396	9.5
33	102.00	247.00	18.67	223.00	931.50	1.416	13.5
34	110.90	261.00	17.88	223.00	932.70	1.465	12.5
35	122.10	278.00	16.95	223.00	934.00	1.531	11.5
36	131.30	278.00	16.67	223.00	935.20	1.576	12.5
37	143.20	271.00	16.17	223.00	931.60	1.742	10.0
38	153.20	277.00	15.20	223.00	932.80	1.870	7.0
39	158.30	271.00	13.94	223.00	933.50	1.999	10.0
40	103.00	249.00	18.66	450.00	930.20	1.463	11.0
41	112.80	255.00	18.35	450.00	931.40	1.558	10.0
42	133.60	260.00	17.55	450.00	932.60	1.709	10.0
43	143.10	262.00	15.42	450.00	932.90	1.870	8.0
44	101.00	246.00	19.52	450.00	929.70	1.432	11.0
45	60.30	225.00	23.69	223.00	875.80	1.153	8.0
46	69.00	229.00	22.92	223.00	880.60	1.261	12.5

TABLE A3.2: continued

No.	P 10^{-1} MN/m^2	G kg/m^{2}s	$\frac{W_n}{W_w}$	K	H_i kJ/kg	X_{IC}	ψ s
47	78.90	244.00	21.50	223.00	881.90	1.285	13.5
48	89.10	256.00	20.83	223.00	881.90	1.363	13.0
49	95.80	264.00	19.51	223.00	882.60	1.419	11.0
50	124.60	436.00	16.97	223.00	1131.70	1.780	4.0
51	103.30	261.00	18.45	223.00	929.30	1.440	12.0
52	113.40	282.00	17.00	223.00	930.50	1.479	11.0
53	98.10	187.00	22.55	665.00	849.20	1.387	4.5
54	123.00	292.00	16.36	223.00	932.20	1.541	11.5
55	133.00	282.00	16.19	223.00	932.40	1.708	9.5
56	140.10	283.00	15.83	223.00	932.80	1.802	9.5
57	150.50	292.00	15.05	223.00	933.70	1.900	7.0
58	160.50	294.00	14.85	223.00	934.40	2.060	10.5
59	84.20	524.00	17.14	223.00	845.50	1.626	4.5
60	83.30	534.00	17.05	223.00	845.40	1.589	4.5
61	129.10	672.00	15.50	17.00	1342.50	1.535	6.5
62	151.10	685.00	14.49	18.00	1343.70	1.777	6.0
63	166.40	705.00	13.77	17.00	1343.50	1.997	6.0
64	180.50	713.00	13.33	18.00	1342.30	2.350	6.0
65	121.20	554.00	9.89	18.00	1346.80	1.600	7.0
66	150.50	598.00	8.81	18.00	1343.20	1.991	6.0
67	120.20	607.00	16.81	17.00	1312.70	1.460	7.0
68	150.60	606.00	16.33	17.00	1347.20	1.678	7.0
69	165.70	616.00	16.02	19.00	1343.00	1.882	7.0
70	180.80	618.00	15.71	16.00	1341.70	2.191	6.0
71	136.60	570.00	17.26	17.00	1135.00	1.709	6.0
72	80.50	676.00	14.81	18.00	1134.00	1.359	7.5
73	99.80	731.00	13.72	18.00	1135.70	1.474	7.0
74	121.90	726.00	13.48	17.00	1134.10	1.622	7.0
75	152.60	755.00	12.97	17.00	1134.40	1.912	6.5
76	167.10	729.00	13.28	18.00	1135.40	2.098	7.0
77	181.50	700.00	13.49	18.00	1265.10	2.367	6.0
78	157.50	633.00	13.77	17.00	1237.30	1.877	7.0
79	139.90	630.00	14.73	15.00	1237.50	1.680	7.0
80	62.10	665.00	14.62	19.00	844.10	1.296	6.5
81	79.00	678.00	14.23	16.00	856.40	1.368	5.5
82	99.90	688.00	13.66	18.00	857.20	1.576	7.0
83	124.20	694.00	10.54	17.00	1337.40	1.669	5.5
84	135.50	708.00	10.18	15.00	1344.10	1.770	5.2
85	81.20	540.00	18.49	16.00	1137.40	1.286	8.5
86	100.10	583.00	16.54	17.00	1138.70	1.414	8.0
87	120.50	626.00	15.20	16.00	1139.50	1.563	7.5
88	148.80	608.00	15.44	18.00	1139.30	1.878	6.0
89	81.10	601.00	16.13	17.00	1300.60	1.297	7.5
90	89.60	615.00	15.80	18.00	1343.40	1.334	6.0
91	99.50	642.00	14.87	19.00	1387.10	1.372	6.0
92	109.70	642.00	14.87	15.00	1420.50	1.443	5.0

TABLE A3.2: continued

No.	P 10^{-1} MN/m^2	G kg/m^{2}s	$\frac{W_n}{W_w}$	K	H_i kJ/kg	X_{IC}	ψ s
93	139.30	491.00	19.54	25.00	1431.10	1.510	8.0
94	160.20	523.00	17.75	19.00	1469.60	1.725	6.0
95	164.50	514.00	18.12	15.00	1485.20	1.823	5.5
96	180.20	515.00	17.98	18.00	1487.40	2.163	4.5
97	139.50	572.00	16.14	19.00	1372.70	1.653	5.0
98	148.90	582.00	15.68	18.00	1371.00	1.742	5.5
99	159.60	597.00	15.09	23.00	1370.90	1.881	5.5
100	169.00	603.00	14.88	18.00	1367.10	2.021	6.0
101	179.00	605.00	14.78	18.00	1373.30	2.277	5.0
102	155.80	587.00	15.30	17.00	1370.20	1.815	5.0
103	140.10	347.00	25.26	27.00	1126.80	1.516	10.5
104	159.80	366.00	23.26	24.00	1136.80	1.663	11.5
105	180.50	386.00	22.17	25.00	1137.80	1.918	11.5
106	190.60	395.00	21.57	24.00	1137.70	2.117	13.0
107	139.80	442.00	11.37	24.00	969.50	1.872	9.0
108	99.30	404.00	18.18	24.00	971.60	1.501	7.5
109	120.00	436.00	16.41	26.00	972.60	1.608	7.5
110	149.30	482.00	14.82	26.00	974.70	1.853	9.0
111	169.20	512.00	13.90	24.00	975.90	2.143	10.0
112	132.40	486.00	16.99	20.00	1128.20	1.708	7.0
113	149.40	505.00	16.12	19.00	1138.80	1.877	6.5
114	132.30	491.00	16.29	21.00	1345.60	1.492	8.5
115	142.90	505.00	15.74	21.00	1339.90	1.580	8.5
116	153.00	520.00	15.12	20.00	1341.30	1.674	8.5
117	163.00	531.00	14.69	19.00	1341.00	1.822	8.0
118	170.20	537.00	14.35	18.00	1340.90	1.935	7.5
119	180.80	512.00	14.36	20.00	1339.50	2.293	9.0
120	170.40	657.00	13.47	17.00	1341.50	2.036	7.0
121	133.20	669.00	14.28	18.00	1343.80	1.587	6.5
122	143.10	675.00	13.92	18.00	1343.40	1.711	6.0
123	150.50	698.00	13.46	17.00	1338.20	1.752	6.0
124	160.60	713.00	12.99	18.00	1342.40	1.898	6.0
125	170.30	720.00	12.64	18.00	1347.50	2.116	6.0
126	170.00	768.00	11.69	19.00	1339.80	2.181	6.0
127	99.90	419.00	19.97	24.00	856.80	1.496	9.0
128	119.50	446.00	18.91	25.00	857.70	1.564	10.0
129	139.30	462.00	17.80	22.00	859.00	1.724	10.5
130	159.20	462.00	17.76	21.00	859.90	1.875	10.0
131	184.70	498.00	16.55	20.00	874.80	2.254	11.0
132	189.10	501.00	16.41	21.00	861.70	2.375	13.0
133	99.00	404.00	14.98	26.00	855.40	1.562	8.5
134	119.70	442.00	13.41	23.00	856.80	1.711	8.0
135	140.10	478.00	12.46	20.00	857.70	1.873	8.5
136	88.90	410.00	20.65	25.00	855.90	1.450	8.5
137	109.00	443.00	19.00	20.00	856.80	1.542	8.5
138	120.00	393.00	10.53	21.00	1339.00	1.544	7.5

TABLE A3.2: continued

No.	P 10^{-1} MN/m^2	G kg/m^{2}s	$\frac{W_n}{W_w}$	K	H_i kJ/kg	X_{IC}	ψ s
139	138.50	414.00	10.25	15.00	1337.20	1.715	7.0
140	60.30	350.00	12.29	21.00	1082.90	1.299	9.0
141	75.40	378.00	11.44	20.00	1082.90	1.390	6.5
142	119.50	444.00	19.12	18.00	1340.70	1.371	10.0
143	139.20	420.00	20.09	20.00	1326.80	1.492	8.0
144	159.50	398.00	20.14	19.00	1342.50	1.864	6.0
145	179.90	412.00	20.23	26.00	1340.70	2.121	7.0
146	79.60	514.00	18.24	20.00	856.40	1.491	6.0

APPENDIX 4

ECONOMIC ASPECTS OF NUCLEAR POWER IN TURKEY

In this appendix, the reprint of a paper presented during a IAEA Symposium on the economic aspects of nuclear power in Turkey is given. For the evaluation of the paper, the following explanations are considered essential.

a - In the paper the lifetimes of nuclear and thermal power plants were taken to be 30 years, and the lifetimes of hydro-power plants to be 50 years. These lifetimes were given to the author by the Turkish State Planning Department or were taken from the references given in the paper. Although economic lifetimes of power plants in industrialized countries are much lower than the above given values, the latter seem justified for Turkey, which is due to the following reasons: Turkey has to import a power plant, whatever kind it may be. During the last three decades, there has always been a considerable unbalance for foreign payments in Turkey's budget, i.e., foreign money is scarce. Therefore an imported power plant has to be used over a longer period than an economic lifetime valid for an industrialized country. This longer period is in fact also an economic lifetime but only applying to Turkey. For example in 1967, a coal fired power plant in Istanbul had been in operation for more than 30 years.

b - The load factor foreseen for 1972 is 60.5% in Table I, as compared to 56.9% in Table II. As the latter refers to the interconnected system, it should be larger rather than smaller than the value given in Table I. The reason for this discrepancy can be explained as follows: These tables were prepared by two different groups and at that time there were no sound statistical data on the subject. It is logical then to expect that there should be inconsistenties in these tables.

c - Table XIII seems to contain an anomaly: Whereas the capital costs of the BWR's are much lower, unit cost differences decrease with increasing plant capacity. This is in fact no anomaly, as illustrated with an example. For a 500 MW(e) BWR, the fixed charges, fuel cost, operation cost and plutonium credit plus the last core are 2.68, 3.59, 0.65 and -0.36 kuruş/kWh

respectively. This implies that the share of the fixed charges in the unit energy cost is about 41%. This is probably due to the penalty paid for foreign expenditure (i.e., 1$ (USA) being taken as 12 Turkish Liras instead of official rate of 9 Turkish Liras in the paper). However, the unit energy cost difference decreases with increasing plant capacity. This difference is 0.19 krş/kWh per 100 MW(e) installed capacity from 400 to 500 MW(e) and 0.12 krş/kWh from 500 to 700 MW(e). This difference fades away at about 900 MW(e).

Reprint from

"NUCLEAR ENERGY COSTS AND ECONOMIC DEVELOPMENT"

INTERNATIONAL ATOMIC ENERGY AGENCY
VIENNA, 1970

A4.3

ECONOMIC ASPECTS OF NUCLEAR POWER IN TURKEY

H.Ç. ÜNAL
Çekmece Nuclear Research and Training-Center,
Istanbul, Turkey

Abstract

ECONOMIC ASPECTS OF NUCLEAR POWER IN TURKEY. This paper outlines Turkey's energy resources, the past, present and future electric power situations and the large hydro and thermal power plant projects, planned and studied by the State Planning Department to be built possibly during the time covered by the second or the third five-year plan (1967-1972 or 1972-1977). The data are reviewed to obtain a future power balance. Then an economical comparison is made of the power plant projects with the 300-, 400-, 500- and 700-MW(e) BWR and PHWR nuclear power plants on the basis of the unit energy cost. The results indicate that the cost of the nuclear power will be comparable with the cost of the hydro power and cheaper than the cost of the conventional thermal power for the next decade in Turkey. Besides the fact that nuclear power generating will be cheap, the distant location of most of the large hydro potential, and the insufficient coal, lignite and oil resources together urge the necessity of launching a long-range nuclear power development program to generate electricity if the country wants to use its energy resources efficiently. It is anticipated that the first nuclear power station will be generating electricity by 1977 at the latest.

1. INTRODUCTION

Throughout the world at present nuclear energy is mainly used to generate electricity. Therefore, this paper considers nuclear energy only as a source of generating electricity and gives, on the basis of unit energy cost, the economic comparison of nuclear power plants with the big hydro- and thermal power plant projects studied and planned by the State Planning Department (DPT) to be built possibly during the time covered by the second or third five-year plan in Turkey.

The unit energy costs of the 300-, 400-, 500-, and 700-MW(e) BWR and PHWR type nuclear power plants, the 300-MW(e) SEYITÖMER lignite-fired, the 220-MW(e) AMBARLI, the 100-MW(e) SILAHTAR, the 300-MW(e) IZMIR fuel oil-fired power plants, and sixteen hydro-power plants with capacities from 90 MW(e) up to 1280 MW(e), are calculated with the present-worth method.

Although it is clear that, on the basis of unit energy cost, the economic comparison of the large hydro and thermal power plant projects, which are at the study and planning phase by DPT, with the nuclear power plants, which are in development stage, is not so very sound, it will still give a fairly good idea of the place of nuclear power among other possibilities in Turkey. The criterion of unit energy cost is not sufficient in the economic analysis of the different types of power plants. Additional factors such as flow control, irrigation, unemployment, status of energy reserves, credit conditions etc., must also be taken into consideration. Nevertheless, for the analysis of different types of power plants, which must be built solely for electrical power generation, the criterion of unit energy cost is valid, and the power plants proposed by DPT are intended for electricity only.

2. THE PRESENT POWER SITUATION

In 1967 there were about 134 hydro and 260 thermal power plants, all comparatively large, producing 6166.7 GWh electric energy with a capacity of 1985 MW(e). (The actual number of power plants in operation was more than 1000.) The largest unit size in the hydro and thermal power plants is 110 MW(e) for each type. The over-all load factor is rather low because many small individual plants are not in the interconnected system which covers the western and north-western parts of the country where the power is needed much more than elsewhere.

TABLE I. THE ACTUAL AND ESTIMATED DEMANDS IN ELECTRIC POWER AND ENERGY [1]

Year	Production		Installed capacity	Net production per capita	
	(GWh)	Growth-rate per year (%)	(MW(e))	(kWh)	Growth-rate per year (%)
1950	789.6	14.9	408	38	11.7
1955	1579.8	12.3	612	66	8.9
1960	2815.1	11.9	1272	101	9.2
1965	4941.5	11.7	1516	157	9.2
1967	6166.7		1985	187	
1972	11400	13.0	2150	306	10.4
1977	20700	12.7	3950	492	10.0
1982	36800	12.2	6950	776	9.5
1987	62900	11.3	11900	1185	8.8
1992	100000	9.2	18700	1689	7.4
2000	180000	7.6	33600	2580	5.4

TABLE II. THE ACTUAL AND ESTIMATED DEMANDS IN ELECTRIC POWER AND ENERGY FOR INTERCONNECTED SYSTEM [2]

Year	Peak load (MW(e))	Production (GWh)	Implied load factor
1961	489	2379	55.5
1962	542	2854	60.0
1963	679	3212	54.0
1964	733	3600	56.1
1965	900	4700	59.7
1967	1130	5640	56.9
1972	2040	10170	56.9
1973	2315	11490	56.5
1974	2630	13000	56.4
1975	3000	14700	56.0
1976	3420	16610	55.5
1977	3910	18770	54.8
1978	4465	21200	54.2

TABLE III. ENERGY RESERVES OF TURKEY [1]

Type of reserve		Reserves: 10^6 ton, 10^9 kWh
Bituminous coals:		
(a) Proved reserves		232.7
(b) Probable reserves		292.9
(c) Possible reserves		404.0
(d) Geological reserves		458.0
	Total:	1387.6
Lignite:		
(a) Proved reserves		167.4
(b) Probable reserves		407.5
(c) Possible reserves		219.1
(d) Geological reserves		228.7
	Total:	1022.7
Oil:		
(a) Proved reserves		50
(b) Possible reserves		473
Hydro-electric potential (economically usable)		57
Oil shale:		
(a) Proved reserves		275
(b) Probable reserves		1829
(c) Possible reserves		3250
	Total:	5354
Uranium U_3O_8		
(a) Proved reserves		0.0010
(b) Probable reserves		0.0014
Dried dung and agricultural residues		17500

The actual and estimated demands both in electric power and in electric energy for the whole country and for the interconnected system alone are given in Tables I and II.

Turkey's present energy sources are mainly hydro, coal, lignite and dried dung, wood and agricultural residues. The total energy reserves are given in Table III. The actual and predicted contributions of different types of energy sources for electricity production are given in Tables IV and V.

The hydro potential is comparatively large and is one of the important sources for obtaining electric energy both now and for the future. It is unfortunate that most of this potential is located in scarcely populated areas which have no industry. Turkey's big cities and industries are located in the west and north-west, where electric energy is most needed.

TABLE IV. THE ACTUAL CONTRIBUTIONS OF VARIOUS ENERGY SOURCES TO ELECTRICITY GENERATION [1]

Year	Coal		Lignite		Liquid fuels		Hydro		Others		Total
	(GWh)	(%)	(GWh)	(%)	(GWh)	(%)	(GWh)	(%)	(GWh)	(%)	(GWh)
1950	540.7	68.5	137.2	17.4	59.8	7.5	30.1	3.8	21.8	2.8	789.6
1955	953.5	60.4	339.0	21.4	158.3	10.0	89.2	5.6	39.8	2.6	1 589.8
1960	1007.7	35.8	532.9	18.9	233.0	8.3	1001.4	35.6	40.5	1.4	2815.1
1961	1109.9	36.9	356.9	11.8	234.8	7.8	1265.2	42.0	44.3	1.5	3011.1
1962	1520.3	42.7	600.0	16.8	270.6	7.6	1123.7	31.6	45.2	1.3	3559.8
1963	969.0	24.4	554.6	13.9	292.3	7.3	2104.3	52.7	63.2	1.7	3983.4
1964	1412.7	31.7	976.0	21.9	317.7	7.2	1648.1	37.0	96.4	2.2	4450.9
1965	1258.0	25.4	998.0	20.2	430.3	8.7	2167.2	43.9	88.0	1.8	4941.5
1966	1444.2	26.0	1210.0	21.9	446.0	8.1	2317.8	41.9	117.0	2.1	5535.0
1967	1074.1	17.5	1063.3	17.2	1505.9	24.4	2369.8	38.4	153.5	2.5	6166.7

TABLE V. PREDICTED CONTRIBUTIONS OF DIFFERENT ENERGY SOURCES TO ELECTRICITY GENERATION [3]

Year	Coals and lignites		Hydro		Liquid fuels		Others	
	(GWh)	(%)	(GWh)	(%)	(GWh)	(%)	(GWh)	(%)
1972	3700	21.3	9600	55.1	3950	22.7	150	0.9
1977	3300	12.7	18200	70.0	4300	16.5	200	0.8
1982	4500	11.7	25800	67.0	8000	20.8	200	0.5

TABLE VI. ACTUAL AND PREDICTED HYDRO-POWER CONSUMPTION FOR ELECTRICITY [1]

Year	Installed capacity (MW(e))	Average production (10^6 kWh)	Ratio of the consumption to the total potential
1950	17.9	30.1	0.05
1955	38.1	89.2	0.14
1960	411.9	1 001.4	1.53
1965	505.6	2 167.2	3.47
1967	731.2	2 369.8	3.63
1972	1850.0	9 700.0	14.9
1977	2900.0	14 100.0	21.6
1982	5600.0	28 200.0	43.2
1987	6600.0	30 500.0	46.7
1992	7600.0	33 000.0	50.5
2000	9100.0	36 000.0	55.1

The actual and predicted hydro-power consumption for electricity are given in Table VI.

From Tables I-VI it can be concluded that:

2.1. The main energy sources for generating electricity are coal, lignite, liquid fuels (fuel-oil and diesel-oil) and hydro-power. The contributions of hydro-power and liquid fuels to electricity generation have increased while other sources have remained constant or decreased since 1950. In the future, the contribution of hydro-power will increase while others will remain nearly the same or decrease (Tables IV and V).

2.2. The net production per capita was very low in comparison with many other countries, i.e., 187 kWh in 1967 (Table I).

2.3. During the next two five-year plan periods, the predicted increase in production and capacity will be about 12.85% and 11.2%, respectively (Table I).

2.4. For the interconnected system, from 1972 to 1978, the annual growth-rate of installed capacity will vary from 275 MW(e)/yr to 490 MW(e)/yr (Table II).

2.5. Although it is predicted that 43.2% of the total hydro potential will be used in 1982, it is doubtful whether such an optimistic estimate will be obtained because most of the hydro potential is in the eastern part of the country (6.2% in the west; 15.9% in the south-west; 65.9% in the east and 12% in the centre) and long high-voltage transmission lines to the western

parts will be difficult if not impossible to build. Coal reserves are poor and moreover large quantities are needed by industry.

Lignite is planned to be used mostly for household purposes and small industries while 55% of the oil is at present imported.

2.6. In 1967 Turkey's population was 32 900 000 and it increases by 2.5% p.a. The total power consumption was 25×10^6 ton coal equivalent in 1967 and it increases by 8% p.a. The cumulative energy consumption will be 3138.1×10^6 ton coal equivalent in 2000. Energy reserves of the country are poor and will hardly meet the demand till the end of this century even if they are used only for electricity generation (Table II).

Bearing those facts in mind, it is obvious that today the country faces the problem of developing a new power source, i.e. nuclear power for electricity in order to use the energy reserves economically to meet future demands.

3. COSTS OF HYDRO, THERMAL AND NUCLEAR POWER

To calculate the unit energy costs, the following assumptions are made:

3.1. Power plants with a capacity of 300 MW(e) or more can only be put into operation after the completion of the KEBAN Hydro Power Plant in 1974. Therefore, it is accepted that all the power plants compared here can be commissioned only after 1974.

3.2. For the prediction of the unit energy cost the present-worth method is used. The economic parameters of the method are chosen as follows:

3.3.1. The reference date is taken as commissioning date.

3.3.2. The lifetime for thermal power plants as well as for nuclear power plants and for hydro-power plants are taken as 30 and 50 years respectively. (For PHWR, see Appendix 3.)

3.3.3. The load factors and nominal powers are given in the following sections.

3.3.4. The annual interest rate is taken as 10%. Although the official interest rate fixed by the Provinces Bank (Iller Bankası) for investments is 7% and the interest rates of foreign loans are much lower than 10%, the actual annual interest rate even exceeds 10% with the additional charges for the loans borrowed by the Provinces Bank. Furthermore, DPT accepts 10% interest rate for the analysis of the investment projects.

3.4. For the foreign expenditure components of the power station costs, one US $ is accepted as equal to 12 TL (Turkish Lira) although the official rate is 9 TL per US $. DPT also uses the above assumption to favour projects which depend on internal rather than on foreign expenditure in the analysis of the investment projects. However, it is believed that this assumption clearly reflects the value of the Turkish currency on the foreign market.

3.5. Although, at present, no duty is charged on the foreign expenditure components of the hydro-power plants in Turkey, the same is not valid for thermal power plants. The foreign expenditure components of the nuclear power plants are duty free but 5% registration fee is charged on them. To make an objective comparison, duties and registration fees are not considered on the foreign expenditure component of any type of power plant.

3.6. Foreign expenditure component in the operation and maintenance costs is 25%.

3.7. During the construction period, the expenses are distributed homogeneously.

3.8. As the capital costs of the hydro and thermal power plants, data given by DPT are used.

3.9. No escalation is considered. Since the escalation rate in Turkey is much higher than in the countries where nuclear power plants can be bought, and percentages of the foreign expenditure components of nuclear power stations are higher than the other types, the assumption is in favour of the conventional power plants. Since DPT data was issued in 1966, 1966 prices are used for all power plants.

3.10. The unit energy costs include costs of the high-voltage transmission lines, i.e. they are the costs at load centre.

3.11. Other assumptions are given in the Appendices.

3.I. Costs of the hydro and thermal power

The unit energy costs of sixteen hydro, three fuel-oil-fired and one lignite-fired power plant projects, which are under study and in the planning phase by DPT, to be built possibly during the second or third five-year plan, are predicted. The locations of these plants are given in Fig. 1. Further assumptions and characteristics of these power plants necessary to calculate the unit energy costs are given in Appendices 1 and 2. The capital and calculated unit energy costs are given in Tables VII to X and in Figs 2 to 5.

Figure 5 reveals that there are attractive hydro-power plant projects although, in the production range covered by thermal power plants, the cost of the thermal power averages the cost of the hydro power. However, it is obvious that there are some hydro-power plants which generate electricity cheaper than the thermal power plants.

At present, the unit energy cost varies considerably and the average cost is above that predicted, because the electricity generating system in Turkey consists of more than a thousand small units.

It is clear that the predicted figures do not give the real unit energy cost of the thermal power because the import duties are not considered, but they are applicable to hydro power. To show the power market, the unit energy costs are calculated by taking the import duties into consideration and they are given in Fig. 6. These figures show what the electricity would cost the producer. (In Turkey, there are various owners of the power plants, i.e.

TABLE VII. CHARACTERISTICS OF HYDRO-POWER PLANT PROJECTS [4]

Name of project	Place (Name of river)	Capacity (MW(e))	Production (GWh)	Construction period (yr)	Capital cost	
					Foreign expenditure component (9TL = US$1) ($10^6$ TL)	Total (10^6 TL)
Kızıltaş	Ceyhan	93	325	5	60	121
Kargı	Sakarya	100	380	6	125	500
Yumula	Kızılırmak	100	430	6	137	350
Çatalan	Seyhan	120	660	6	150	600
Fatlı	Yeşılırmak	124	286	5	90	179
Homa	Manavgat	140	930	5	130	400
Şahınkaya	Kızılırmak	146	640	5	75	250
Sandalcık	Dalaman	150	750	6	125	500
Kumbel	Kızılırmak	185	810	6	75	220
Boyabat	Kızılırmak	280	1230	7	144	600
Iyıdere	Ikizdere	360	1100	6	100	450
Ayvacık	Yeşılırmak	380	1080	8	230	570
Kavşak	Seyhan	440	1757	7	450	1150
Taşüstü	Fırat	1050	4546	8	350	2755
Karakaya	Fırat	1280	7000	8	570	2322
Halfetı	Fırat	1280	6543	8	460	2424

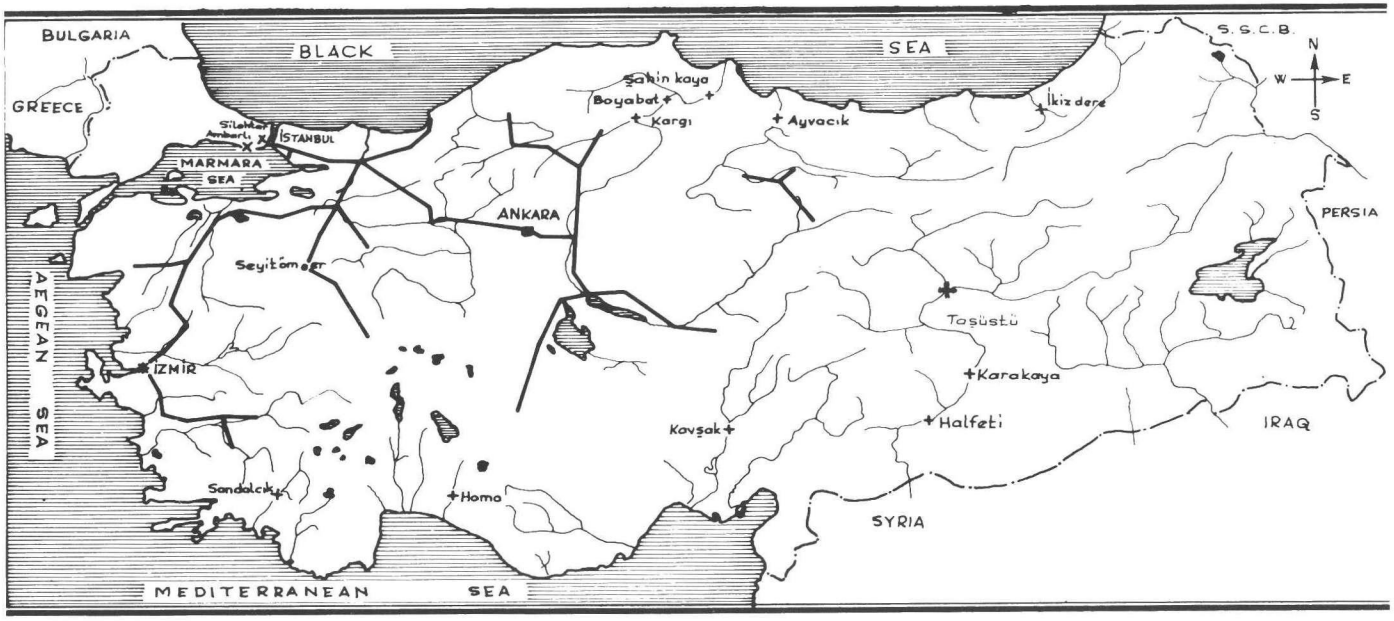

FIG.1. Locations of the hydro- and thermal-power plants.

——— = Interconnected system (the power lines in operation and scheduled for construction)
* = Fuel-oil-fired power plants
● = Lignite-fired power plants
✚ = Hydro-power plants

TABLE VIII. UNIT ENERGY COSTS OF THE DIFFERENT HYDRO-POWER-PLANT PROJECTS

Name of project	Unit energy cost (kuruş/kWh)[a]
Kızıltaş	6.48
Kargı	20.83
Yamula	14.23
Çatalan	15.44
Fatli	10.67
Homa	6.95
Şahinkaya	6.48
Sandalcık	11.00
Kumbel	4.89
Boyabat	8.61
Iyıdere	6.63
Ayvacik	10.43
Kavşak	11.56
Taşüstü	11.12
Karakaya	6.37
Halfetı	6.99

[a] 0.9 kuruş/kWh = 1.0 mill/kWh (9 TL = US $1)

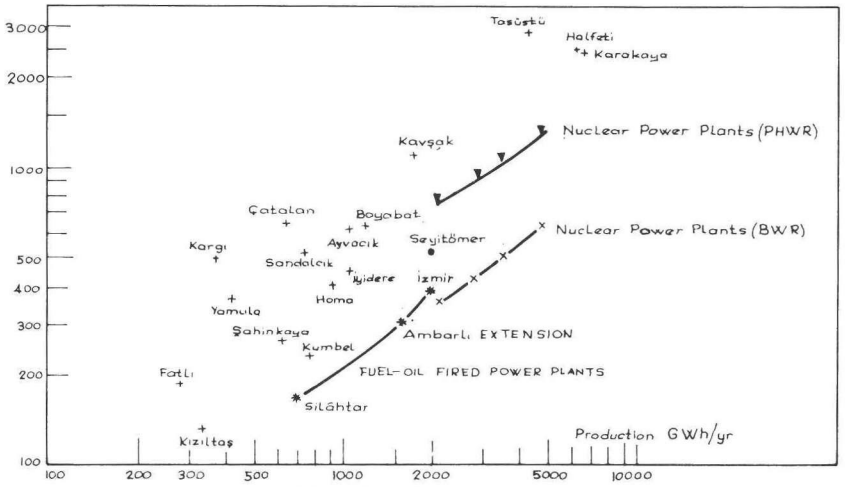

FIG. 2. Total capital costs of the hydro-, thermal- and nuclear-power plants (10^6 TL).

✚ = Hydro-power plants
✲ = Fuel-oil-fired plants
● = Lignite-fired plants
x = Nuclear power plants (BWR)
▼ = Nuclear power plants (PHWR)

TABLE IX. CHARACTERISTICS OF THERMAL-POWER-PLANT PROJECTS [4]

Name of project	Place	Load factor	Capacity (MW(e))	Production (GWh)	Capital cost	
					Foreign expenditure component (9 TL = US $1) ($10^6$ TL)	Total[a] (10^6 TL)
Lignite-fired power plant	Seyitömer	0.76	2 x 150	2000	347	719.6
Fuel-oil-fired power plant extension	Ambarlı (Istanbul)	0.83	2 x 110	1600	208	424.8
Fuel-oil-fired power plant	Silâhtar (Istanbul)	0.80	2 x 50	700	110	230.0
Fuel-oil-fired power plant	Izmir	0.76	2 x 150	2000	263	536.0

[a] Includes import taxes and duties.

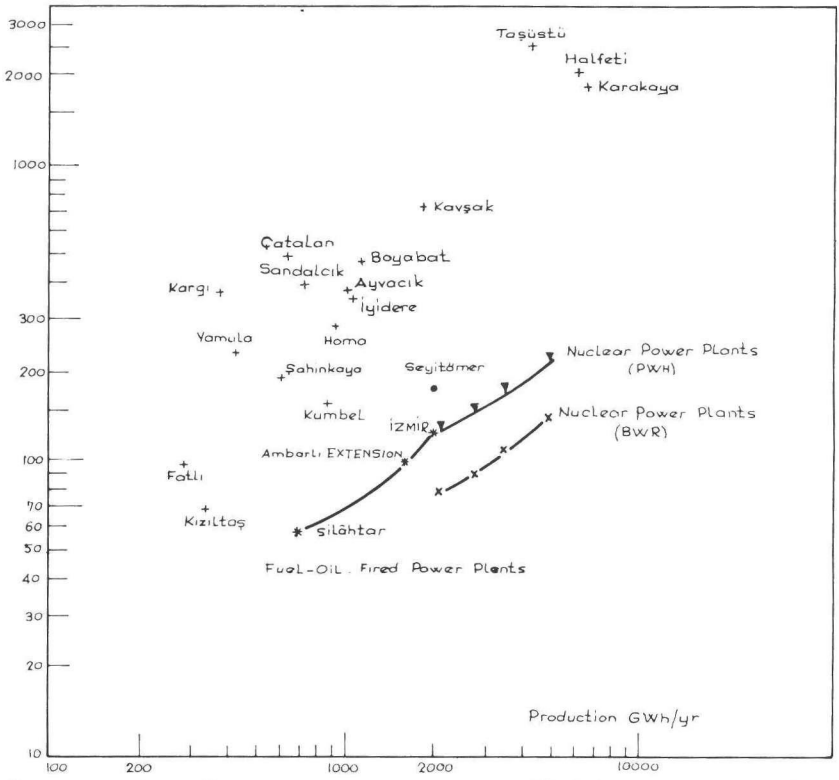

FIG. 3. Internal expenditure components of the capital costs of the hydro-, thermal- and nuclear-power plants. (10^6 TL).

✚ = Hydro-power plants
✲ = Fuel-oil-fired plants
● = Lignite-fired plants
× = Nuclear power plants (BWR)
▼ = Nuclear power plants (PHWR)

TABLE X. UNIT ENERGY COSTS OF THE DIFFERENT THERMAL-POWER-PLANT PROJECTS

Name of project	Unit energy cost (kuruş/kWh)
Lignite-fired power plant (Seyitömer)	8.99
Fuel-oil-fired power plant extension (Ambarlı)	8.67
Fuel-oil-fired power plant (Silâhtar)	7.98
Fuel-oil-fired power plant (Izmir)	8.00

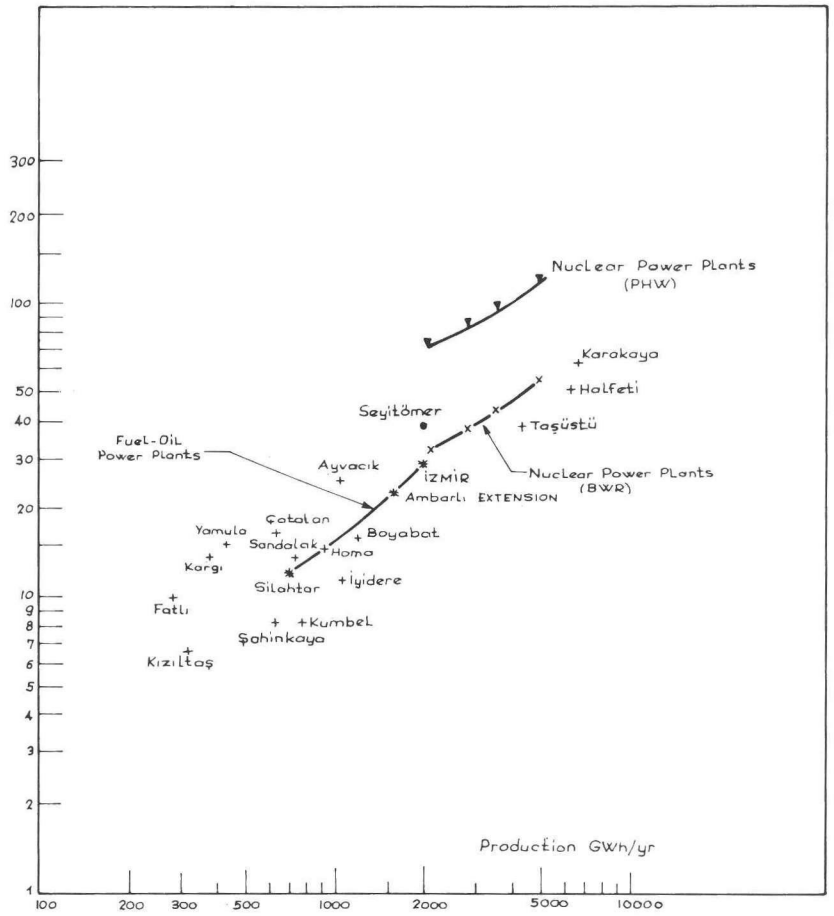

FIG.4. Foreign expenditure components of the capital costs of the hydro-, thermal- and nuclear-power plants (US$).

✚ = Hydro-power plants
● = Lignite-fired plants
✲ = Fuel-oil-fired plants
× = Nuclear power plants (BWR)
▼ = Nuclear power plants (PHWR)

the State Hydraulic Works, Etibank, two state organizations, municipalities, and some private firms which generate electricity for their own use but not for sale.) They clearly indicate that hydro power is cheaper. This is purely because import duties are included in the cost of the thermal power but not in the cost of the hydro power.

Here, there is another point worth mentioning. The lack of capital in developing countries may give preference to the power plant with minimum capital over a more economical one. Figures 2 to 5 reveal that thermal power plants have such an advantage over hydro-power plants.

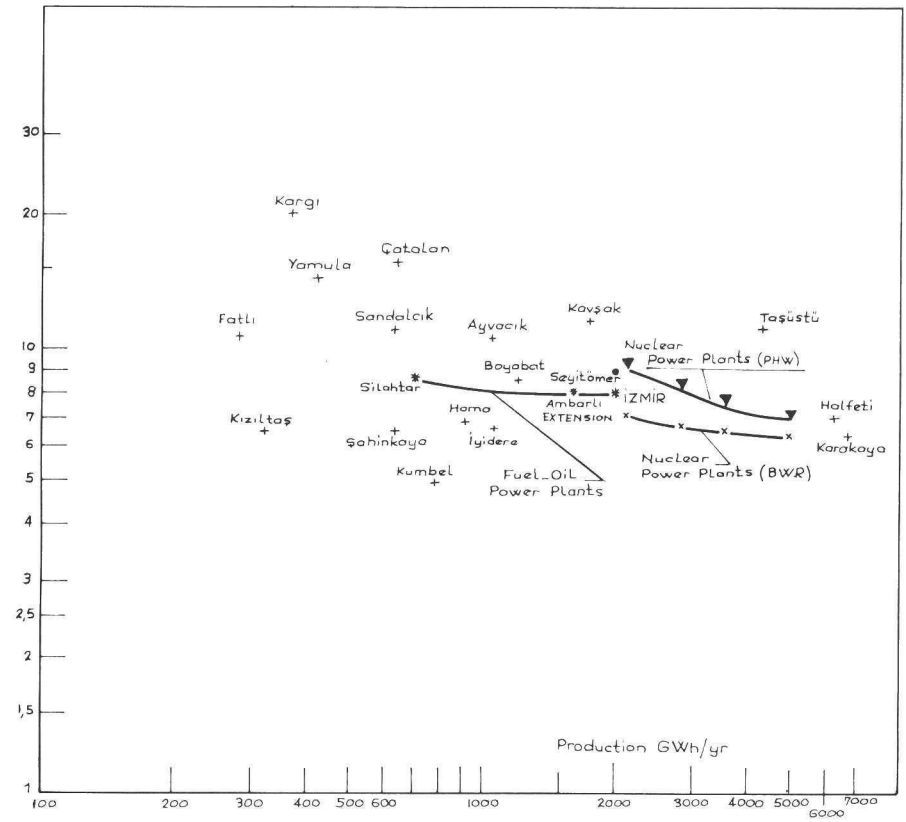

FIG. 5. Unit energy costs of the hydro-, thermal- and nuclear-power plants (kuruş/kWh); (1 kuruş/kWh = 0.9 mill/kWh).

- ✚ = Hydro-power plants
- ● = Lignite-fired plants
- ✲ = Fuel-oil-fired plants
- × = Nuclear power plants (BWR)
- ▼ = Nuclear power plants (PHWR)

TABLE XI. TOTAL CAPITAL COSTS OF BWR NUCLEAR POWER PLANTS

Capacity (MW(e))	Foreign expenditure component (US $1 = 9 TL) ($10^6$ TL)	Internal expenditure component (10^6 TL)	Total cost (10^6 TL)
300	294.00	76.68	370.68
400	342.00	89.64	431.64
500	394.00	109.35	503.35
700	502.00	140.50	642.50

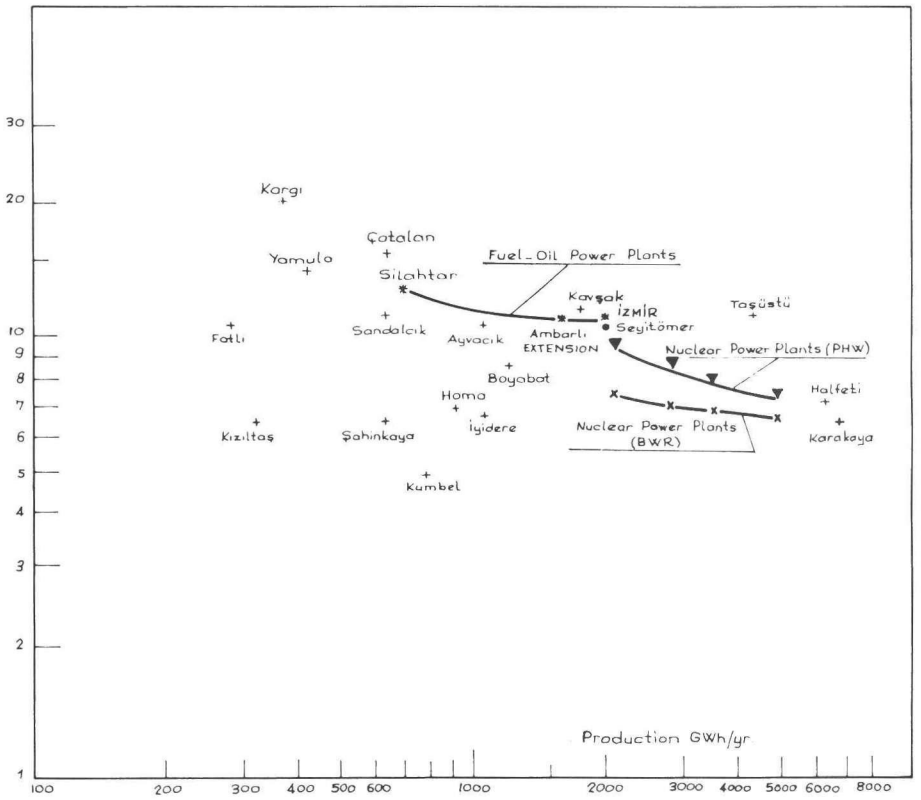

FIG.6. Unit energy costs of the hydro-, thermal- and nuclear-power plants, including import duties (kuruş/kWh).

✚ = Hydro-power plants
● = Lignite-fired plants
✲ = Fuel-oil-fired plants
× = Nuclear power plants (BWR)
▼ = Nuclear power plants (PHWR)

3.II. Cost of the nuclear power

At present, no nuclear power plant exists in operation or in planning or in the construction phase. However, an extensive feasibility report for the Turkish Authorities is being prepared by Motor Columbus Ltd. Consulting Engineers, Baden, Switzerland, to evaluate the economic aspects of nuclear power plants with the aim of building one in Turkey. This report will probably be ready before this symposium and will show the fate of the nuclear energy for the near future in Turkey.

The unit energy costs of eight nuclear power plants, BWR and PHWR types with capacities of 300, 400, 500 and 700 MW(e), are calculated here. The data and assumptions used in the calculations are given in Appendix 3. The capital and predicted unit energy costs are shown in Tables XI, XII and XIII and in Figs 2 to 5.

TABLE XII. TOTAL CAPITAL COSTS OF PHWR NUCLEAR POWER PLANTS

Capacity (MW(e))	Foreign expenditure component (US $1 = 9 TL) ($10^6$ TL)	Internal expenditure component (10^6 TL)	Total capital costs (10^6 TL)
300	125.5	653.7	779.2
400	148.7	767.5	916.2
500	175.9	851.4	1027.3
700	223.6	1091.2	1314.8

TABLE XIII. UNIT ENERGY COSTS OF THE NUCLEAR POWER PLANTS (kuruş/kWh)

Capacity (MW(e))	Type of nuclear power plant	
	PHWR	BWR
300	9.10	7.16
400	8.22	6.75
500	7.51	6.56
700	7.04	6.32

Figure 5 shows that the unit energy cost of a BWR nuclear power plant is cheaper than the unit energy cost of any other type of thermal power plant and it is about the same level with the unit energy cost of hydro-power plant when the capacity increases. PHWR nuclear power plants generate electricity more expensively than BWR power plants.

The GCR and AGR nuclear power plants should also be mentioned. However, a previous study shows that the unit energy cost difference between the GCR (Magnox) and PHWR nuclear power plants is about twice as high as the unit energy cost difference between BWR and PHWR power plants of 500-700 MW(e) capacity [6].

The necessary financial sources to build a large power plant are difficult to obtain for a developing country. In this respect, oil-fired power plants have more favourable conditions than any other type. (See Figs 2 to 4. The costs of the first cores of the nuclear power plants are not included in the capital costs.)

Having taken the criterion of the unit energy cost only, the economic comparative ranking of the different types of power plants is as follows:

(a) Hydro-power plants and/or BWR nuclear power plants
(b) Fuel-oil-fired power plants
(c) Lignite-fired power plants
(d) PHWR nuclear power plants

The unit energy costs of the nuclear power plants are also given in Fig. 6 when registration fees are charged on their foreign expenditure components. The previous conclusion is also valid for this case. The above comparisons clearly indicate that nuclear electricity generation has attractive aspects for Turkey.

4. CONCLUSIONS

The cost of the nuclear power will be comparable with the cost of hydro-power and cheaper than the cost of thermal power for the next decade in Turkey.

The energy reserves of the country, with the exception of the huge hydro potential, are rather poor and will be insufficient to meet the increasing electricity demands. Most of the hydro potential lies in the areas where the population is scarce and where there is no industry. Furthermore, it will be rather difficult to build hydro-power plants as fast as the electricity demand increases. Also the initial investments of hydro-power plants are rather high.

At present Turkish industry is incapable of building a nuclear power plant with the capacity needed by the interconnected system. But its participation in the construction of some types of small nuclear power plants, which must be built as soon as possible to obtain design and operation experience, may be considerable.

It now seems to be the right time for the country to launch its long-range nuclear power development program.

APPENDIX 1

COST OF HYDRO POWER

The capacities, construction periods and capital costs of the sixteen hydro-power plants mentioned earlier are given in Table VII and Figs 2 to 4 according to the DPT [4].

Further assumptions made to calculate the unit energy costs of these hydro-power plants are as follows:

(a) The figures given in Table VII include only the construction costs of the dams and power plants, but not the costs of the high-voltage transmission lines [2]. Most hydro-power plants are located remotely; therefore, for the costs of transmission lines the internal expenditure components of the capital costs are increased 10% for Kızıltaş, Yamula, Çatalan, Fatlı, Şahinkaya and Ayvacik Hydro-Power Plants; and 5% for Homa, Şandalcık, Boyabat, Kavşak, Taş Üştü, Halfetı, Karakaya Hydro-Power Plants. No modification is made for Kargı and Iyidere Hydro-Power Plants. For the above estimates, which are highly conservative, the locations of the hydro plants and transmission lines under construction and in planning phase are taken into consideration.

(b) For the transmission losses, the production given in Table VII is reduced 2% for the first eight hydro plants, 3% for the successive four hydro plants, and 5% for the last ones. These estimates are also highly conservative.

(c) Operation and maintenance costs are 0.19 kuruş/kWh [5].

Using the present-worth method with the assumptions given in section 3 and above, the calculations of the unit energy costs are straightforward and their details are not given here, but only the results. The unit energy costs of the hydro-power plants are given in Table VIII and in Fig. 5.

APPENDIX 2

COST OF THERMAL POWER

The capacities and the capital costs of the three fuel-oil-fired power plants and one lignite-fired power plant mentioned before are given in Table IX and in Figs 2 to 4, according to DPT[1]. The feasibility reports of the above power plants have been prepared [4].

Further assumptions made to calculate the unit energy costs of the different thermal power plants are as follows:

(a) As the capital costs in Table IX also include the import duties, the amounts equal to these items, i.e. 56.3% of the foreign expenditure components, must be subtracted from the total capital costs.

(b) The construction period is three years.

(c) The load factors for the first twenty years are given in Table IX. For the last ten years, these factors are reduced by 5%.

(d) For Seyitömer lignite-fired power plant, the fuel cost is 3.08 kuruş/kWh, and operation and maintenance cost 1.25 kuruş/kWh [6].

(e) For the fuel-oil-fired plants, operation and maintenance costs are 0.4 kuruş/kWh [6].

(f) The net thermal efficiency of the fuel-oil-fired plants is 36% and calorific value of the fuel oil (number 5) is 10 000 kcal/kg.

(g) Fuel oil costs 136 TL/ton. (This figure does not include taxes and duties of any kind.)

(h) As the above power plants will be located at the load centres, no transmission costs are considered.

The calculated unit energy costs according to the assumptions mentioned in section 3 and above, are given in Table X and in Fig. 5.

[1] At present, Ambarlı fuel-oil and Seyitömer lignite-fired power plants are being constructed.

APPENDIX 3

COST OF NUCLEAR POWER

To calculate the unit energy costs of the BWR and PHWR types of eight nuclear power plants with capacities of 300, 400, 500 and 700 MW(e), the following additional assumptions are made.

I. General

(a) At present, the Turkish industry is not capable of manufacturing any type of nuclear power plant. Therefore, with the exception of site and improvements, buildings and structures, the other services and reactor plant equipment, turbo-generator plant, electrical equipment and auxiliary plant equipment etc., must be imported.

(b) The costs of the nuclear power plants are based on developments which nuclear power plants will reach in 1970 because the earliest commissioning date of any considerable sized thermal power plant to be built in Turkey is 1975.

(c) The construction period is 3.5 years.

(d) Transportation costs of the imported equipments are 5% of their values.

(e) Transport is by Turkish ships.

(f) Fuel is changed every year, so the payment for the fresh fuel is made one year before charging it into the reactor and plutonium credit is obtained one year later than the discharge of the fuel from the reactor.

(g) The load factor is 80% for the first 20 years and 75% for the last 10 years.

(h) Insurance with a rate of 0.5% is charged on all cost items except on the costs of transport and civil works.

(i) All the cost figures are selected from the literature. Domestic workmanship and land are cheaper than in countries where the nuclear power plants are developed. Therefore, the values given in the literature for the costs of the site and improvements and buildings and structures are reduced by 25%, and no foreign expenditure is accepted on them.

(j) Uranium content of the last core is considered.

(k) Nuclear power stations are assumed to be located near the load centres.

II. BWR-type nuclear power plants

As a light-water reactor, BWR type is considered. For the analysis of this level, BWR and PWR types of nuclear power plants would yield identical results. The components of the unit capital costs and total capital costs and

the necessary data for the fuel cycle are given in Tables XI, XIV and XV and in Figs 2 to 4. Operation and maintenance costs are considered as 0.55 kurus/kWh [8-15].

TABLE XIV. COMPONENTS OF THE UNIT CAPITAL COSTS OF THE BWR NUCLEAR POWER PLANTS

Component of unit capital cost (US $/kW(e))	Capacity (MW(e))			
	300	400	500	700
Site and improvements	2.0	2.0	3.0	3.0
Buildings and structures	13.2	11.6	10.6	9.7
All reactor and power plant equipment	73.5	64.5	59.0	53.5
Engineering design, inspection and administrative works	31.7	27.0	25.5	23.2
Contingencies	12.8	11.2	10.4	9.5
Insurance	0.6	0.5	0.5	0.5
Transportation	3.6	3.2	3.0	2.7
Total unit capital cost:	137.4	120.0	112.0	102.1

TABLE XV. BWR FUEL-CYCLE DATA [11, 14]

Type of data	Value
Net thermal efficiency of plant (%)	33.0
Burn-up (MWd/ton U)	24 000.0
Cost of first core (US $/kW(e))	59.75
Transport of first core (TL/kW(e))	27.00
Fuel price ($/kg U): total	331.5
(a) Fabrication	80.0
(b) Feed uranium	148.2
(c) Spent fuel recovery	42.0
(d) Plutonium credit	-40.2
(e) Discharge uranium	-20.9
Transport of fuel (TL/kg U)	132.0
Fuel requirement per year (kg U/kW(e))	0.03662

TABLE XVI. COMPONENTS OF UNIT CAPITAL COSTS OF PHWR NUCLEAR POWER PLANTS

Component of the unit capital cost (US $/kW(e))	Capacity (MW(e))			
	300	400	500	700
Site and improvements	2	2	3	3
Buildings and structures	20	17.6	17	15
Heavy water	42	37	33.4	31.5
Reactor and its components	57	50.5	44.5	40.5
All the plant equipment except 4	86	75.5	67.5	61.5
Engineering, design, inspection and administrative works	41.5	36.5	31.2	28
Contingencies	29.9	26.3	23.6	21.6
Insurance	1	0.9	0.8	0.8
Transport	9.2	8.1	7.3	6.8
Total unit capital cost:	288.6	254.4	228.3	208.7

TABLE XVII. PHWR FUEL-CYCLE DATA [7, 8, 11]

Type of data	Value
Net thermal efficiency (%)	0.30
Burn-up (MWd/t U)	12000
Fuel price (US $/kg)	41.53
Fuel transport (TL/kg)	51.5
Fuel requirement for first core (g U/kW(e))	204
Annual fuel requirement (g U/kW(e)-yr)	130

III. PHWR-type nuclear power plants

Candu-type nuclear power plants developed in Canada have been analysed. Owing to their natural uranium fuel cycle they are attractive. The components of the unit capital costs and the total capital costs and the necessary data for the plant and fuel cycle are given in Tables XII, XVI and XVII and in Figs 2 to 4. Further assumptions are given below [7-13, 15].

(a) The reactor and its components are renewed after 15 years of operation. Renewal lasts six months and the costs for the reactor and its components for 300-, 400-, 500- and 700-MW(e) capacities are, respectively, US $/kW(e) 57, 50.5, 44.5 and 40.5. No transportation is calculated on these items due to the cost reductions which are expected in the future.

(b) Operation and maintenance costs are 0.59 kuruş/kWh.

(c) The lifetime for a heavy-water reactor and its components are, respectively, 40 and 15 years. For the rest of the plant it is 30.5 years. (Six months renewal time is added to 30 years.)

(d) The salvage value of heavy water is US $12.6/kg.

(e) No plutonium credit is considered.

The calculated unit energy costs of the nuclear power stations based on the assumptions are given in Table XII and in Fig. 3.

REFERENCES

[1] Total Energy Report for Turkey, September 1968, prepared by a Commission for the 2nd Conf. Total Energy in Turkey, 18-20 November, 1968, Ankara (in Turkish).

[2] INTERNATIONAL ATOMIC ENERGY AGENCY, Report of an IAEA Mission to Turkey, 23 December, 1965; Revised, May 1966.

[3] Proc. 3rd Technical Conf. for Electrical Engineering of Turkey, 15-17 November, 1967, Ankara (in Turkish).

[4] Report on 2nd Five-Year Plan, Special Commission for Electricity of the State Planning Office (DPT), printed by Department for Study and Planning of Electrical Works (EIEI), February, 1966 (in Turkish).

[5] Electrical Engineering, 9 No. 102 (June 1965) (in Turkish).

[6] Feasibility Report, The Extension of Ambarli Thermal Power Plant, Electric Power Resources Survey and Planning Administration, Republic of Turkey, January 1966.

[7] ÜNAL, Ç., Cost of the nuclear power in our country, ÇNAEM Rep. 41 (Oct. 1966) (in Turkish).

[8] HAYWOOD, L.R., Trends in atomic power costs, AECL-2534, (March 1966).

[9] ENEA, Basic assumptions for nuclear power estimates in Europe, ENEA, Paris, 1960.

[10] INTERNATIONAL ATOMIC ENERGY AGENCY, Introduction to the Methods of Estimating Nuclear Power Generating Costs, TRS N°. 5, IAEA, Vienna (1961).

[11] OECD First Report on Power Reactor Characteristics, OECD, 1966 (internal Rep.).

[12] INTERNATIONAL ATOMIC ENERGY AGENCY, Small and Medium Power Reactors (Proc. Conf. Vienna, 1960) 2, IAEA, Vienna (1961).

[13] WILLEMS, M. et al., Euratom Economic Handbook, 3079 e, Euratom (1966).

[14] LANE, A.J., "Calculating fuel cycle costs for light water reactors", presented at the IAEA International Survey Course on Economical and Technical Aspects of Nuclear Power, 5-16 September, 1966, Vienna.

[15] ÜNAL, Ç., Economical comparison of the nuclear power plants with thermal and hydraulic plants which are considered to be built in our country, ÇNAEM Rep. 43 (Feb. 1967) (in Turkish).

DISCUSSION

S. YIFTAH: In section 3.II of your paper you say that a feasibility report is being prepared for the Turkish authorities by Motor Colombus Ltd., consulting engineers in Switzerland, for an evaluation of the economic aspects of a nuclear power plant to be built in Turkey. Is this report ready, and what are its conclusions?

H.C. ÜNAL: Perhaps Mr. Aybers would like to answer this question.

N. AYBERS: The feasibility report for our nuclear power project has been submitted to us but we have not yet had time to evaluate it.

B.J. CSIK: You give a figure of three to five years for the construction time. I do not think any nuclear power plant can be built in such a short time today. Also, the generating cost of 10 mill/kWh which you arrive at

for a 300-MW HWR seems extremely high. According to the parameters used in the paper, operating maintenance and fuel cost together would account for less than 2 mill/kWh; this leaves more than 8 mill/kWh for capital charges. How did you arrive at this figure? Have you included any other items not mentioned in the paper?

H.C. ÜNAL: I agree that the construction period given is rather short, but it may not be unreasonable as the reactor will be bought on a turnkey basis.

Since the interest rate is taken as 10% and the rate of exchange used is US $1 = 12 TL, instead of the official rate of US $1 = 9 TL, the unit energy cost becomes higher. This also applies to the fuel cycle.

A.M. AIKIN: I would like to comment on two points made in this paper. You have gone to a lot of trouble to assess the competitiveness of nuclear power with hydro, coal or oil power, but unfortunately, you have used data that are not correct today. The capital cost figures for LWRs are low by at least a factor of two since, as pointed out on several occasions at this symposium, there has been a rapid rise in costs during the past three years. I wonder whether you have since had an opportunity to recalculate the generating costs.

My second point concerns the statement made in Appendix 3, section III of the paper that the PHWR reactor would have to be rebuilt after 15 years. This is certainly not true for the CANDU-PHW reactors being built in Canada, where the design life is at least 30 years.

N. AYBERS: I also think that the unit capital costs given in Table XI for BWR power stations are very low; I believe the figures should be approximately doubled. Could any of the United States participants comment on this?

H.C. ÜNAL: The figures are taken from report AECL-2534 by Haywood, dated March 1966.

I. SPIEWAK: As pointed out in my own paper and in papers presented by other United States participants, the capital costs of 500-MW(e) light-water reactors bought in 1969 in the United States are about $225/kW.

J. BARTH: May I refer again to Table XI in the paper under discussion. The opinion has just been expressed that the cost per kW of the 700-MW(e) reactor should be doubled. I don't agree that the increase should be as much as this. One reason for the low cost is that you do not seem to have taken the interim interest into account, and it would seem that this should be added. Then also, between 1966 and 1969 the price escalation can be roughly estimated at 25%, and taken together all this means that the cost per kW for the 700-MW(e) reactor would reach $150/170 - a perfectly feasible figure for western European industries. But the point is that this is still much less of an increase than has just been suggested.

H.C. ÜNAL: Again according to AECL-2534, in Canada and the United States the escalation rate is only 1%. It is assumed that we shall import our nuclear plant from either the USA or Canada.

L. BOXER: In Section 3.d of the paper you state that the foreign expenditure components of nuclear power plants are duty free, but are subject to a 5% registration fee. In the paper presented by Mr. Aybers, however, (IAEA-SM-126/17)[1], customs duties were estimated to form a considerable part of the total costs. Is there not some discrepancy here?

[1] These Proceedings

H.C. ÜNAL: At present, all that is charged on nuclear devices imported into Turkey is a 5% registration fee. However, one can interpret the currently valid legislation differently in the case of an electricity generating facility, and there is no clear ruling on the point at present.

N. AYBERS: Perhaps I should explain that equipment for research and development imported by the Turkish AEC is free of duty. The power station will probably be built by ETIBANK, however, and the utility company will have to pay taxes amounting to about 33%.

APPENDIX 5

SUMMARY AND CONCLUSIONS IN DUTCH
SAMENVATTING EN CONCLUSIES IN HET NEDERLANDS

Dit proefschrift is gebaseerd op reeds gepubliceerde [U2, U3, U4, U6, U7, U8, U9], of nog te publiceren artikelen [U10, U11] van de auteur in wetenschappelijke tijdschriften en de door hem gehouden lezingen tijdens internationale symposia [U1, U5].

Het doel van dit proefschrift is een licht te werpen op de fysische verschijnselen van sommige aspecten van twee-fasen stroming, warmte-overdracht en dynamische instabiliteiten in stoomgeneratoren voor middelhoge- en hoge druk en het afleiden van nauwkeurige modellen en correlaties voor thermische en hydrodynamische ontwerpen en het veilig bedrijven van deze stoomgeneratoren. Voor deze doeleinden werden experimenten uitgevoerd in zes natriumverhitte stoomgeneratorpijpen van verschillende lengte en in één natriumverhit grootschalig verdampermodel. Bij deze experimenten werden hoofdzakelijk gegevens verkregen voor dampfractie, beginpunt van koken, beginpunt van netto-dampontwikkeling, bellendynamica, droogkoken, twee-fasen drukverlies en dichtheidgolfoscillaties. De binnendiameters van de testpijpen varieerden van 7,86 mm tot 18 mm en de lengten van 10 m tot 44,43 m. De bedrijfscondities van de experimenten waren identiek aan die van natriumverhitte stoomgeneratoren voor snelle kweekreactoren. In totaal werden 1036 gegevens verkregen. Ook werden relevante experimentele gegevens uit de literatuur geanalyseerd.

Hieronder volgen de samenvatting en de conclusies van het uitgevoerde onderzoek.

A5.1 DAMPFRACTIE (hoofdstuk 3 van het proefschrift)

Er is een methode ontwikkeld, te weten: een ultra-snelle fotografische techniek, om een snelheidsveld in twee-fasen stroming te bepalen. Het gemeten snelheidsveld is gebruikt om de dampfractie te bepalen.

A5.1.1 Vertikale Pijpen

a - Het theoretische model van Zuber en Findlay [Z2] voor de evaluatie van de dampfractie werd eerst geverifieerd door proeven in een

vertikale stoomgeneratorpijp met een kleine diameter voor $P = 4,1 - 18$ MN/m^2 en $G = 51 - 2237$ kg/m^{2}s. Deze verificatie leverde de nauwkeurige waarden van de in het model gebruikte parameters op. Deze waarden verschilden aanmerkelijk van die welke door Zuber en Findlay en andere onderzoekers werden gegeven [B2, K7, S13, Z3]. Vervolgens werd aangetoond dat de verkregen resultaten toegepast konden worden om de dampfractie nauwkeurig te voorspellen voor de adiabatische en diabatische stroming van stoom/water mengsels in vertikale pijpen met cirkelvormige en rechthoekige doorsnede en in vertikale annulaire kanalen met kleine en middelgrote diameter voor $d = 4,74 - 34,3$ mm; $P = 1 - 18$ MN/m^2; $G = 51 - 3504$ kg/m^{2}s en $\bar{\alpha} = 0,08 - 99\%$. Voor dit doel werden 642 gegevens gebruikt. 62 hiervan werden verkregen tijdens de beschreven studie.

b - Voor de in paragraaf (a) genoemde condities is de waarde van de distributiefactor bijna gelijk aan 1. Dit houdt in dat voor deze condities de radiale verdelingen voor dampfractie en volumetrische stroomdichtheid van geen belang zijn voor het voorspellen van de distributiefactor en dat het verschil tussen de over de pijpdoorsnede gemiddelde snelheid van de stoomfase en de gemiddelde volumetrische stroomdichtheid van een stoom/water mengsel praktisch gelijk is aan de over de doorsnede gemiddelde driftsnelheid. De bovenstaande resultaten betekenen een aanzienlijke vereenvoudiging van de welbekende twee theorieën, te weten: de theorie van Zuber en Findlay [Z2] en die van Bankoff [B2] voor de bepaling van de dampfractie en het snelheidsveld in een twee-fasen stroming in vertikale pijpen van kleine en middelgrote diameter.

c - Voor de in paragraaf (a) genoemde condities blijkt de gewogen gemiddelde drift-snelheid slechts weinig afhankelijk te zijn van de heersende druk.

A5.1.2 Schroefgewonden Pijpen

a - Er zijn experimentele gegevens en correlaties gegeven voor de dampfractie in schroefgewonden stoomgeneratorpijpen voor $d = 18$ mm; $d_c/d = 38,9$; $P = 4 - 18$ MN/m^2; $G = 429 - 1518$ kg/m^{2}s; $\beta = 0,00018 - 0,58$. Voor het bovengegeven drukgebied worden geen gegevens voor de dampfractie voor water in de literatuur vermeld. In

totaal werden 44 gegevens verkregen. De nauwkeurigheid van de correlaties is circa 12,5%.

b - Voor de stroming van stoom/water mengsels in schroefgewonden pijpen en voor β = 0,4 - 0,58; P = 4,2 - 8,1 MN/m^2; G = 429 - 1493 kg/m^{2}s en d_c/d = 38,9 wordt de distributiefactor niet beïnvloed door centrifugale krachten. Deze is constant en gelijk aan 0,875. Voor de stroming van lucht/water mengsels in schroefgewonden pijpen is de waarde van genoemde factor eveneens constant en gelijk aan 1,1 voor β = 0,18 - 0,99 en d_c/d = 11 - 48.

c - Bij hogere drukken en voor β = 0,4 - 0,58 is de distributiefactor voor de stroming van stoom/water mengsels in schroefgewonden pijpen kleiner dan de distributiefactor voor de stroming van stoom/water mengsels in horizontale pijpen. Deze conclusie is ook van toepassing op de stroming van lucht/water mengsels voor β = 0,3 - 0,9.

d - Voor de stroming van stoom/water mengsels in schroefgewonden pijpen wordt de distributiefactor beïnvloed door centrifugale krachten en de volumetrische snelheidsverhouding voor damp voor β = 0,00018 - 0,4; P = 4 - 18 MN/m^2; G = 754 - 1518 kg/m^{2}s en d_c/d = 38,9.

A5.2 BEGINPUNT VAN KOKEN EN BEGINPUNT VAN NETTO-DAMPONTWIKKELING VOOR ONDERKOELD STROMINGSKIEMKOKEN (hoofdstuk 4 in het proefschrift)

In een kanaal waarin koken optreedt is het beginpunt van koken het punt waarop de eerste bel ontstaat en zich van de pijpwand losmaakt en het beginpunt van netto-dampontwikkeling het punt waarop de dampfractie plotseling stijgt. Deze punten zullen respectievelijk aangeduid worden als IPB en IPNVG.

a - In een vertikale pijp en twee schroefgewonden cirkelvormige stoomgeneratorpijpen, werd het IPB gemeten voor P = 4 - 18 MN/m^2 en G = 757 - 2208 kg/m^{2}s en het IPNVG voor P = 4 - 18 MN/m^2 en G = 1435 - 2203 kg/m^{2}s. Voor de metingen werd een directe methode, dat wil zeggen een ultrasnelle fotografische techniek, gebruikt. De aldus verkregen 22 gegevens en nog eens 143 gegevens uit de literatuur werden geanalyseerd.

b - Zowel het IPB als het IPNVG staan in nauw verband met het warmte-

overdrachtsmechanisme voor onderkoeld stromingskiemkoken. Daarom werd een dimensieloos getal dat karakteristiek is voor deze punten afgeleid uit een fenomenologische warmteoverdrachtsvergelijking. Dit dimensieloze getal geeft de verhouding van de warmtestroomdichtheid als gevolg van onderdrukte gedwongen convectie tot de totale warmtestroomdichtheid bij het IPB en IPNVG. Voor water is de waarde van dit dimensieloze getal constant en

b1- is gelijk aan 0,665 voor het IPB in vertikale pijpen van cirkelvormige en ringvormige doorsnede en op een vlakke plaat voor $P = 0,15 - 19,6$ MN/m^2; $G = 470 - 17355$ kg/m^{2}s; $q = 0,13 - 9,8$ MW/m^2; $\Delta T_{sub} = 2,6 - 108$ K en $d = 2,13 - 32$ mm; en

b2- is gelijk aan 0,445 voor het IPB in schroefgewonden pijpen voor $P = 4 - 18$ MN/m^2; $G = 757 - 1518$ kg/m^{2}s; $q = 0,082 - 0,39$ MW/m^2; $\Delta T_{sub} = 4,4 - 12,5$ K en $d = 18$ mm; en

b3- is gelijk aan 0,24 als $u \geq 0,45$ m/s en gelijk aan 0,11 als $u < 0,45$ voor het IPNVG in vertikale pijpen van cirkelvormige en rechthoekige doorsnede, vertikale pijpen van ringvormige doorsnede en in schroefgewonden pijpen voor $P = 0,1 - 18$ MN/m^2; $G = 132 - 2818$ kg/m^{2}s; $q = 0,128 - 1,92$ MW/m^2; $\Delta T_{sub} = 1,2 - 42$ K en $d = 4,1 - 19,8$ mm.

b4- Voor het IPNVG in vertikale pijpen en voor Refrigerant-22 is de waarde van het bovengenoemde dimensieloze getal gelijk aan 0,18 als $u \geq 0,45$ m/s en gelijk aan 0,11 als $u < 0,45$ voor $P = 1,2 - 3,3$ MN/m^2; $G = 180 - 1391$ kg/m^{2}s; $q = 0,02 - 0,06$ MW/m^2; $\Delta T_{sub} = 3,2 - 7,3$ K en $d = 10,2$ mm.

c - Het IPB in schroefgewonden pijpen is vertraagd ten opzichte van het IPB in vertikale pijpen. Dit is waarschijnlijk het gevolg van de warmtegeleiding in de wand van een schroefgewonden stoomgeneratorpijp in de omtreksrichting van de pijp.

d - Er werd ook een opschalingswet opgesteld om het IPNVG te voorspellen voor andere vloeistoffen dan water en Refrigerant-22 door gebruik te maken van eerdergenoemde fenomenologische warmteoverdrachtsvergelijking voor onderkoeld stromingskiemkoken.

A5.3 BELLENDYNAMICA VOOR ONDERKOELD STROMINGSKIEMKOKEN (hoofdstuk 5 in het proefschrift)

a - Een door warmteoverdracht gecontroleerd bellenmodel gaf drie

semi-empirische correlaties om belgroeisnelheid, maximum beldiameter en maximum belgroeitijd te bepalen voor het onderkoeld stromingskiemkoken van water. Het model werd getoetst aan de gegevens verkregen voor P = 0,1 - 17,7 MN/m^2; u = 0,08 - 9,15 m/s; q = 0,47 - 10,64 MW/m^2; ΔT_{sub} = 3 - 86 K; d_m = 0,08 - 1,24 mm en t_m = 0,175 - 5 ms. Voor dit doel werden 60 gegevens gebruikt, waarvan er 12 werden verkregen in de huidige studie. Het model komt goed overeen met de experimentele resultaten.

b - Het model toonde aan dat het droge oppervlak onder een bel die in het onderkoeld stromingskiemkokengebied van een stoomgeneratorpijp ontstaat, verdwijnt bij een druk hoger dan 1 MN/m^2.

c - Het gedrag van een bel gevormd bij het IPB verschilt van het gedrag van de doorsnee-bel van een bellenpopulatie die uit talrijke bellen bestaat. Beide typen bellen zijn in deze studie geanalyseerd.

A5.4 DROOGKOKEN EN TWEE-FASEN DRUKVERLIES IN NATRIUMVERHITTE SCHROEFGEWONDEN STOOMGENERATORPIJPEN BIJ HOGE DRUKKEN (hoofdstuk 6 van het proefschrift)

A5.4.1 Droogkoken

a - De condities waaronder droogkoken optreedt werden bepaald in drie door natrium verhitte schroefgewonden cirkelvormige pijpen van 18 mm inwendige diameter. De verwarmde langs de schroeflijn gemeten lengten van deze pijpen waren 40,13, 35,50 en 26,67 m en de diameters van de schroeffiguren waren respectievelijk 1,5, 0,7 en 0,7 m. De proeven werden uitgevoerd voor het volgende gebied van bedrijfsomstandigheden: P = 14,7 - 20,2 MN/m^2; G = 112 - 1829 kg/m^2s; ΔT_{sub} = 35,6 - 156,8 K; X_d = 0,08 - 1; q_d = 41 - 731 kW/m^2.

b - Droogkoken werd gemeten aan de buiten- en binnenzijde, boven- en onderkant van een testpijp en trad steeds op in de laatste kwartlengte van de pijp. De afstand tussen de plaatsen waar het eerste en het laatste droogkoken geconstateerd werd, varieerde van 0,2 tot 5,1 m. Deze afstand was een klein gedeelte van de lengte van een testpijp, nl. max. 15%. Uit het bovenstaande zou men kunnen opmaken dat de plaats waar voor het eerst droogkoken gemeten wordt, praktisch samenvalt met de plaats waar droogkoken werkelijk voor de eerste maal

optreedt en dat de plaats waar voor het laatst droogkoken gemeten wordt, samenvalt met de plaats waar droogkoken in feite eindigt. Dit resultaat is van belang voor praktische toepassingen.

c - Bij massastroomsnelheden groter dan ongeveer 850 kg/m^{2}s werd geconstateerd dat droogkoken het eerst optrad aan de binnenwand van een testpijp. De laatste plaats waar droogkoken geconstateerd werd was aan de buitenkant van de pijp. Bij massastroomsnelheden kleiner dan 850 kg/m^{2}s waren de plaatsen waar het eerst en het laatst droogkoken geconstateerd werd, respectievelijk de bovenkant en de onderkant. De plaats van droogkoken blijkt af te hangen van, onder andere, centrifugale krachten en de zwaartekracht.

d - Bij hoge massastroomsnelheden waren de fluctuaties in wandtemperatuur op de plaats waar voor het eerst droogkoken werd geconstateerd, zeer klein, en deze fluctuaties werden groter ter plaatse van het laatst geconstateerde droogkookverschijnsel. Bij verlaging van de massastroom werden de temperatuurfluctuaties groter.

e - De 203 gegevens die tijdens de huidige studie werden verkregen voor het eerste en het laatst gemeten droogkoken en de 674 gegevens van verschillende onderzoekers verkregen bij proeven in vertikale, korte en lange elektrisch verhitte cirkelvormige pijpen en in een lange, vertikale, door natrium verhitte cirkelvormige pijp werden gecorreleerd. De opgestelde correlatie voorspelt de warmtestroomdichtheid bij droogkoken binnen 20% nauwkeurigheid voor 98% van de gegevens. De standaarddeviatie van de fouten voor alle 877 gegevens is 9,01%. De pijpgeometrieën en bedrijfsomstandigheden waarvoor de gegevens werden verkregen die gebruikt zijn om de correlatie te bepalen, zijn de volgende: L_h = 0,25 - 40,13 m; d = 7,86 - 18 mm; d/(2 δ) = 1,90 - 6,67; d_c/d = 38,9 - 83,3; P = 4,3 - 20,2 MN/m^2; G = 112 - 5542 kg/m^{2}s; ΔT_{sub} = 8 - 273 K; X_d = 0 - 1; q_d = 41 - 4931 kW/m^2. Het gebruik van de correlatie is niet aan te raden voor korte pijpen voor P < 9,7 MN/m^2.

f - De zogenaamde equivalente lengte hypothese zou een fysische betekenis hebben voor de verklaring van het mechanisme van droogkoken.

g - De correlaties voor droogkoken die gebaseerd zijn op gegevens die verkregen werden voor gelijkmatig verhitte (dat wil zeggen elektrisch verhitte) pijpen worden niet aangeraden voor niet gelijkmatig verhitte pijpen.

A5.4.2 Twee-fasen Drukverlies

a - In bovengenoemde schroefgewonden pijpen werd ook het drukverlies voor twee-fasen stroming gemeten. De 70 gegevens die werden verkregen tijdens deze studie en de 299 gegevens uit de literatuur voor een 10 m lange, vertikale, natriumverhitte, cirkelvormige pijp van 7,86 mm inwendige diameter, werden gecorreleerd binnen een nauwkeurigheid van 20% voor 98% van de gegevens. De standaarddeviatie van de fouten voor alle 369 gegevens is 9,87%. De proefomstandigheden waarbij de gegevens werden verkregen die gebruikt zijn om de correlatie te bepalen, zijn: $P = 14,3 - 20,1$ MN/m^2; $G = 296 - 3498$ kg/m^{2}s; $X_{bt} = 0,06 - 1$; $\Delta P = 3,0 - 226$ kN/m^2.

A5.5 TWEE-FASEN STROMINGSINSTABILITEITEN IN STOOMGENERATORPIJPEN (hoofdstuk 7 van het proefschrift)

A5.5.1 Dichtheidgolfoscillaties

Dichtheidgolfoscillaties zijn laagfrequente oscillaties waarvan de periode varieert tussen één en tweemaal de verblijftijd van een vloeistofdeeltje in een stoomgeneratorpijp. Deze zullen aangeduid worden als DWO.

a - De DWO werden bestudeerd in vier oververhitte stoom producerende stoomgeneratorpijpen met $L_t/d = 1272 - 2468$ en in een grootschalig verdampermodel met $L_t/d = 1535$ voor $P = 5,3 - 19,1$ MN/m^2; $G = 187 - 1365$ kg/m^{2}s; $X_{IC} = 1,10 - 2,38$; $\Delta T_{sub} = 3,2 - 168$ K en $K = 0 - 713$. Alle testpijpen en de verdamper werkten met gedwongen stroming en werden door natrium verhit.

b - De DWO in oververhitte stoom producerende stoomgeneratorpijpen met gedwongen stroming zijn zogenaamde tijdvertragingsoscillaties. De lengte van het oververhitte-stoomgebied en de verblijftijd van een vloeistofdeeltje in dit gebied zijn van groot belang voor het mechanisme van de DWO. Ten einde het veelvoudige regeneratieve terugkoppelmechanisme in werking te stellen dat de DWO opwekt in een oververhitte stoom producerende stoomgeneratorpijp met gedwongen stroming wanneer de uitlaatdruk en de inlaatsmoring constant worden

gehouden, moet de lengte van het oververhitte stoomgedeelte een constante waarde bereiken. Dan beginnen de DWO op te treden en wordt het veelvoudige regeneratieve terugkoppelmechanisme in werking gesteld. Smoren ter plaatse van de inlaat vertraagt dit mechanisme.

c - Voor het mechanisme van de DWO in een oververhitte stoom produceren stoomgeneratorpijp met gedwongen stroming werd een empirische relatie vastgesteld door gebruik te maken van de dimensieloze verblijftijden van een vloeistofdeeltje in verschillende warmteoverdrachtsgebieden van de pijp. De relatie is in feite een stabiliteitsmodel en werd getoetst aan de hand van 176 gegevens die verkregen werden in een 44,43 m lange schroefgewonden pijp en een 20,45 m lange pijp bestaande uit een vertikale en een horizontale V-vormige pijp, voor $P = 7,6 - 19$ MN/m^2; $G = 262 - 1020$ kg/m^{2}s; $\Delta T_{sub} = 20,4 - 168$ K en $X_{IC} = 1,37 - 2,20$.

d - De stoomkwaliteit ter plaatse van de uitlaat van een oververhitte stoom producerende stoomgeneratorpijp met gedwongen stroming bij het begin van het optreden van de DWO is voornamelijk een functie van de druk voor een gegeven inlaatsmoring, terwijl de invloed van alle andere proefomstandigheden op de stoomkwaliteit van secundair belang zijn. Dit werd ook aangetoond door de relatie te gebruiken ter verklarii van het mechanisme van de DWO vermeld in bovengenoemde paragraaf.

e - De paragrafen (b) en (d) suggereren dat de gegevens voor de DWO verkregen in oververhitte stoom producerende stoomgeneratorpijpen met gedwongen stroming nauwkeurig gecorreleerd kunnen worden op verschillende manieren. Twee correlaties werden bepaald voor een groot gebied van proefomstandigheden en geometrieën.

f - De parameters die in de eerste correlatie werden gebruikt zijn de dimensieloze inlaat-onderkoelingenthalpie, de gereduceerde druk, de inlaat-smoringcoefficient en de verhouding van verwarmde pijplengte tot pijpdiameter. Het gebied van geometrieën en proefomstandigheden is: geometrie: cirkelvormige rechte pijpen, cirkelvormige serpentine pijpen, cirkelvormige schroefgewonden pijpen, pijpen bestaande uit een cirkelvormige vertikale pijp en een cirkelvormige horizontale pijp in V-vorm, en een rechte pijp met rechthoekige doorsnede; soort verwarming: verwarming door natrium of elektriciteit; $L_h/d = 153 - 9502$; $d = 4,49 - 29,9$ mm; $X_{IC} = 0,27 - 2,38$;

$P = 4,1 - 19,1$ MN/m^2; $G = 118 - 2088$ kg/m^{2}s; $\Delta T_{sub} = 2,8 - 245,9$ K en $K = 0 - 2882$. Het aantal gebruikte gegevens bedroeg 413. De correlatie is zowel van toepassing op een oververhitte stoom producerende stoomgeneratorpijp met gedwongen stroming als op een stoomgeneratorpijp met gedwongen stroming waarin geen oververhitte stoom wordt geproduceerd. De correlatie voorspelt het vermogen bij het begin van de DWO uit deze 413 gegevens tot op 8% nauwkeurig voor 87% van de gegevens. De standaarddeviatie van de fouten is 5,97%.

g - De parameters gebruikt in de tweede correlatie omvatten praktisch alle proefomstandigheden en geometrieën in dimensieloze vorm. De gebieden van geometrieën en proefomstandigheden van de gegevens die werden gebruikt om deze correlatie te bepalen, zijn: geometrie: cirkelvormige rechte pijpen; cirkelvormige schroefgewonden pijpen, een cirkelvormige serpentine pijp, en pijpen, elk samengesteld uit een cirkelvormige vertikale pijp en een cirkelvormige horizontale pijp in V-vorm; soort van verwarming: verwarming door natrium of elektriciteit; $L_t = 10 - 223,3$ m; $L_t/d = 1272 - 10150$; $d = 7,86 - 22$ mm; $d_c/d = 47,4 - 83,3$; $P = 4,3 - 19,1$ MN/m^2; $G = 118 - 1365$ kg/m^{2}s; $\Delta T_{sub} = 3,2 - 245,9$ K; $X_{IC} = 1,01 - 2,38$ en $K = 0 - 2882$. Het aantal gebruikte gegevens bedroeg 380. De correlatie is slechts van toepassing op oververhitte stoom producerende stoomgeneratorpijpen en voorspelt het vermogen bij het begin van de DWO uit deze 380 gegevens tot op 7,5% nauwkeurig voor 98% van de gegevens. De standaarddeviatie van de fouten is 3,33%.

h - Voor oververhitte stoom producerende stoomgeneratorpijpen en $L_t/d > 4167$, wordt de uitlaatstoomkwaliteit of het vermogen bij de begincondities van de DWO niet beïnvloed door de inlaatsmoring.

i - Een correlatie om de periode te kunnen voorspellen van de DWO die optreden in oververhitte stoom producerende stoomgeneratorpijpen met gedwongen stroming en in een stoomgeneratorpijp met gedwongen stroming waarin geen oververhitte stoom wordt geproduceerd, werd ook opgesteld voor $L_t = 0,68 - 44,43$ m; $d = 4,49 - 18$ mm; $P = 4,1 - 19$ MN/m^2; $G = 262 - 2088$ kg/m^{2}s; $X_{IC} = 0,27 - 2,20$; $\Delta T_{sub} = 2,8 - 168$ K; $\psi = 0,345 - 12,5$ s en $K = 0 - 450$. Het aantal gebruikte gegevens bedroeg 188. De correlatie voorspelt uit deze gegevens de periode van de DWO binnen een nauwkeurigheid van 30% voor 95% van de gegevens. De standaarddeviatie van de fouten is 15,1%.

j - Het blijkt dat inlaatsmoring invloed heeft op de periode van de DWO.

k - Het is gerechtvaardigd te concluderen dat de condities waaronder de DWO optreden in oververhitte stoom producerende stoomgeneratorpijpen met gedwongen stroming met behulp van eenvoudige vergelijkingen kunnen worden voorspeld, wat het gebruik van tijdrovende gecompliceerde stabiliteitscorrelaties in de vorm van een computerprogramma, tenminste voor het gebied van geometrieën en proefomstandigheden zoals gebruikt in de huidige studie, overbodig maakt. Er dient in dit geval op te worden gewezen dat de huidige correlaties afgeleid werden uit het fysische mechanisme van de DWO in oververhitte stoom producerende stoomgeneratorpijpen met gedwongen stroming.

l - Ter ondersteuning van de conclusie genoemd in paragraaf (k), werden de 110 gegevens verkregen door verschillende onderzoekers bij proeven in stoomgeneratorpijpen met natuurlijke circulatie voor de begincondities van de DWO eveneens met behulp van eenvoudige vergelijkingen gecorreleerd. Het gebied van geometrieën en proefomstandigheden waarvoor deze gegevens werden verkregen, zijn: geometrie: vertikale cirkelvormige pijpen en vertikale pijpen met ringvormige doorsnede; d = 8,51 - 36 mm; L_h = 0,91 - 4,89 m; L_h/d = 34 - 489; P = 0,2 - 7,1 MN/m^2; X_{IC} = 0,04 - 0,62; G = 529 - 1230 kg/m^2s en ΔT_{sub} = 0 - 244 K. De gevonden correlatie voorspelt uit bovenstaande gegevens het vermogen bij het begin van het optreden van de DWO binnen een nauwkeurigheid van 20% voor 95% van de gegevens. De standaarddeviatie van de fouten is 10,6%.

m - Een geringe mate van smoren ter plaatse van de inlaat heeft geen invloed op de aanvangscondities waaronder de DWO optreden in stoomgeneratorpijpen met natuurlijke circulatie.

A5.5.2 Stromingspatrooninstabiliteiten

a - De oorzaak van deze instabiliteiten die zijn waargenomen in twee lange stoomgeneratorpijpen met verschillende geometrieën schijnt te liggen in de onderdrukking van de bellengroei maar niet in het verschil in drukverlies tussen het bellen-prop-stromingsgebied en het annulaire stromingsgebied.

A5.5.3 Instabiliteiten als gevolg van het Ontbreken van Thermodynamisch Evenwicht tussen de Fasen

a - In de aanwezigheid van deze instabiliteiten kunnen noch de ware stoomkwaliteit noch de temperatuur van de stoom langs de lengte van een oververhitte stoom producerende stoomgeneratorpijp nauwkeurig worden gemeten door gebruik te maken van conventionele methoden voorbij de plaats waar de thermodynamische stoomkwaliteit de waarde van 1 bereikt. Dit houdt in dat de bovengenoemde grootheden bij de huidige stand van kennis op dit gebied slechts theoretisch geëvalueerd kunnen worden.

STELLINGEN

1. In spite of the considerable advances that have been made in the field of digital computers, we are not yet able to predict adequately the dynamic behaviour of a shell - and - tube type evaporator using a numerical method if we assume the properties of the shell- and tube fluid to be space- and time-dependent. This justifies the use of dimensional analysis for predicting the dynamics of a heat exchange equipment for both large and small transients.

2. Two-phase flow conservation equations can be written in different forms: local instantaneous equations, instantaneous space-averaged equations, local time-averaged equations and space-time (or time-space) averaged equations. In spite of the considerable advances made in the two-phase flow field, the space-time averaged equations are the only ones available for practical applications.

3. The huge number of data published on the various aspects of two-phase flow would warrant the establishment of an international centre in which these data can be classified by operating conditions, geometry, quality, etc. This would prevent unnecessary duplication of much experimental research work.

4. Some recent books and courses on two-phase flow imply that this subject is not only interesting for scientists but also for businessmen.

5. Of the many proposals for recovering energy from the sun, air, wind or oceans, only a very limited number promise to make a significant contribution to meet the world's future energy demands with reasonable economics.

6. Let the politicians who decide to make a war fight at the front. This will at least prevent unnecessary wars caused by inferiority or superiority complexes.

7. Imprisonment of an individual is the failure of society. The heavier a prison sentence, the more imperfect the society that administers it.

8. Even the worst operating democracy is better than the best military dictatorship.

9. The future need for psycho-analysts will exceed that of M.D.'s.

10. Every person possessing a driving licence should be examined for his manners. If he fails, his driving licence should be withdrawn. This will help considerably to protect the life and property of the individual.

H.C. Ünal